

UNIVERSITÀ DI PISA

Scuola di Dottorato in Ingegneria “Leonardo da Vinci”



Corso di Dottorato di Ricerca in
SICUREZZA NUCLEARE E INDUSTRIALE

Tesi di Dottorato di Ricerca

**DEVELOPMENT OF METHODOLOGY FOR
EVALUATION OF UNCERTAINTIES OF
SYSTEM THERMAL-HYDRAULIC CODES'
INPUT PARAMETERS**

Autore:

Andriy Kovtonyuk

*Firma*_____

Relatori:

Prof. Ing. Francesco D'Auria

*Firma*_____

Dott. Ing. Giorgio M. Galassi

*Firma*_____

Dott. Ing. Alessandro Petruzzi

*Firma*_____

Anno 2014

*To my dearest parents
and my beloved Marina*

ACKNOWLEDGEMENTS

I would like to express my deepest gratitude to all colleagues, friends and family who supported me in this endeavor.

First of all, I would like to acknowledge Prof. Francesco D'Auria, who provided the opportunity and means to perform this research activity and gave access to immense expertise in nuclear engineering that undoubtedly defined the bases of this work.

My special acknowledgments are to my tutors Dr. Alessandro Petruzzi and Dr. Ing. Giorgio Galassi whose good advices, comments and sometimes heated discussions provided me with guiding light even in those situations when all seemed lost and objectives of this research were galloping from me at the speed of a racing horse.

I also would like to thank my colleagues from OECD PREMIUM project – my discussions with them had an impact on this work no less than a direct.

Greetings and thanks to my friends and colleagues from Nuclear Research Group of San Piero a Grado and other institutions, who have been there with a word of advice or a good joke to cheer me up.

And finally, my deepest and sincere gratitude to all my family – the people who helped me become who I am today, who, staying close or even being thousand miles away, have been there for me in every darkest second or every joyful moment. The dedication of this work to you, my dear ones, is only a small token of my praise for your support and love.

ABSTRACT

The purpose of the present doctoral research is to improve on two issues identified in the frame of use of Best Estimate Plus Uncertainty approach in nuclear safety studies: proper estimation of code input parameter uncertainties and quality assurance in qualification of best-estimate models. The application of best-estimate computer codes and models implies the evaluation of uncertainties. This is connected with the imperfect nature of the codes and of the process of codes application. While the 'code user effect' is already a well-known issue in the frame of the deterministic analysis and application of system thermal-hydraulic codes, the adoption of BEPU approach poses a new problem – so called uncertainty methodology user effect. Lessons learnt from the international benchmarks showed that the use of engineering judgment in identification of considered code input parameters and imperfect knowledge of the code input parameter uncertainties, greatly affects the results of performed uncertainty analysis. The application of computer codes to calculation of experimental tests provides a first step to obtain code-specific uncertainties of input parameters representative of a studied correlation. A proper methodology of treatment of calculation and experimental results has to be adopted in this case. Therefore, in order to address this issue an Input Parameter Range Evaluation Methodology (IPREM) has been developed. The IPREM adopts the mathematical apparatus of Fast Fourier Transform Based Method (FFTBM) that has been previously developed at University of Pisa and applied for quantification of accuracy of thermal-hydraulic calculations. The proper IPREM procedure, figures-of-merit and criteria have been established in order to quantify the variation ranges of an input parameter. The IPREM has been applied to evaluation of uncertainty of reflood-related input parameters and models of RELAP5 Mod3.3 and CATHARE2 codes. In this framework, the simulations of various experimental tests of FEBA, PERICLES and ACHILLES separate effect test facilities have been performed. The obtained results in the form of variation ranges of input parameters have been subjected to various "internal" qualifications and extensive validation. The validation has been carried out through uncertainty analysis of "blind" thermal-hydraulic calculations of numerous reflood tests performed at different experimental facilities and at different conditions. The values of experimentally measured peak cladding temperature have been compared with maximum of evaluated upper uncertainty ranges of predicted temperature trends. The majority of evaluated uncertainty bands encompasses the measured values of peak cladding temperature and allows to confirm the validity of the application of the IPREM methodology for the evaluation of uncertainty of code input parameters. Although the IPREM is based on rather engineering considerations than on substantial statistical basis (and therefore does not provide the probability distribution of considered parameters), it proved to be code-, geometry- and condition-independent. The methodology is cost efficient, in general does not require code modification and requires few experimental tests with time-dependent measurements in order to quantify and validate the ranges of variation of input parameters of interest.

On the other hand, a key feature of the activities performed in nuclear reactor safety technology is constituted by the necessity to demonstrate the qualification level of each tool adopted within an assigned process and of each step of the concerned

process. Therefore, the qualification of best-estimate codes, models and “best modeling practices” must be considered of great importance in order to ensure the validity of performed BEPU analysis. A consistent code assessment supported by a qualified experimental database is an important step for developing a solid ground for the uncertainty evaluation in the frame of BEPU approach. Thus, a methodology has to be developed in order to address the issue of quality assurance in the process of code assessment. The solution to quality assurance problem has been proposed in a form of a Standard Consolidated Reference Experimental Database (SCRED), which includes a series of documents which goal is to demonstrate the qualification level of the achieved code results. The structure and procedure to set up reference data sets, qualification report and engineering handbook has been outlined. In the framework of application of the SCRED to validation of thermal-hydraulic code RELAP5-3D®, the RDS, model for LOBI-MOD1 and LOBI-MOD2 integral test facilities and Engineering Handbook have been developed. The calculation of large break LOCA and small break LOCA tests has been performed and calculation results have been subjected to qualification process. The obtained documents and code calculation results demonstrate the maturity level and the effectiveness of the procedures itself, which is reflected in the excellent results of the performed simulations. This confirms that the use of qualified experimental databases has the key role in providing the quality assurance to the “best nodalization practices”, which currently is the only viable approach in consideration of nodalization-related uncertainties.

INDEX

ACKNOWLEDGEMENTS	v
ABSTRACT	vii
INDEX.....	ix
ABBREVIATIONS	xiv
LIST OF FIGURES	xvi
LIST OF TABLES.....	xxiv
1 INTRODUCTION	1
1.1. Objectives of the research	1
1.2. Framework.....	2
1.3. Description of the performed activity	2
1.4. Structure of the document	4
2 UNCERTAINTY ANALYSIS IN THERMAL-HYDRAULIC CALCULATIONS	5
2.1. Sources of uncertainty	5
2.2. Common approaches for evaluation of uncertainty of thermal- hydraulic calculations	8
2.2.1. Input error propagation	8
2.2.1.1. CSAU method.....	8
2.2.1.2. GRS method	10
2.2.2. Output error propagation.....	12
2.2.3. Approaches based on adjoint sensitivity procedures.....	14
2.3. Evaluation of uncertainty of code input parameters	16
2.3.1. Overview of CIRCÉ method.....	17
2.3.2. Overview of Data Adjustment and Assimilation.....	19
2.4. Overview of EU projects related to uncertainty analysis of TH- SYS calculations.....	21
3 DEVELOPMENT OF INPUT PARAMETER RANGE EVALUATION METHODOLOGY	23
3.1. Needs and objectives.....	23
3.2. Fast Fourier Transform Based Method.....	26

3.3. Description of methodology for input parameter range evaluation: the IPREM	31
3.4. Verification step: application to Edwards pipe problem	36
3.4.1. Modeling Edwards pipe experiment with RELAP5 code.....	36
3.4.2. Quantification of uncertainty of model input parameters	38
3.4.3. Internal qualification: uncertainty analysis of Edwards pipe calculation	45
4 APPLICATION AND VALIDATION OF IPREM.....	48
4.1. Reflood in Nuclear Safety	50
4.2. Application of IPREM: quantification of variation ranges of reflood-related input parameters of RELAP5 code	54
4.2.1. Description of FEBA facility.....	54
4.2.2. Modeling of FEBA with RELAP5 code	56
4.2.2.1. Simulation of reflood with various TH-SYS codes.....	60
4.2.3. Identification of influential parameters.....	64
4.2.4. Quantification of input parameter uncertainties	74
4.2.5. Internal qualification.....	84
4.2.5.1. Uncertainty analysis of test FEBA 216	84
4.2.5.2. Sensitivity on limit for $CR(\alpha)$	87
4.2.5.3. Sensitivity on type of Probability Density Function.....	91
4.3. Validation of IPREM: uncertainty analysis of reflood simulation with thermal-hydraulic codes	95
4.3.1. Validation against FEBA facility	95
4.3.2. Validation against PERICLES facility	98
4.3.2.1. Description of PERICLES facility	98
4.3.2.2. Modeling of PERICLES facility with RELAP5 code	100
4.3.2.3. Uncertainty analysis of PERICLES tests	101
4.3.3. Validation against ACHILLES facility.....	105
4.3.3.1. Description of ACHILLES facility	105
4.3.3.2. Modeling of ACHILLES facility with RELAP5 code	106
4.3.3.3. Uncertainty analysis of ACHILLES tests	107

4.4. External qualification: test-independence and facility-independence checks.....	109
4.4.1. Quantification of input parameter uncertainties using FEBA test 222	109
4.4.2. Quantification of input parameter uncertainties using PERICLES facility.....	115
4.4.2.1. Post-test calculation of PERICLES test RE79.....	115
4.4.2.2. Quantification and input parameter uncertainties.....	117
4.5. External qualification: application of IPREM to CATHARE2 code 124	
4.5.1. Modeling of FEBA facility with CATHARE2 code	124
4.5.2. Quantification of input parameter uncertainties	128
4.5.3. Validation of input parameter uncertainties	134
4.5.3.1. Modeling of ACHILLES facility with CATHARE2 code	134
4.5.3.2. Uncertainty analysis of reflood tests simulations.....	136
4.6. Summary of performed analysis.....	138
5 CONSIDERATIONS ON BEST-ESTIMATE MODEL QUALIFICATION.....	140
5.1. Use of qualified experimental database for a system code assessment.....	141
5.1.1. Setting up RDS facility and RDS test	143
5.1.2. Writing an input deck	144
5.1.3. Qualification Report	146
5.1.4. Engineering Handbook	146
5.2. Application of SCRED for assessment of RELAP5 code against LOCA scenarios in LOBI facility.....	149
5.2.1. Description of LOBI facility.....	149
5.2.2. Reference Data Set of LOBI facility	152
5.2.3. Modeling of LOBI facility with RELAP5-3D© code	152
5.2.4. Code validation for LBLOCA scenario.....	155
5.2.5. Code validation for SBLOCA scenario	158
5.3. Summary considerations	161
6 CONCLUSIONS	162

REFERENCES	165
APPENDIX A. CODES APPLIED IN THE FRAMEWORK OF RESEARCH	170
A.1. RELAP5 Mod3.3 code	170
A.1.1. Code overview.....	170
A.1.2. Reflood-related correlations.....	171
A.1.2.1. Interphase friction	171
A.1.2.2. Dispersed flow interphase heat transfer	171
A.1.2.3. Wall to fluid Heat Transfer (film boiling and transition boiling)	172
A.1.2.4. Weber number	175
A.1.2.5. Minimum droplet diameter	175
A.2. CATHARE2 code	176
A.3. RELAP5-3D© code	177
A.3. References to APPENDIX A	178
APPENDIX B. MODIFICATIONS OF RELAP5 SOURCE CODE	179
B.1. RELAP5 Mod3.3 source package.....	179
B.2. Modifications of main subroutine.....	179
B.3. Reflood-relevant subroutines and parameters	181
B.3.1. Interphase friction	181
B.3.2. Interphase heat transfer.....	182
B.3.3. Film/Transition boiling heat transfer	183
B.3.4. Minimum droplet diameter	184
B.5. References to APPENDIX B	184
APPENDIX C. DESCRIPTION OF THE LOBI-MOD2 NODALIZATION FOR RELAP5-3D© CODE	185
C.1. Description of the nodalization.....	185
C.2. Model qualification	193
C.3. References to APPENDIX C.....	199
APPENDIX D. EXAMPLE OF REFERENCE DATA SET FOR LOBI FACILITY	200
D.1. Reference Data Set for Facility	200

D.2.	Reference Data Set for Experimental Test	212
D.3.	References to APPENDIX D	220
APPENDIX E.	EXAMPLE OF ENGINEERING HANDBOOK OF	
	RELAP5 MODEL OF LOBI FACILITY	221
E.1.	Pressure Vessel hydraulic model	221
E.1.1.	Downcomer hydraulic model.....	226
E.2.	Pressure Vessel heat structure data	227
E.2.1.	Downcomer heat structure data.....	231
E.3.	General tables	236
E.4.	Material properties.....	237
E.5.	Control logic.....	237
E.5.1.	Control variables.....	237
E.5.2.	Trips	238
E.6	References to APPENDIX E.....	238

ABBREVIATIONS

1-D	One Dimensional
2-D	Two Dimensional
3-D	Three Dimensional
AA	Average Amplitude
ACC	Accumulator
AAG	Global Average Amplitude
ASAP	Adjoint Sensitivity Analysis Procedure
BE	Best Estimate
BEMUSE	Best Estimate Methods, Uncertainty and Sensitivity Evaluation
BEPU	Best Estimate Plus Uncertainty
BC	Boundary Conditions
BIC	Boundary and Initial Conditions
BL	Broken Loop
BWR	Boiling Water Reactor
CEA	Commissariat à l'Energie Atomique
CFD	Computational Fluid Dynamics
CFR	Code of Federal Regulation
CHF	Critical Heat Flux
CIAU	Code with capability of Internal Assessment of Uncertainty
CL	Cold Leg
CSAU	Code Scaling, Applicability and Uncertainty
CSNI	Committee on the Safety of Nuclear Installations
DAA	Data Adjustment and Assimilation
DBA	Design Basis Accident
DC	Downcomer
DIMNP	Department of Mechanical, Nuclear and Production Engineering of University of Pisa, Italy
ECC	Emergency Core Cooling
ECCS	Emergency Core Cooling System
EH	Engineering Handbook
E-M	Expectation-Maximization
FD	Fully Developed
FFT	Fast Fourier Transform
FFTBM	Fast Fourier Transform Based Method
GASAP	Global Adjoint Sensitivity Analysis Procedure
GRNSPG	Gruppo Ricerca Nucleare a San Piero a Grado
GRS	Gesellschaft für Anlagen- und Reaktorsicherheit
HL	Hot Leg
HTC	Heat Transfer Coefficient
HPIS	High Pressure Injection System
IAEA	International Atomic Energy Agency
ID	Identification number
IL	Intact Loop
IPREM	Input Parameter Range Evaluation Methodology
ITF	Integral Test Facility
KWU	Kraftwerk Union AG

LB-LOCA	Large Break LOCA
LOCA	Loss of Coolant Accident
LPIS	Low Pressure Injection System
LS	Loop Seal
MCP	Main Circulation Pump
NEA	Nuclear Energy Agency
NPP	Nuclear Power Plant
OECD	Organization for the Economic Cooperation and Development
PCT	Peak Cladding Temperature
PDF	Probability Distribution Function
PIRT	Phenomena Identification and Ranking Table
Ph.W.	Phenomenological Window
PREMIUM	Post-BEMUSE Reflood Models Input Uncertainty Methods
PRZ	Pressurizer
PS	Primary Side
PWR	Pressurized Water Reactor
QA	Quality Assurance
QF	Quench Front
QR	Qualification Report
RDS	Reference Data Set
RPV	Reactor Pressure Vessel
SBLOCA	Small Break LOCA
SCRED	Standard Consolidated Reference Experimental Database
SETF	Separate Effect Test Facility
SG	Steam Generator
SoT	Start of Transient
SS	Steady State
SYS	System
TAF	Top of Active Fuel
T-H	Thermal-Hydraulic
WF	Weighted Frequency
WWER	Water cooled Water moderated Energy Reactor
UA	Uncertainty Analysis
UE	User Effect
UMAE	Uncertainty Method based on the Accuracy Extrapolation
UNIPI	University of Pisa
US NRC	United States Nuclear Regulatory Commission
V&V	Validation and Verification

LIST OF FIGURES

<i>Figure 1 – Flowchart of performed research activity.</i>	3
<i>Figure 2 – Uncertainty methods based upon propagation of input uncertainties.</i>	8
<i>Figure 3 – Uncertainty methods based upon propagation of input uncertainties.</i>	9
<i>Figure 4 – Uncertainty methods based upon propagation of output uncertainties.</i>	13
<i>Figure 5 – UMAE process flow diagram.</i>	13
<i>Figure 6 – Uncertainty methods based on Adjoint Sensitivity Analysis Procedure and Data Adjustment/Assimilation.</i>	15
<i>Figure 7 – Important issue in input error propagation method.</i>	16
<i>Figure 8 – Inputs and outputs of CIRCÉ.</i>	18
<i>Figure 9 – IPREM in the framework of BEPU approach.</i>	25
<i>Figure 10 – Sample Fourier Transform representation.</i>	27
<i>Figure 11 – Flowchart of IPREM procedure</i>	32
<i>Figure 12 – Sample trend of CR quantity.</i>	35
<i>Figure 13 – Edward pipe experimental setup.</i>	36
<i>Figure 14 – RELAP5 nodalization of Edward pipe experimental.</i>	37
<i>Figure 15 – Edward pipe: predicted pressure in reference calculation.</i>	38
<i>Figure 16 – Edward pipe: predicted void fraction in reference calculation.</i>	38
<i>Figure 17 – Edwards pipe: AAz1jS – R and AAz1jS – E for initial liquid temperature.</i>	40
<i>Figure 18 – Edwards pipe: AAz2jS – R and AAz2jS – E for break flow area.</i>	40
<i>Figure 19 – Edwards pipe: AAz3jS – R and AAz3jS – E for Kloss at the break.</i>	41
<i>Figure 20 – Edwards pipe: AAz4jS – R and AAz4jS – E for discharge coefficient.</i>	41
<i>Figure 21 – Edwards pipe: AAG1jS – R and AAG1jS – E for initial liquid temperature.</i>	42
<i>Figure 22 – Edwards pipe: AAG2jS – R and AAG2jS – E for break flow area.</i>	42
<i>Figure 23 – Edwards pipe: AAG3jS – R and AAG3jS – E for K_{loss} at the break.</i>	43
<i>Figure 24 – Edwards pipe: AAG4jS – R and AAG4jS – E for discharge coefficient.</i>	43
<i>Figure 25 – Edwards pipe: CRα1j for initial liquid temperature.</i>	44
<i>Figure 26 – Edwards pipe: CRα2j for break flow area.</i>	44
<i>Figure 27 – Edwards pipe: CRα3j for Kloss at the break.</i>	45
<i>Figure 28 – Edwards pipe: CRα4j for discharge coefficient.</i>	45

Figure 29 – Edwards pipe: evaluated uncertainty for predicted pressure response.	47
Figure 30 – Example of rod surface temperature time trend during reflood.....	53
Figure 31 – Example of quench front propagation time trend during reflood.	53
Figure 32 – FEBA rod bundle – cross-section view.	54
Figure 33 – Cross-section view of the FEBA heater rod.	55
Figure 34 – Axial view of the FEBA heater rod and axial power profile distribution.	55
Figure 35 – Sketch of FEBA nodalization for RELAP5 code.....	57
Figure 36 – FEBA test 216: predicted by RELAP5 steady-state temperature distribution.	58
Figure 37 – FEBA test 216: predicted by RELAP5 cladding temperature at 2/3 height.	59
Figure 38 – FEBA test 216: predicted by RELAP5 cladding temperature at TAF. .	59
Figure 39 – FEBA test 216: predicted by RELAP5 quench front propagation.	60
Figure 40 – PREMIUM benchmark: fidelity of adopted nodalizations.	61
Figure 41 – PREMIUM benchmark: predicted cladding temperature at 2/3 height.	62
Figure 42 – PREMIUM benchmark: predicted cladding temperature at TAF.	62
Figure 43 – PREMIUM benchmark: predicted quench front propagation.	63
Figure 44 – Example of classification of Input Parameters for Weismann correlation.	65
Figure 45 – Procedure for identification of influential Input Parameters.	66
Figure 46 – Illustration of criteria #1 and #2 for selection of influential input parameters.....	67
Figure 47 – Illustration of criterion #3 for selection of influential input parameters.	67
Figure 48 – PREMIUM benchmark: Initially considered input parameters.....	70
Figure 49 – PREMIUM benchmark: Identified influential input parameters.	72
Figure 50 – PREMIUM benchmark: Cladding temperature vs. Wall HTC (multiplier).	73
Figure 51 – PREMIUM benchmark: Time of rewet vs. Wall HTC (multiplier).....	73
Figure 52 – PREMIUM benchmark: Cladding temperature vs. Interphase friction coefficient (multiplier).....	74
Figure 53 – FEBA 216: AAz1jS – R and AAz1jS – E for interphase HTC.	76
Figure 54 – FEBA 216: AAz2jS – R and AAz2jS – E for interphase friction coefficient.	76

Figure 55 – FEBA 216: $AAz3jS - R$ and $AAz3jS - E$ for film boiling HTC.....	77
Figure 56 – FEBA 216: $AAz4jS - R$ and $AAz4jS - E$ for convection to vapor HTC.	77
Figure 57 – FEBA 216: $AAG1jS - R$ and $AAG1jS - E$ for interphase HTC.	78
Figure 58 – FEBA 216: $AAG2jS - R$ and $AAG2jS - E$ for interphase friction coefficient.....	78
Figure 59 – FEBA 216: $AAG3jS - R$ and $AAG3jS - E$ for film boiling HTC.....	79
Figure 60 – FEBA 216: $AAG4jS - R$ and $AAG4jS - E$ for convection to vapor HTC.	79
Figure 61 – FEBA 216: $CR\alpha1j$ for interphase HTC.....	80
Figure 62 – FEBA 216: $CR\alpha2j$ for interphase friction coefficient.	80
Figure 63 – FEBA 216: $CR\alpha3j$ for film boiling HTC.	81
Figure 64 – FEBA 216: $CR\alpha4j$ for convection to vapor HTC.	81
Figure 65 – FEBA 216: variation of relevant responses at min & max values of interphase HTC.....	82
Figure 66 – FEBA 216: variation of relevant responses at min & max values of interphase friction coefficient.	83
Figure 67 – FEBA 216: variation of relevant responses at min & max values of film boiling HTC.	83
Figure 68 – FEBA 216: variation of relevant responses at min & max values of convection to vapor HTC.	84
Figure 69 – FEBA 216: predicted uncertainty band for cladding temperature at 2/3 height.	85
Figure 70 – FEBA 216: predicted uncertainty band for cladding temperature at top.	86
Figure 71 – FEBA 216: predicted uncertainty band for quench front elevation.....	86
Figure 72 – FEBA 216: application of $limit=0.1$ to $CR\alpha1j$ for interphase HTC.....	87
Figure 73 – FEBA 216: application of $limit=0.1$ $CR\alpha2j$ for interphase friction coefficient.....	88
Figure 74 – FEBA 216: application of $limit=0.1$ $CR\alpha3j$ for film boiling HTC.	88
Figure 75 – FEBA 216: application of $limit=0.1$ $CR\alpha4j$ for convection to vapor HTC.	89
Figure 76 – FEBA 216: predicted uncertainty band with $limit=0.1$ for cladding temperature at 2/3 height.....	90
Figure 77 – FEBA 216: predicted uncertainty band with $limit=0.1$ for cladding temperature at top.	90

Figure 78 – FEBA 216: predicted uncertainty band with limit=0.1 for quench front elevation.	91
Figure 79 – FEBA 216: Probability Density Functions for interphase friction.....	93
Figure 80 – FEBA 216: Results of PDF-sensitivity analysis for cladding temperature at 2/3 height.	93
Figure 81 – FEBA 216: Results of PDF-sensitivity analysis for cladding temperature at top.	94
Figure 82 – FEBA 216: Results of PDF-sensitivity analysis for quench front elevation.	94
Figure 83 – Results of uncertainty analysis of RELAP5 calculation of FEBA 223.	96
Figure 84 – Results of uncertainty analysis of RELAP5 calculation of FEBA 220.	96
Figure 85 – Results of uncertainty analysis of RELAP5 calculation of FEBA 218.	97
Figure 86 – Results of uncertainty analysis of RELAP5 calculation of FEBA 214.	97
Figure 87 – Results of uncertainty analysis of RELAP5 calculation of FEBA 222.	98
Figure 88 – Sketch of 2D PERICLES experimental test section.	99
Figure 89 – Horizontal section of one assembly of 2D PERICLES.	99
Figure 90 – Power profiles in 2D PERICLES.	99
Figure 91 – Sketch of PERICLES nodalization for RELAP5 code.	100
Figure 92 – Results of uncertainty analysis of RELAP5 calculation of PERICLES RE62.	102
Figure 93 – Results of uncertainty analysis of RELAP5 calculation of PERICLES RE64.	102
Figure 94 – Results of uncertainty analysis of RELAP5 calculation of PERICLES RE69.	103
Figure 95 – Results of uncertainty analysis of RELAP5 calculation of PERICLES RE79.	103
Figure 96 – Results of uncertainty analysis of RELAP5 calculation of PERICLES RE80.	104
Figure 97 – Results of uncertainty analysis of RELAP5 calculation of PERICLES RE86.	104
Figure 98 – Cross-section view of ACHILLES test section.	105
Figure 99 – Axial power profile and temperature measurement location in ACHILLES test section.	106
Figure 100 – Sketch of ACHILLES nodalization for RELAP5 code.	107
Figure 101 – Results of uncertainty analysis of RELAP5 calculation of ACHILLES A1R030.	108

Figure 102 – Results of uncertainty analysis of RELAP5 calculation of ACHILLES A1R048.	108
Figure 103 – FEBA 222: AAG5jS – R and AAG5jS – E for transition boiling HTC.	110
Figure 104 – FEBA 222: CR α 1j for interphase HTC.	111
Figure 105 – FEBA 222: CR α 2j for interphase friction coefficient.	111
Figure 106 – FEBA 222: CR α 3j for film boiling HTC.	111
Figure 107 – FEBA 222: CR α 4j for convection to vapor HTC.	112
Figure 108 – FEBA 222: CR α 5j for transition boiling HTC.	112
Figure 109 – Uncertainty analysis of RELAP5 calculation of FEBA 216 with [α^L ; α^U] derived from FEBA 222.	114
Figure 110 – Uncertainty analysis of RELAP5 calculation of PERICLES RE80 with [α^L ; α^U] derived from FEBA 222.	114
Figure 111 – Post-test calculation of PERICLES RE79: cladding temperature at 2/3 height of hot assembly.	116
Figure 112 – Post-test calculation of PERICLES RE79: cladding temperature at 2/3 height of cold assembly.	116
Figure 113 – Post-test calculation of PERICLES RE79: cladding temperature at top of hot assembly.	116
Figure 114 – Post-test calculation of PERICLES RE79: cladding temperature at top of cold assembly.	117
Figure 115 – PERICLES RE79: AAG1jS – R and AAG1jS – E for interphase HTC.	118
Figure 116 – PERICLES RE79: AAG2jS – R and AAG2jS – E for interphase friction coefficient.	119
Figure 117 – PERICLES RE79: AAG3jS – R and AAG3jS – E for film boiling HTC.	119
Figure 118 – PERICLES RE79: AAG4jS – R and AAG4jS – E for convection to vapor HTC.	119
Figure 119 – PERICLES RE79: AAG4jS – R and AAG4jS – E for transition boiling HTC.	120
Figure 120 – PERICLES RE79: CR α 1j for interphase HTC.	120
Figure 121 – PERICLES RE79: CR α 2j for interphase friction coefficient.	120
Figure 122 – PERICLES RE79: CR α 3j for film boiling HTC.	121
Figure 123 – PERICLES RE79: CR α 4j for convection to vapor HTC.	121
Figure 124 – PERICLES RE79: CR α 5j for transition boiling HTC.	121

Figure 125 – Uncertainty analysis of RELAP5 calculation of FEBA 216 with $[\alpha^L ; \alpha^U]$ derived from PERICLES RE79.	123
Figure 126 – Uncertainty analysis of RELAP5 calculation of PERICLES RE80 with $[\alpha^L ; \alpha^U]$ derived from PERICLES RE79.	123
Figure 127 – CATHARE model of the FEBA rod bundle.	125
Figure 128 – FEBA test 216: predicted by CATHARE2 steady-state clad (a) and housing (b) temperature distributions.	126
Figure 129 – FEBA test 216: predicted by CATHARE2 cladding temperature at 2/3 height.	127
Figure 130 – FEBA test 216: predicted by CATHARE2 cladding temperature at TAF.	127
Figure 131 – FEBA test 216: predicted by CATHARE2 quench front propagation.	128
Figure 132 – CATHARE2 sensitivity to variations in wall-fluid global heat transfer.	129
Figure 133 – CATHARE2 sensitivity to variations in conduction near quench front.	130
Figure 134 – CATHARE2 sensitivity to variations in interfacial friction.	130
Figure 135 – CATHARE2: AAG1jS – R and AAG1jS – E for wall-fluid global heat transfer.	131
Figure 136 – CATHARE2: AAG2jS – R and AAG2jS – E for conduction near quench front.	131
Figure 137 – CATHARE2: AAG3jS – R and AAG3jS – E for interfacial friction. ...	132
Figure 138 – CATHARE2: CR α 1j for wall-fluid global heat transfer.	132
Figure 139 – CATHARE2: CR α 2j for conduction near quench front.	133
Figure 140 – CATHARE2: CR α 3j for interfacial friction.	133
Figure 141 – CATHARE model of the ACHILLES rod bundle.	135
Figure 142 – ACHILLES A1R030: predicted by CATHARE2 steady-state temperature distributions.	136
Figure 143 – Uncertainty analysis of CATHARE2 calculation of FEBA test 214 with $[\alpha^L ; \alpha^U]$ derived from FEBA 216.	137
Figure 144 – Uncertainty analysis of CATHARE2 calculation of ACHILLES test A1R030 with $[\alpha^L ; \alpha^U]$ derived from FEBA 216.	137
Figure 145 – Uncertainty analysis of CATHARE2 calculation of ACHILLES test A1R048 with $[\alpha^L ; \alpha^U]$ derived from FEBA 216.	137
Figure 146 – Flow chart of the RDS, Input Deck, QR and EH interconnections. .	142
Figure 147 – The RDS-facility and the RDS-Tests.	144

Figure 148 – Flow chart of the nodalization qualification procedure.	147
Figure 149 – Flow Chart of the Input Development, Review and Qualification Procedures.	148
Figure 150 – LOBI MOD2 Primary Cooling System Configuration.	150
Figure 151 – Example of modules of RDS for LOBI-MOD2 facility.	152
Figure 152 – Example of Upper Plenum module of RDS for LOBI-MOD2 facility.	153
Figure 153 – Example of RELAP5 ASCII input deck commenting: hydraulic components.	154
Figure 154 – Example of RELAP5 ASCII input deck commenting: control logic components.	154
Figure 155 – Engineering Handbook: example of description of LOBI-MOD2 RPV nodalization for RELAP5 code.	155
Figure 156 – LOBI A1-06 RELAP5 calculation: primary side pressure.	156
Figure 157 – LOBI A1-06 RELAP5 calculation: Break mass flow rate (pump side).	156
Figure 158 – LOBI A1-06 RELAP5 calculation: Mass flow rate ACC HL IL.	156
Figure 159 – LOBI A1-06 RELAP5 calculation: Differential pressure across BL SG U-tubes.	157
Figure 160 – LOBI A1-06 RELAP5 calculation: Heater rod temperature 2/3 of the core height.	157
Figure 161 – LOBI A1-83 RELAP5 calculation: primary side pressure.	159
Figure 162 – LOBI A1-83 RELAP5 calculation: primary side residual mass.	159
Figure 163 – LOBI A1-83 RELAP5 calculation: core differential pressure.	160
Figure 164 – LOBI A1-83 RELAP5 calculation: Heater rod temperature 2/3 of the core height.	160
Figure 165 – Fuel Rod Showing Variables used by the Reflood Model.	173
Figure 166 – Modification to relap5.ff.	180
Figure 167 – Modification at the beginning of all affected *.ff.	181
Figure 168 – Structure of externally read data.txt.	181
Figure 169 – RELAP5-3D© - LOBI/MOD2 nodalization, general scheme.	188
Figure 170 – RELAP5-3D© of LOBI/MOD2 reactor pressure vessel and upper head simulator.	189
Figure 171 – PS volume vs. elevation.	196
Figure 172 – Pressure drop Vs. length in IL.	197
Figure 173 – Pressure drop Vs. length in BL.	197

<i>Figure 174 – Subdivision of LOBI facility into modules.</i>	<i>200</i>
<i>Figure 175 – Primary Side Volume versus Height Curve.</i>	<i>201</i>
<i>Figure 176 – Modules of Steam Generator of Primary Side Broken Loop.</i>	<i>202</i>
<i>Figure 177 – Modules of Surge Line Piping.</i>	<i>202</i>
<i>Figure 178 – Measurement Insert Location in Reactor Pressure Vessel.</i>	<i>205</i>
<i>Figure 179 – Heater Rod Measurement Insert Location in Reactor Pressure Vessel.</i>	<i>206</i>
<i>Figure 180 – Heat Losses of LOBI-MOD2 primary Loop at Steady State.</i>	<i>210</i>
<i>Figure 181 – Break Insert with Discharge Line, [D-2].</i>	<i>213</i>
<i>Figure 182 – Break Assembly: Configuration for Small Break, [D-2].</i>	<i>213</i>
<i>Figure 183 – Pressure Drop versus Length in the Intact Loop.</i>	<i>218</i>
<i>Figure 184 – Core Power, Short Time.</i>	<i>218</i>
<i>Figure 185 – HPIS Mass Flow as Function of Time.</i>	<i>218</i>
<i>Figure 186 – Primary and Secondary System Pressure.</i>	<i>219</i>
<i>Figure 187 – Primary System Fluid Inventory.</i>	<i>219</i>
<i>Figure 188 – Collapsed Liquid Level in the Vessel.</i>	<i>219</i>
<i>Figure 189 – Mean Temperature in Heater Rods.</i>	<i>220</i>
<i>Figure 190 – LOBI/MOD2 RPV and UH simulator with subdivision in modules [E1].</i>	<i>222</i>
<i>Figure 191 – RELAP5-3D© nodalization of LOBI/MOD2 RPV and UH simulator.</i>	<i>223</i>
<i>Figure 192 – LOBI/MOD2 Reactor Pressure Vessel.</i>	<i>224</i>
<i>Figure 193 – RELAP5-3D© nodalization of LOBI/MOD2 Reactor Pressure Vessel.</i>	<i>225</i>
<i>Figure 194 – LOBI/MOD2 Pressure Vessel, Heat Structures.</i>	<i>228</i>
<i>Figure 195 – LOBI/MOD2 Lower Flange of the Pressure Vessel.</i>	<i>232</i>
<i>Figure 196 – LOBI/MOD2 Upper Flange of the Pressure Vessel.</i>	<i>234</i>

LIST OF TABLES

<i>Table 1 – GRS method: number of required calculations.</i>	12
<i>Table 2 – FFTBM weighting factor components for typical thermal-hydraulic parameters.</i>	30
<i>Table 3 – Weighting factors for IPREM procedure.</i>	34
<i>Table 4 – Edwards pipe facility characteristics.</i>	37
<i>Table 5 – Edwards pipe IPREM settings for reference calculation.</i>	39
<i>Table 6 – Edwards pipe: quantified variation ranges of input parameters.</i>	45
<i>Table 7 – Edwards pipe: uncertainty analysis settings.</i>	47
<i>Table 8 – Experimental tests used in application and validation of IPREM against reflood phenomena.</i>	49
<i>Table 9 – Boundary conditions of FEBA tests.</i>	50
<i>Table 10 – Boundary conditions of FEBA tests.</i>	50
<i>Table 11 – Boundary conditions of ACHILLES tests.</i>	50
<i>Table 12 – List of SETF investigating reflood.</i>	51
<i>Table 13 – List of ITF simulating reflood phase of LBLOCA.</i>	52
<i>Table 14 – FEBA cladding temperature measurements.</i>	56
<i>Table 15 – Summary of RELAP5 model of FEBA facility.</i>	57
<i>Table 16 – PREMIUM benchmark: list of participating organizations.</i>	61
<i>Table 17 – PREMIUM benchmark: Summary of reference calculations.</i>	63
<i>Table 18 – Reflood: list of initially considered input parameters for RELAP5 code.</i>	68
<i>Table 19 – Reflood: identified influential input parameters RELAP5 code for reflood simulation.</i>	69
<i>Table 20 – PREMIUM benchmark: Input parameters initially considered by majority.</i>	71
<i>Table 21 – FEBA 216 IPREM settings for reference calculation.</i>	75
<i>Table 22 – FEBA 216: quantified variation ranges of input parameters for RELAP5</i>	82
<i>Table 23 – FEBA 216: uncertainty analysis settings.</i>	85
<i>Table 24 – FEBA 216: quantified variation ranges with limit=0.1.</i>	89
<i>Table 25 – FEBA 216: settings for sensitivity analysis on type of PDF.</i>	92
<i>Table 26 – Validation: settings for uncertainty analysis.</i>	95
<i>Table 27 – Summary of RELAP5 model of PERICLES facility.</i>	101

<i>Table 28 – Summary of RELAP5 model of ACHILLES facility.</i>	107
<i>Table 29 – FEBA 222 reference calculation Average Amplitude values.</i>	110
<i>Table 30 – FEBA 222: quantified variation ranges.</i>	112
<i>Table 31 – Modification in post-test model of RELAP5 model of PERICLES facility.</i>	115
<i>Table 32 – PERICLES RE79 IPREM settings for reference calculation.</i>	118
<i>Table 33 – PERICLES RE79: quantified variation ranges.</i>	122
<i>Table 34 – Summary of CATHARE2 model of FEBA facility.</i>	126
<i>Table 35 – FEBA 216 IPREM settings for reference calculation with CATHARE2.</i>	129
<i>Table 36 – Identified influential reflood-related input parameters for CATHARE2.</i>	129
<i>Table 37 – FEBA 216: quantified variation ranges of input parameters for CATHARE2.</i>	134
<i>Table 38 – Summary of CATHARE2 model of ACHILLES facility.</i>	135
<i>Table 39 – Summary of reflood calculations for validation of IPREM.</i>	138
<i>Table 40 – Summary of reflood calculations for validation of IPREM.</i>	151
<i>Table 41 – Example of Analysis of Relevant Thermal-hydraulic Aspects.</i>	158
<i>Table 42 – List of predicted events in LOBI A1-83.</i>	161
<i>Table 43 – RELAP5 subroutine modifications for interphase friction.</i>	182
<i>Table 44 – RELAP5 subroutine modifications for interphase heat transfer.</i>	183
<i>Table 45 – RELAP5 subroutine modifications for film boiling heat transfer.</i>	183
<i>Table 46 – RELAP5 subroutine modifications for transition boiling heat transfer.</i>	183
<i>Table 47 – RELAP5 subroutine modifications for minimum droplet diameter.</i>	184
<i>Table 48 – Code nodes and hydraulic zones correspondence, RELAP5-3D©.</i>	190
<i>Table 49 – Adopted code resources for RELAP5-3D© LOBI/MOD2 nodalization.</i>	192
<i>Table 50 – Criteria for nodalization qualification at the steady-state level.</i>	194
<i>Table 51 – Comparison between measured and calculated relevant initial and boundary conditions.</i>	198
<i>Table 52 – Steam Generator Geometrical Data: Primary Side Broken Loop. Module 101.</i>	203
<i>Table 53 – Pressurizer Surge Line Geometrical Data. Module 606.</i>	204
<i>Table 54 – Example of pressure losses evaluation.</i>	208
<i>Table 55 – Material Properties of Passive Structures.</i>	209

<i>Table 56 – Example of data of facility individual heat losses.</i>	<i>211</i>
<i>Table 57 – Configuration of the Facility in test A1-83.....</i>	<i>212</i>
<i>Table 58 – Test Relevant Initial Conditions.</i>	<i>217</i>
<i>Table 59 – Summary Table: Geometry Data of Pressure Vessel and Upper Head.</i>	<i>229</i>
<i>Table 60 – Summary Table: Junction Data of Pressure Vessel and Upper Head.</i>	<i>230</i>
<i>Table 61 – Summary Table: Heat Structure Data of RPV.....</i>	<i>235</i>
<i>Table 62 – Core Power Table.....</i>	<i>236</i>
<i>Table 63 – Inconel 625 Thermal Conductivity.</i>	<i>237</i>
<i>Table 64 – Summary Table for Level control variables.</i>	<i>239</i>

1 INTRODUCTION

Without any doubt, Best-Estimate plus Uncertainty Evaluation (BEPU) methods are gaining increased interest in the licensing process. However, the application of best-estimate (realistic) computer codes and models implies the evaluation of uncertainties. This is connected with the imperfect nature of the codes and of the process of codes application. In other words, 'sources of errors' or 'sources of uncertainty' affect the predictions by best-estimate codes and must be taken into account. While the 'code user effect' is already a well-known issue in the frame of the deterministic analysis and application of system thermal-hydraulic codes, the adoption of BEPU approach poses a new problem – so called uncertainty methodology user effect. Lessons learnt from the BEMUSE benchmark and others showed that the use of engineering judgment for identifying the code input uncertainty parameters and for bypassing the imperfect knowledge of the code input parameter uncertainties, greatly affects the results of performed uncertainty analysis. Often it occurs that the uncertainties of the input parameters derived solely from experimental data and therefore not specific to any computer code, are adopted in the uncertainty methods. In this case it shall be noted that the codes seldom feature the exact implementation of the analytical form of correlations (which are approximations of the experimental results) and thus the use of these uncertainties is not correct from logical point of view. In some other case, the use of the input parameter uncertainties simply 'guessed' by engineering judgment is not uncommon either. Thus, it is evident that improvements of the present uncertainty evaluation methods are necessary, especially developing methods to properly estimate input parameter uncertainties - their ranges of variation and probability distributions. Among these input parameters, a special attention must be paid to the physical models, because they are often very influential and the determination of their uncertainty raises difficulties, due to the fact that they are not directly measurable.

On the other hand, a key feature of the activities performed in nuclear reactor safety technology is constituted by the necessity to demonstrate the qualification level of each tool adopted within an assigned process and of each step of the concerned process. Therefore, the qualification of best-estimate codes, models and "best modeling practices" must be considered of great importance in order to ensure the validity of performed BEPU analysis. At this juncture, it should be pointed out that a consistent code assessment supported by a qualified experimental database is an important step for developing a solid ground for the uncertainty evaluation in the frame of BEPU approach. Thus, the availability of an experimental qualified database is of outmost importance for the validation and qualification of code calculations.

1.1. Objectives of the research

The performed research activity is aimed to improve on two issues identified in the frame of the use of BEPU approach in nuclear safety studies: proper estimation of code input parameter uncertainties and quality assurance in qualification of best-estimate models. To fulfil both objectives, a methodology for code input uncertainties evaluation and a methodology to set up a qualified experimental database for code

assessment have to be developed respectively. The methodologies shall provide a clearly defined procedures and means to fulfill the posed tasks, contributing to reduce the code user effect and the uncertainty method user effect, being cost-effective and easily adaptable for industrial applications.

1.2. Framework

The research has been carried out in the framework of the OECD/NEA PREMIUM project (2011-2014) and EU NURESAFE project. These projects are aimed at developing advanced tools and methods for a multi-scale and multi-physics analysis and progress on the issue of the quantification of the uncertainty of the physical models in system thermal-hydraulic codes.

Thus, the present research has profited from the availability of experimental databases as well as cooperation with a number of experts in the fields of nuclear reactor safety, validation and verification of thermal-hydraulic codes and uncertainty analysis.

1.3. Description of the performed activity

The activities performed to address the objectives of the research are outlined in the flowchart on *Figure 1*. The following steps below have been carried:

- investigation of the issues related to use of Best Estimate Plus Uncertainty approach in thermal-hydraulic analysis;
- acquisition of expertise in the field of uncertainty analysis and model calibration;
- development of a Input Parameter Range Evaluation Methodology (IPREM);
- application of the IPREM for evaluation of uncertainty of reflood-related code input parameters;
- validation and “external qualification” of the IPREM through a series of uncertainty analysis of simulations of numerous experimental reflood tests and various checks for test, facility and code-independence;
- development of an approach to establish a qualified experimental database in support of code assessment and Best Estimate model qualification.

The presented research activity has been carried out at San Piero a Grado Nuclear Research Group (GRNSPG) of University of Pisa and made use of the expertise acquired in the framework of various international benchmarks, meetings, workshops, project related to validation of thermal-hydraulic codes, nuclear reactor safety studies etc..

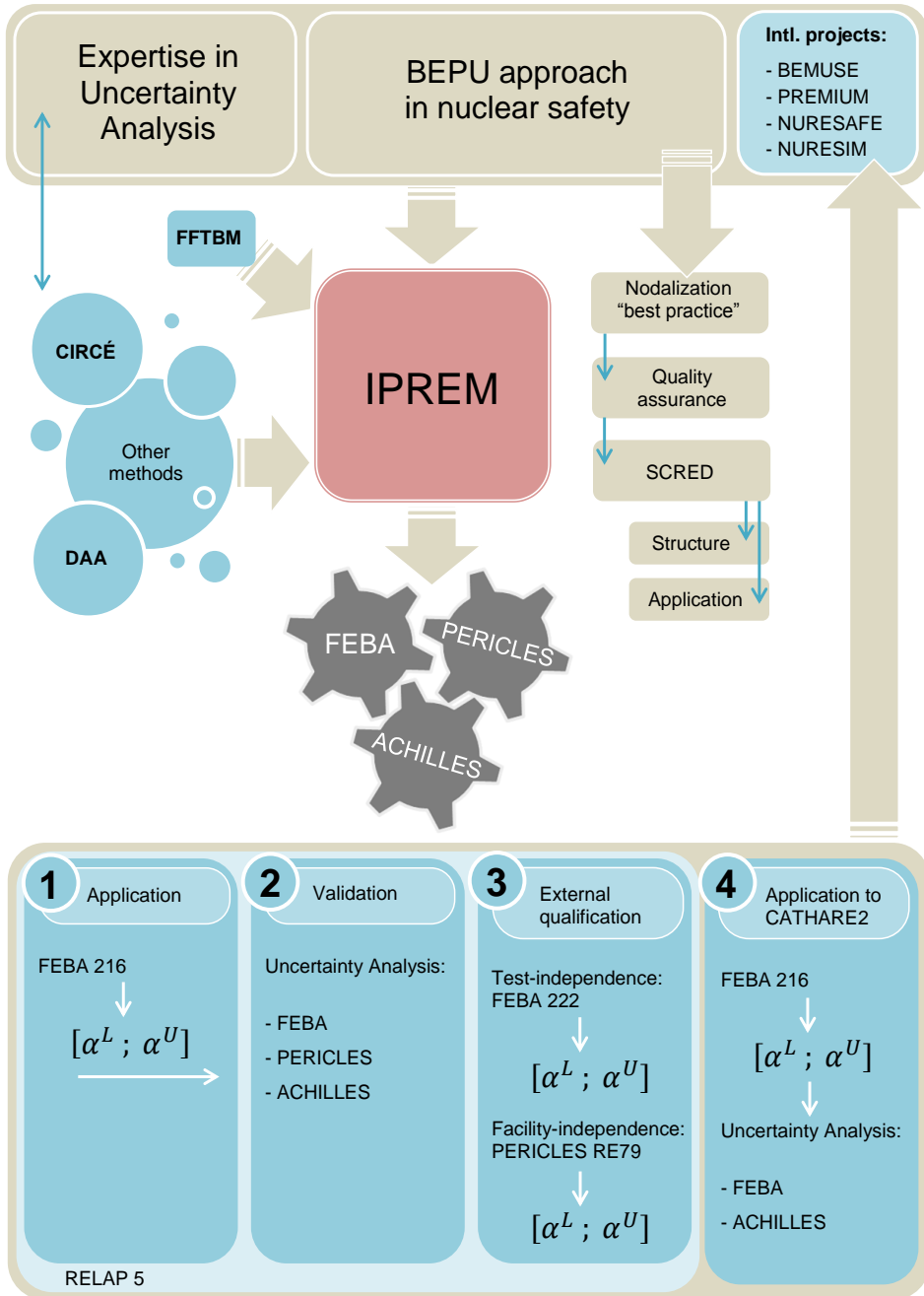


Figure 1 – Flowchart of performed research activity.

1.4. Structure of the document

The thesis is divided in six chapters and five appendixes.

The **Introduction** contains the background information and main objectives of the activity.

Chapter 2 describes the framework of uncertainty analysis of thermal-hydraulic calculations and provides an overview of the current state-of-the-art in uncertainty analysis approaches and methodologies for the evaluation of uncertainties of code input parameters.

Chapter 3 provides the description of the developed methodology for input parameter range evaluation. The procedure, formula and adopted criteria are described. An example application of this methodology for the evaluation of uncertainties of RELAP5 input parameters for blowdown problem is presented.

Chapter 4 demonstrates the application of the IPREM to simulation of reflood phenomena by thermal-hydraulic codes. The process and results of extensive methodology verification and validation activities is provided.

Chapter 5 contains the insights into an issue of using experimental data for qualification of “best modeling practice” which constitutes the basis for application of Best-Estimate models. The needs for quality assurance of code assessment process are discussed and solutions are presented in a form of a qualified experimental database.

Chapter 6 finally presents conclusions from the performed research activity.

2 UNCERTAINTY ANALYSIS IN THERMAL-HYDRAULIC CALCULATIONS

2.1. Sources of uncertainty

Application of best-estimate (realistic) computer codes to the safety analysis of nuclear power plants implies the evaluation of uncertainties. This is connected with the (imperfect) nature of the codes and of the process of codes application. In other words, 'sources of errors' or 'sources of uncertainty' affect the predictions by best-estimate codes and must be taken into account. Three major sources of error are mentioned in the Annex II of the IAEA guidance Accident Analyses for Nuclear Power Plants, ref. [1]:

- Code or model uncertainty.
- Representation or 'simulation uncertainty'.
- Plant uncertainty.

A more detailed list of uncertainty includes the following items, ref. [2]:

A) Balance (or conservation) equations are approximate:

- not all the interactions between steam and liquid are included,
- the equations are solved within cylindrical pipes: no consideration of geometric discontinuities, situation not common for code applications to the analysis of Nuclear Power Plants transient scenarios;

B) Presence of different fields of the same phase: e.g. liquid droplets and film. Only one velocity per phase is considered by codes, thus causing another source or uncertainty.

C) Geometry averaging at a cross section scale: the need "to average" the fluid conditions at the geometry level makes necessary the 'porous media approach'. Velocity profiles happen in the reality: These correspond to the 'open media approach'. The lack of consideration of the velocity profile, i.e. cross-section averaging, constitutes an uncertainty source of 'geometric origin'.

D) Geometry averaging at a volume scale: only one velocity vector (each phase) is associated with a hydraulic mesh along its axis. Different velocity vectors may occur in the reality (e.g. inside lower plenum of a typical reactor pressure vessel, at the connection between cold leg and down-comer, etc.). The volume-averaging constitutes a further uncertainty source of 'geometric origin'.

E) Presence of large and small vortex or eddy. Energy and momentum dissipation associated with vortices are not directly accounted for in the equations at the basis of the codes, thus introducing a specific uncertainty source. In addition, a large vortex may determine the overall system behaviour (e.g. two-phase natural circulation between hot and cold fuel bundles), not necessarily consistent with the prediction of a code-discretized model.

F) The 2nd principle of thermodynamics is not necessarily fulfilled by codes. Irreversible processes occur as a consequence of accident in nuclear reactor systems. This causes 'energy' degradation, i.e. transformation of kinetic energy into

heat. The amount of the transformation of energy is not necessarily within the capabilities of current codes, thus constituting a further specific energy source.

G) Models of current interest for thermal-hydraulic system codes are constituted by a set of partial derivatives equations. The numerical solution is approximate, therefore, approximate equations are solved by approximate numerical methods. The 'amount' of approximation is not documented and constitutes a specific source of uncertainty.

H) Extensive and unavoidable use is made of empirical correlations. These are needed 'to close' the balance equations and are also reported as 'constitutive equations' or 'closure relationships'. Typical situations are:

- The ranges of validity are not fully specified. For instance, pressure and flowrate ranges are assigned, but void fraction, or velocity (or slip ratio) ranges may not be specified.

- Relationships are used outside their range of validation. Once implemented into the code, the correlations are applied to situations, where, for instance, geometric dimensions are different from the dimensions of the test facilities at the basis of the derivation of the correlation. One example is given by the wall-to-fluid friction in the piping connected with reactor pressure vessel: no facility has been used to derive (or to qualify) friction factors in two phase conditions when pipe diameters are of the order of one meter. In addition, once the correlations are implemented into the code, no (automatic) action is taken to check whether the boundaries of validity, i.e. the assigned ones, are over-passed during a specific application.

- Correlations are implemented approximately into the code. The correlations, apart from special cases, are derived by scientists or in laboratories that are not necessarily aware of the characteristics or of the structure of the system code where the correlations are implemented. Furthermore, unacceptable numeric discontinuities may be part of the original correlation structure. Thus, correlations are 'manipulated' (e.g. extrapolated in some cases) by code developers with consequences not always ascertained.

- Reference database is affected by scatter and errors. Correlations are derived from ensembles of experimental data that unavoidably show 'scatter' and are affected by errors or uncertainties. The experimentalist must interpret those data and achieve an 'average-satisfactory' formulation.

I) A paradox: shall be noted: 'Steady State' & 'Fully Developed' (SS & FD) flow condition is a necessary prerequisite or condition adopted when deriving correlations. In other terms, all qualified correlations must be derived under SS & FD flow conditions. However, almost in no region of the Nuclear Power Plant those conditions apply during the course of an accident.

J) The state and the material properties are approximate. Various materials used in a NPP are considered in the input deck, including liquids, gases and solids. Thermo-physical properties are part of the codes or constitute specific code user input data. These are of empirical nature and typically subjected to the limitations discussed under item H). A specific problem within the current context can be associated with the derivatives of the water properties.

K) Code User Effect (UE) exists. Different groups of users having available the same code and the same information for modelling a Nuclear Power Plant do not achieve the same results. UE (see also below) is originated by:

- Nodalization development, see also item N), below.
- Interpreting the supplied (or the available) information, usually incomplete, see also item M) below;
- Accepting the steady state performance of the nodalization;
- Interpreting transient results, planning and performing sensitivity studies, modifying the nodalization and finally achieving “a reference” or “an acceptable” solution;

The UE might result in the largest contribution to the uncertainty and is connected with user expertise, quality and comprehensiveness of the code-user manual and of the database available for performing the analysis.

L) Computer/compiler effect exists. A computer code is developed making use of the hardware selected by the code developers and available at the time when the code development starts. A code development process may last a dozen years during which period profound code hardware changes occur. Furthermore, the code is used on different computational platforms and the current experience is that the same code with the same input deck applied within two computational platforms produces different results. Differences are typically small in ‘smoothly running transients’, but may become noticeable in the case of threshold- or bifurcation-driven transients.

M) Nodalization (N) effect exists. The N is the result of a wide range brainstorming process where user expertise, computer power and code manual play a role. There is a number of required code input values that cannot be covered by logical recommendations: the user expertise needed to fix those input values may reveal inadequate and constitutes the origin of a specific source of uncertainty.

N) Imperfect knowledge of Boundary and Initial Conditions (BIC). Some BIC values are unknown or known with approximation: the code user must add information. This process unavoidably causes an impact on the results that is not easily traceable and constitutes a specific source of uncertainty.

O) Code/model deficiencies cannot be excluded. The system code development started toward the end of the sixties and systematic assessment procedures were available since the eighties. A number of modelling errors and inadequacies have been corrected or dealt with and substantial progress has been made in improving the overall code capabilities. Nevertheless, deficiencies or lack of capabilities cannot be excluded nowadays. Examples, not applicable to all thermal-hydraulic system codes, are connected with the modelling of:

- the heat transfer between the free liquid surface and the upper gas-steam space,
- the heat transfer between a hotter wall and the cold liquid down-flowing inside a steam-gas filled region.

Those deficiencies are expected to have an importance only in special transient situations.

2.2. Common approaches for evaluation of uncertainty of thermal-hydraulic calculations

An uncertainty analysis consists of identification and characterization of relevant input parameters (input uncertainty) as well as of the methodology to quantify the global influence of the combination of these uncertainties on selected output parameters (output uncertainty). These two main items are treated in different ways by the various methods, ref. [3].

2.2.1. Input error propagation

The propagation of code input errors (*Figure 2*): this can be evaluated as being the most adopted procedure nowadays, endorsed by industry and regulators. It adopts the statistical combination of values from selected input uncertainty parameters (even though, in principle an unlimited number of input parameters can be used) to calculate the propagation of the errors throughout the code.

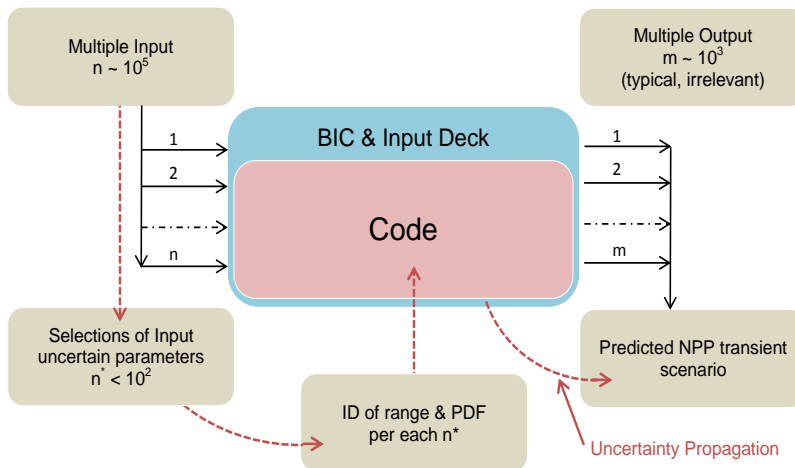


Figure 2 – Uncertainty methods based upon propagation of input uncertainties.

The main drawbacks of such methods are connected with: a) the need of engineering judgment for limiting (in any case) the number of the input uncertain parameters; b) the need of engineering judgment for fixing the range of variation and the PDF for each input uncertain parameter; c) the use of the code-nodalization for propagating the uncertainties: if the code-nodalization is wrong, not only the reference results are wrong but also the results of the uncertainty calculations.

2.2.1.1. CSAU method

The pioneering work in the area of the BEPU (Best Estimate Plus Uncertainty) methods was done by US NRC and its contractors and consultants while revising the acceptance rules on ECCS (Emergency Core Cooling System, ref. [4]). The revised rule, stating an alternate ECCS performance analysis based on best-estimate methods, may be used to provide more realistic estimates of the plant

safety margins if the licensee quantifies the uncertainty of the estimates and includes that uncertainty when comparing the calculated results with prescribed acceptance limits. To support the revised ECCS rule a method called the Code Scaling, Applicability and Uncertainty (CSAU) was developed, ref. [5]. A simplified flow sheet of CSAU method is given in *Figure 3*.

The method is intended to investigate the uncertainty of safety-related output single-valued parameters (e.g. PCT). A procedure is proposed to evaluate the code applicability to a selected plant scenario and experts shall identify and rank phenomena, examining experimental data and code predictions of the studied scenario. In the resulting Phenomena Identification and Ranking Table (PIRT), ranking is accomplished by expert judgment. The PIRT and code documentation is compared, and it is decided if the code is applicable to the plant scenario.

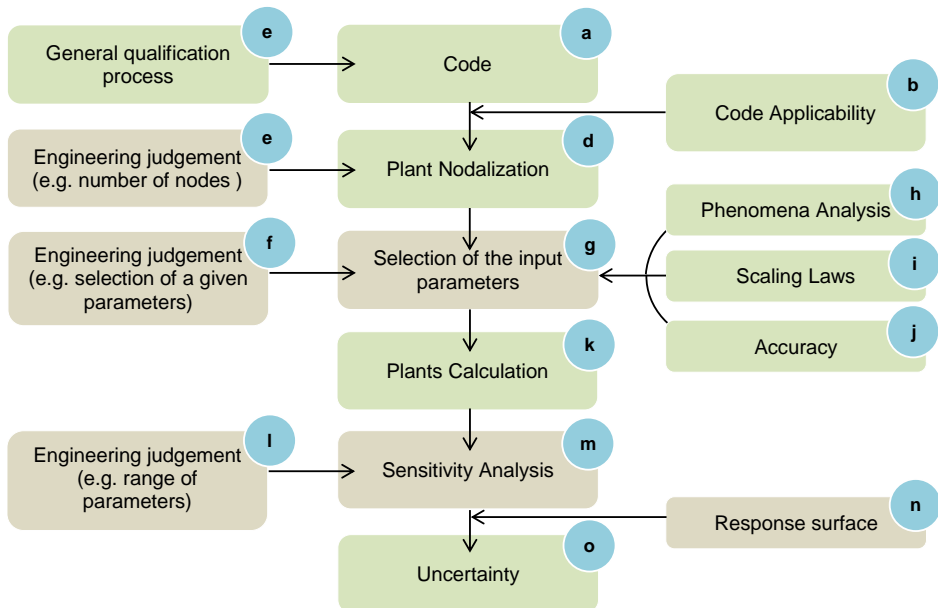


Figure 3 – Uncertainty methods based upon propagation of input uncertainties.

All the sensitivity calculations are performed by using an optimized nodalization. This represents a compromise between accuracy and cost, based on experience obtained by analyzing separate effects tests and integral experiments. No particular method or criteria are applied to accomplish this task. Only those parameters modeling the high ranked phenomena are selected to be considered as uncertain input parameters. The selection is based on the judgment about their influence on the output parameters. Additional output biases are introduced to consider the uncertainty of other phenomena not included in the sensitivity calculations.

Information from experiments, manufacturing, and prior calculations performed have been utilized when defining the mean value and the standard deviation of uncertain parameters, for both the Large Break (LB) and the Small Break (SB) LOCA analyses. Uncertainty ranges are defined by intervals of plus/minus two standard deviations from the mean value. Additional biases can be introduced to the input uncertainties.

Uniform and normal distributions were utilized in the two applications performed up to date. Output uncertainty is the result of the propagation of input uncertainties through a number of code calculations. Input parameter uncertainty can be either due to stochastic nature (i.e. code-independent) or due to un-precise knowledge of the parameter values. No statistical method is formally proposed in the CSAU definition. A response surface approach has been used in the applications performed up to date. The response surface fits the code predictions obtained for selected parameters, and is further used instead of the original computer code. Such an approach then implies the use of a limited number of uncertain parameters, in order to reduce the number of code runs and the cost of analysis. However, within the CSAU frame the response surface approach is not required, and other methods may be applied.

Scaling is considered by CSAU, identifying several issues based on test facilities and on code assessment. The effect of scale distortions on main processes, the applicability of the existing database to the NPP range, the scale-up capability of closure relationships and their applicability to the NPP range is evaluated at a qualitative level. Biases are introduced if the scaling capability is not provided, by including either before or after the probabilistic analysis.

2.2.1.2. GRS method

The GRS method, ref. [6] and [7], is a probabilistic method based on the concept of propagating the input uncertainties. All relevant uncertain parameters including the code, representation and plant uncertainties are identified, any dependencies between uncertain parameters are quantified and ranges and/or PDF for each uncertain parameter are determined. Expert judgment and experience from code applications to separate and integral test and full plant application are principal sources of information for uncertain parameters identification and quantification. Peculiarities of the GRS method are:

- The uncertainty space of input parameters (defined by their uncertainty ranges) is sampled at random according to the combined “subjective” probability distribution of the uncertain parameters and code calculations are performed by sampled sets of parameters.
- The number of code calculations is determined by the requirement to estimate a tolerance/confidence interval for the quantity of interest (such as peak clad temperature). The Wilks formula, ref. [8] is used to determine the number of calculations needed for deriving the uncertainty bands.
- Statistical evaluations are performed to determine the sensitivities of input parameter uncertainties on the uncertainties of key results (parameter importance analysis).
- There are no limits for the number of uncertain parameters to be considered in the analysis and the calculated uncertainty has a well-established statistical basis.
- The method relies only on actual code calculations without using approximations like fitted response surfaces.

For the selected plant transient, the method is applied to an integral effects test simulating the same scenario prior to the plant analysis. If experimental data are not bounded, the set of uncertain input parameters has to be modified. Experts identify

significant uncertainties to be considered in the analysis, including the modelling uncertainties, and the related parameters, and identify and quantify dependencies between uncertain parameters. Subjective Probability Density Functions are used to quantify the state of knowledge of uncertain parameters for the specific scenario. The term “subjective” is used here to distinguish uncertainty due to imprecise knowledge from uncertainty due to stochastic or random variability.

Uncertainties of code model parameters are derived based on validation experience. The scaling effect has to be quantified as model uncertainty. Additional uncertain model parameters can be included or PDF can be modified, accounting for results from the analysis of Separate Effects Tests. Input parameter values are simultaneously varied by random sampling according to the subjective PDF and dependencies. A set of parameters is provided to perform the required number n of code runs. For example, the 95% percentile and 95% confidence limit of the resulting subjective distribution of the selected output quantities is directly obtained from the n code results, without assuming any specific distribution. No response surface is used or needed.

Sensitivity measures by using regression or correlation techniques from the sets of input parameters and from the corresponding output values allow the ranking of the uncertain input parameters in relation to their contribution to output uncertainty. Therefore, the ranking of parameters is a result of the analysis, not of prior expert judgment. The 95% percentile, 95% confidence limit and sensitivity measures for continuous-valued output parameters are provided.

Upper statistical tolerance limits are the upper β confidence for the chosen α percentile. The percentile indicates the probability content of the probability distributions of the code results (e.g. $\alpha = 95\%$ means that PCT is below the tolerance limit with at least $\alpha = 95\%$ probability). One can be β % confident that at least α % of the combined influence of all the characterized uncertainties are below the tolerance limit. The confidence level is specified because the probability is not analytically determined. It accounts for the possible influence of the sampling error due to the fact that the statements are obtained from a random sample of limited size. The smallest number n of code runs is determined by the Wilks formula:

$$(1 - \alpha)^n \geq \beta \quad (1)$$

and is representing the size of a random sample (a number of calculations) such that the maximum calculated value in the sample is an upper statistical tolerance limit. For two-sided statistical tolerance intervals (investigating the output parameter distribution within an interval) the formula is:

$$1 - \alpha^n - n \cdot (1 - \alpha) \cdot \alpha^{n-1} \geq \beta \quad (2)$$

The minimum number n of calculations for both one-sided and two-sided can be found in *Table 1*. As a consequence, the number n of code runs is independent of the number of selected input uncertain parameters, only depending on the percentage of the fractile and on the desired confidence level percentage. The number of code runs for deriving sensitivity measures is also independent of the number of parameters. As an example, a total number of 100 runs is typical for the application of the GRS method. For regulatory purposes where the margin to

licensing criteria is of primary interest, the one-sided tolerance limit may be applied, i.e. for a 95th/95th percentile 59 calculations should be performed.

Table 1 – GRS method: number of required calculations.

β / α	One-sided Statistical Tolerance Limit			Two-sided Statistical Tolerance Limit		
	0.90	0.95	0.99	0.90	0.95	0.99
0.90	22	45	230	38	77	388
0.95	29	59	299	46	93	473

2.2.2. Output error propagation

The method focuses not on the evaluation of individual parameter uncertainties but on the propagation of errors from a suitable database calculating the final uncertainty by extrapolating the accuracy from relevant integral experiments to full scale NPP (*Figure 4*). The Uncertainty Method based on the Accuracy Extrapolation (UMA), whose flow diagram is given in *Figure 5*, is the prototype method, ref. [9], for the description of “the propagation of code output errors” approach. Considering integral test facilities of a reference water cooled reactor, and qualified computer codes based on advanced models, the method relies on code capability, qualified by application to facilities of increasing scale. Direct data extrapolation from small scale experiments to reactor scale is difficult due to the imperfect scaling criteria adopted in the design of each scaled down facility. So, only the accuracy (i.e. the difference between measured and calculated quantities) is extrapolated. Experimental and calculated data in differently scaled facilities are used to demonstrate that physical phenomena and code predictive capabilities of important phenomena do not change when increasing the dimensions of the facilities.

Other basic assumptions are that phenomena and transient scenarios in larger scale facilities are close enough to plant conditions. The influence of user and nodalization upon the output uncertainty is minimized in the methodology. However, user and nodalization inadequacies affect the comparison between measured and calculated trends; the error due to this is considered in the extrapolation process and gives a contribution to the overall uncertainty. The method utilizes a database from similar tests and counterpart tests performed in integral test facilities that are representative of plant conditions. The quantification of code accuracy is carried out by using a procedure based on the Fast Fourier Transform, ref. [10], characterizing the discrepancies between code calculations and experimental data in the frequency domain, and defining figures of merit for the accuracy of each calculation.

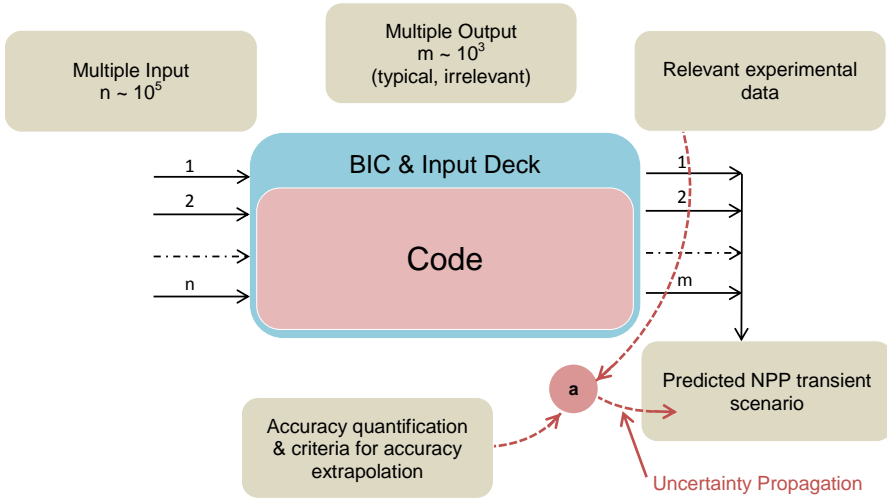
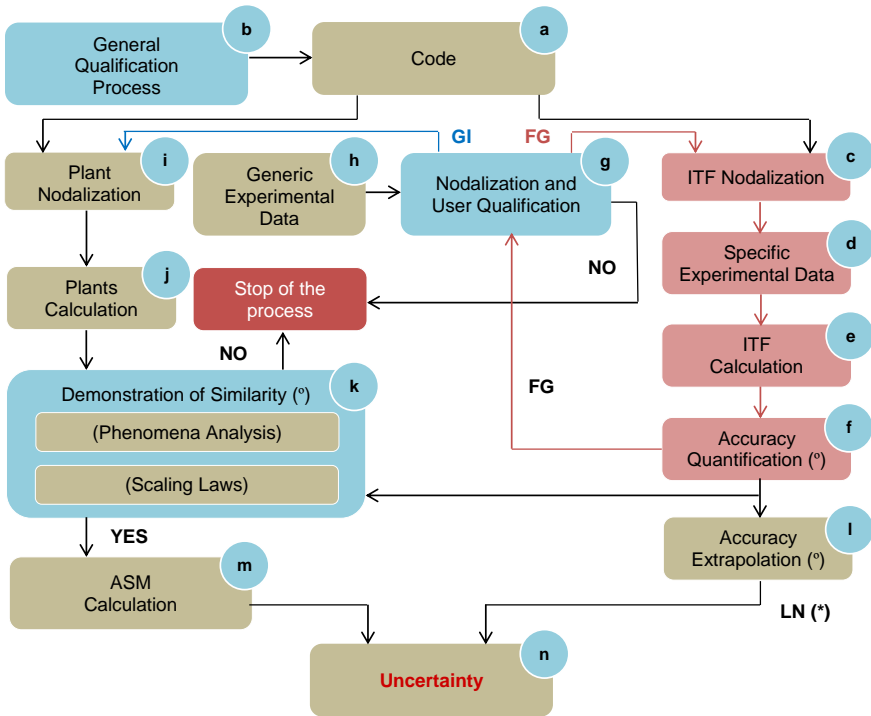


Figure 4 – Uncertainty methods based upon propagation of output uncertainties.



(*) Special methodology developed

Figure 5 – UMAE process flow diagram.

If these errors comply with a number of acceptability conditions, ref. [9], then the resulting (error) database is processed and the ‘extrapolation’ of the error takes place. Relevant conditions for the extrapolation are:

- Building up the NPP nodalization with the same criteria as was adopted for the ITF nodalizations;
- Performing a similarity analysis and demonstrating that NPP calculated data are “consistent” with the data measured in a qualified ITF experiment.

Calculations of both ITF experiments and NPP transients are used to attain uncertainty from accuracy. Nodalizations are set up and qualified against experimental data by an iterative procedure, requiring that a reasonable level of accuracy is satisfied. Similar criteria are adopted in developing plant nodalization and in performing plant transient calculations (see left loop FG in *Figure 5*). The demonstration of the similarity of the phenomena exhibited in test facilities and in plant calculations, accounting for scaling laws considerations (step ‘k’ in *Figure 5*), leads to the Analytical Simulation Model, i.e. a qualified nodalization of the NPP.

The UMAE methodology has been ‘embedded’ into a Code with capability of Internal Assessment of Uncertainty (CIAU), ref. [11] and [12], in order to overcome the issues inherent to all uncertainty methods:

- The resources needed for their application may be very demanding, ranging up to several man-years;
- The achieved results may be strongly method/user dependent.

Within CIAU, the database of errors is set up by recognized experts separately by iterative code application to various thermal-hydraulic scenarios performed and/or registered at experimental facilities and NPPs. The user, in order to perform uncertainty analysis of a thermal-hydraulic calculation, needs to perform only one calculation and apply the specifically developed software that would analyze the transient, extract the appropriate error from the database and evaluate the uncertainties through extrapolation process.

However, it should be noted, that this class of uncertainty evaluation methods includes only a few applications from industry.

The main drawbacks of this method are as follows: (i) the method is not applicable in the absence of relevant experimental information; (ii) a considerable amount of resources is needed to establish a suitable error database, however this is a one-time effort, independent of subsequent applications of this method; (iii) the process of combining errors originating from different sources (e. g, stemming from different ITF or SETF (Separate Effect Test Facility), different but consistent nodalizations, different types of transient scenarios) is not based upon fundamental principles and requires detailed validation.

2.2.3. Approaches based on adjoint sensitivity procedures

The ‘third’ approach, (*Figure 6*): this is an independent way, i.e. different from propagation of code input errors or from propagation of code output errors is based on Adjoint Sensitivity Analysis Procedure (ASAP), Global Adjoint Sensitivity Analysis Procedure (GASAP), and Data Adjustment/Assimilation (DAA) methodology, by which experimental and calculated data, including the computation of sensitivities

(derived from ASAP), are mathematically combined for the prediction of the uncertainty scenarios, ref. [13].

ASAP, GASAP and DAA are the powerful mathematical tools which allow to consider all parameters α that affect any prediction, being part of either the code models or the input deck. The Adjoint Sensitivity Analysis Procedure, ref. [14] and [15], is the most efficient deterministic method for computing local sensitivities \mathbf{S} of large-scale systems, when the number of parameters and/or parameter variations exceeds the number of responses \mathbf{R} of interest (that is the case of most problems of practical interest). In addition, also system's critical points y (i.e. bifurcations, turning points, saddle points, response extrema) can be considered and determined by the Global Adjoint Sensitivity Analysis Procedure (in the combined phase-space formed by the parameters, forward state variables, and adjoint variables. Subsequently the local sensitivities of the responses \mathbf{R} located at critical points y are analyzed by the ASAP.

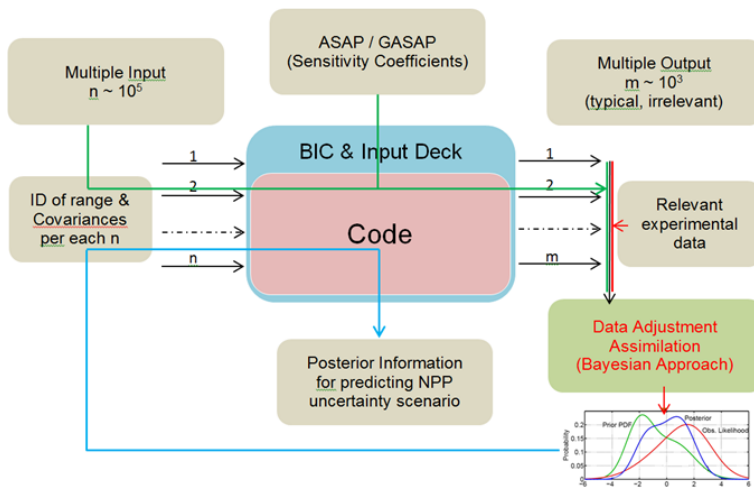


Figure 6 – Uncertainty methods based on Adjoint Sensitivity Analysis Procedure and Data Adjustment/Assimilation.

Once the sensitivity matrix \mathbf{S} of the responses \mathbf{R} respect to the parameters α is available, the moment propagation equation is adopted to obtain the computed covariance matrix \mathbf{C}_R of the responses starting from the covariance matrix \mathbf{C}_α of the system parameters. The elements of the matrix \mathbf{C}_α reflect the state of knowledge about the input (uncertainty) parameters that can be characterized by ranges and PDF.

The main drawbacks of this approach are as follows: (i) the method is not applicable in the absence of relevant experimental information; (ii) the adjoint model, needed for computing the sensitivity \mathbf{S} , requires relatively modest additional resources to develop and implement if this is done simultaneously with the development of the original code; however if the adjoint model is constructed a posteriori, considerable skills may be required for its successful development and implementation; (iii) a considerable amount of resources is needed to establish a suitable database of improved estimates for the input parameters (α^{IE}) and for the respective input covariance matrix (\mathbf{C}_α^{IE}), but this is a one-time effort, independent of subsequent applications of the method.

2.3. Evaluation of uncertainty of code input parameters

The lessons learnt from various international benchmarks on BEPU application to safety analysis (e.g. OECD/NEA BEMUSE, ref. [16]) showed that improvements of the present uncertainty evaluation methods are necessary, especially developing methods to properly estimate input parameter uncertainties (*Figure 7*). Among these input parameters, a special attention must be paid to the physical models, because they are often very influential and the determination of their uncertainty raises difficulties, due to the fact that they are not directly measurable.

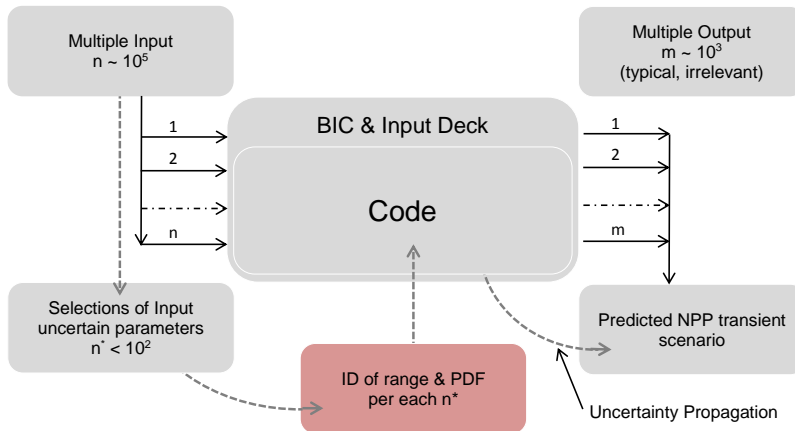


Figure 7 – Important issue in input error propagation method.

It is very well known that in system thermal-hydraulics only few code input parameter uncertainties are obtained from experimental observations (mainly from Separate Effect Test Facilities), whereas for the major part of them engineering judgment is adopted for deriving ('first') guess values of ranges and PDF. The imperfect knowledge of the input uncertainty parameter and of its uncertainties obviously affects the computed responses and the relative uncertainties of the responses and constitutes the main reason for which proper experimental data (i.e. connected with the specific NPP transient scenario under investigation for uncertainty evaluation) are needed.

Currently, an analyst in order to perform a BEPU analysis of a selected transient has different options for characterizing the ranges of variation of input parameters, each one has advantages and disadvantages. In order of preference (ref. [17]):

- Evaluation based on code calculation of experimental tests
 - Results are code-specific
 - Reflect the actual code parameter uncertainty
 - Possibility to evaluate the uncertainty of "nodalization" parameters
 - Available experimental data are needed
 - Requires significant resources for implementation
- Evaluation based on experimental data
 - Physical model / correlation parameter uncertainties

- Not specific to any code
- Statistically relevant sample of qualified experimental data is rarely available
- Literature review
 - Physical model / correlation parameter uncertainties
 - Not specific to any code
- Engineering/expert judgment.

Little information regarding uncertainty of physical models or correlations may be found in the available literature. However, it is a rare case and most typically this data are not specific to any computer code (evaluated from experiments). Evaluation of an available large experimental matrix of specific phenomena may result in higher confidence uncertainties of studied correlation. It should be noted that typically the availability of such extensive experimental matrices is limited to few research institutions and reactor vendors. Nevertheless, the uncertainties evaluated on experimental data only are not specific to any computer code, which seldom feature the exact implementation of an analytical form of correlation.

The application of computer codes to calculation of experimental tests provides a first step to obtain code-specific uncertainties of input parameters representative of a studied correlation. A proper methodology of treatment of calculation and experimental results has to be adopted in this case. It should be noted that estimating uncertainties of some parameters is a difficult problem because these models are, in the majority of the cases, not directly measurable: for instance, interfacial friction between liquid and vapor phases cannot be measured. However, there are SET (Separate Effect Tests) experiments, the results of which are a priori sensitive to the considered models. In a case of very simple SET experiments where only one physical phenomenon, described by one physical model, is clearly dominant, the quantification of its uncertainty is rather simple. It is sufficient to shift the parameter associated with the involved physical model in order to fit the code value with each experimental data, and after that to do statistics with the different values of the parameter obtained with all the experimental data. But in the most frequent case, several physical models must be considered together, and this method does not apply any more. Such experiments are called “intermediate” (e.g. the reflood experiments).

As a last resort, an analyst may assume a range of variation of input parameters of interest, based on professional experience. However the use of such ranges decreases the confidence in obtained uncertainty analysis results.

2.3.1. Overview of CIRCÉ method

The CIRCÉ method, ref. [18], which stands for “Calculation of the Uncertainties Related to the Elementary Correlations” (from *fr. Calcul des Incertitudes Relatives aux Corrélations Élémentaires*), is a statistical approach of data analysis and is applied as an alternative to the expert judgment often used to determine the uncertainty of the physical models. The method and corresponding tool is developed by Commissariat à l’Énergie Atomique (CEA).

CIRCÉ is a statistical tool of data analysis that uses measured data sensitive to some particular physical models to determine a probabilistic representation of their associated parameters. CIRCÉ estimates the mean value and the standard

deviation, as well as the type of probability density function (PDF): normal or log-normal, of the parameters associated to the physical models, for which uncertainty must be quantified. Thus it is apparent that the uncertainty representation made by CIRCÉ is of probabilistic type.

For a given experiment of intermediate type, the user determines the physical models describing the physical phenomena potentially influential on the experimental data. This choice is made by expert judgment and with the help of sensitivity calculations. On this basis, CIRCÉ uses the measured quantities of the intermediate experiment, called experimental responses, and the corresponding code values, called code responses.

More precisely, the parameters considered by CIRCÉ and associated with the physical models relevant in the considered experiment are denoted as α_i . CIRCÉ gives an estimation of the b_i mean value (also called bias) and the standard deviation σ_i of each α_i parameter. To obtain these results, CIRCÉ combines the differences between the experimental results and the corresponding code results, denoted as $(R_j^{exp} - R_j^{code})$ and the derivatives of each code response with respect to each parameter: $\partial R_j^{code} / \partial \alpha_i$. It is also possible to take into account the experimental uncertainties of the responses, denoted as δR_j^{exp} . This process is summarized on *Figure 8*.

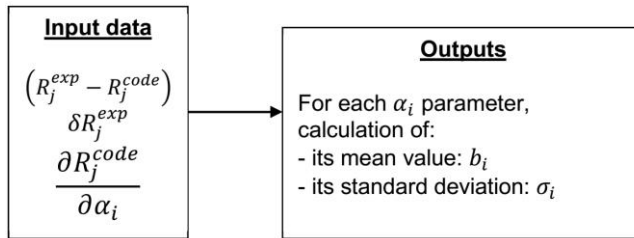


Figure 8 – Inputs and outputs of CIRCÉ.

For CATHARE 2, the derivatives are obtained with the ASM (Adjoint Sensitivity Method, ref. [14]) if the description of the experiment requires the use of only 1-D modules, without reflood and fuel. In other cases, finite differences are used with some precautions.

CIRCÉ uses an algorithm well-known in statistics: the E-M (Expectation-Maximization) algorithm, ref. [19] and [20]. This algorithm is based on the principle of maximum of likelihood and Bayes' theorem.

Two main hypotheses are made by CIRCÉ:

- Normality of the α_i parameters. A hypothesis on the probability density function of the parameters is compulsory since the principle of maximum of likelihood is applied in the E-M algorithm.
- Linearity between the code responses and each α_i parameter. Without giving a detailed description of the E-M algorithm, this hypothesis seems fairly obvious since first order derivatives are used.

Both hypotheses, linearity and normality, must be systematically checked: it is an important part of the methodology developed for a proper use of CIRCÉ.

So far, CIRCÉ has been applied to the dimensionless multipliers of the physical Models of CATHARE thermal-hydraulic code, but it would be possible to consider also single coefficients inside the physical models or even additive parameters.

2.3.2. Overview of Data Adjustment and Assimilation

The proposed technique by which experimental observations are combined with code predictions and their respective errors to provide an improved estimate of the system state is known as Data Adjustment and Assimilation (DAA), ref. [21], and it is based on a Bayesian inference process.

The idea at the basis of DAA can be made more specific as follows: the computed results \mathbf{R} and the respective statistical errors \mathbf{C}_R predicted by mathematical models and based on 'prior' or 'first' guess PDF for the input parameters (i.e. \mathbf{C}_α) are combined with proper experimental observations \mathbf{M} of the states of a system to generate 'adjusted' values for the system parameters (α^{IE} , where the suffix IE stays for improved estimate values) and the respective input covariance matrix ($\mathbf{C}_{\alpha^{IE}}$, or 'posterior' PDF). From this process, which can be considered as improved estimate analysis of the system's states, the responses \mathbf{R}^{IE} and the respective covariance matrix (\mathbf{C}_R^{IE}) are finally derived. The outline of the DAA basis is as follows, ref. [22].

If α^v is the column vector of system parameters represented in every time node \mathbf{v} , then \mathbf{R}^v is the vector of the system responses which can be a function of not only the system parameters at time node \mathbf{v} , but also of the system parameters at all previous time nodes \mathbf{n} . Additional observations (e.g., experimental evidence, inferences based on theoretical models) generally provide new information about system parameters. Such observations provide "observed" values α^v of the "true," but unknown, parameter values, and also provide "observational errors" $\Delta\alpha^v$. Such errors are represented by block-matrices which describe the intrinsic correlations at different time steps but also the cross-correlations between different time steps. The matrix of parameter correlations:

$$C_\alpha = \begin{bmatrix} C_\alpha^{11} & C_\alpha^{12} & \dots & \dots \\ C_\alpha^{21} & C_\alpha^{22} & \dots & \dots \\ \dots & \dots & \dots & \dots \\ \dots & \dots & \dots & C_\alpha^{N_t N_t} \end{bmatrix}, \quad C_{\alpha,ij}^{v\mu} = \langle \Delta\alpha_i^v \Delta\alpha_j^\mu \rangle \quad (3)$$

contains blocks $\mathbf{C}^{v\mu}$, describing the correlation between parameter α_i at time step \mathbf{v} and parameter α_j at time step μ . The covariances in the model parameters induce uncertainties in the responses computed by the model, which can be computed via the "sandwich rule":

$$C_R^{v\mu} = \sum_\rho \sum_\eta S^{v\rho} C_\alpha^{\rho\eta} (S^T)^{\mu\eta}, \quad \rho, \eta \in J_v; \quad v, \mu \in J_t \quad (4)$$

where $\mathbf{S}^{v\mu}$ is the sensitivity matrix with elements $s_{ni}^{v\mu}$ defined as

$$s_{ni}^{v\mu} = \{ \partial R_n^v / \partial \alpha_i^\mu \}, \quad 1 \leq \mu \leq v \leq N_t, \quad \text{and} \quad s_{ni}^{v\mu} = 0, \quad v < \mu \leq N_t \quad (5)$$

The aim of "model calibration" is to update the parameters in a numerical simulation tool by using additional, externally obtained, experimental data, denoted henceforth by the vector \mathbf{M}^v .

Model calibration includes estimation of discrepancies in the data and, more importantly, estimation of the biases between model predictions and experimental data. Model calibration can be done only by taking into account systematically (i.e., using sensitivities) all of the uncertainties (computational, experimental, etc.). The concept of prior probability distribution characterizes the existing knowledge of (degree of belief in) each model parameter, before incorporating any additional from experiments. Such prior knowledge is combined consistently with new information by using Bayesian inference. The additional information introduced by drawing inferences from the observational data should improve the knowledge about the system. Furthermore, this added knowledge (contained in the posterior probability density function) should lead to a reduction of uncertainties in both the responses and the system parameters. It can be shown that such a Bayesian inference procedure leads to the following posterior "best-estimated" responses

$$(R^{BE})^v = R_M^v + \sum_{\mu} \{ (C_M^{v\mu} - \sum_{\eta} C_{\alpha R}^{v\eta} (S^{\mu\eta})^T) \times [\sum_{\eta} (C_d^{-1})^{\mu\eta} d^{\eta}] \}, \quad \mu \in J_t, \eta \in J_t \quad (6)$$

best-estimated parameters

$$(\alpha^{BE})^v = \alpha_o^v + \sum_{\mu} \{ ((C_{\alpha R}^{v\mu})^T - \sum_{\eta} C_{\alpha}^{v\eta} (S^{\mu\eta})^T) \times [\sum_{\eta} (C_d^{-1})^{\mu\eta} d^{\eta}] \}, \quad \mu \in J_t, \eta \in J_t \quad (7)$$

best-estimated parameter covariances

$$(C_{\alpha}^{BE})^{v\mu} = C_{\alpha}^{v\mu} - \sum_{\eta} \left[\sum_{\rho} \left((C_{\alpha R}^{v\rho})^T - \sum_{\pi} C_{\alpha}^{v\pi} (S^{\rho\pi})^T \right) (C_d^{-1})^{\rho\eta} \right] \left(C_{\alpha R}^{\eta\mu} - \sum_{\pi} S^{\eta\pi} (C_{\alpha}^{\pi\mu})^T \right), \quad (8)$$

$v, \mu, \eta, \rho, \pi \in J_t$

best-estimated response covariances

$$(C_R^{BE})^{v\mu} = C_M^{v\mu} - \sum_{\eta} \left[\sum_{\rho} \left(C_M^{v\rho} - \sum_{\pi} C_{\alpha R}^{v\pi} (S^{\rho\pi})^T \right) (C_d^{-1})^{\rho\eta} \right] \left(C_M^{\eta\mu} - \sum_{\pi} S^{\eta\pi} (C_{\alpha R}^{\pi\mu})^T \right), \quad (9)$$

$v, \mu, \eta, \rho, \pi \in J_t$

and best-estimated parameter-response covariances

$$(C_{\alpha R}^{BE})^{v\mu} = C_{\alpha R}^{v\mu} - \sum_{\eta} \left[\sum_{\rho} \left(C_M^{v\rho} - \sum_{\pi} C_{\alpha R}^{v\pi} (S^{\rho\pi})^T \right) (C_d^{-1})^{\rho\eta} \right] \left(C_{\alpha R}^{\eta\mu} - \sum_{\pi} S^{\eta\pi} (C_{\alpha}^{\pi\mu})^T \right), \quad (10)$$

$v, \mu, \eta, \rho, \pi \in J_t$

In the above expressions, the matrices \mathbf{d} and \mathbf{C}_d are defined as follows:

$$C_d = C_R + C_M - SC_{\alpha R}^T - C_{\alpha R} S^T; \quad d = R - M \quad (11)$$

In conclusion, to reduce uncertainties in both the system parameters and responses, the Bayesian inference procedure is used to consistently assimilate computational and experimental information. There are several approaches possible when performing a DAA process in conjunction with time dependent nonlinear systems, but the "on-line data adjustment/assimilation," is the best suited for uncertainty analysis of large-scale highly nonlinear time-dependent problems. It can be performed on-line (i.e., sequentially in time and interactively with the code that calculates the system's dependent variables and responses), by decomposing the

original system into simpler but interacting subsystems. In the present case, the assimilation process involves, at every time node, the minimization of a quadratic objective function subject to constraints.

Once a suitable database of improved estimates for the input parameters (α^{IE}) and for the respective input covariance matrix (C_{α}^{IE}) is available, the application of the method to a NPP scenario is straightforward and requires: a) the calculation of the reference responses R^{NPP} , where here the word 'reference' is connected with the reference NPP boundary and initial conditions supplemented by improved estimates of the input parameters (α^{IE}) when other information is not available; b) the computation of the sensitivity coefficients S , c) the application of the moment propagation equation to obtain the computed covariance matrix C_R^{NPP} of the responses starting from the covariance matrix C_{α}^{NPP} of the system parameters supplemented by improved estimates of the input covariance matrix (C_{α}^{IE}) when other information is not available.

The Data Adjustment and Assimilation has been applied to calibrate and reduce systematically the uncertainties in the predictions of thermal-hydraulic calculations [23]. However it should be noted that so far this methodology has been applied to codes/models that are relatively simpler than system thermal-hydraulic codes like RELAP5, TRACE or CATHARE.

The main drawbacks of this approach are as follows [13]: (i) the method is not applicable in the absence of relevant experimental information; (ii) the adjoint model, needed for computing the sensitivity S , requires relatively modest additional resources to develop and implement if this is done simultaneously with the development of the original code; however if the adjoint model is constructed a posteriori, considerable skills may be required for its successful development and implementation; (iii) a considerable amount of resources is needed to establish a suitable database of improved estimates for the input parameters (α^{IE}) and for the respective input covariance matrix (C_{α}^{IE}), but this is a one-time effort, independent of subsequent applications of the method.

2.4. Overview of EU projects related to uncertainty analysis of TH-SYS calculations

There are important research projects and initiatives that have been carried out or are in progress in the area of uncertainty analysis of TH-SYS:

- **BEMUSE**: The BEMUSE (Best Estimate Methods – Uncertainty and Sensitivity Evaluation) Programme, ref. [26] and [27], has been promoted by the Working Group on Accident Management and Analysis (GAMA) and endorsed by the CSNI. Operational objectives include an assessment of the applicability of best-estimate and uncertainty methods to integral tests and their use in reactor applications. The scope of the Programme is to perform LBLOCA analyses making reference to experimental data and to a NPP in order to address the issue of “the capabilities of the present computational tools” including scaling/uncertainty analysis.

- PREMIUM: PREMIUM (Post-BEMUSE REflood Models Input Uncertainty Methods) is an activity launched with the aim to progress on the issue of the quantification of the uncertainty of the physical models in system thermal-hydraulic codes, by considering a concrete case: the physical models involved in the prediction of core reflooding, ref. [28]. It is endorsed by OECD/NEA/CSNI/WGAMA. It is based on a selected case of uncertainty analysis application to the simulation of quench front propagation (which takes place in reflood scenarios) in an experimental test facility. The scope of the benchmark comprises a review of the existing methods, the identification of potentially important uncertain input parameters for selected case, a quantification of uncertainties using experimental data and, finally, a confirmation/validation of the performed quantification on the basis of blind calculation of a second experiment.
- NURESIM: The Project aims at establishing the basis for the realization of a common European standard software platform for nuclear reactor simulations, ref. [29]. The key objectives of the Project are the following:
 - the integration of advanced physical models in a shared and open software platform;
 - promoting and incorporating the latest advances in reactor and core physics, thermal-hydraulics, and coupled (multi-) physics modelling progress assessment by using deterministic and statistical sensitivity and uncertainty analyses, verification and benchmarking;
 - training, dissemination, best practice and quality assurance.
- NURESAFE WP3.1: Work Package 3.1 of the NURESAFE European collaborative project aims at developing advanced tools and methods for a multi-scale and multi-physics analysis and simulation of LOCAs and other system thermal-hydraulic transients. Such transients are currently treated by system thermal-hydraulic codes such as CATHARE-2 and ATHLET. The addition of two-phase CFD tools and of advanced fuel models allows to revisiting these transients for more accurate and reliable predictions. This may require coupling of CFD with system codes, coupling of fuel thermomechanics with thermal-hydraulic codes and new methods for evaluation of accuracy, sensitivity and uncertainty of coupled simulation tools.

3 DEVELOPMENT OF INPUT PARAMETER RANGE EVALUATION METHODOLOGY

3.1. *Needs and objectives*

It has become evident that the correct evaluation of ranges and PDF of uncertain input parameters have a crucial influence on the results of the uncertainty analysis of thermal-hydraulic calculations. Moreover, the uncertainties of code models and other input parameters should be code-specific as the correlations are seldom implemented in the codes in their analytical form. There are available methodologies, typically based on Bayesian update approach, for evaluating the uncertainties of code input parameters (e.g. CIRCÉ, DAA etc.). However, these methods have a number of serious disadvantages that may impede interested parties from its application:

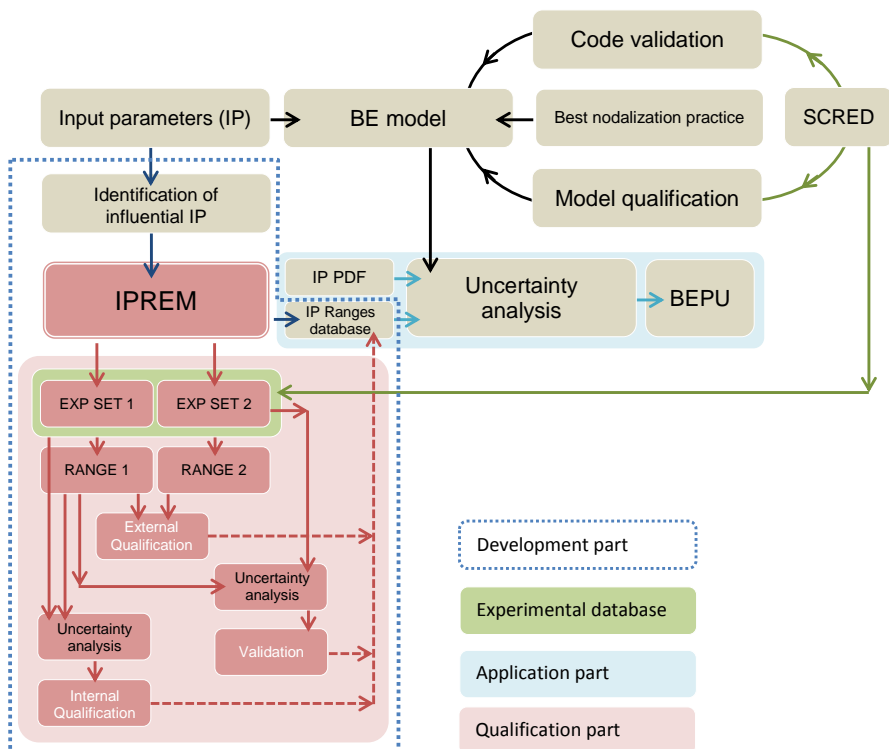
- The computation of sensitivity matrix (response-parameter derivatives) and/or the adjoint system must be introduced to the thermal-hydraulic code, which poses a rather non-trivial task at best and often requires access to the source of the code which is not always available;
- In case of using the “brute force” approach to compute the sensitivity matrix, the introduced input parameter perturbations are often rather large (otherwise the variation in response is not detectable in calculation results) which violate the assumption of linear parameter-response dependence in many cases;
- In some methods (such as CIRCÉ) the number of considered responses should be limited for practical applications, therefore these responses are “pinpointed” at the corresponding time trends (e.g. cladding temperature) which involves a great deal of engineering judgment;
- The aforementioned methods use model calibration which results in updated/calibrated values of both input parameter values α^{IE} and corresponding uncertainties C_{α}^{IE} . This means that at further application of the selected thermal-hydraulic code to a NPP analysis would require reference code calculation with calibrated values of input parameters instead of code default once. This may not be accepted by national regulatory bodies which typically endorse the application of “frozen” versions of a code with non-altered models/correlations.

Having said that, in order to develop a methodology that would overcome the aforementioned issues, the following objectives have been set for the present research:

- The methodology should use data from ‘intermediate’ experimental tests which produce time-dependent measured responses;
- The methodology should not require large experimental matrix to evaluate the uncertainty of code input parameters;
- The methodology should be code independent;
- The methodology should reduce the use of engineering judgment as much as possible;

- The methodology should be able to analyze any code input parameter and any code output parameter (given the accessibility to input parameter in standard input deck);
- The methodology should not require modifications of source of thermal-hydraulic code (at condition that interested input parameters are accessible from standard input file);
- The required resources to implement and apply the methodology for a code of interest should be sufficiently low;
- The resulting evaluated uncertainty of code input parameters should be applicable to reference/default values of these parameters.

Considering the posed requirements, it has been decided to adopt the mathematical apparatus and figures-of-merit of Fast Fourier Transform Based Method (FFTBM) that has been previously developed at University of Pisa and applied for quantifying the accuracy of thermal-hydraulic calculations, ref. [10]. Additional criteria in order to quantify the ranges of variation of uncertain code input parameters have been developed and added to the FFTBM apparatus, thus resulting into the Input Parameter Range Evaluation Methodology (hence labeled “**IPREM**”). The use of the IPREM in the framework of Best Estimate Plus Uncertainty approach is shown on



the
Figure 9 below.

The description of the original FFTBM tool and IPREM are provided in the following subsections.

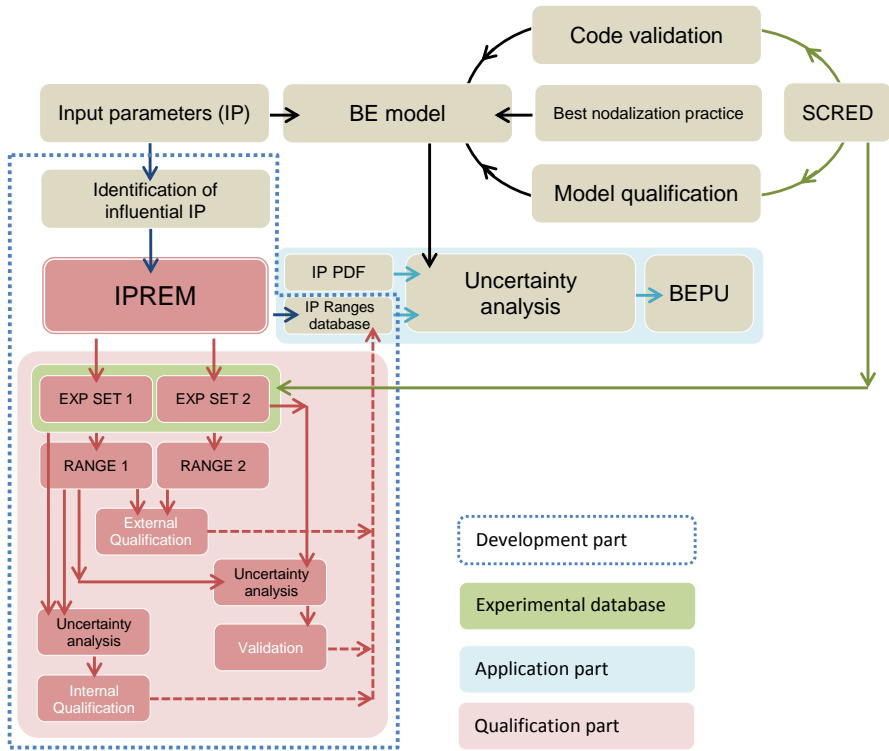


Figure 9 – IPREM in the framework of BEPU approach.

3.2. Fast Fourier Transform Based Method

The proposed methodology is originating from the UMAE methodology [9], which focuses not on the evaluation of individual parameter uncertainties but on the propagation of errors by extrapolating the accuracy from relevant experiments to another experiment or a full scale NPP. Within the UMAE, the quantification of the accuracy of code calculations is performed, using the amplitude of the Fourier Transform of the experimental signal and of the difference between this one and the calculated trend. The accuracy of a code calculation can be evaluated through these values, by representing the discrepancies of the addressed calculation with respect to the experimental data with a dimensionless Average Amplitude (AA) which represents the relative magnitude of these discrepancies [10, 31]. The FFTBM tool has been validated and applied in the numerous international benchmarks [32-35]. Hereafter, the mathematical background of FFTBM is provided.

Generally, the starting point of each method is an error function, by means of which the accuracy is evaluated. Some requirements were fixed which an objective error function should satisfy:

1. at any time of the transient this function should remember the previous history;
2. engineering judgment should be avoided or reduced;
3. the mathematical formulation should be simple;
4. the function should be non-dimensional;
5. it should be independent upon the transient duration;
6. compensating errors should be taken into account (or pointed out);
7. its values should be normalized.

The simplest formulation about the accuracy of a given code calculation, with reference to the experimental measured trend, is obtained by the difference function:

$$\Delta g(t) = g_{calc}(t) - g_{exp}(t) \quad (12)$$

The information contained in this time dependent function, continuously varying, should be condensed to give a limited number of values which could be taken as indexes for quantifying accuracy. This is allowed because the complete set of instantaneous values of $\Delta \mathbf{g}(\mathbf{t})$ is not necessary to draw an overall judgment about accuracy. Integral approaches satisfy this requirement, since they produce a single value on the basis of the instantaneous trend of a given function of time. On the other hand, searching for functions expressing all the information through a single value, some interesting details could be lost. Therefore, it would be preferable to define methodologies leading to more than one value in order to characterize the code calculation accuracy. Information that comes from the time trend of a certain parameter, either being it a physical or a derivate one, may be not sufficient for a deep comprehension of the concerned phenomenon; in such a case, it may be useful to study the same phenomenon from other points of view, free of its time dependence. In this context, the complete behavior of a system in periodic regime conditions (periodic conditions due to instability phenomena are explicitly excluded) can be shown by the harmonic response function that describes it in the frequency domain. Furthermore, the harmonic analysis of a phenomenon can point out the presence of perturbations otherwise hidden in the time domain.

It is well known that the Fourier transform is essentially a powerful problem solving technique. Its importance is based on the fundamental property that one can analyse any relationship from a completely different viewpoint, with no lack of information with respect to the original one. The Fourier transform can translate a given time function $\mathbf{g}(t)$, in a corresponding complex function defined, in the frequency domain, by the relationship:

$$\tilde{g}(f) = \int_{-\infty}^{+\infty} g(t) e^{-j2\pi ft} dt \quad (13)$$

The graphical display of a transformed signal is obtained through the two spectral coordinates: amplitude and frequency. In *Figure 10* is illustrated an example of the Fourier transform of a simple time function, ref. [36].

Afterwards, it is assumed that the experimental and calculated trends, to which the Fourier transform is applied, verify the analytical conditions required by its application theory; i.e., it is assumed that they are continuous (or generally continuous)¹ in the considered time intervals with their first derivatives, and absolutely integrable in the interval $(-\infty, +\infty)$ ². This last requirement can be easily satisfied in our case, since the addressed functions assume values different from zero only in the interval $(0, T)$. Therefore:

$$\tilde{g}(f) = \int_0^T g(t) e^{-j2\pi ft} dt \quad (14)$$

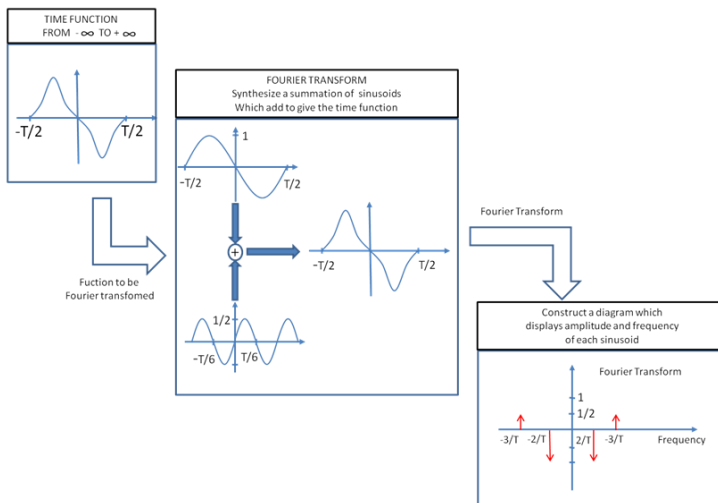


Figure 10 – Sample Fourier Transform representation.

The Fourier integral Eq. (14) is not suitable for machine computation, because an infinity of samples of $\mathbf{g}(t)$ is required. Thus, it is necessary to truncate the sampled

¹ i.e. discontinuous only in a finite number of points. The existence of the Fourier Transform is guaranteed if $g(t)$ is summable according to Lebesgue on the real axis.

² i.e. $\int_{-\infty}^{+\infty} |g(t)| dt < \infty$

function $\mathbf{g}(\mathbf{t})$ so that only a finite number of points are considered, or in other words, the discrete Fourier transform is evaluated. Truncation introduces a modification of the original Fourier transform (the Fourier transform of the truncated $\mathbf{g}(\mathbf{t})$ has a rippling); this effect can be reduced choosing the length of the truncation function as long as possible.

By analogy with the Fourier transform for a continuous function $\mathbf{g}(\mathbf{t})$, the Fourier transform for a discrete set of $g_k = g(t_k)$ ($k = 0, 1, 2, \dots, N-1$) may be defined as below:

$$\tilde{g}(f_n) = \int_0^{T_d} g(t) e^{-i2\pi f_n t} dt \approx \frac{1}{N} \sum_{k=0}^{N-1} g_k e^{-i2\pi f_n t_k} \Delta t = \Delta t \frac{1}{N} \sum_{k=0}^{N-1} g_k e^{-i2\pi f_n t_k} \quad (15)$$

When using functions sampled in digital form, the Fast Fourier Transform (FFT) can be used. The FFT is an algorithm that can compute more rapidly the discrete Fourier transform. To apply the FFT algorithm, functions must be identified in digital form by a number of values which is a power of 2, ref. [37] and [38]. Thus, if the number of points defining the function in the time domain $N = 2^{m+1}$ then according to the sampling theorem the sampling frequency is given by the equation (16).

$$\frac{1}{\Delta t} = f_s = 2f_{max} = \frac{N}{T_d} = \frac{2^{m+1}}{T_d} \quad (16)$$

Where, \mathbf{T}_d is the transient time duration of the sampled signal and \mathbf{f}_{max} is the highest (maximum) frequency component of the signal. The sampling theorem does not hold beyond \mathbf{f}_{max} . From the relation in (16) is seen that selection of the number of points is strictly connected to sampling frequency. The FFT algorithm determines the number of points, equally spaced, which is a power with base 2 (\mathbf{N} range from 2^9 to 2^{12}). Generally, an interpolation is necessary to satisfy this requirement. Taking in account that the available subroutine packages evaluate the FFT normalized to the time duration \mathbf{T}_d , from the equations (14) and (16), it can be easily seen that $|\tilde{\mathbf{g}}(\mathbf{0})|$ represent the mean value of the function $\mathbf{g}(\mathbf{t})$ in the interval $(\mathbf{0}, \mathbf{T}_d)$ while $|\tilde{\mathbf{g}}(\mathbf{f}_n)|$ represent the amplitude of the n -th term of the Fourier polynomial expansion $\mathbf{g}(\mathbf{t})$. To apply the methodology described above, after selecting the signals to be analyzed, it is necessary to choose the following parameters: number of points, sampling frequency and cut frequency.

The method developed for the code accuracy quantification of an individual calculation is based on the amplitude of the FFT of the experimental signal and of the difference between this one and the calculated trend. In particular the method introduces the definition of 2 *figures of merits*: Average Amplitude (AA) Eq. (17) and Weighted Frequency (WF) Eq. (18), which provide a synthesis of the information about the error function Eq. (12):

$$AA = \frac{\sum_{n=0}^{2^m} |\Delta F(f_n)|}{\sum_{n=0}^{2^m} |F_{exp}(f_n)|} \quad (17)$$

$$WF = \frac{\sum_{n=0}^{2^m} |\Delta F(f_n)| \cdot f_n}{\sum_{n=0}^{2^m} |\Delta F(f_n)|} \quad (18)$$

The Average Amplitude represents the relative magnitude of the discrepancy deriving from the comparison between the addressed calculation and the corresponding experimental trend: the lower is the AA – the better is agreement between the experiment and calculation. The Weighted Frequency factor characterizes the kind of error, because its value emphasizes if the error has more

relevance at low or high frequencies. Depending upon the transient, high frequency errors can be more acceptable than low frequency ones. In other terms, better accuracy is achieved by low AA values at high WF values.

Trying to give an overall picture of the accuracy of a given calculation, it is required to combine the information obtained for the single parameters into average indexes of performance. This is obtained by defining the following quantities: the total weighted \mathbf{AA}_{tot} Eq. (19) and the total \mathbf{WF}_{tot} Eq. (20).

$$(\mathbf{AA})_{tot} = \sum_{i=1}^{N_{var}} \mathbf{AA} \cdot (w_f)_i \quad (19)$$

$$(\mathbf{WF})_{tot} = \sum_{i=1}^{N_{var}} (\mathbf{WF})_i (w_f)_i \quad (20)$$

With

$$\sum_{i=1}^{N_{var}} (w_f)_i = 1 \quad (21)$$

Where \mathbf{N}_{var} is the number of analyzed parameters and $(w_f)_i$ are weighting factors that take into account the different importance of each parameter from the viewpoint of safety analyses. This introduces some degree of engineering judgment that has been fixed by a proper and unique definition of the weighting factors, necessary to account for the different relevance, from the point of view of safety and reliability of the measurement, of the various addressed quantities.

In the framework of application of FFTBM to thermal-hydraulic calculations, the settings are adopted for the following parameters:

- Sampling frequency
- Number of points
- Cut frequency
- Weights

The choice of the sampling frequency depends on transient, kind of parameter trend to be investigated (i.e. pressure, flow rate, clad temperature, etc.). Obviously, the fulfillment of the sampling theorem is required to avoid distortion of sampled signals due to aliasing occurrence.

$$T = \frac{1}{2f_c} \quad (22)$$

where f_c is the highest frequency component of Fourier transform characterizing the spectrum of the continuous function $\mathbf{g}(t)$. Therefore, experimental data acquisition should be characterized by sampling frequency greater than $2 f_c^3$; similar frequencies of acquisition should have the corresponding calculated trends. A typical value of f_c related to parameters of interest in thermal hydraulic transients is 1 Hz; however, specific responses like break flow rates or pressure drops measurements may require higher values.

Since the FFT algorithm requires that functions are identified by a number of values, equally spaced, which is a power of 2, an interpolation is necessary to satisfy this requirement. On the other hand, the comparison of experimental and calculated signals, and the evaluation of their difference function $\Delta\mathbf{g}(t)$, imposes that they have

³ Normally 3-4-5 times f_c is used

the same time scale. Furthermore, after selecting the number of points N , the maximum frequency of transformed functions by the FFT, is given by:

$$f_{max} = \frac{2^m}{T_d} = \frac{f_c}{2} \quad (23)$$

Thus, the number of points is strictly associated with the adopted sampling frequencies; it is meaningless to choose a number of points corresponding to a frequency⁴ greater than the f_{max} achievable using a certain f_c .

To filter any spurious contribution, a cut frequency has been introduced. This cut frequency characterizes the frequency upper value which has to be considered in evaluating the AA and WF factors, as defined by Eq. (17) and (18). Typical thermal hydraulic parameter trends (for different kinds of transients) have been analyzed [39], aiming at defining a unique suitable value of cut frequency, in such a way to avoid partial loss of information. A cut frequency value of 1 Hz is generally suitable to analyze trends of thermal hydraulics parameters; only flow rates and densities require cut frequency values up to 2 Hz.

The need of $(w_f)_j$ definition derives from the fact that the addressed parameters are characterized among other things by different importance and reliability of measurement. The weighting factor for the generic j -th parameter, is defined as:

$$(w_f)_j = \frac{(W_{exp})_j \cdot (W_{saf})_j \cdot (W_{norm})_j}{\sum_{j=1}^{N_{var}} (W_{exp})_j \cdot (W_{saf})_j \cdot (W_{norm})_j} \quad (24)$$

where

- N_{var} is the number of parameters to which the method is applied
- $(W_{exp})_j$ is the contribution related to the experimental accuracy
- $(W_{saf})_j$ is the contribution expressing the safety relevance of the parameter
- $(W_{norm})_j$ is component of normalization with reference to the average amplitude evaluated for the primary side pressure

This introduces a degree of engineering judgment that has been fixed by a proper and unique definition of the weighting factors (see *Table 2*, ref. [39]).

Table 2 – FFTBM weighting factor components for typical thermal-hydraulic parameters.

Parameter	ID	W_{exp}	W_{saf}	W_{norm}
Primary pressure	PP	1.0	1.0	1.0
Secondary pressure	SP	1.0	0.6	1.1
Pressure drops	PD	0.7	0.7	0.5
Mass inventories	MS	0.8	0.9	0.9
Flow rates	FR	0.5	0.8	0.5
Fluid temperatures	FT	0.8	0.8	2.4
Clad temperatures	CT	0.9	1.0	1.2
Collapsed levels	LV	0.8	0.9	0.6
Core power	PW	0.8	0.8	0.5

⁴ Beyond $f_j/2$ the sampling theorem doesn't hold, and we have no further information about these frequencies.

3.3. *Description of methodology for input parameter range evaluation: the IPREM*

The feature of FFTBM to provide a quantitative evaluation of an accuracy of a time-dependent code output parameter with respect to experimental data has been used to establish a methodology for evaluating the range of variation of input parameter: the IPREM.

The approach, adopted in IPREM, is based on the simulation of a selected 'intermediate' experimental test with a thermal-hydraulic code of interest (e.g. RELAP5) and on the comparison of the calculated thermal-hydraulic responses with the available experimental measurements via the mathematical apparatus of FFTBM.

The quantification of variation ranges of input parameters for physical models is achieved through a) running the calculations of the reference case of a physical model and of the "sensitivity" cases, constituted by a single-parameter variation, b) the application of the FFTBM for quantifying the accuracy of calculated responses respect to experimental data and c) further comparison of differences between **AA** values obtained from sensitivity cases and an **AA** of the reference case. The flowchart of the IPREM procedure is shown on *Figure 11*. In essence, an analyst should take the following actions:

1. To perform Reference Case calculation;
2. To select relevant Responses (output parameters);
3. To derive by FFTBM the AA for each selected response and to compute the global AA for the calculation;
4. To select a set of Uncertain Input Parameters;
5. To perform Sensitivity cases calculations and conduct a qualitative check;
6. To apply FFTBM to the sensitivity cases:
 - Perform FFTBM for "Sensitivity calculation – Experiment data" pair;
 - Perform FFTBM for "Sensitivity calculation – Reference calculation " pair;
7. To apply established CRiterion for the quantification of the variation range.

It should be noted that the development of the model of experimental facility for the code of interest should be performed following the "best nodalization" practices, i.e. no special tuning should be applied. This is to ensure the applicability of evaluated uncertainties of input parameters to further uncertainty analyses of thermal-hydraulic calculations with this code (simulation of ITF tests, NPP scenarios etc.).

Once the model has been set up, the analyst performs the reference calculation of experimental test and performs the qualitative check of obtained results:

- The relevant thermal-hydraulic phenomena observed in the experiment must be predicted by the code
- Discrepancy between predicted and measured parameters should be qualitatively acceptable.

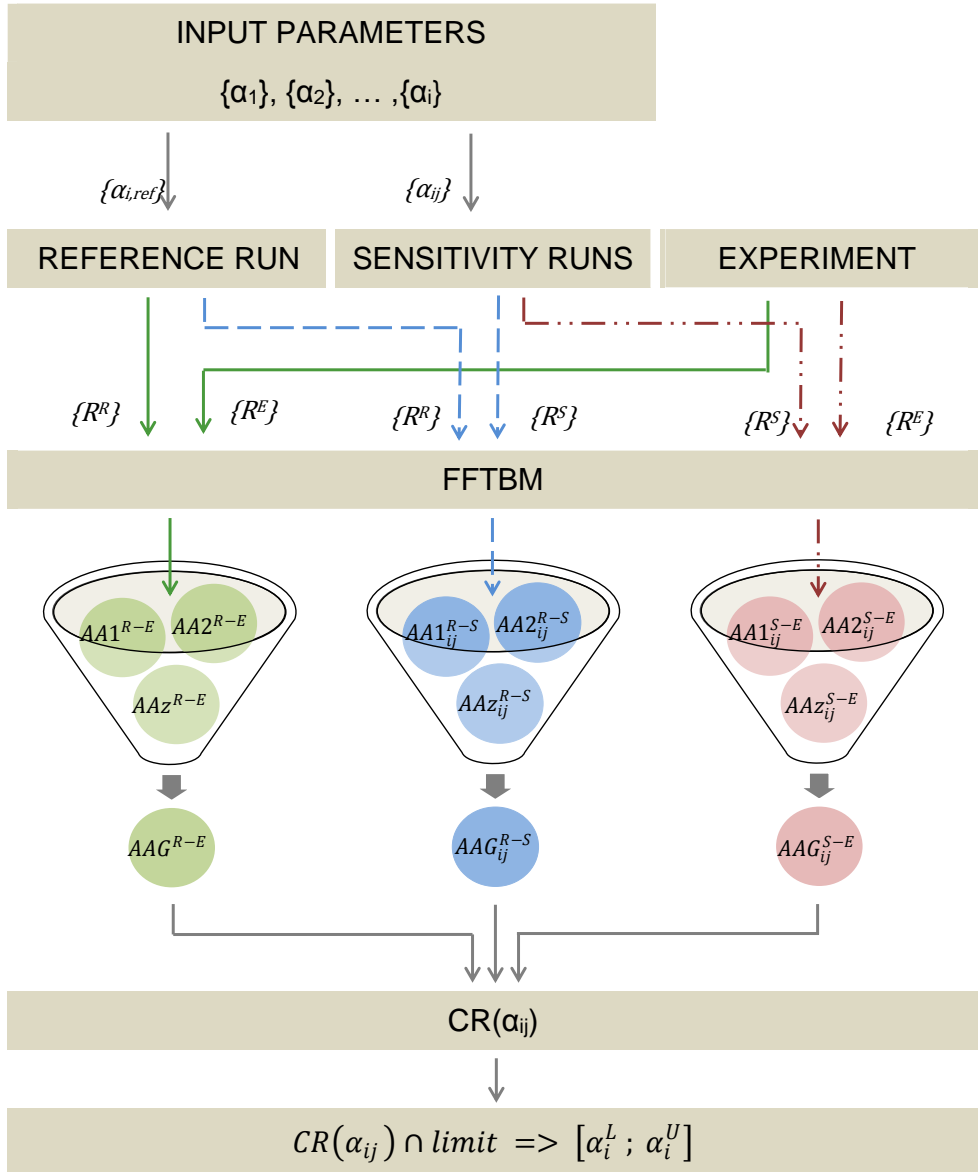


Figure 11 – Flowchart of IPREM procedure

The relevant thermal-hydraulic parameters that describe the phenomena of interest should be selected as responses. The reliable and rather precise experimental measurement must be available for the responses of interest. The selected code responses must be sensitive to the analyzed input parameters. At the current stage of the validation of the methodology, it is advised to use few (up to 3-4) responses to be analyzed. Once the types of responses are identified, the set of calculated $\{R^R\}$ and experimental $\{R^E\}$ time trends is defined.

The list of studied input parameters $\{\alpha_i\}$ should be established. A preliminary sensitivity analysis may be applied to identify those parameters that are influential to the selected responses. For each i -th input parameter a vector of j multipliers should be defined. The values of multipliers may be arbitrary with the condition that they cover the sufficiently large but reasonable span of possible values of an input parameter.

For each i -th input parameter of interest a number of j calculations must be performed, by varying only the i -th parameter. As a results, each response Rz^S has $i \times j$ time trend results $\{R_{ij}^S\}$, e.g. in case of selection of 3 responses ($z=1,2,3$): $[R1_{ij}^S; R2_{ij}^S; R3_{ij}^S]$.

As it has been mentioned above (see step 6), two FFTBM analyses must be performed for each j -th sensitivity run of each i -th input parameter:

- $\{R_{ij}^S\}$ vs $\{R^E\}$
- $\{R_{ij}^S\}$ vs $\{R^R\}$

As a result, the analyst obtains two sets of Average Amplitudes (**AA**) for each j -th sensitivity run of each i -th input parameter:

- AAz_{ij}^{S-R} , that quantifies the “deviation” of sensitivity run from reference case
- AAz_{ij}^{S-E} , that quantifies the “accuracy” of sensitivity run with respect to experimental data

where z is the consecutive number of a response. For example, in case of 3 responses it would be:

- $[AA1_{ij}; AA2_{ij}; AA3_{ij}]^{S-R}$
- $[AA1_{ij}; AA2_{ij}; AA3_{ij}]^{S-E}$

At this point, the set of AAz_{ij} values is available for each selected response for each j -th sensitivity run of each i -th input parameter. A next step is performed in order to produce a single Figure-of-Merit that allows to:

- Quantify the sensitivity of entire nodalization to the input parameter variation;
- Quantify the accuracy of entire nodalization performance in each sensitivity run with respect to experimental data.

This is achieved by the calculation of a Global AA (**AAG**) for each of two sets of AAz_{ij} derived from the j -th sensitivity run of the i -th input parameter. The **AAG** is calculated as a weighted sum of AAz_{ij} values over the z responses:

$$AAG = \sum_z w_z AA_z \quad (25)$$

where w_z is the weighting factor assigned for each type of response. The weighting factors are determined by the type of thermal-hydraulic parameter selected as a response. A proposed set of weighting factors has been developed for 'intermediate' experimental tests on the basis of Eq. (24) and of the contributors presented in *Table 2*. The resulting values are shown in *Table 3*.

Table 3 – Weighting factors for IPREM procedure.

Parameter type	W_z
Primary pressure	1.000
Secondary pressure	0.660
Pressure drop	0.245
Mass Inventory	0.648
Flow rate	0.200
Fluid temperature	0.256
Cladding temperature	1.080
Level	0.432
Power	0.320
Quench front elevation	0.864

After the weights are selected and assigned to the $AA_{z_{ij}}$ of corresponding responses, they are normalized in order to obtain:

$$w_z = \frac{W_z}{\sum_{i=1}^{NZ} W_i} \quad (26)$$

The following properties of AAG^{S-E} and AAG^{S-R} may be noted:

- AAG^{S-R} has a minimum value of $AAG^{S-R} = 0$ at the value of α^{ref} and monotonically increases (around α^{ref}) with values of α deviating from α^{ref}
- AAG^{S-E} has a minimum value at some α_j , which may not necessarily be α^{ref} .

Once the Global AA values are calculated for each j -th value of input parameter α_i , the criterion quantity $CR(\alpha_{ij})$ is computed:

$$CR(\alpha_{ij}) = \frac{AAG^{S-E}(\alpha_{ij}) + AAG^{S-R}(\alpha_{ij}) - AAG^{R-E}}{(1 - AAG^{S-E}(\alpha_{ij}))} \quad (27)$$

where AAG^{R-E} is calculated from comparison of reference calculation and experimental data.

In equation (27) the following constituents are included:

- $AAG^{S-E} + AAG^{S-R}$ is a measure of the total "deviation" of a sensitivity calculation from both the reference calculation and the experimental data;

- AAG^{R-E} is calculated from the comparison of reference calculation and experimental data;
- $(1 - AAG^{S-E})$ “slows” the increase of CR if the change of an input parameter leads to improvement of results with respect to experiment.

The obtained dependence $CR(\alpha)$ is convenient to be analyzed in graphical mode. A typical trend obtained for an input parameter is showed on the *Figure 12*.

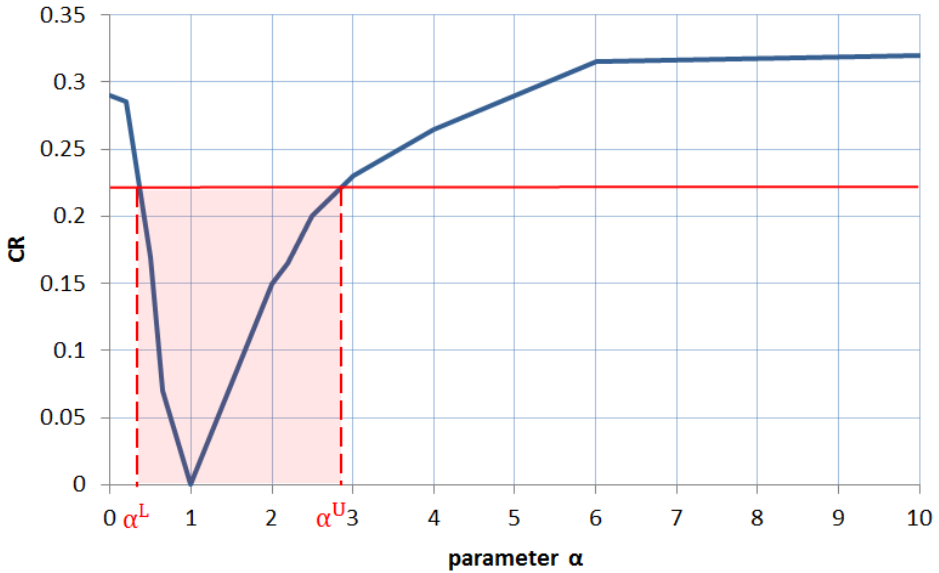


Figure 12 – Sample trend of CR quantity.

As a last step, the variation ranges of each parameter α are quantified by applying the limiting value (threshold) to $CR(\alpha)$. The lower and upper bounds of α are therefore defined as:

$$[\alpha^L; \alpha^U] = CR(\alpha) \cap \text{limit} \quad (28)$$

The **limit** value must be set once and consistently applied for all the analyses performed. The variation of this values is not allowed unless proper justification.

In the present research a value of **limit** = 0.22 has been adopted.

The value of 0.22 is based on the consideration that the maximum allowed “deviation” of responses (at extremes of the range of input parameters) be 10% (using the FFTBM metrics of Average Amplitude) in the hypothetical case when reference calculation exactly matches the experimental data ($AAG^{S-E} = AAG^{S-R}$):

$$CR = \frac{2 \cdot AAG}{(1 - AAG)} \leq 0.22 \iff AAG \leq 0.1 \quad (29)$$

The application of **limit** = 0.22 to the example of $CR(\alpha)$ shown in *Figure 12* results in ranges of parameter α : [0.35; 2.8].

The proposed procedure for evaluating the variation ranges of uncertain input parameters is based rather on engineering considerations than on statistical treatment. Therefore, it does not take account or provide as a result the Probability Density Function for each input parameter. However, for practical thermal-hydraulic applications it is suggested to use the type of distribution which corresponds to the “limited” knowledge of it: uniform distribution, triangular distribution or histogram law. In Section 4 of this thesis, the results of sensitivity analysis on choice of PDF for input parameters are presented.

Summing up, the following features of the proposed methodology can be outlined, ref. [40]:

- It is neither a statistical procedure nor is based on perturbation theory;
- Any kind of input/output parameter can be analyzed, since the procedure involves only post-processing of calculation results;
- The procedure is code-independent;
- The whole time trend of responses and experimental measurements is taken into account;
- The software (for performing FFT analysis) is rather simple to develop.

3.4. Verification step: application to Edwards pipe problem

At the stage of development of the IPREM methodology, a blowdown experiment has been selected in order to set up and benchmark the considered quantities, factors and criteria. Particularly, the “Edwards pipe” experiment, ref. [41], has been selected to be modeled with RELAP5 Mod3.3 code due to the relatively simple geometry and limited number of measured parameters. The process of application of IPREM to quantify the variation ranges of blowdown-related code input parameters and their further verification is described in the following subsections.

3.4.1. Modeling Edwards pipe experiment with RELAP5 code

In its original setting, “Edwards pipe” experiment models a depressurization of a pipe, filled initially with single-phase water at a pressure of 7 MPa and temperature of 502 K. The layout of the facility is shown in *Figure 13* and geometrical properties and boundary conditions are summarized in *Table 4*. The transient depressurization of the single-phase water is initiated by releasing one end of the pipe (by means of rupture disk). The time dependent behavior of the liquid, namely water turning into a two-phase mixture during the pipe depressurization, simulates basic features of a loss of coolant accident in a pressurized water reactor.

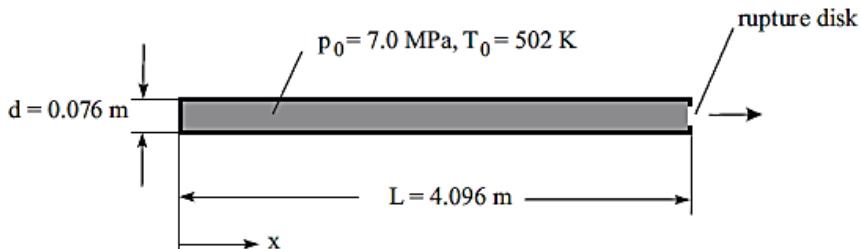


Figure 13 – Edward pipe experimental setup.

Table 4 – Edwards pipe facility characteristics.

Parameter	Value	Note
Pipe length, m	4.096	
Pipe diameter, mm	76	
Break diameter, mm	71	reduction of 13% of the pipe area
Initial pressure, MPa	7.0	
Initial temperature, K	502	
Ambient pressure, MPa	0.1	

The first 10ms of the transient are characterized by the propagation of a rarefaction wave from the opening end into the pipe and the reflection of the wave at the closed end of the pipe where a distinct undershoot of the pressure occurs. During the later phase of the blowdown the depressurization is controlled by the strong evaporation (flashing) of the liquid phase. The main thermal-hydraulic phenomena occurring in this experiment are:

- Depressurization
- Phase change
- Flashing
- Stratification
- Interphase momentum and energy transfer
- Critical flow

The RELAP5 Mod3.3 code, ref. [42], has been applied to model the thermal-hydraulic phenomena occurring in Edwards pipe experiment. More detailed description of the code is provided in Appendix A.

The pipe is modeled with a 1-D *pipe* component consisting of 40 nodes of equal length (see *Figure 14*). The atmosphere is simulated as fixed boundary conditions (saturated steam at pressure of 7 MPa) in *time-dependent volume* component. The break is represented by means of *trip valve* component which opens instantly at the beginning of the transient. The Henry-Fauske critical flow model, ref. [43], has been activated at the break. The reference case calculation has been performed and predicted responses $\{R^R\}$ have been compared with experimentally measured data $\{R^E\}$: pressure (*Figure 15*) and void fraction (*Figure 16*) at measurement station of 1.64m.

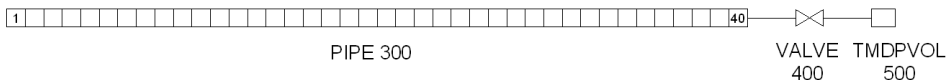


Figure 14 – RELAP5 nodalization of Edward pipe experimental.

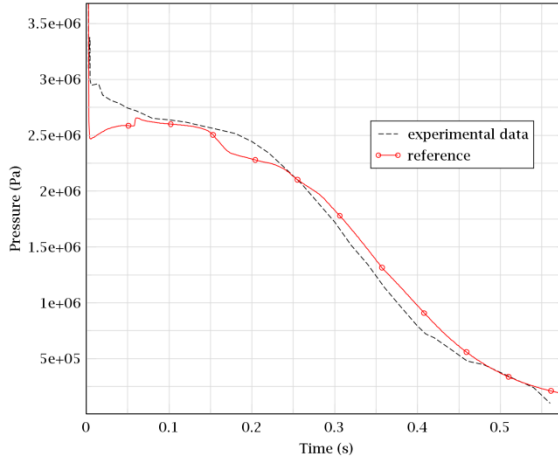


Figure 15 – Edward pipe: predicted pressure in reference calculation.

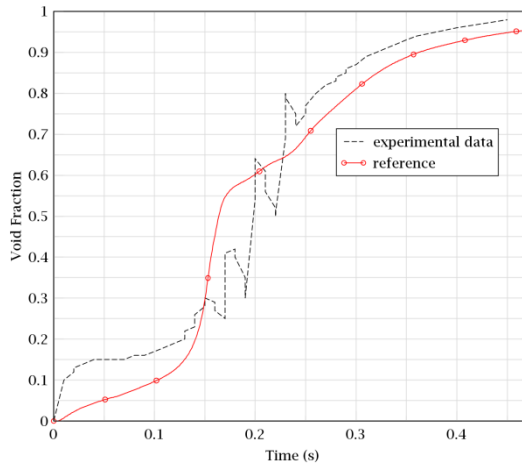


Figure 16 – Edward pipe: predicted void fraction in reference calculation.

The code predicts the experimental data rather well, although Henry-Fauske model tends to overpredict the subcooled liquid discharge rate, ref. [44], hence the predicted pressure undershoot immediately after break opening. All the relevant thermal-hydraulic phenomena (including pressure wave propagation flashing and critical flow) are predicted by the model.

3.4.2. Quantification of uncertainty of model input parameters

As the next step, the most influential parameters of the RELAP5 model of Edwards pipe have been determined through a series of sensitivity calculations with single-parameter variation. Therefore, the following parameters have been identified to be subjected to IPREM analysis (the reference values $\{\alpha^{ref}\}$ are presented in Table 5):

- α_1 - Initial liquid temperature in the pipe
- α_2 - Break flow area
- α_3 - Pressure loss coefficient K_{loss} at the break
- α_4 - Henry-Fauske model discharge coefficient

At the next step, the FFTBM tool has been applied to calculate $\{\mathbf{AA}^{\text{R-E}}\}$ (comparison of reference calculation and experimental data). The results are shown in *Table 5*. It may be noticed that pressure Average Amplitude $\mathbf{AA}_p^{\text{R-E}}$ is lower than corresponding value for void fraction response $\mathbf{AA}_v^{\text{R-E}}$. It is consistent with the discrepancy between predicted void fraction and experimental data that shows somewhat oscillatory behavior which is not present in calculation.

The “pressure” and “level” weights \mathbf{W}_z from *Table 3* are used in equation (26) in order to calculate weights \mathbf{w}_z for both responses (shown in *Table 5*). The “level” weighting factor \mathbf{W}_z has been used, since the collapsed level in thermal-hydraulic calculations is typically evaluated from the void fraction. Finally, the Global Average Amplitude value $\mathbf{AAG}^{\text{R-E}}$ is computed with equation (25) to characterize the performance of the entire model in reference case against experimental data.

Table 5 – Edwards pipe IPREM settings for reference calculation.

	Parameter	Value
$\{\alpha_i^{\text{ref}}\}$	α_1 – Initial liquid temperature	502 K
	α_2 – Break flow area	3.967E-2 m ²
	α_3 – K_{loss} at the break	15.0
	α_4 – discharge coefficient	1.0
$\mathbf{AA}_z^{\text{R-E}}$	$\mathbf{AA}_p^{\text{R-E}}$ – pressure	0.064
	$\mathbf{AA}_v^{\text{R-E}}$ – void fraction	0.156
\mathbf{w}_z	w_p – pressure	0.698
	w_v – void fraction	0.302
\mathbf{AAG}	$\mathbf{AAG}^{\text{R-E}}$	0.092

As the next step, a series of j (about 10-15) sensitivity calculations have been performed with various values for each of 4 input parameters α_i . FFTBM tool has been applied twice to each of these sensitivity calculations in order to quantify:

- $\begin{bmatrix} \mathbf{AA}p_{1j}^{S-R} & \mathbf{AA}p_{2j}^{S-R} & \mathbf{AA}p_{3j}^{S-R} & \mathbf{AA}p_{4j}^{S-R} \\ \mathbf{AA}v_{1j}^{S-R} & \mathbf{AA}v_{2j}^{S-R} & \mathbf{AA}v_{3j}^{S-R} & \mathbf{AA}v_{4j}^{S-R} \end{bmatrix}$
- $\begin{bmatrix} \mathbf{AA}p_{1j}^{S-E} & \mathbf{AA}p_{2j}^{S-E} & \mathbf{AA}p_{3j}^{S-E} & \mathbf{AA}p_{4j}^{S-E} \\ \mathbf{AA}v_{1j}^{S-E} & \mathbf{AA}v_{2j}^{S-E} & \mathbf{AA}v_{3j}^{S-E} & \mathbf{AA}v_{4j}^{S-E} \end{bmatrix}$

Obtained values AAz_{ij}^{S-R} and AAz_{ij}^{S-E} (where \mathbf{z} is \mathbf{p} for pressure and \mathbf{v} for void) are plotted in *Figure 17*, *Figure 18*, *Figure 19* and *Figure 20* for each of 4 input parameters α_i .

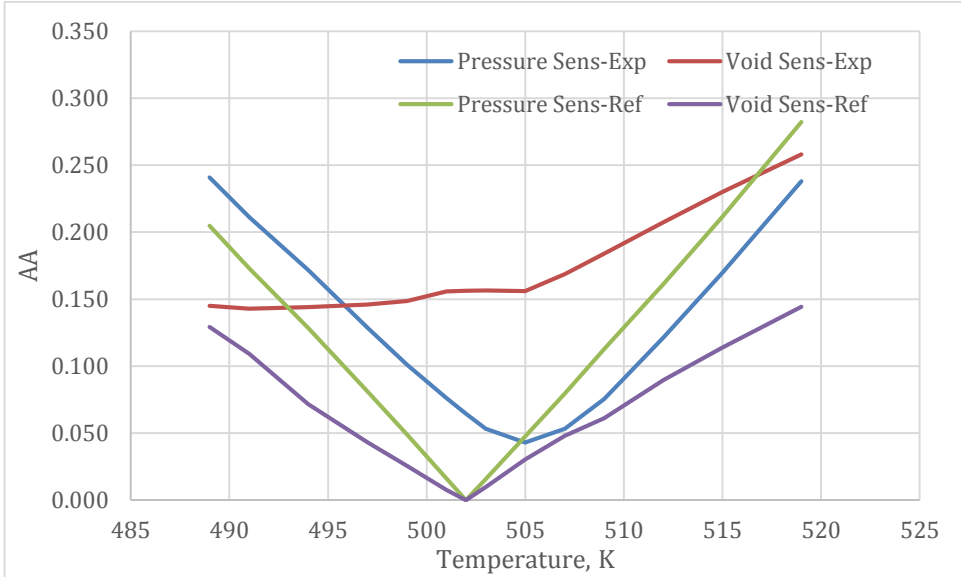


Figure 17 – Edwards pipe: AAz_{1j}^{S-R} and AAz_{1j}^{S-E} for initial liquid temperature.

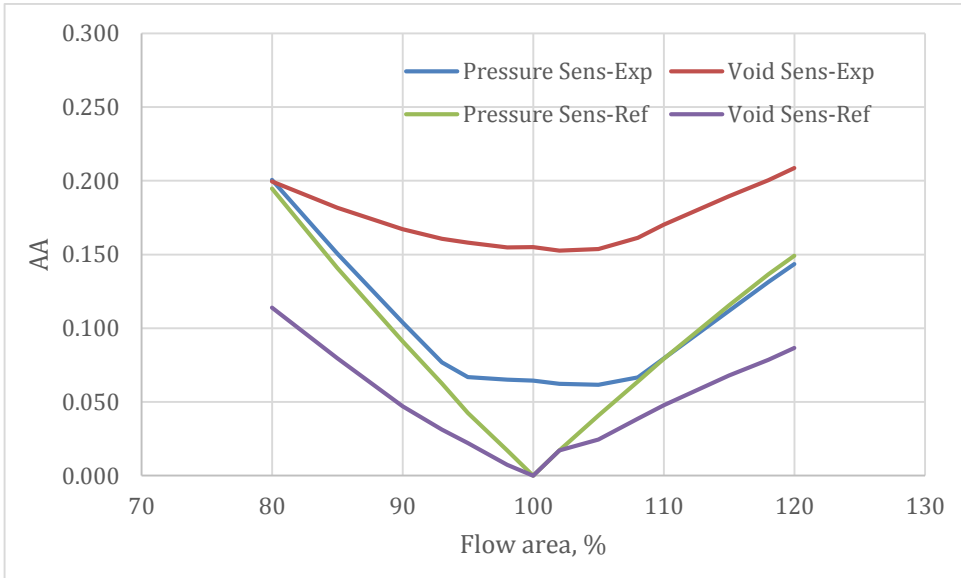


Figure 18 – Edwards pipe: AAz_{2j}^{S-R} and AAz_{2j}^{S-E} for break flow area.

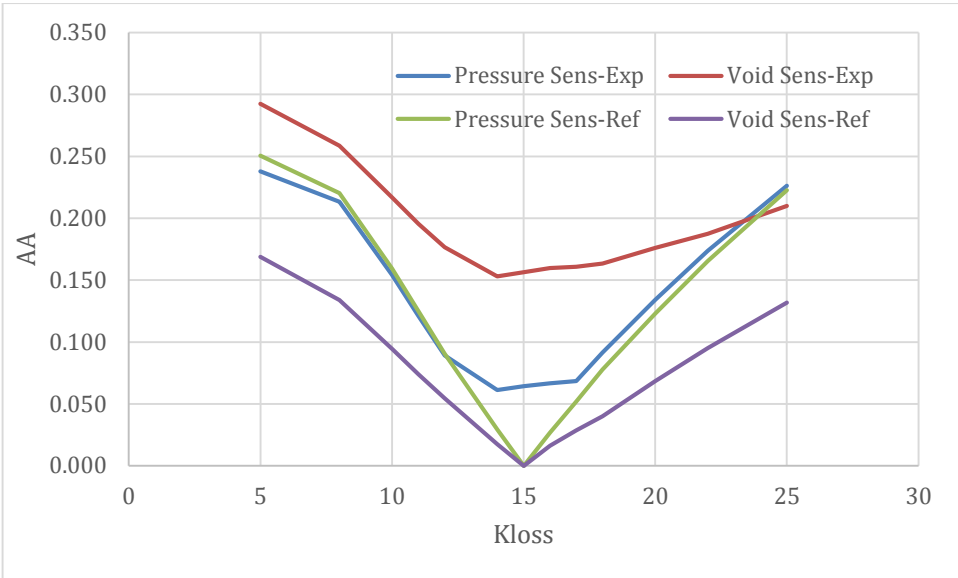


Figure 19 – Edwards pipe: AAz_{3j}^{S-R} and AAz_{3j}^{S-E} for Kloss at the break.

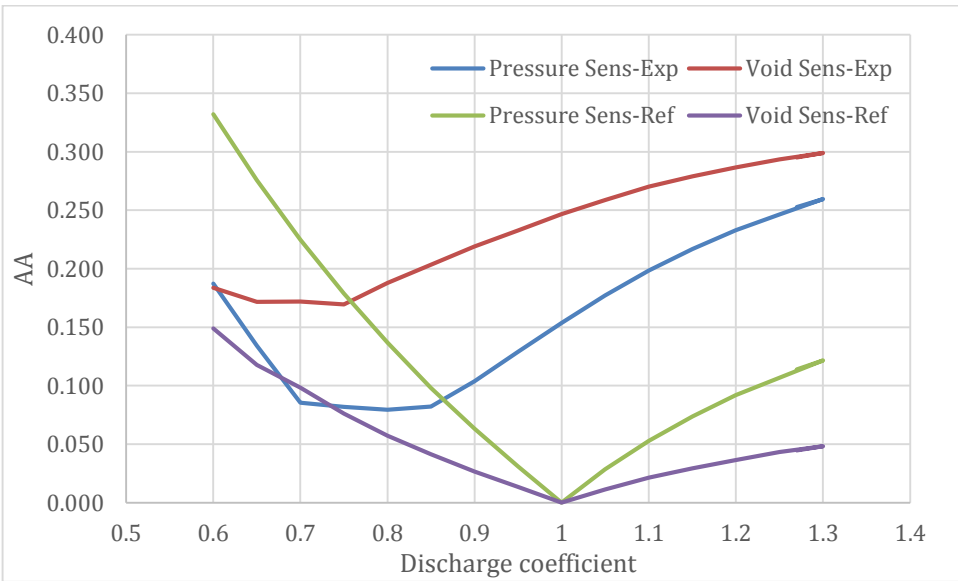


Figure 20 – Edwards pipe: AAz_{4j}^{S-R} and AAz_{4j}^{S-E} for discharge coefficient.

It may be noticed that all values AAz_{ij}^{S-R} are monotonically (and almost symmetrically except for discharge coefficient) increasing around reference value of α_i . The values AAz_{ij}^{S-E} show their minimum extrema at α_{ij} very close to reference values for break flow area, K_{loss} and initial water temperature. It confirms that the model is set correctly in terms of geometry, boundary and initial conditions. Instead, Figure 20

shows that calculation results (expressed by pressure and void fraction) improve with respect to experimental data while decreasing discharge coefficient of Henry-Fauske critical flow model towards value of 0.75.

At the next step the equation (25) is applied to all AAz_{ij}^{S-R} and AAz_{ij}^{S-E} with the weights listed in *Table 5*, in order to calculate the pairs of Global Average Amplitude (AAG_{ij}^{S-R} and AAG_{ij}^{S-E}) for each input parameter. The results are shown in *Figure 21*, *Figure 22*, *Figure 23* and *Figure 24*.

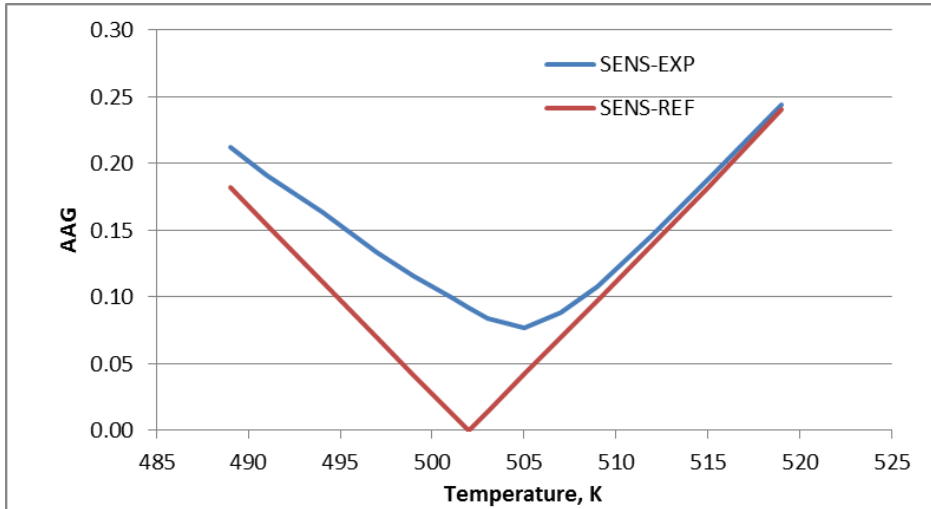


Figure 21 – Edwards pipe: AAG_{1j}^{S-R} and AAG_{1j}^{S-E} for initial liquid temperature.

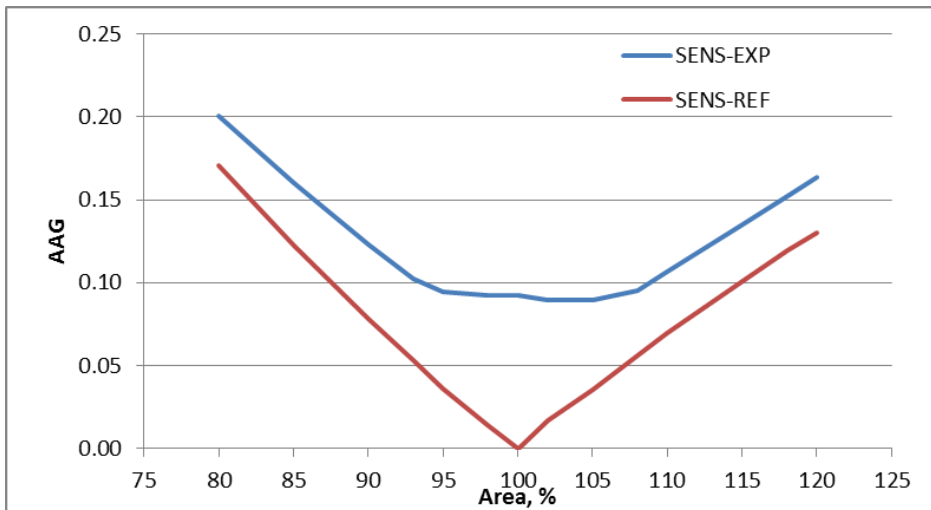


Figure 22 – Edwards pipe: AAG_{2j}^{S-R} and AAG_{2j}^{S-E} for break flow area.

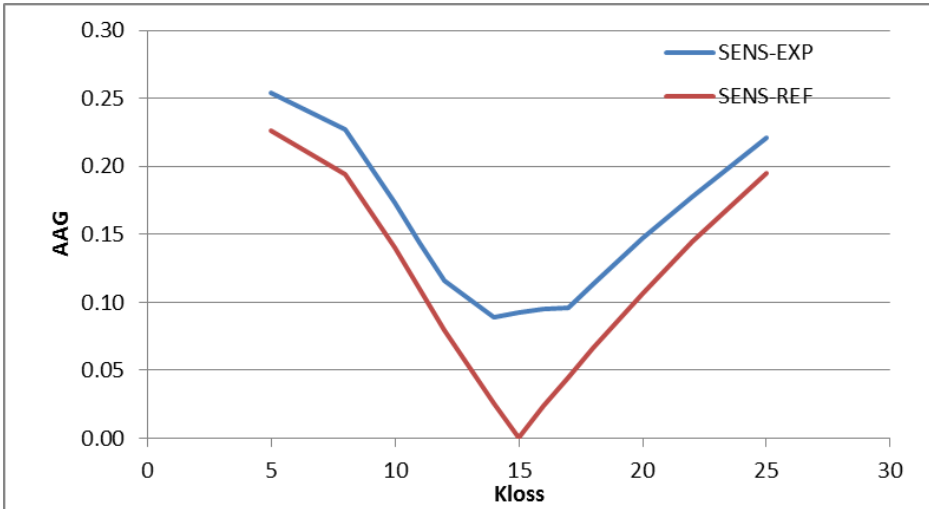


Figure 23 – Edwards pipe: AAG_{3j}^{S-R} and AAG_{3j}^{S-E} for K_{loss} at the break.

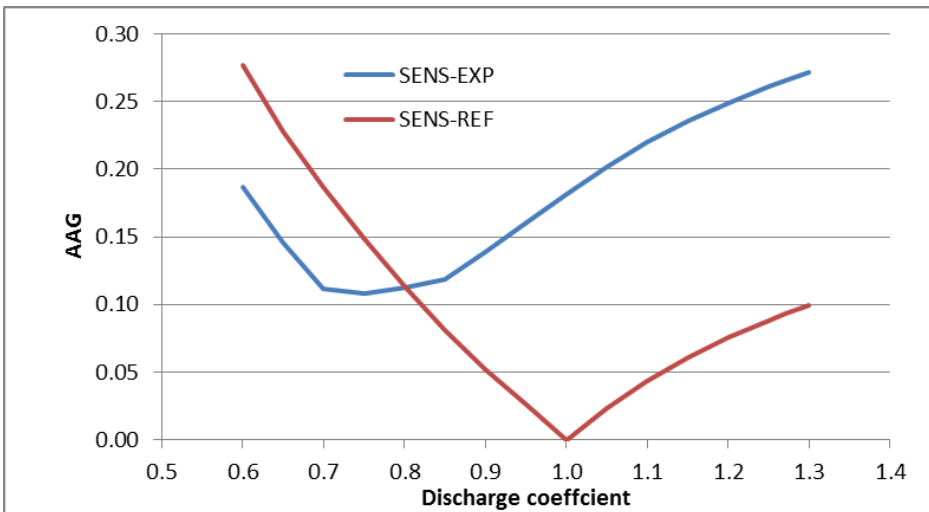


Figure 24 – Edwards pipe: AAG_{4j}^{S-R} and AAG_{4j}^{S-E} for discharge coefficient.

One may note that AAp_{1j}^{S-E} and AAv_{1j}^{S-E} on Figure 17 have the contrary trends: pressure response improves with increasing temperature around reference value, while void fraction response improves with decreasing temperature. However, given that pressure response has higher weight than void fraction, the resulting AAG_{1j}^{S-E} on Figure 21 has minimum value at 505 K comparing to reference 502 K.

The $CR(\alpha_{ij})$ is computed for each of 4 input parameters according to equation (27). The results are shown on Figure 25, Figure 26, Figure 27 and Figure 28.

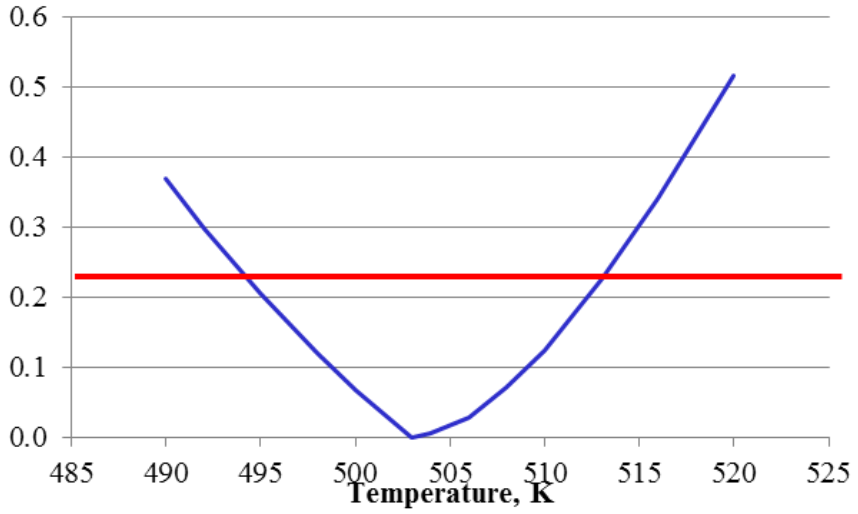


Figure 25 – Edwards pipe: $CR(\alpha_{1j})$ for initial liquid temperature.

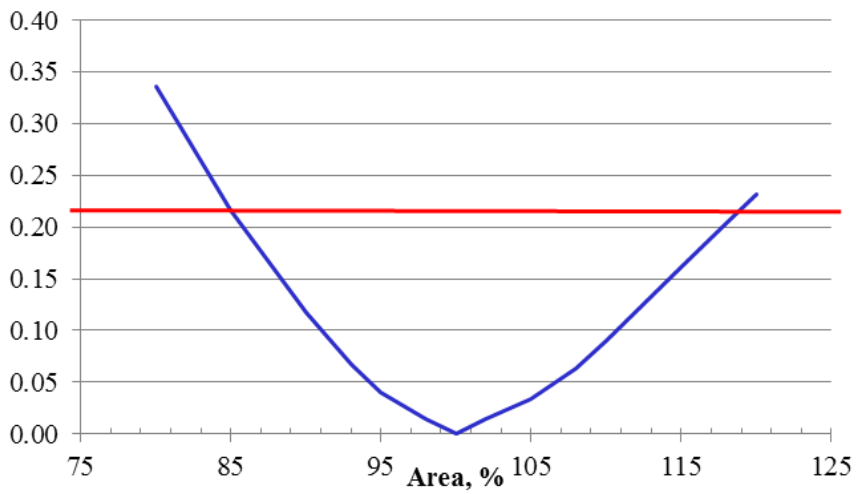


Figure 26 – Edwards pipe: $CR(\alpha_{2j})$ for break flow area.

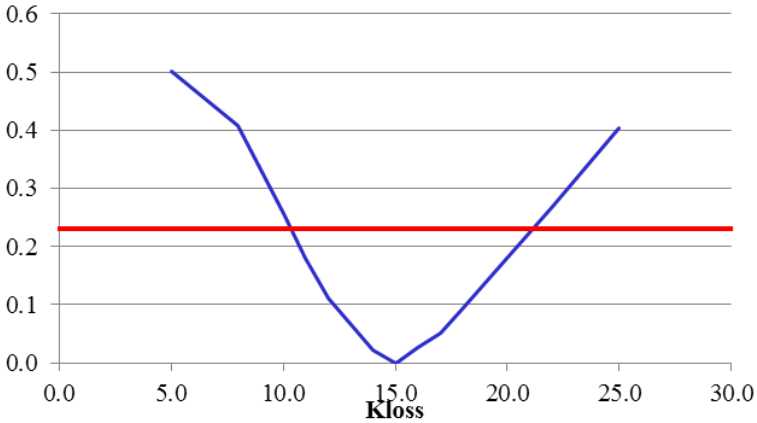


Figure 27 – Edwards pipe: $CR(\alpha_{3j})$ for K_{loss} at the break.

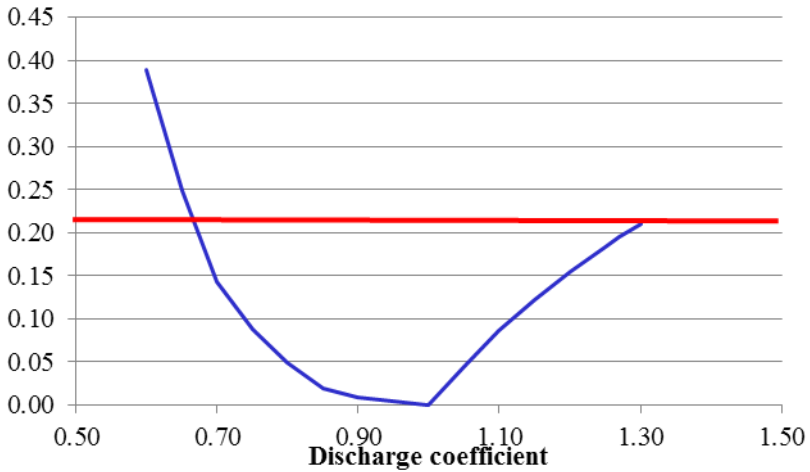


Figure 28 – Edwards pipe: $CR(\alpha_{4j})$ for discharge coefficient.

Table 6 – Edwards pipe: quantified variation ranges of input parameters.

α_i	Parameter	Min	Max
α_1	Initial liquid temperature	0.7 K_{ref}	1.4 K_{ref}
α_2	Break flow area	0.85 A_{ref}	1.19 A_{ref}
α_3	K_{loss} at the break	-8.5 K	+10 K
α_4	discharge coefficient	0.66	1.3

Finally, the **limit** = 0.22 (red line on Figure 25, Figure 26, Figure 27 and Figure 28) has been applied to each $CR(\alpha_{ij})$ in order to quantify the variation ranges of input parameters (Table 6).

3.4.3. Internal qualification: uncertainty analysis of Edwards pipe calculation

In order to verify the consistency of the variation ranges of input parameters for the blowdown problem obtained with IPREM, the uncertainty analysis of the RELAP5 calculation of Edwards pipe experiment has been performed. Since the variation ranges have been derived on the basis of the same Edwards pipe test, this verification can be considered as “internal qualification” than an actual validation.

The qualification is performed by using the quantified ranges of input model parameters (*Table 6*) for the uncertainty analysis of thermal-hydraulic calculation of experimental test. The consistency is achieved verifying whether the resulting uncertainty bands of relevant thermal-hydraulic response encompass the experimental data.

The uncertainty analysis of RELAP5 calculation of Edwards pipe test has been performed with GRS method, ref. [6] and [7], considering 1st order statistics. The 5% and 95% percentiles, obtained with 95% confidence, have been chosen to represent the two-sided uncertainty band. Therefore, Wilks formula (equation (1)) determines the required number of samples/uncertainty calculations to be performed, which is **93**.

In order to perform uncertainty analysis with GRS method, a Probability Distribution Function has to be specified for each uncertain input parameter. As suggested by IPREM, a **uniform PDF** has been selected as the one with “minimum knowledge” about a parameter. The pressure has been identified as the relevant thermal-hydraulic response. The settings of the GRS analysis are summarized in *Table 7*.

The resulting uncertainty bands are shown in *Figure 29*. The uncertainty bands sufficiently cover the experimental data. Hence, it may be concluded that the input parameter ranges, quantified for the blowdown problem with the IPREM methodology, are consistent.

Table 7 – Edwards pipe: uncertainty analysis settings.

Parameter	Description
Method applied	GRS
Uncertainty band	[5%; 95%]
Confidence level	95%
Number of calculations	93
Probability Distribution Function of input parameters	uniform
Analyzed response	pressure

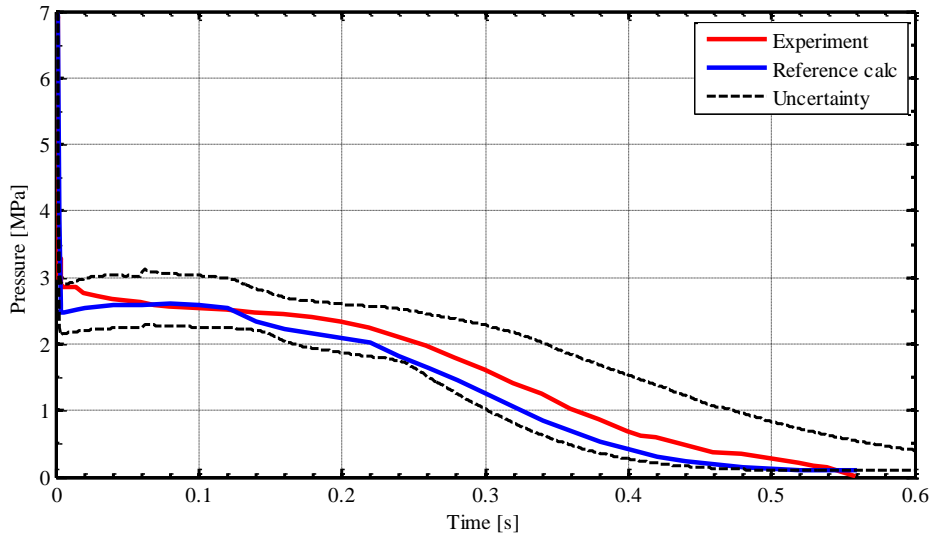


Figure 29 – Edwards pipe: evaluated uncertainty for predicted pressure response.

4 APPLICATION AND VALIDATION OF IPREM

In this section, the IPREM methodology (described in section 3) is being applied to evaluation of uncertainty of input parameters and models of code RELAP5 Mod3.3 which are relevant for the simulation of reflood phenomena. The evaluation is performed using the experimental FEBA test 216. Once the variation ranges are quantified, these results are extensively validated against numerous experimental tests through uncertainty analysis of thermal-hydraulic calculations. Additional analyses have been performed in order to provide an “Internal Qualification” (using the same FEBA test 216) and “External Qualification” (using other experimental tests) of the IPREM:

- Internal Qualification
 - Perform sensitivity analysis on consistency of chosen value of **limit = 0.22**;
 - Perform sensitivity analysis on selection of type of PDF for quantified ranges;
- External Qualification
 - Perform test-independence check: apply IPREM to FEBA test 222 (same geometry but different boundary conditions) and to compare the obtained variation ranges of input parameters and consequent uncertainty bands of thermal-hydraulic calculations with those obtained from test 216.
 - Perform facility-independence check: apply IPREM to PERICLES test RE79 (different geometry but similar boundary conditions) and to compare the obtained variation ranges of input parameters and consequent uncertainty bands of thermal-hydraulic calculations with those obtained from FEBA test 216.
 - Perform code-independence check: apply IPREM to CATHARE2 T-H code to obtain input parameter variation ranges from FEBA test 216 and further validate those against thermal-hydraulic calculations of tests FEBA and ACHILLES.

These steps of performed analysis in the framework of PhD research are shown in *Figure 1*. *Table 8* summarizes the experimental tests used during the application and validation of IPREM against reflood phenomena. The *Table 9*, *Table 10* and *Table 11* provide main boundary conditions of considered experimental tests.

Table 8 – Experimental tests used during the application and validation of IPREM against reflood phenomena.

		RELAP5						CATHARE2	
		Application	Validation	Internal Qualification		External Qualification		Application	Validation
				limit	PDF	Test-independence	Facility-independence		
FEBA	223		X						
	216	X		X	X	V*	V*	X	
	220		X						
	218		X						
	214		X						X
	222		X			X			
PERICLES	RE62		X						
	RE64		X						
	RE69		X						
	RE79		X				X		
	RE80		X			V*	V*		
	RE86		X						
ACHILLES	A1R030		X						X
	A1R048		X						X

* V - experimental tests used to validate the evaluated input parameter uncertainties from test X

Table 9 – Boundary conditions of FEBA tests.

Test	Reflood rate, cm/s	Pressure, bar	Liq. temperature, °C	Bundle power, kW
223	3.8	2.2	44-36	120% ANS
216	3.8	4.1	48-37	120% ANS
220	3.8	6.2	49-37	120% ANS
218	5.8	2.1	42-37	120% ANS
214	5.8	4.1	45-37	120% ANS
222	5.8	6.2	43-36	120% ANS

Table 10 – Boundary conditions of PERICLES tests.

Test No	Φ_{nom} (HA) W/cm ²	Φ_{nom} (CA) W/cm ²	F_{xy}	GO (HA) g/cm ² s	GO (CA) g/cm ² s	T_{wi} (HA) °C	T_{wi} (CA) °C	DT °C	P (bar)
RE62	2.93	2.93	1	3.6	3.6	600	600	60	3
RE64	4.2	2.93	1.435	3.6	3.6	600	475	60	3
RE69	2.93	2.93	1	3.6	3.6	475	475	60	3
RE79	4.2	2.93	1.435	3.6	3.6	600	475	90	3
RE80	4.2	2.93	1.435	5	5	600	475	60	3
RE86	4.2	2.93	1.435	3.6	3.6	600	475	60	4

Table 11 – Boundary conditions of ACHILLES tests.

Test	Pressure [bar]	Reflood rate [cm/s]	Inlet subcooling [C]	Max linear heat rate [W/cm]
A1R030	2.1	2.0	24	11.5
A1R048	2.1	4.0	24	11.5

4.1. Reflood in Nuclear Safety

Large break scenarios involve a very rapid depressurization with significant emptying of the primary system and core uncover taking place within only tens of seconds. When the primary system pressure falls below the injection pressure of the various ECC systems, borated coolant enters the primary system and flows through the available paths to refill the lower-plenum and then to reflood and finally recover the core.

The reflood phase begins as soon as the ECC reaches the hot fuel rods at the bottom of the core. A quench front is formed on the fuel rods and large amounts of steam are generated by the energy released from the rods at a high temperature. This steam produces a back-pressure opposing the driving head of coolant in the annulus and thereby slowing or even reversing the water level rise in the core. Thus, reflooding of the core proceeds with level oscillations (strong at the beginning, moderate later) occurring in both the core and downcomer.

The quenching front progression can be followed by cladding temperature measurements located on different axial levels in the fuel rod. Thermocouples both on the inner and outer sides of the cladding have been demonstrated to provide useful data. Due to the time constants of the thermocouples there is only limited possibility for measuring the rapid cooling characteristics in the precursory phase and during the final rewetting. The filler material of the fuel rod simulator also has a significant effect to the rewetting characteristics.

In addition to the surface temperature measurements it is essential that the two-phase flow parameters are measured sufficiently accurately. The minimum instrumentation includes:

- system pressure measurements;
- pressure difference measurements for the core water inventory;
- water inventory measurement in the upper plenum;
- inlet flow measurement both for the net flow and for oscillations.

For a more detailed analysis, useful instrumentation includes:

- steam temperature measurement above the swell level;
- droplet size distribution;
- entrained water weighting;
- cladding temperature measurements in different circumferential positions.

Table 12 provides a list of some Separate Effect Test Facilities, ref. [45], investigating reflood-related phenomena. Table 13 provides the list of Integral Test Facilities, ref. [46], simulating Large break LOCA including reflood phase which are suitable for code assessment.

Table 12 – List of SETF investigating reflood.

Facility	Notes	Relevant parameters ranges		
		Pressure (MPa)	Inlet mass flow (kg/m ² s)	Heat flux (W/cm ²)
REWET-II	Triangular array	0.1-1.0	0-15	20
PERICLES rectangular	Rod bundle	0.2-0.4	0-5	30-90
PERICLES cylindrical	Rod bundle	0.2-0.4	1-19	60
TPTF JAERI	Core heat transfer, PWR and BWR bundle	0.5-12	≤ 120	≤ 20
SCTF JAERI	Large scale	0.6	-	10 MW
CCTF JAERI	Large scale, system	0.6	-	10 MW
GÖTA BWR ECC	Spray cooling, bundle	0.1-2.0	0.045-2.20 kg/s	150-350 kW
ACHILLES reflood loop	PWR bundle	0.3	4 cm/s	220 kW
NEPTUN-I and -II	Bundle	0.1-0.4	1.5-15 cm/s	80-140 kW
BWR-FLECHT/GE	Spray cooling, bundle	0.1	1.6-15 cm/s	10-390
LTSF blowdown/INEL	Single rod, bundle	7	0.4-6.0 m/s	-

Table 13 – List of ITF simulating reflood phase of LBLOCA.

Facility name	Facility scale
CCTF	1:25
LOFT	1:50
BETHSY	1:100
PKL	1:145
SEMISCALE	1:1600
ROSA-III	1:424
FIST	1:624
PIPER1	1:2200

The rewetting characteristics of the overheated core after the large LOCA was one of the most interesting research topics in 70's and still has a significant influence on acceptance criteria in licensing and deterministic safety analyses. The main interest is related to the maximum temperature in the core, but this turn-over temperature is determined by the liquid dispersed flow well before quenching. Depending on the amount of water available the cooldown takes place earlier or later.

The large temperature gradient in the cladding gives rise to a mechanical stress on the cladding and it may affect fuel damage and radioactivity leakages. The rapid temperature drop is also associated with strong steam generation and this may have an effect on system characteristics including:

- liquid entrainment rate;
- counter current flow limitation in the upper tie plate;
- steam binding in the steam generator;
- multi-dimensional flow distribution in the core.

Relevant responses for reflood are:

- Rod surface temperature T_{clad} ;
- Time when rewet starts t_{rew} (i.e. time when abrupt change occurs in the rod surface temperature).

These parameters are presented in a form of time trends of rod surface temperature as shown on *Figure 30*. Additionally, the information on quench front propagation can be summarized plotting the quench front elevation versus time of its occurrence as presented on *Figure 31*.

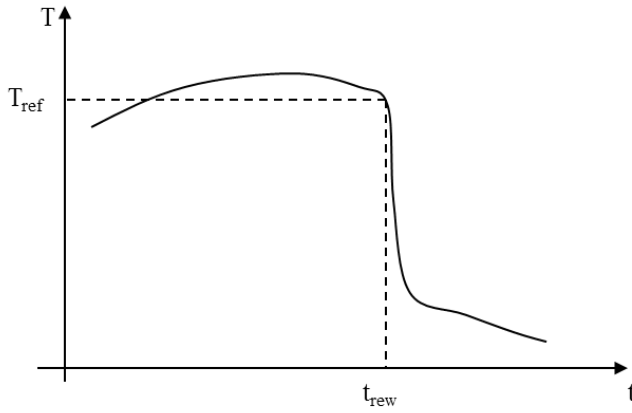


Figure 30 – Example of rod surface temperature time trend during reflood.

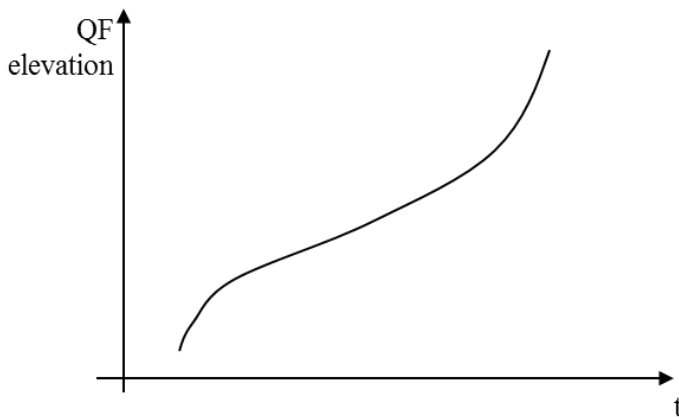


Figure 31 – Example of quench front propagation time trend during reflood.

4.2. Application of IPREM: quantification of variation ranges of reflood-related input parameters of RELAP5 code

4.2.1. Description of FEBA facility

The FEBA/SEFLEX program has been performed at KfK Karlsruhe, Germany, ref. [47] and [48]. The test facility was designed for the reflooding tests with possibility of maintaining constant flooding rates and constant back pressure. The test section consists of a full-length 5 x 5 rod bundle of PWR fuel rod dimensions utilizing electrically heated rods with a cosine power profile approximated by 7 steps of different power density in axial direction. The rod bundle is placed in housing made of stainless steel and insulated with Triton Kao Wool to reduce heat losses to environment. The cross-section of the FEBA rod bundle is shown in *Figure 32*.

The outer diameter of the heater rod is 10.75 mm (*Figure 33*). The pitch of the rod grid is 14.3 mm. The dimensions of the quadratic housing are: inner side length 78.5 mm and wall thickness 6.5 mm. The inner size of the housing is chosen in such a way that the hydraulic diameter of the bundle array for all rods is the same and equal 13.47 mm. The heated length is 3900 mm. The spacers decrease the flow cross section about 20%. The applied spacers were original PWR spacers as used by KWU. The location of the spacers can be found in *Figure 34*.

Prior to the test run the fuel rod simulators were heated in stagnant steam to desired initial cladding temperature, using a low rod power. In the meantime the test bundle housing was being heated up passively to the requested initial temperature by radiation from the rods. The aim of choosing the thick wall ("active wall") was to prevent premature quenching of the wall relative to the bundle quench front progression.

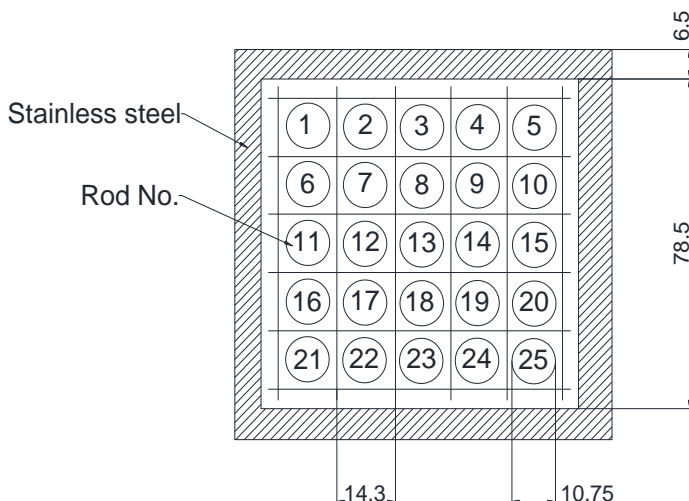


Figure 32 – FEBA rod bundle – cross-section view.

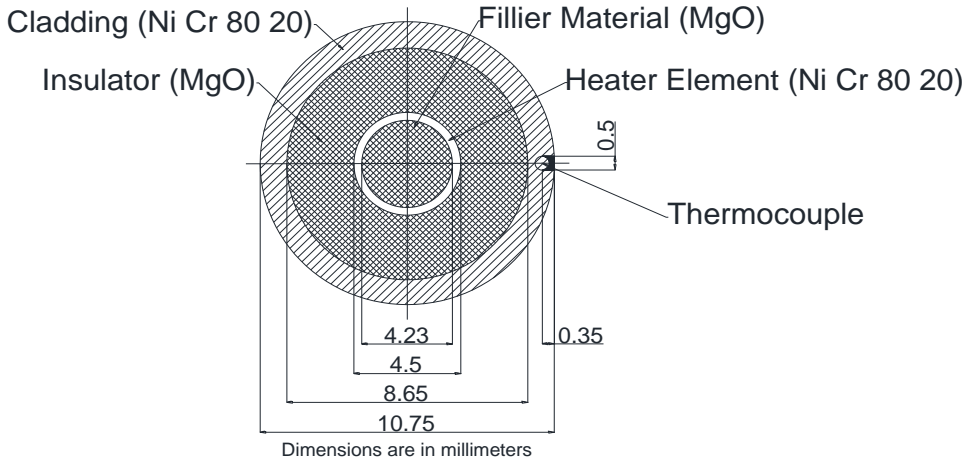


Figure 33 – Cross-section view of the FEBA heater rod.

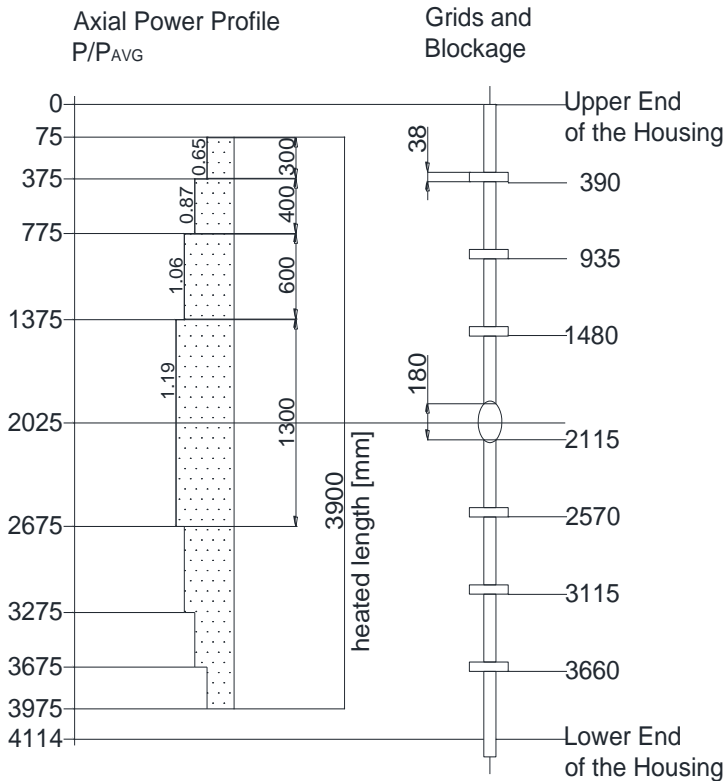


Figure 34 – Axial view of the FEBA heater rod and axial power profile distribution.

During the heat up period the inlet plenum was cooled by circulating water to maintain the desired temperature. The steam filled ducts were heated up to a temperature slightly above the saturation temperature.

By starting of the test run the bundle power was increased to the required level simulating decay heat according to 120% ANS-Standard about 40 s after reactor shut down. Simultaneously the water supply was activated.

During test runs cladding temperatures at several axial positions have been measured (*Table 14*). Pressure and pressure differences were measured with pressure transducers. In addition to inlet and outlet pressure, the pressure differences were measured along the bottom middle and upper part of the channel as well as along the whole channel. The flooding rate was measured with a turbo flow-meter. The amount of the water carried over was measured continuously by a pressure transducer at the water collecting tank.

Table 14 – FEBA cladding temperature measurements.

Label	Position from top, mm
18a4	3860
18a3	3315
18a2	2770
18a1	2225
12b4	1680
12b3	1135
12b2	590
12b1	45

4.2.2. Modeling of FEBA with RELAP5 code

A 1-D nodalization has been developed for RELAP5 Mod3.3 code, ref. [42], to model the FEBA test section (*Figure 35*). It should be noted that the model has been developed using the available description of FEBA facility and experimental measurements of test 216. However, no special tuning has been applied to get the best possible agreement with experimental data, i.e. the so called “best practice” has been used during the model development. The model consists of the heated part of test section (*pipe 110*), lower (*branch 100*) and upper plena (*branch 120*). The heated part of the section has been modeled with 20 hydraulic nodes (of 200 mm length, except for the bottom at top parts of the bundle that are modeled with 150 mm nodes). Spacer grids have been taken into account during calculation of the free hydraulic volume and the proper K_{loss} coefficients have been allocated at corresponding junctions in order to simulate the pressure loss due to flow restriction. However, no flow area reduction or change in hydraulic diameter has been modeled at locations of the spacer grids. The upper plate has been simulated by setting a proper flow area and hydraulic diameter at the junction above the heated part of the bundle. The heater rods are modeled with a single heat structure component with

power profile imposed as in experiment specifications. Additional boundary options using 9-word format have been specified for this heat structure such as heated diameter, heated length forward/reverse, grid spacer length forward/reverse etc. The housing is modeled with a heat structure, isolated on the external side. Reflood and rod bundle without cross-flow options were activated for this heat structure. The housing is modelled with a heat structure isolated on the external side. Pressure at the top, flow energy and velocity at the bottom were imposed as the boundary conditions. The main model properties are summarized in *Table 15*.

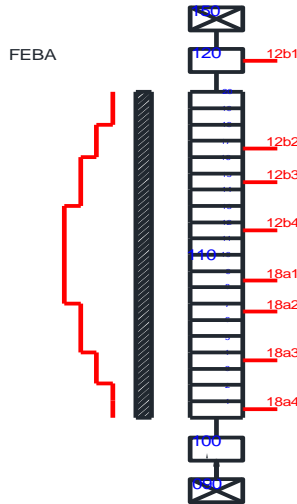


Figure 35 – Sketch of FEBA nodalization for RELAP5 code.

Table 15 – Summary of RELAP5 model of FEBA facility.

Parameter	Value
Total height/length	4.322 m
Nodes in heated length	20
Flow area	$3.893 \cdot 10^{-3} \text{ m}^2$
Hydraulic diameter	$1.347 \cdot 10^{-2} \text{ m}$
Wall roughness	$2.0 \cdot 10^{-5}$
Spacer grid K_{loss}	0.2
Total heat transfer area of the heated part of heater rods	9.034 m^2
Maximum linear heat rate	2.44 kW/m
<i>Special options activated:</i>	
Rod bundle interphase friction (b=1 in hydraulic nodes)	
Vertical bundle without cross flow (110 in heat structures)	

The boundary conditions to the model have been applied by means of time-dependent volume and time-dependent junction components:

- Pressure has been imposed by *time-dependent volume 150*
- Flooding coolant temperature has been imposed by *time-dependent volume 90*
- Flooding velocity has been imposed by time-dependent junction 95 (connecting *tm dpvol 90* and *branch 100*)
- Power has been imposed to the corresponding heat structure by means of general table with specified power curve
- Heat losses were not simulated

The model has been initialized at “cold” conditions:

- Pressure at 4.1 MPa
- Hydraulic nodes filled with vapor at saturation temperature
- No flow imposed in the nodes and boundary conditions
- Heater rod heat structure meshes initialized at vapor temperature (420 K)

The heat-up conditioning phase has been simulated in order to reach the Start of Transient (SoT) conditions. The obtained axial temperature distribution in heater rods and housing at the SoT instant are provided in the *Figure 36* below.

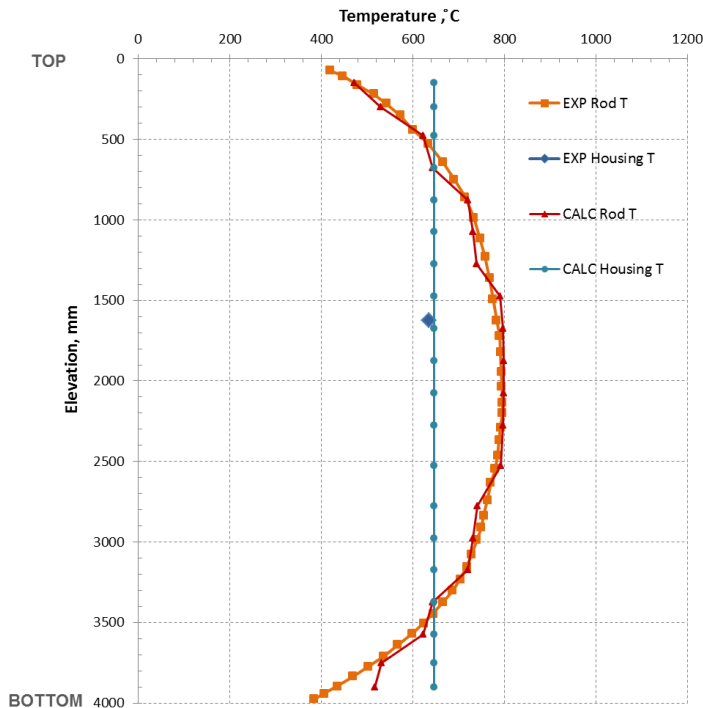


Figure 36 – FEBA test 216: predicted by RELAP5 steady-state temperature distribution.

The results of reference calculation of test 216 are shown in *Figure 37*, *Figure 38* and *Figure 39*. RELAP5 calculation underestimates the peak cladding temperature (PCT) and predicts faster quench front propagation comparing to experimental data. The quench at the very top of the bundle is simulate by RELAP5 code as top-down reflow, on the contrary to the shown bottom-up reflow in *Figure 39*, and is not considered in the framework of evaluation of uncertainty of input parameters. It should be noted that calculations have been performed as “post-test”, i.e. experimental results were available to the analyst. However, no special tuning has been applied to the model in order to achieve best agreement possible with experimental data. Instead, the observed discrepancies of calculation results using the standard nodalization practices with respect to the experimental data were deemed as acceptable.

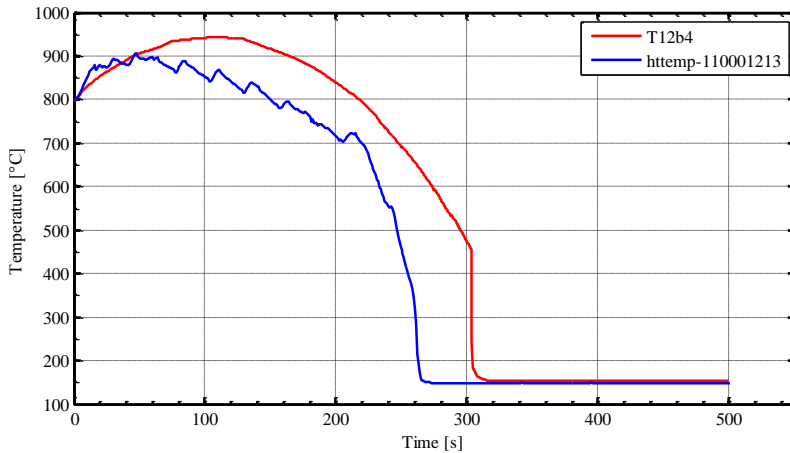


Figure 37 – FEBA test 216: predicted by RELAP5 cladding temperature at 2/3 height.

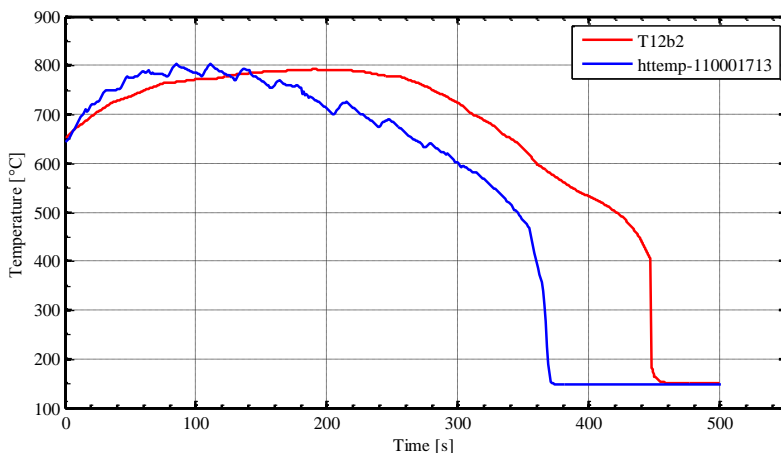


Figure 38 – FEBA test 216: predicted by RELAP5 cladding temperature at TAF.

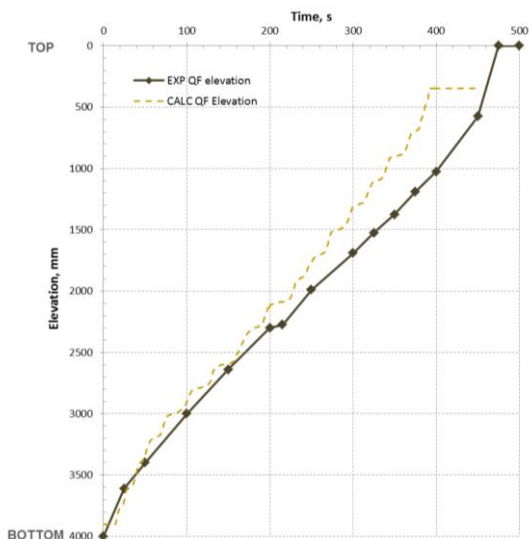


Figure 39 – FEBA test 216: predicted by RELAP5 quench front propagation.

4.2.2.1. Simulation of reflood with various TH-SYS codes

The activity, presented in section 4.2, contributed to OECD/NEA PREMIUM benchmark, ref. [49]. In Phase II of the benchmark the participants applied their codes of choice to simulate reflood phenomena in FEBA test 216 and further identified the models and parameters influential on the results of reflood simulation. Main outcomes from reflood simulation are presented in this subsection in order to demonstrate the current state-of-the-art in modeling of reflood phenomena with system thermal-hydraulic codes.

In total, 13 participating organizations submitted their results for Phase II, ref. [49]. The list of the participants and the codes applied are provided in *Table 16*. All applied codes are 1-D system thermal-hydraulic codes, except COBRA-TF module applied by KAERI which is a sub-channel code.

Most of participants adopted a nodalization representing the test section of FEBA with single vertical channel and single heater rod/heat structure. Different approaches were adopted by participants for modeling the spacer grids: some organizations actually reduced the flow area at the location of the grids and activated special models for heat transfer enhancement; others took into account the grids only by applying form loss coefficients at the corresponding elevations.

The number of axial nodes, representing the test section, in the participants' nodalizations ranges from 20 to 78 (*Figure 40*) and depends on the type of the numerical scheme adopted by each code and by the nodalization techniques adopted in different organizations. It should be mentioned, that the provided number of axial nodes does not take into account the possible refinement, as it can be the case in the vicinity of the quench front to calculate the axial conduction (whenever performed by a code).

Table 16 – PREMIUM benchmark: list of participating organizations.

Participant	Country	Code
Bel V	Belgium	CATHARE 2 V2.5_2 mod8.1
TRACTEBEL	Belgium	RELAP5/MOD3.3
NRI	Czech Republic	ATHLET 2.1A
VTT	Finland	APROS 5.11.02
CEA	France	CATHARE 2 V2.5_2 mod8.1
IRSN	France	CATHARE 2 V2.5_2 mod8.1
GRS	Germany	ATHLET 2.2B
KIT	Germany	TRACE Version 5 patch3
UNIPI	Italy	RELAP5/MOD3.3 patch3
KAERI	Republic of Korea	COBRA-TF Module of MARS-KS Code
KINS	Republic of Korea	MARS-KS-003
OKBM	Russian Federation	RELAP/SCDAPSIM/MOD3.4
UPC & CSN	Spain	RELAP5/MOD3.3 patch4

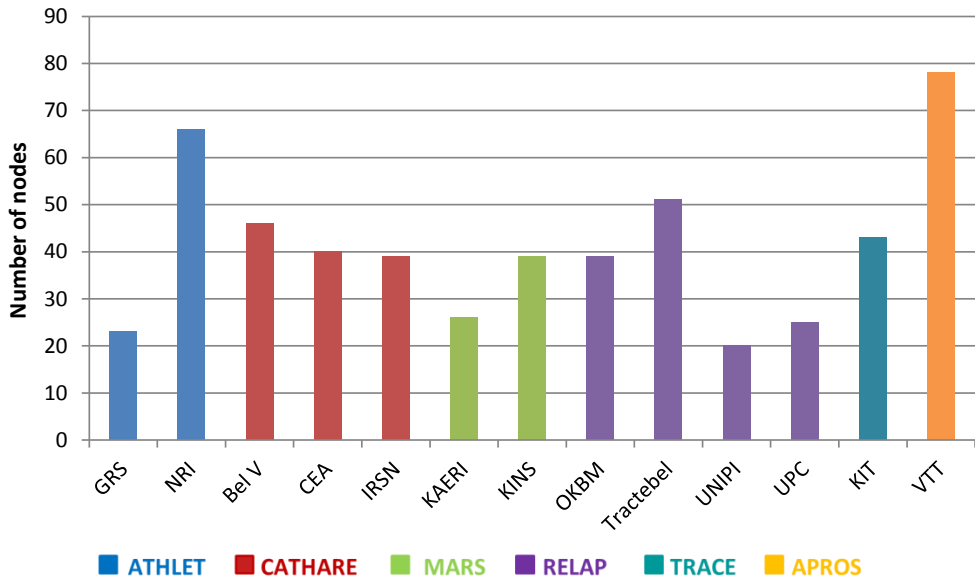


Figure 40 – PREMIUM benchmark: number of nodes in the test section.

The results of reference calculations performed by participants are shown in Figure 41, Figure 42 and Figure 43 and are summarized in Table 17.

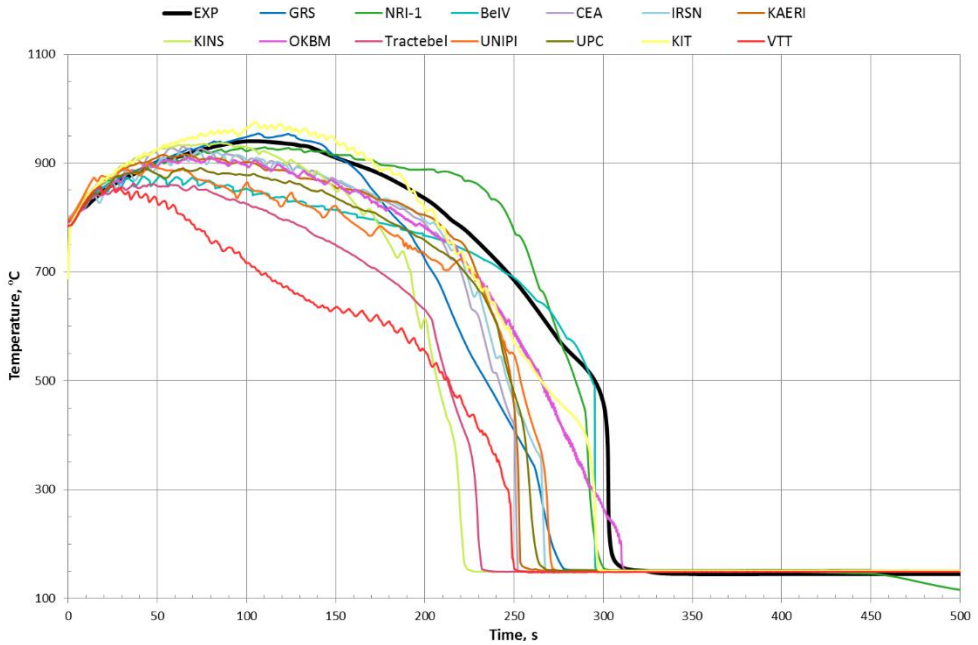


Figure 41 – PREMIUM benchmark: predicted cladding temperature at 2/3 height.

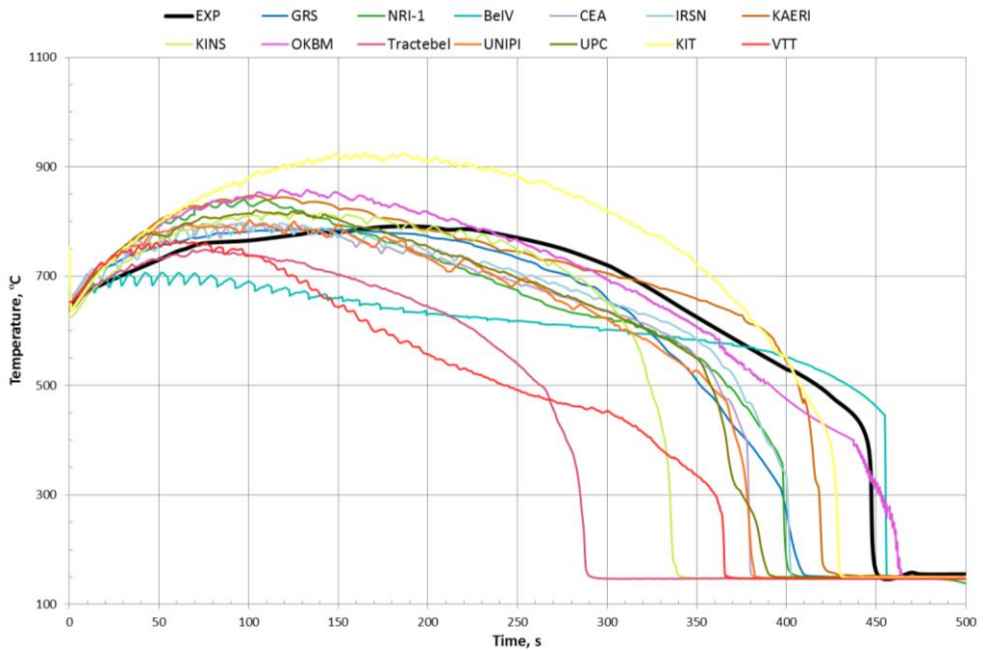


Figure 42 – PREMIUM benchmark: predicted cladding temperature at TAF.

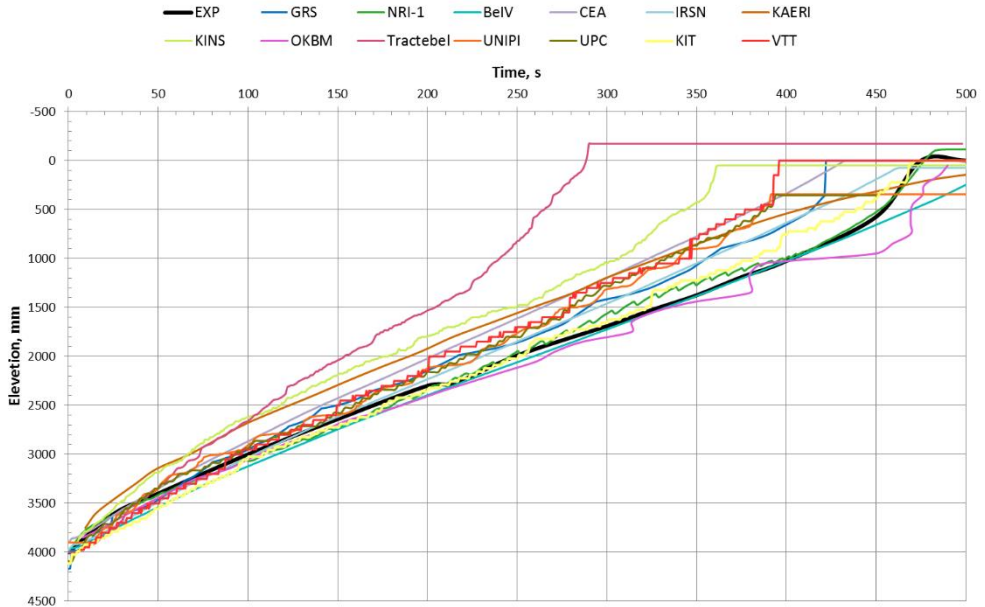


Figure 43 – PREMIUM benchmark: predicted quench front propagation.

Table 17 – PREMIUM benchmark: Summary of reference calculations.

Participant	Code	PCT, °C	Bundle quenched, s
Experiment		940	~450
GRS	ATHLET 2.2B	958	422
NRI	ATHLET 2.1A	933	477
Bel V	CATHARE 2 V2.5_2 mod8.1	877	516
CEA	CATHARE 2 V2.5_2 mod8.1	931	429
IRSN	CATHARE 2 V2.5_2 mod8.1	925	462
KAERI	MARS-KS1.3 (COBRA-TF Module)	921	587
KINS	MARS-KS-003	946	350
OKBM	RELAP/SCDAPSIM Mod3.4	915	489
Tractebel	RELAP5 Mod3.3	870	290
UNIPI	RELAP5 Mod3.3 patch3	908	378
UPC	RELAP5 Mod3.3 patch4	890	392
KIT	TRACE Version 5 patch 3	978	430
VTT	APROS 5.11.02	858	396

The calculated time trends of cladding temperature at different elevations show rather big spread, in terms of maximum temperature and time of rewet, with respect to experimentally measured data. Almost all codes, except RELAP/SCDAPSIM

Mod3.4 applied by OKBM, predict faster quench front propagation. One may also note that results of almost all the participants show somewhat oscillatory behavior which may have the numeric origins and not observed in the experimental trends.

Regarding the overall bundle behavior prediction, i.e. peak cladding temperature and bundle rewet time, most of the participants obtained rather satisfactory results with PCT ranging +42/-82 °C (*Figure 41*). It may be noted that RELAP group and APROS code generally underpredicted the PCT while TRACE code (applied only by one participant) resulted in maximum overprediction.

Considering the results presented above, the following conclusions may be outlined with regards to activity performed in the PhD thesis framework:

- Results, obtained with developed RELAP5 Mod3.3 model of FEBA facility, are consistent with the state-of-the-art simulation of reflood phenomena;
- User effect (spread of results obtained with the same code) has a significant role in accuracy of code calculations;

4.2.3. Identification of influential parameters

Once the RELAP5 model of FEBA facility has been set up and the reference calculation of test 216 has been performed, the sensitivity analysis has been performed in order to identify those code model and input parameters that are influential on results of reflood simulation.

Within the framework of Phase II of PREMIUM benchmark the following definitions, procedure and criteria for identification of influential input parameter has been proposed by the author of this thesis, ref. [50].

The definitions attributing to the “selection of influential input parameters (IP)” concept are introduced. An example of classification of input parameters according to introduced definitions is provided on *Figure 42*.

- **Response (R):** A physical quantity that can be measured or deduced (calculated) from measurements (e.g. cladding temperatures, time when rewet starts, etc.)
- **Input Global Parameter (IGP):** An IP associated with a physical model (e.g. heat transfer coefficient)
- **Input Basic Parameter (IBP):** An IP that can be
 - BIC parameter: e.g. mass flow rate, power, etc.
 - Geometrical parameter: e.g. hydraulic diameter
 - Material property parameter: e.g. conductivity of zircaloy, UO₂, etc.
 - Discretization parameter: e.g. length of nodes, size of meshes, etc.
- **Input Coefficient Parameter (ICP):** a single coefficient inside a correlation with can be distinguished as follows
 - A parameter accessible from input deck for a code: e.g. K_{loss} coefficients in RELAP
 - A numerical constant value not accessible from input deck
 - A derived quantity parameter: e.g. quality, Re , etc.

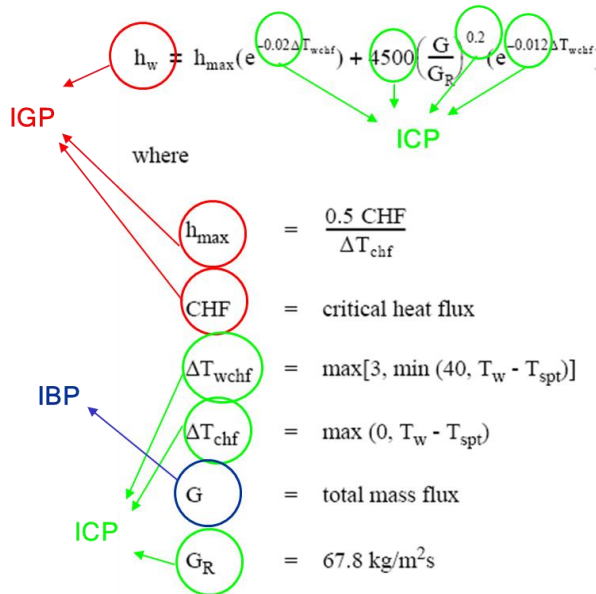


Figure 44 – Example of classification of Input Parameters for Weismann correlation.

The procedure for identification of influential has been proposed to participants of the benchmark (*Figure 45*):

- **Step #1:** Set up an initial list of IP. In order to develop a preliminary list of input parameters, the participant should use their knowledge of the related phenomena physics and corresponding correlations implemented in the code intended for use. At this stage an engineering judgment may be applied to sort out immediately non-influential parameters.
- **Step #2:** The best-estimate values of all the IP from the preliminary list shall be selected and documented. A code reference calculation to be performed and main responses to be documented.
- **Step #3:** Set up and document criteria for selection of influential input parameters.
- **Step #4:** Perform a number of required sensitivity code runs corresponding to the methodology (criteria) set up at the Step #3. One code calculation should be performed for a single variation of a single IP from the preliminary list. Main responses for each sensitivity run to be documented.
- **Step #5:** Apply the criteria for selection of influential Input Parameters. At this stage, the use of engineering judgment shall be minimized. If an analyst decides to keep the parameter that does not meet the criteria, a reasonable justification shall be provided.
- **Step #6:** Document the list of influential Input Parameters and supposed range of variation and/or PDF (if available).

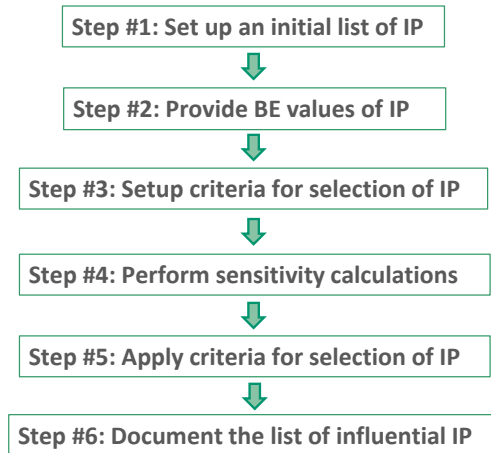


Figure 45 – Procedure for identification of influential Input Parameters.

After an initial list of input parameters has been set up by an analyst and the required sensitivity studies have been performed, a selection of influential IP is performed. With regard to reflood phenomena, the following set of criteria has been adopted: An influential IP has to be such that its extreme value in the range of variation causes the following change in the either of two main reflood responses (at least one out of two criteria should be fulfilled):

- **Criterion #1:** The absolute value of variation in rod surface temperature T_{clad} is $\Delta T_{\text{ref}} = 50\text{K}$ (see Figure 46);
- **Criterion #2:** The variation in rewet time t_{rew} is $\Delta t_{\text{rew}} = 10\%$ (see Figure 46).

Additionally, a confirmation criterion may be applied with respect to the quench front propagation:

- **Criterion #3:** The variation in elevation of the quench front versus time $\Delta QF_{\text{elev}} = 10\%$ (see Figure 47).

Once the potential influential IP have been selected, the following criteria must be applied in order to ensure the “realism” of these Input Parameters:

- **Criterion #4:** Limited qualitative impact on the responses’ time trends. Notably, the variation of an IP should not cause the drastic changes in rod surface temperature time trends (sudden deviations, oscillations) which may be caused by phenomenology different from that of reflood or by physical or numerical instabilities.
- **Criterion #5:** The range of variation (to make the parameter “influential”) shall be consistent with the level of knowledge on the correspondent IP, e.g. the change in Zr density cannot be larger than the real known physical limits.
- **Criterion #6** (if applicable): In case a preliminary uncertainty evaluation is available, the range of variation of the single IP should not be responsible of the overall uncertainty of the responses.

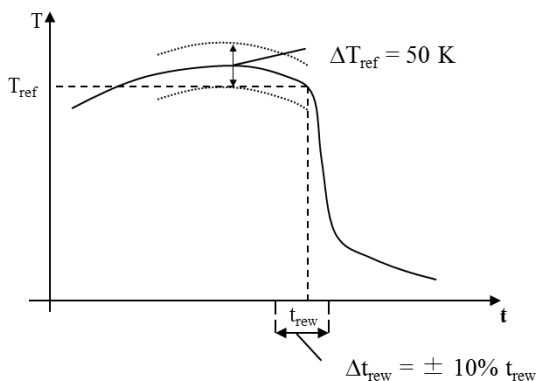


Figure 46 – Illustration of criteria #1 and #2 for selection of influential input parameters.

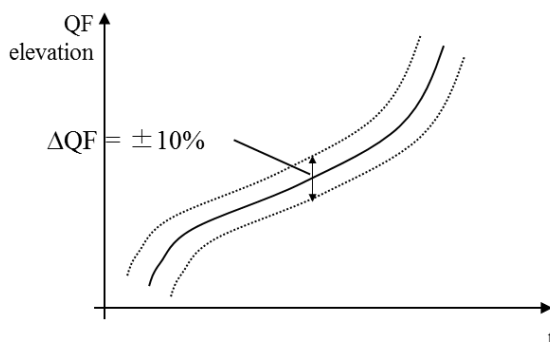


Figure 47 – Illustration of criterion #3 for selection of influential input parameters.

Regarding application of RELAP5 code to reflood phenomena, a list of initially considered input parameters has been established (*Table 18*). RELAP5 correlations (representative coefficients) have been also considered as input parameter. The detailed description of reflood-related RELAP5 correlation is provided in Appendix A.

It shall be noted that by default, in the “frozen” version of RELAP5 Mod3.3 code, there is no possibility to perform a direct sensitivity analysis with constituent correlations (e.g. interphase heat transfer). Therefore, in order to achieve the assigned goals, the RELAP5 Mod3.3 source had to be modified to be able to perform sensitivity studies on selected physical models of the code. These modifications make provisions for introduction of multipliers on the concerned models in the source code of RELAP5 Mod3.3. After such modification and code re-compilation, the values of multipliers are conveniently read by the code from an external text file, allowing to perform extensive sensitivity studies. More detailed information is provided in Appendix B.

After the performing a sensitivity analysis of calculation with single-parameter variation from the initial list of parameters and applying the criteria for identification of influential input parameters, the list of influential parameters has been defined. The list is presented in the *Table 19* together with the preliminary variation range of

the selected parameters and corresponding variations of responses of interest (cladding temperature and time of rewet) at selected elevations.

It may be noticed that only the considered RELAP5 correlations turned up to be influential enough on reflood simulation, while sensitivities on boundary conditions and nodalization parameters (e.g. material properties or pressure loss coefficients) did not result in significant variation of PCT or time of rewet. Hence, the following parameters (representative of corresponding correlations) have been identified as influential for reflood:

- IGP - Interphase heat transfer coefficient
- IGP - Interphase friction coefficient
- IGP - Film boiling heat transfer coefficient
- IGP - Convection to vapor heat transfer coefficient
- ICP - Minimum droplet diameter

Only the resulting interphase friction coefficient has been kept, since the interphase drag for bubbles and drops contributes to the former.

Table 18 – Reflood: list of initially considered input parameters for RELAP5 code.

Input Basic Parameter	
1	Pressure
2	Flooding velocity
3	Fluid temperature
4	Ni Cr Thermal conductivity
5	Ni Cr Heat capacity
6	MgO Thermal conductivity
7	MgO Heat capacity
8	Housing initial temperature
9	Power
10	Grid pressure loss coefficient
Input Global Parameter	
1	Film boiling heat transfer coefficient
2	Transition boiling heat transfer coefficient
3	Junction interface friction coefficient
4	Effective interface friction coefficient
5	Interphase heat transfer
Input Coefficient Parameter	
1	Droplet Weber (critical) number
2	Minimum droplet diameter
3	Quench front threshold distances for HTC transitions

Table 19 – Reflood: identified influential input parameters RELAP5 code for reflood simulation.

Parameter	Subroutine	Fortran variable / Key word	Multiplier REF / REF value	Multiplier MIN	Multiplier MAX	T _{clad} variation [°C]	Position [mm]	t _{rew} variation [s]	Position [mm]
Film boiling wall-to-fluid HTC	PSTDNB	hfb	1.0	0.5	3.0	+13 / -34	1680	+58 / -62	1680
Film boiling wall-to-vapor HTC	PSTDNB	hv	1.0	0.65	4.0	+59 / -44	1680	0 / -30	675
Junction interphase drag for bubbles and droplets	FIDIS2	fic	1.0	0.5	1.5	-15 / +15	1680	-46 / +40	1680
Resulting interphase friction at junctions	PHATNJ	fij	1.0	0.5	1.5	-12 / +11	1680	-55 / +45	1680
Interphase heat transfer in dispersed flow for dry wall	DISPDRYHIF	hifc, hign, hgfc	1.0	0.2 ^{/1/}	5.0 ^{/1/}	+79 / -56	675	+31 / -85	675
Minimum droplet diameter ^{/2/}	FIDIS2 & FIDISV	dcon(2)	1.5 mm	0.7 mm	2.5 mm	0 / 0	675	+55 / -48	675

/1/ The multiplier has been simultaneously applied for all three partitions of the interphase heat transfer

/2/ The multiplier has been simultaneously applied in both subroutines

The identification of influential reflood-related input parameters has also been performed in the framework of Phase II of PREMIUM benchmark, ref. [49]. Following the base case calculation, each participant compiled an initial list of considered influential input parameters. Each participant considered about 20 parameters, except VTT and KIT who initially considered 40 and 56 parameters respectively.

In total, 72 various input parameters were considered by all participants. These parameters were categorized into Input Basic Parameters (IBP), Input Global Parameters (IGP) and Input Coefficient Parameters (ICP) according to the definitions in presented above. This resulted in 26 IBPs, 14 IGPs and 33 ICPs. To each parameter an Identification Number (ID) has been assigned for further convenient reference.

Due to the variety of considered parameters and to the fact that IGP and ICP are code dependent, this list was not easy to establish. Therefore, some actual code-specific parameters considered by participants, such as “forced convection with vapor” or “film boiling heat transfer” are represented by the single “wall heat transfer” parameter (parameter ID 27). In *Figure 48* the statistics shows which parameters were chosen by the majority of the participants. The input parameters considered by majority of participants are listed in *Table 20*.

As the following step, participants performed the sensitivity studies and selected the most influential parameters. The criteria used for selection differ from one participant to another. Some organizations applied the set of criteria proposed in Specifications for Phase II (recited in above), some participants used the proposed criteria as a base but modified the quantitative thresholds (e.g. $\Delta T_{ref} = 30K$ instead of 50K), others applied their own methodology.

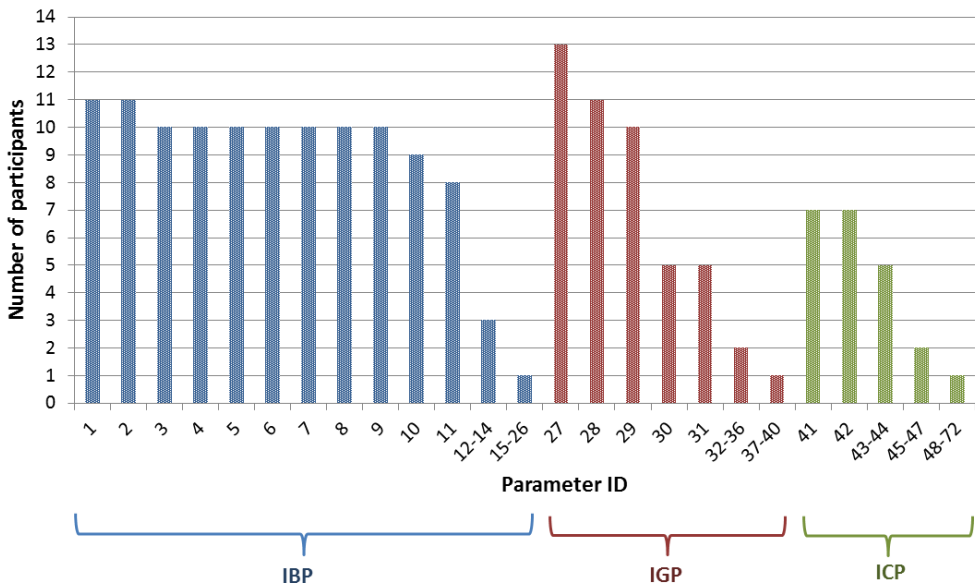


Figure 48 – PREMIUM benchmark: Initially considered input parameters.

Table 20 – PREMIUM benchmark: Input parameters initially considered by majority.

ID	Parameter
Input Basic Parameters	
1	Inlet liquid temperature
2	Power/power density
3	Pressure
4	Inlet liquid mass flow/flux/velocity
5	Thermal conductivity of heater
6	Heat capacity of heater
7	Thermal conductivity of insulation
8	Heat capacity of insulation
9	Spacer Form loss coefficients
10	Initial wall temperatures
11	Hydraulic diameter
12-26	...
Input Global Parameters	
27	Wall heat transfer
28	Interfacial friction
29	Interphase heat transfer
30	Wall friction
31	Heat transfer (enhancement) at the quench front
32-40	...
Input Coefficient Parameters	
41	Droplet diameter
42	Droplet critical Weber number
43-72	...

Applying the adopted set of criteria, participants identified the input parameters, influential for their reflow models. The statistics on influential input parameters identified by participants is shown in *Figure 49* (to compare with *Figure 48*). Therefore, out of total 72 input parameters, initially considered by all participants, only 6 were identified as influential by more than 4 participants:

- Bundle power
- Wall heat transfer coefficient
- Interphase friction coefficient
- Interphase heat transfer coefficient
- Heat transfer (enhancement) at the quench front
- Droplet diameter

It can be seen that results, obtained within the framework of current research activity, are in good agreement with the pool of benchmark participants.

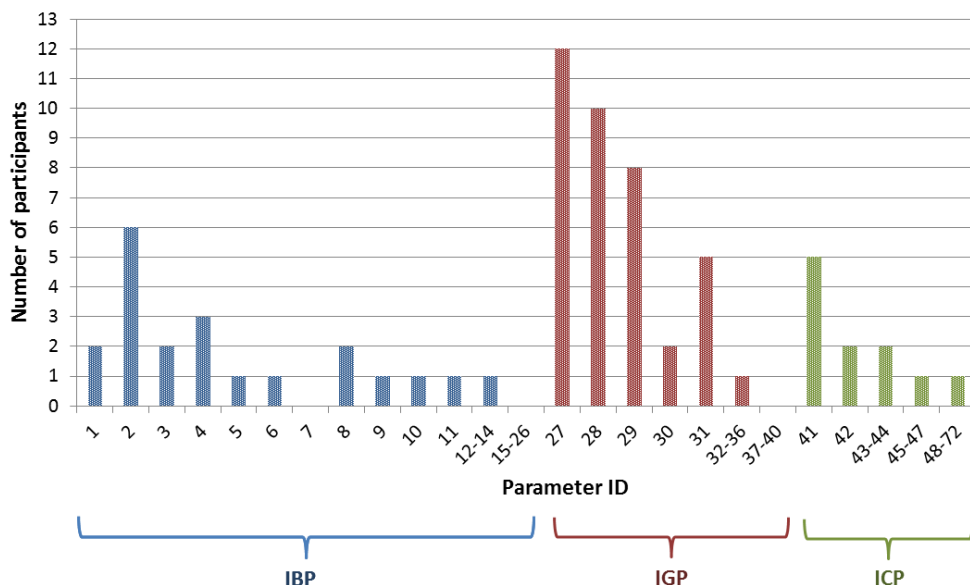


Figure 49 – PREMIUM benchmark: Identified influential input parameters.

Additionally, for each of 6 input parameters (except “heat transfer (enhancement) at the quench front”) identified by majority as influential a data has been provided with indicated range of variation of input parameter and variation of maximum cladding temperature at selected elevation (2225 mm or 1680 mm) and time of rewet at this elevation which correspond to extremes of the aforementioned range. It is worth to show these variations of responses vs. input parameter variations for some influential input parameters.

Eleven participating organizations identified heat transfer coefficient at the wall (ID 27) as an influential input parameter (Figure 49). It may be noticed that variations in cladding temperature show non-linear behavior (Figure 50). The observed behavior is also different between the different codes but more similar for the same code (e.g. RELAP5 or CATHARE “groups”). On the contrary, the variations in time of rewet show significant spread between the different participants and codes (Figure 51).

Ten participating organizations identified interphase friction coefficient (ID 28) as an influential input parameter (Figure 49). The variation ranges chosen by the participants are very different. They range from rather large variations for CATHARE code chosen by CEA and for APROS by VTT to quite small variations ranges chosen for RELAP by OKBM and for TRACE by KIT. Importantly, a contrary (positive and negative) change of cladding temperature with interphase friction variation by participants can be observed (Figure 52). It may be noted that the smaller variation of interfacial friction performed for RELAP by OKBM leads to the larger variation of cladding temperature observed among all RELAP users (which suggests the nodalization-dependency).

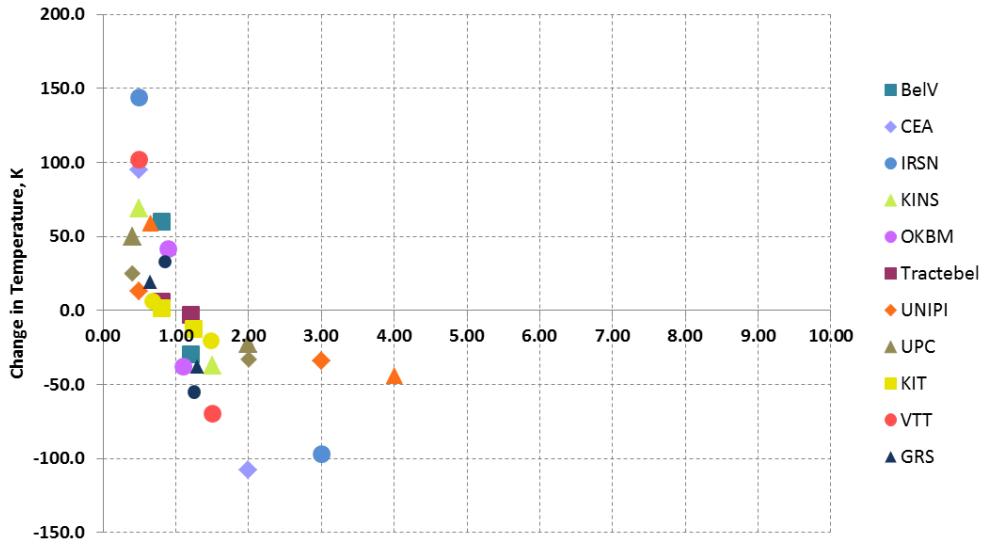


Figure 50 – PREMIUM benchmark: Cladding temperature vs. Wall HTC (multiplier).

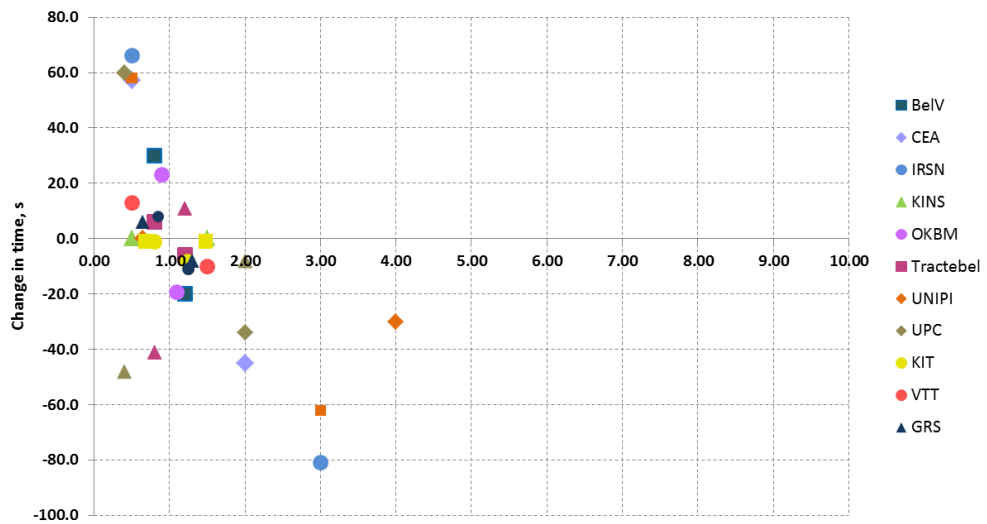


Figure 51 – PREMIUM benchmark: Time of rewet vs. Wall HTC (multiplier).

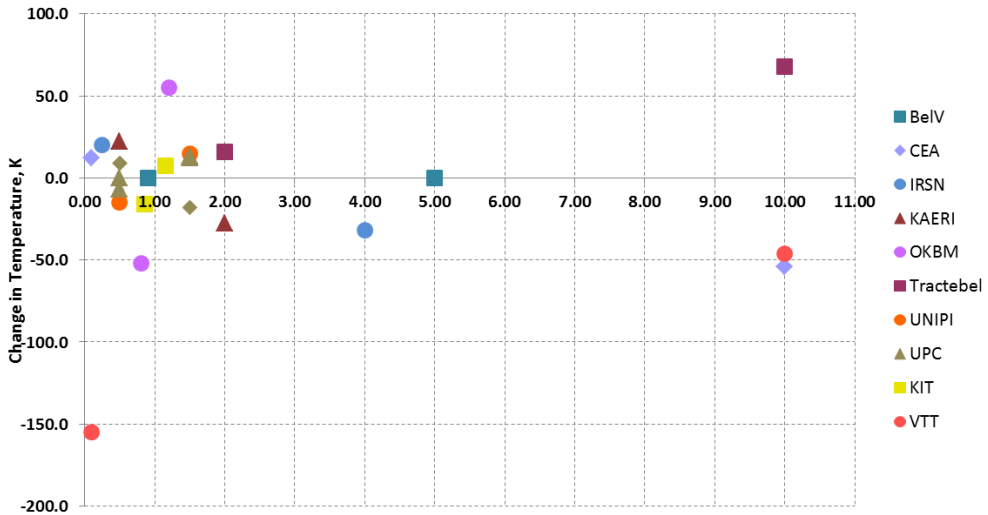


Figure 52 – PREMIUM benchmark: Cladding temperature vs. Interphase friction coefficient (multiplier).

Therefore, an important observation can be drawn from the results presented above: the change in calculation results of different codes may be rather different (even contrary) with a change of the same physical model (i.e. interphase friction). This stresses the importance of availability of code-specific uncertainties of input parameters in order to perform valid uncertainty analysis of a thermal-hydraulic calculation.

4.2.4. Quantification of input parameter uncertainties

IPREM methodology has been further applied for identified influential input parameters. It should be noted that the RELAP5 parameter “minimum droplet diameter” has been discarded from the further analysis since it contributes to other analyzed parameters like interphase friction or heat transfer. Therefore, the following parameters have been identified to be subjected to IPREM analysis:

- α_1 – Multiplier to interphase heat transfer coefficient (HTC)
- α_2 – Multiplier to interphase friction
- α_3 – Multiplier to film boiling HTC
- α_4 – Multiplier to convection to vapor HTC

For each of these 4 input parameters the reference values are $\{\alpha^{ref}\} = 1$ since, essentially, they are multipliers to the code default values.

The following parameters have been selected as responses $\{R\}$ from the pool of available measurement channels:

- 1) Cladding temperature at location 12b4 (where experimental PCT is observed)
- 2) Cladding temperature at location 12b2 (top of heated part)
- 3) Quench front elevation (QF)

These 3 responses represent at best the relevant issues of reflood in nuclear safety: Peak Cladding Temperature and the time of core quench.

At the next step, the FFTBM tool has been applied to calculate $\{AA^{R-E}\}$ (comparison of reference calculation and experimental data). The results are shown in *Table 21*. It may be noticed that quench front Average Amplitude $AA3^{R-E}$ is lower than corresponding value for cladding temperature responses $AA1^{R-E}$ and $AA2^{R-E}$. This is consistent with the discrepancy between predicted cladding temperature and experimental data, while predicted quench front elevation shows a visible better agreement with experiment.

Table 21 – FEBA 216 IPREM settings for reference calculation.

	Parameter	Value
AAz^{R-E}	$AA1^{R-E} - 12b4$	0.342
	$AA2^{R-E} - 12b2$	0.387
	$AA3^{R-E} - \text{quench front}$	0.135
W_z	$w_t - \text{cladding temperature}$	0.357
	$w_{qf} - \text{quench front}$	0.286
AAG	AAG^{R-E}	0.299

The “cladding temperature” and “quench front elevation” weights W_z from *Table 3* are used in equation (26) in order to calculate weights w_z for the responses (shown in *Table 21*). Finally, the Global Average Amplitude value AAG^{R-E} is computed with equation (25) to characterize the performance of the entire model in reference case against experimental data.

As the next step, a series of j (about 15) sensitivity calculations have been performed with various values for each of 4 input parameters α_i . FFTBM tool has been applied twice to each of these sensitivity calculations in order to quantify:

$$\bullet \begin{bmatrix} AA1_{1j}^{S-R} & AA1_{2j}^{S-R} & AA1_{3j}^{S-R} & AA1_{4j}^{S-R} \\ AA2_{1j}^{S-R} & AA2_{2j}^{S-R} & AA2_{3j}^{S-R} & AA2_{4j}^{S-R} \\ AA3_{1j}^{S-R} & AA3_{2j}^{S-R} & AA3_{3j}^{S-R} & AA3_{4j}^{S-R} \end{bmatrix}$$

$$\bullet \begin{bmatrix} AA1_{1j}^{S-E} & AA1_{2j}^{S-E} & AA1_{3j}^{S-E} & AA1_{4j}^{S-E} \\ AA2_{1j}^{S-E} & AA2_{2j}^{S-E} & AA2_{3j}^{S-E} & AA2_{4j}^{S-E} \\ AA3_{1j}^{S-E} & AA3_{2j}^{S-E} & AA3_{3j}^{S-E} & AA3_{4j}^{S-E} \end{bmatrix}$$

Obtained values AAz_{ij}^{S-R} and AAz_{ij}^{S-E} (where z ranges from 1 to 3) are plotted in *Figure 53*, *Figure 54*, *Figure 55* and *Figure 56* for each of 4 input parameters α_i . For interphase heat transfer coefficient (*Figure 53*) a steady improvement of calculation results with respect to experimental data while reducing values of α_1 may be noticed from AAz_{1j}^{S-E} trends.

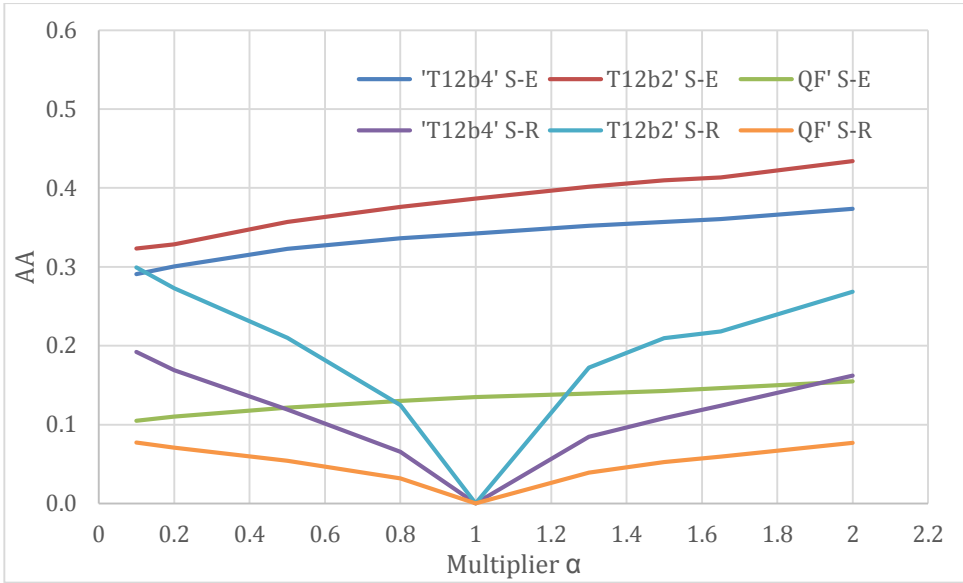


Figure 53 – FEBA 216: AAz_{1j}^{S-R} and AAz_{1j}^{S-E} for interphase HTC.

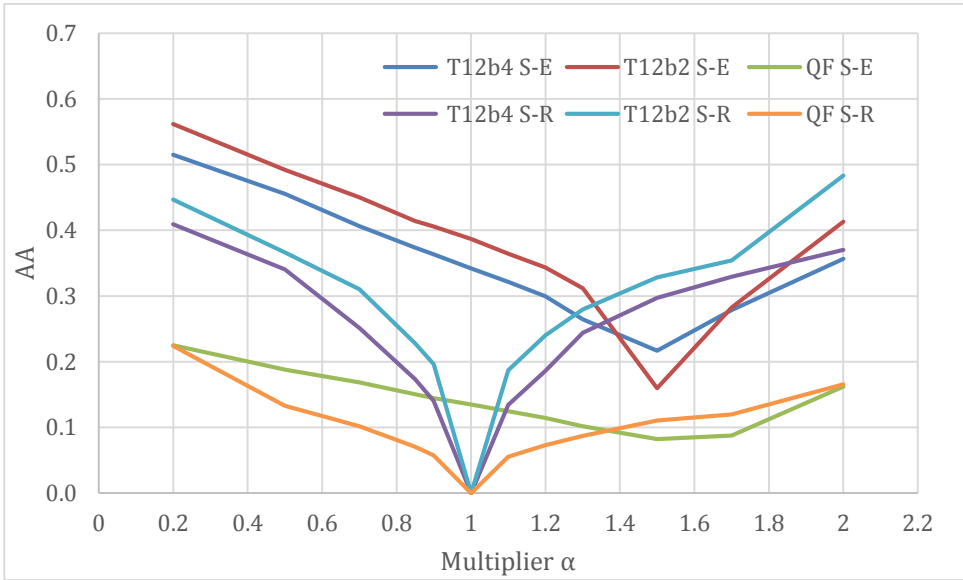


Figure 54 – FEBA 216: AAz_{2j}^{S-R} and AAz_{2j}^{S-E} for interphase friction coefficient.

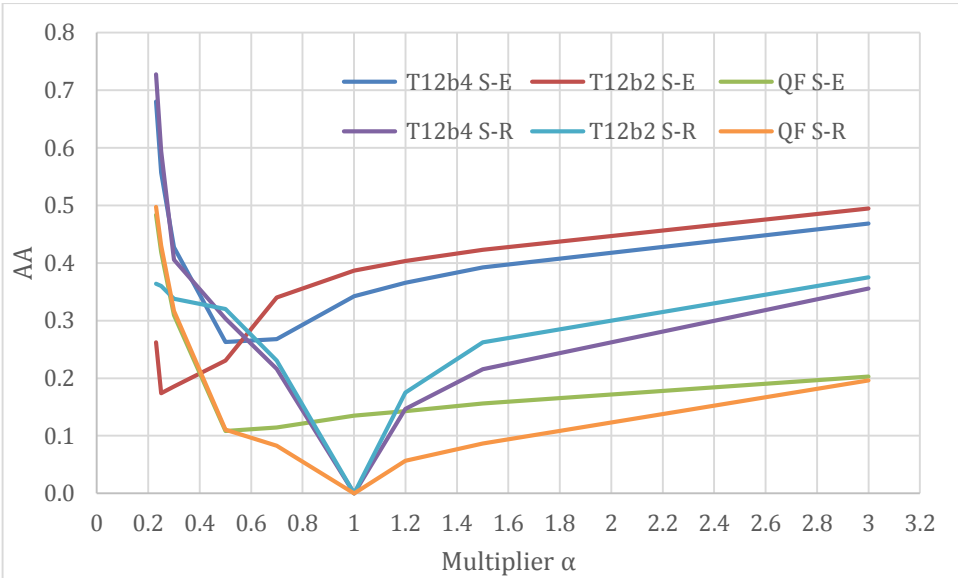


Figure 55 – FEBA 216: AAz_{3j}^{S-R} and AAz_{3j}^{S-E} for film boiling HTC.

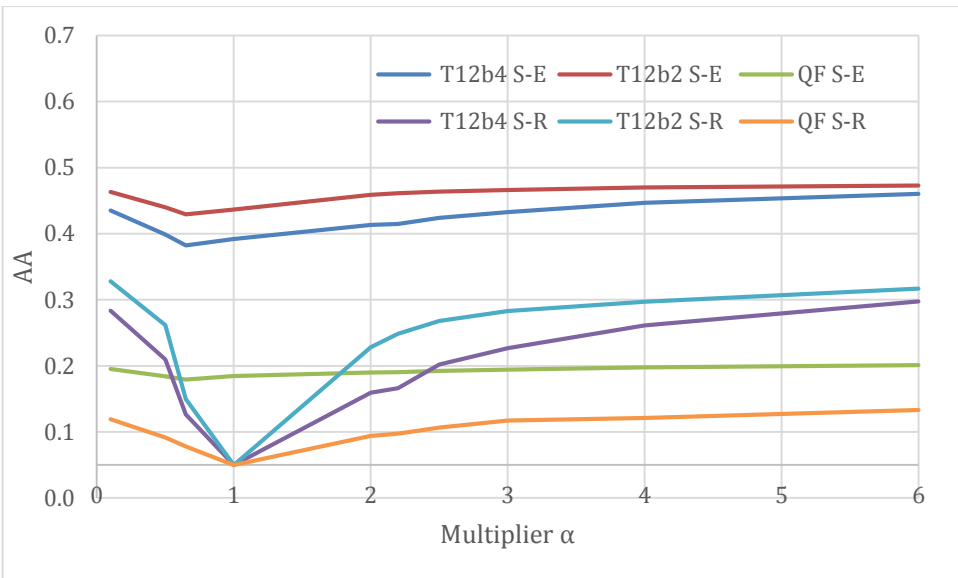


Figure 56 – FEBA 216: AAz_{4j}^{S-R} and AAz_{4j}^{S-E} for convection to vapor HTC.

For interphase friction coefficient (Figure 54) the best agreement of calculation results with respect to experimental data is achieved at the value of $\alpha_2 \approx 1.5$. Reducing the film boiling HTC (Figure 55) results in improvement of code prediction with the minimum values of AAz_{3j}^{S-E} achieved at $\alpha_3 \approx 0.5$. Variations in convection to vapor HTC do not result in drastic changes of AAz_{4j}^{S-E} , although there is a tendency in improvement of code calculation while decreasing the multiplier.

At the next step the equation (25) has been applied to all AAz_{ij}^{S-R} and AAz_{ij}^{S-E} given weights presented in *Table 21*, in order to calculate the pairs of Global Average Amplitude (AAG_{ij}^{S-R} and AAG_{ij}^{S-E}) for each input parameter. The results are shown in *Figure 57*, *Figure 58*, *Figure 59* and *Figure 60*. The trends of both AAG_{ij}^{S-R} and AAG_{ij}^{S-E} which assess the performance of the entire nodalization are consistent with AAz_{ij}^{S-R} and AAz_{ij}^{S-E} obtained for each response separately. Next, the $CR(\alpha_{ij})$ is computed for each of 4 input parameters according to equation (27). The results are shown in *Figure 61*, *Figure 62*, *Figure 63* and *Figure 64*.

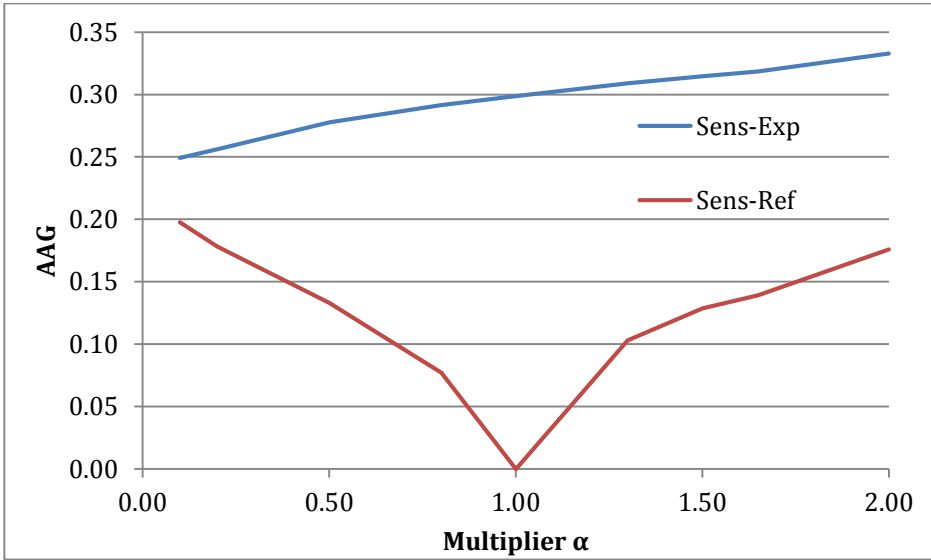


Figure 57 – FEBA 216: AAG_{1j}^{S-R} and AAG_{1j}^{S-E} for interphase HTC.

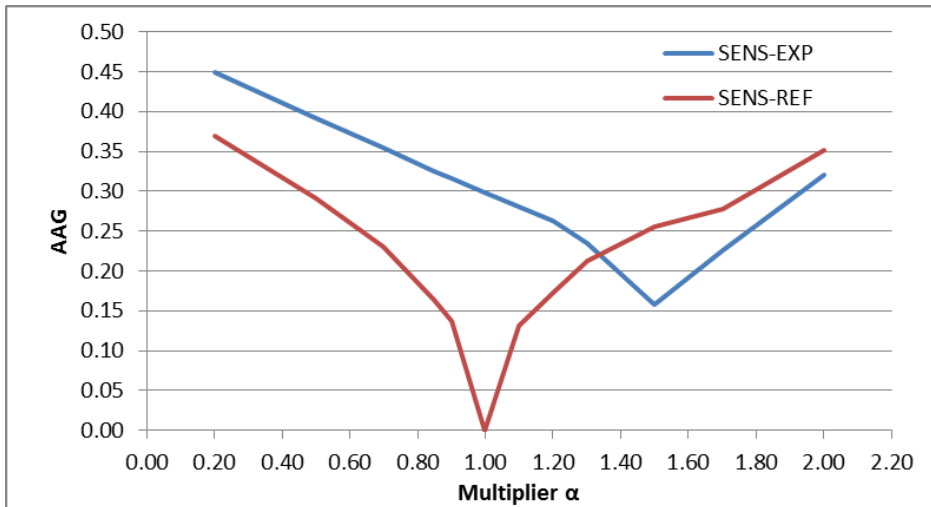


Figure 58 – FEBA 216: AAG_{2j}^{S-R} and AAG_{2j}^{S-E} for interphase friction coefficient.

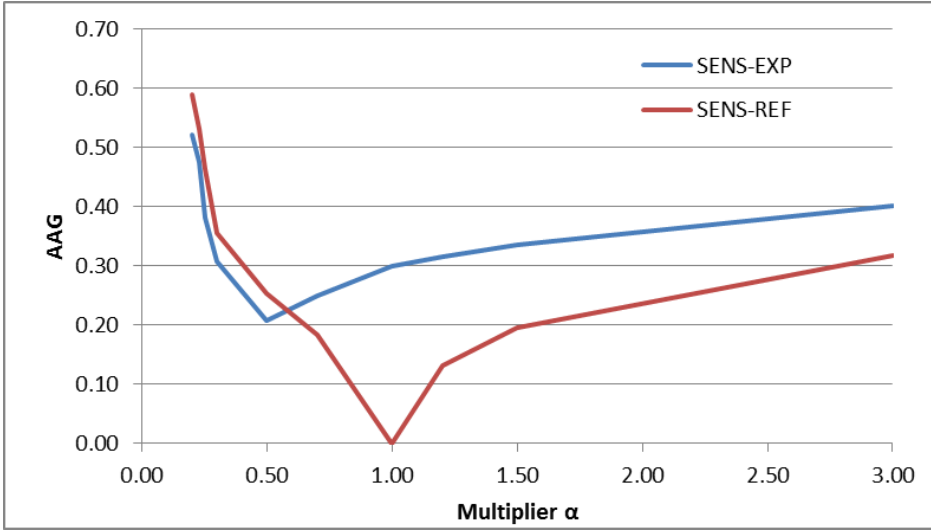


Figure 59 – FEBA 216: AAG_{3j}^{S-R} and AAG_{3j}^{S-E} for film boiling HTC.

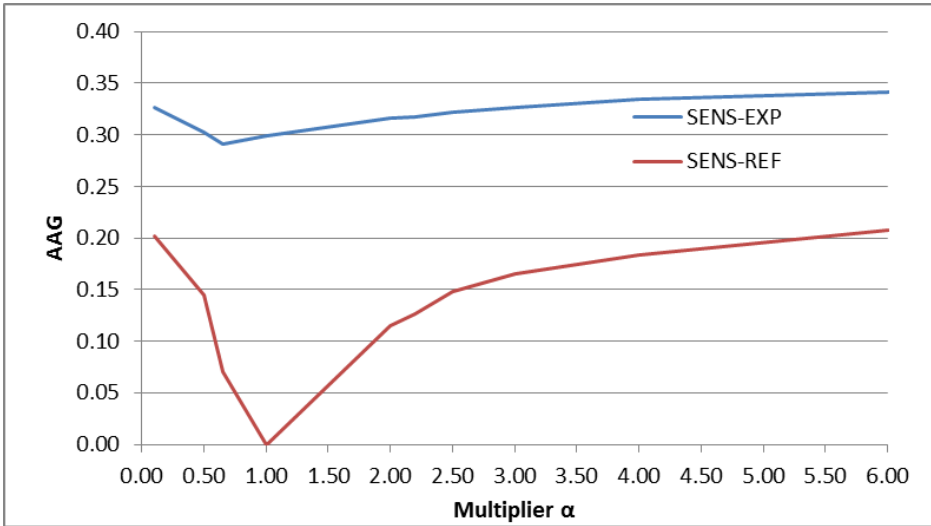


Figure 60 – FEBA 216: AAG_{4j}^{S-R} and AAG_{4j}^{S-E} for convection to vapor HTC.

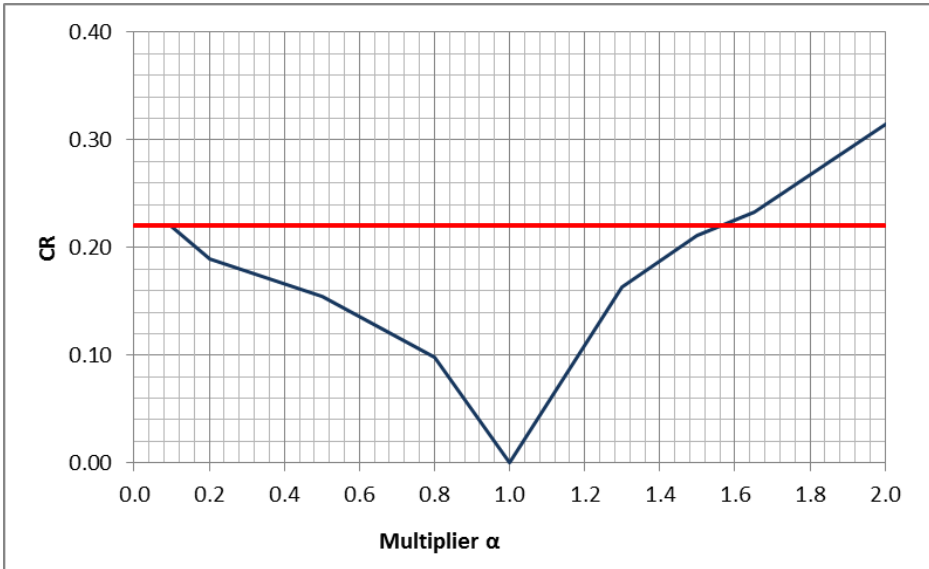


Figure 61 – FEBA 216: $CR(\alpha_{1j})$ for interphase HTC.

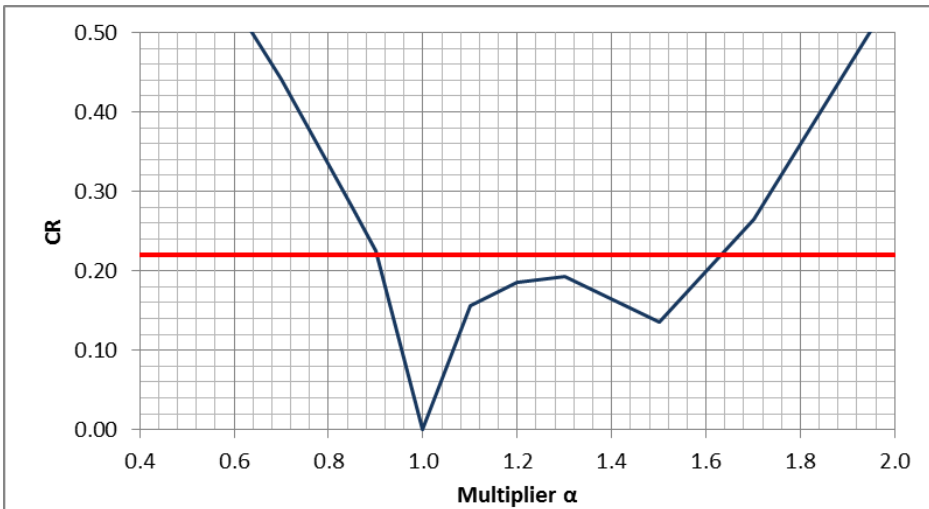


Figure 62 – FEBA 216: $CR(\alpha_{2j})$ for interphase friction coefficient.

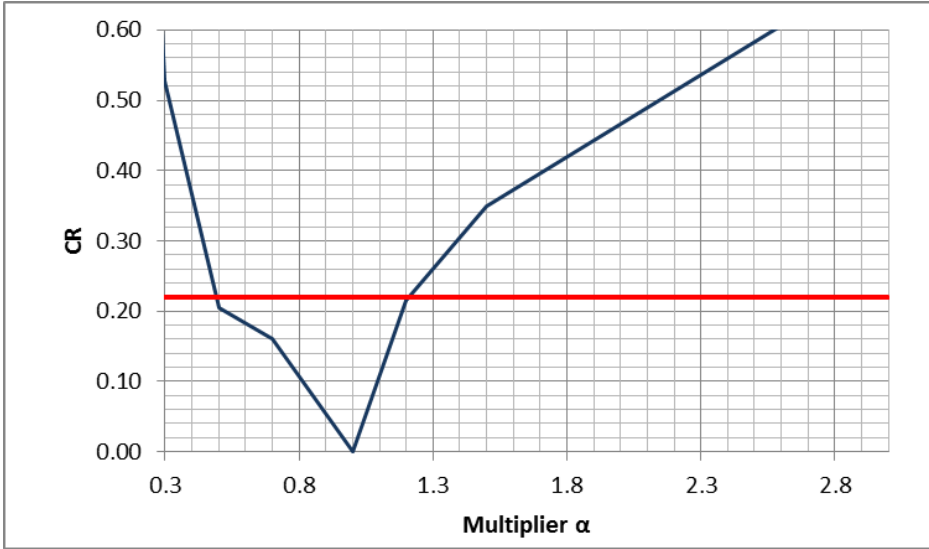


Figure 63 – FEBA 216: $CR(\alpha_{3j})$ for film boiling HTC.

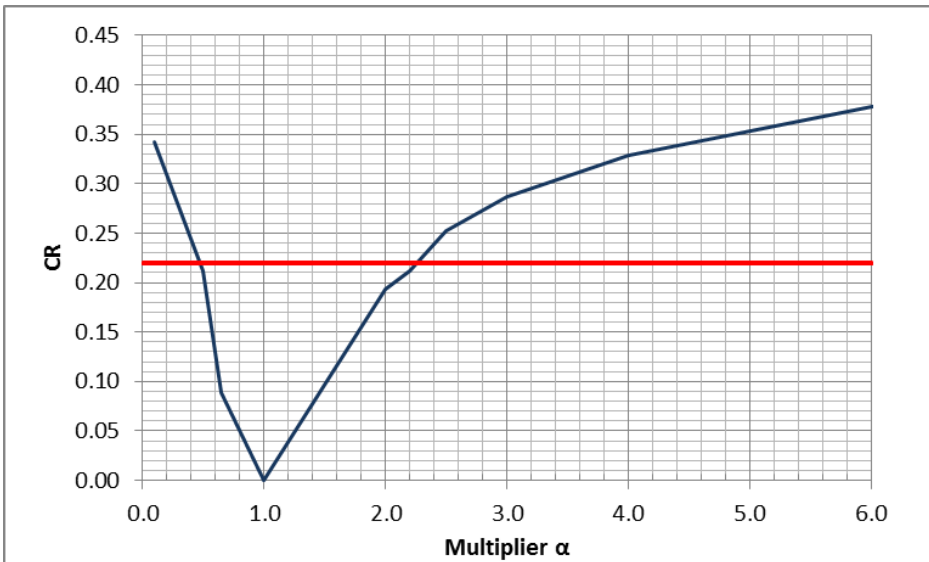


Figure 64 – FEBA 216: $CR(\alpha_{4j})$ for convection to vapor HTC.

Finally, the **limit** = 0.22 (red line in Figure 61, Figure 62, Figure 63 and Figure 64) has been applied to each $CR(\alpha_{ij})$ in order to quantify the variation ranges of the input parameters (Table 22).

The change of considered relevant responses (12b4, 12b2 and quench front) at the extremes of the quantified input parameter ranges (values Min and Max in *Table 22*) are shown in *Figure 65*, *Figure 66*, *Figure 67* and *Figure 68*. It may be noted that the obtained responses obtained at corresponding Min and Max values of input parameters do not do not completely encompass the experimental data, as required in *Criterion #6* of procedure for identification of influential input parameters provided in section 4.2.3.

Table 22 – FEBA 216: quantified variation ranges of input parameters for RELAP5

α_i	Parameter	Ref	Min	Max
α_1	Interphase HTC multiplier	1.0	0.1	1.58
α_2	Interphase friction multiplier	1.0	0.86	1.62
α_3	Film boiling HTC multiplier	1.0	0.5	1.20
α_4	Convection to vapor HTC multiplier	1.0	0.35	2.3

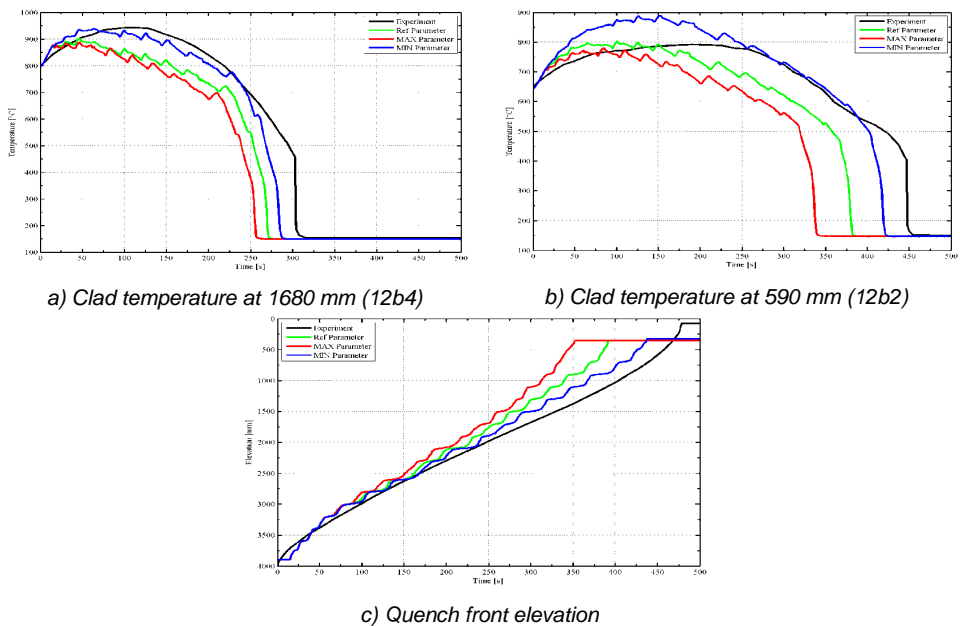


Figure 65 – FEBA 216: variation of relevant responses at min & max values of interphase HTC.

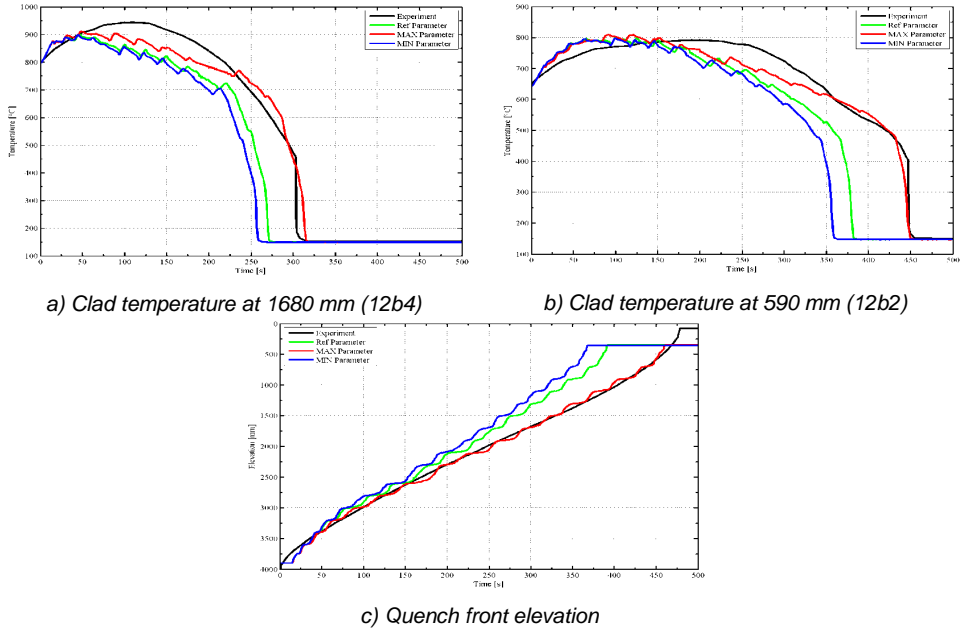


Figure 66 – FEBA 216: variation of relevant responses at min & max values of interphase friction coefficient.

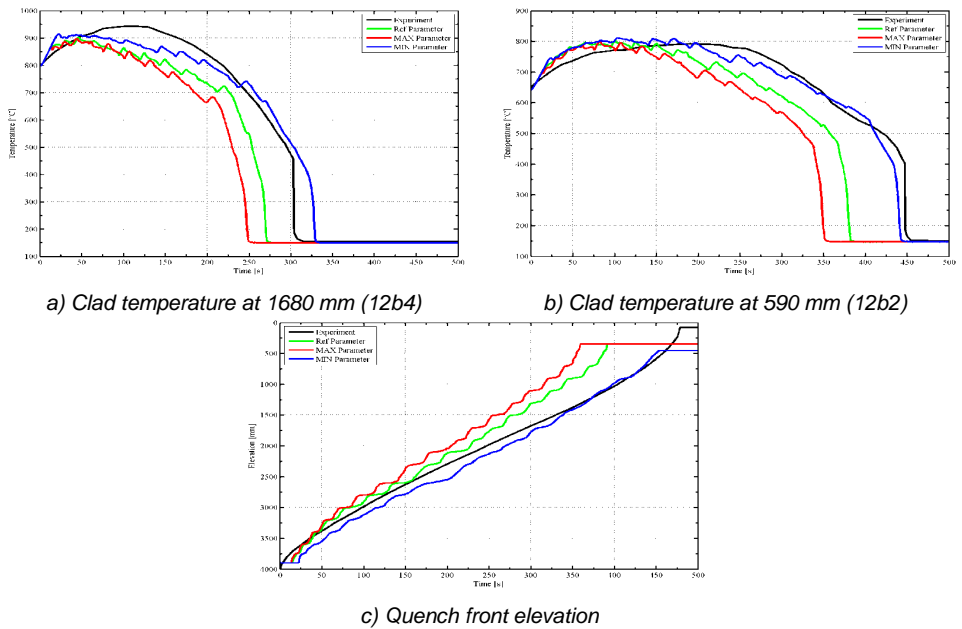


Figure 67 – FEBA 216: variation of relevant responses at min & max values of film boiling HTC.

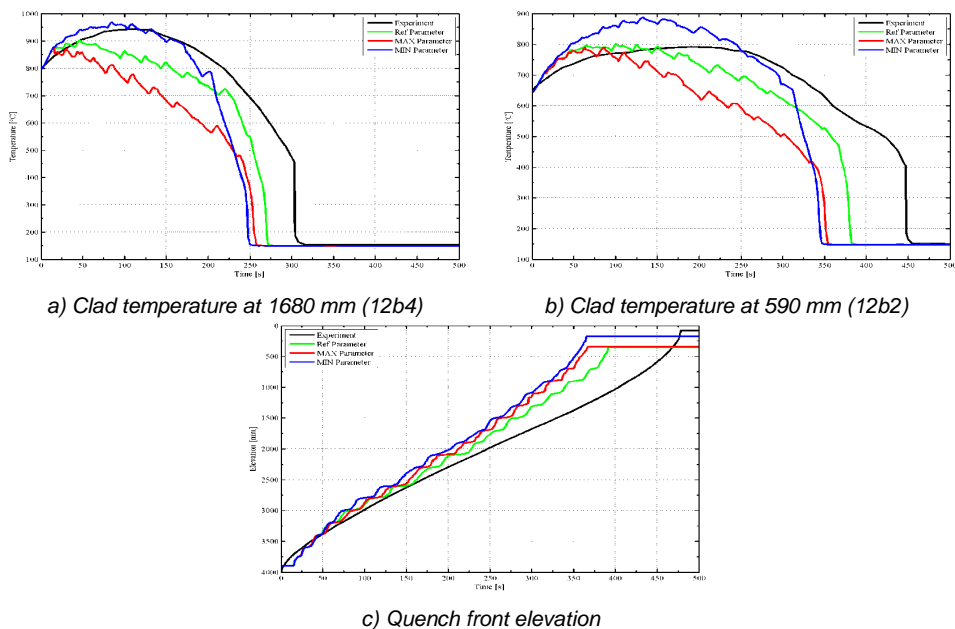


Figure 68 – FEBA 216: variation of relevant responses at min & max values of convection to vapor HTC.

4.2.5. Internal qualification

In this section the input parameter ranges (Table 22), obtained by application of IPREM to experimental test FEBA 216, are put through an “internal qualification” process. The process is defined as “internal” since the ranges are verified against the same test FEBA 216.

4.2.5.1. Uncertainty analysis of test FEBA 216

Similar to the verification process performed for Edwards pipe test (section 3.4.3.), the consistency of variation ranges of input parameters (Table 22) has been verified through the uncertainty analysis of the thermal-hydraulic calculation of test FEBA 216. The consistency is achieved verifying whether the resulting uncertainty bands of relevant thermal-hydraulic response encompass the experimental data.

The uncertainty analysis of RELAP5 calculation of test FEBA 216 has been performed with GRS method, ref. [6] and [7], considering 1st order statistics. The 5% and 95% percentiles, obtained with 95% confidence, have been chosen to represent the two-sided uncertainty band. Therefore, Wilks formula (equation (1)) determines the required number of samples/uncertainty calculations to be performed, which is **93**. A **uniform PDF** has been specified for each uncertain input parameter. The settings of the GRS analysis are summarized in Table 23.

The obtained uncertainty bands are shown in Figure 69, Figure 70 and Figure 71. The uncertainty bands sufficiently cover the experimental data. Hence, it may be

concluded that the input parameter ranges, quantified for reflood problem on the basis of FEBA test 216 with IPREM, are consistent.

Table 23 – FEBA 216: uncertainty analysis settings.

Parameter	Description
Method applied	GRS
Uncertainty band	[5%; 95%]
Confidence level	95%
Number of calculations	93
PDF of input parameters	uniform
Analyzed responses	12b2 12b4 QF

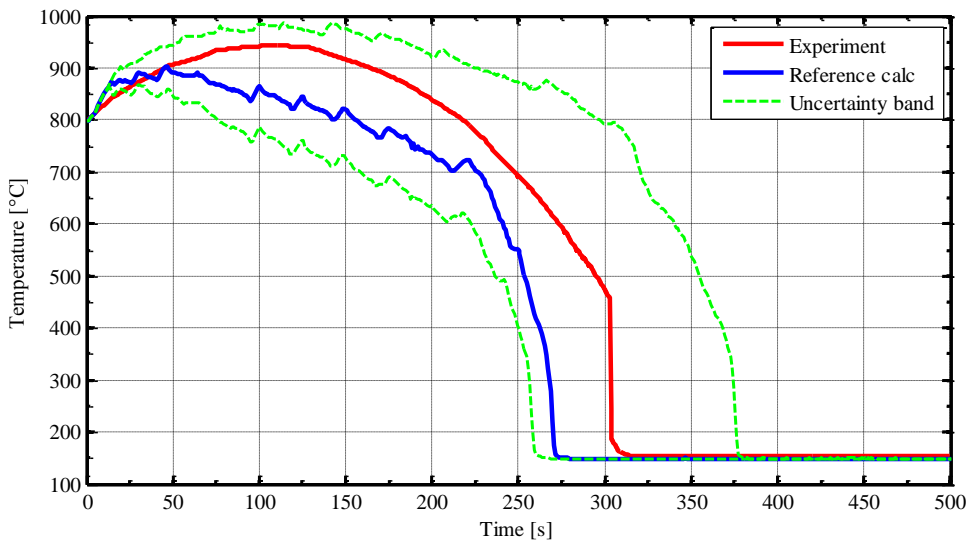


Figure 69 – FEBA 216: predicted uncertainty band for cladding temperature at 2/3 height.

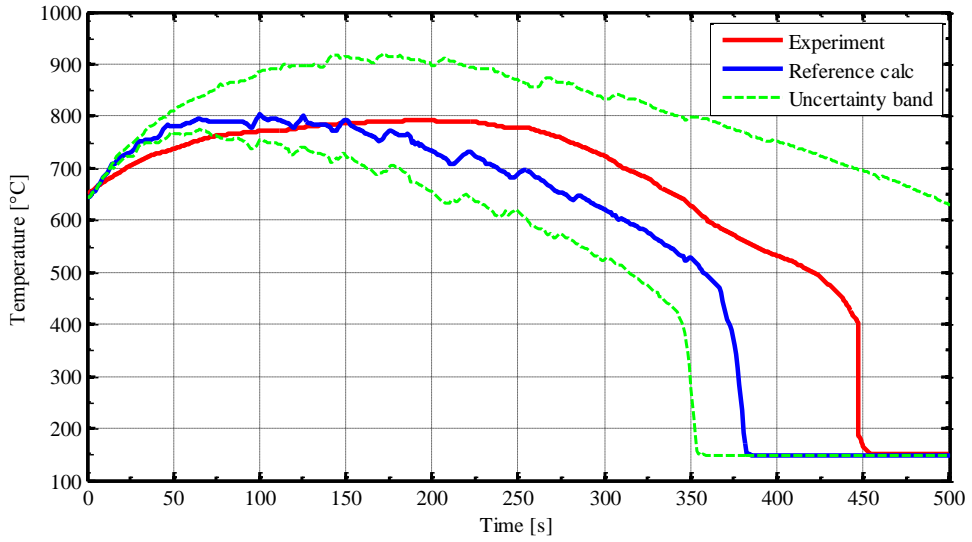


Figure 70 – FEBA 216: predicted uncertainty band for cladding temperature at top.

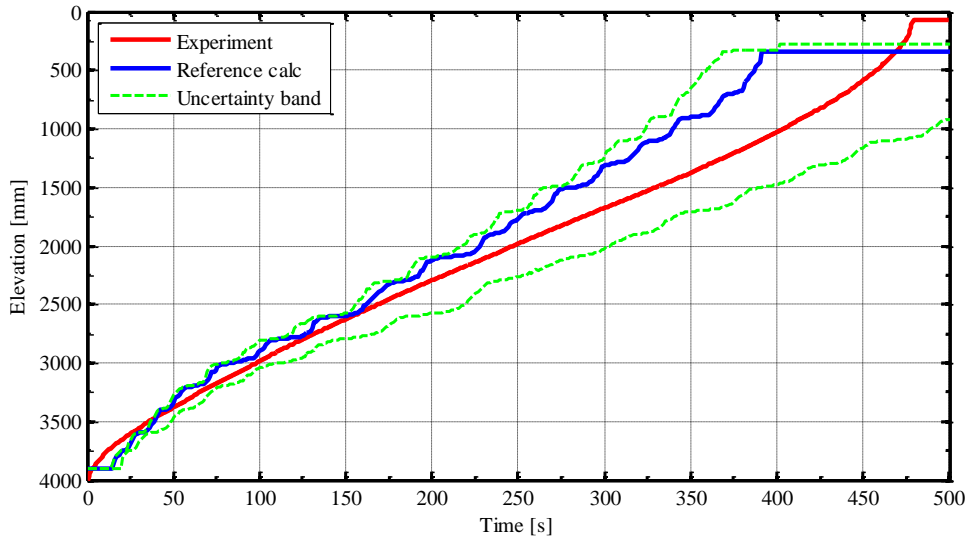


Figure 71 – FEBA 216: predicted uncertainty band for quench front elevation.

4.2.5.2. Sensitivity on limit for $CR(\alpha)$

In IPREM methodology a **limit** value is applied to a calculated $CR(\alpha)$ in order to quantify the input parameter variation ranges by equation (28). In the performed research a value of **limit** = 0.22 has been adopted on the basis of the consideration of a maximum allowed “sensitivity deviation” in a hypothetical case of perfect match between reference calculation and experimental data. In order to verify the impact of the choice of the **limit** value, the input parameter ranges obtained from FEBA test 216 shown in *Figure 61*, *Figure 62*, *Figure 63* and *Figure 64* have been re-quantified using the $CR(\alpha_{ij})$ and applying an alternative value of the **limit** factor (*Figure 72*, *Figure 73*, *Figure 74* and *Figure 75*). Since the $CR(\alpha_{ij})$ do not show rapid change around the value of 0.22 it has been deemed insignificant to attempt a very small variation of limit. Instead, the **limit** = 0.1 has been chosen to verify the changes in input parameter ranges if the **limit** factor is reduced by almost half. The resulting variation ranges are shown in *Table 24* in comparison with those quantified with **limit** = 0.22.

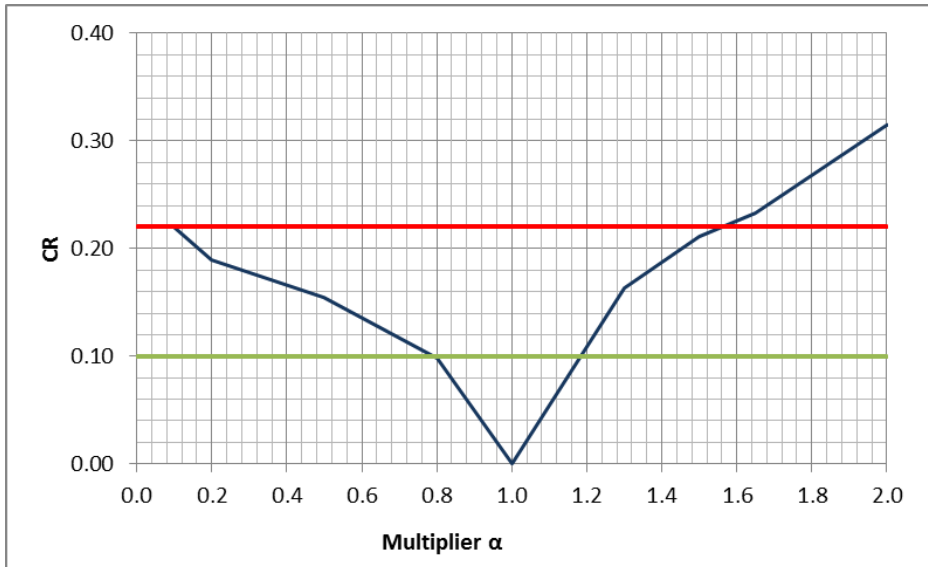


Figure 72 – FEBA 216: application of $limit=0.1$ to $CR(\alpha_{1j})$ for interphase HTC.

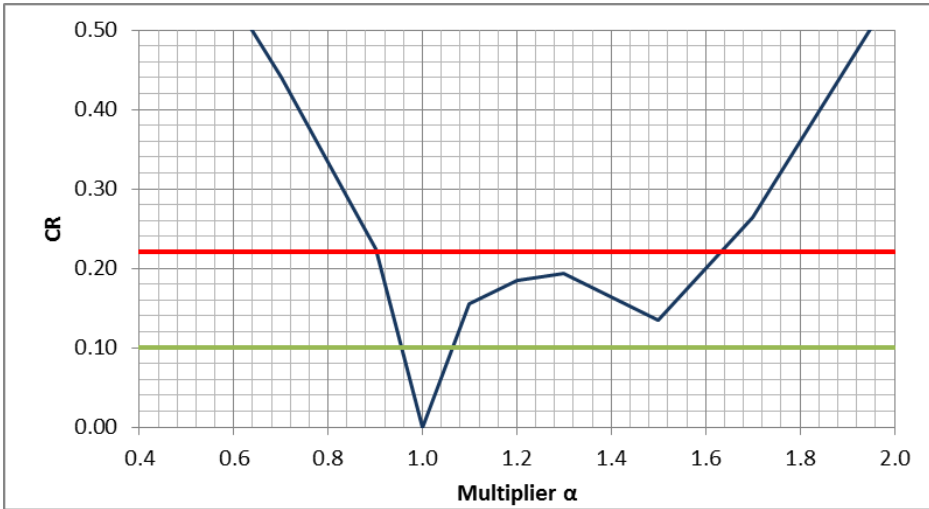


Figure 73 – FEBA 216: application of limit=0.1 $CR(\alpha_{2j})$ for interphase friction coefficient.

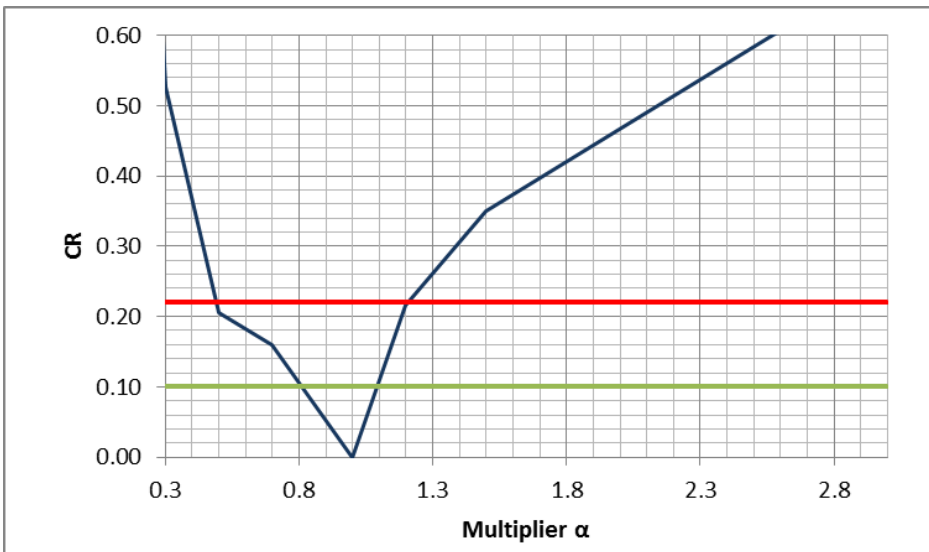


Figure 74 – FEBA 216: application of limit=0.1 $CR(\alpha_{3j})$ for film boiling HTC.

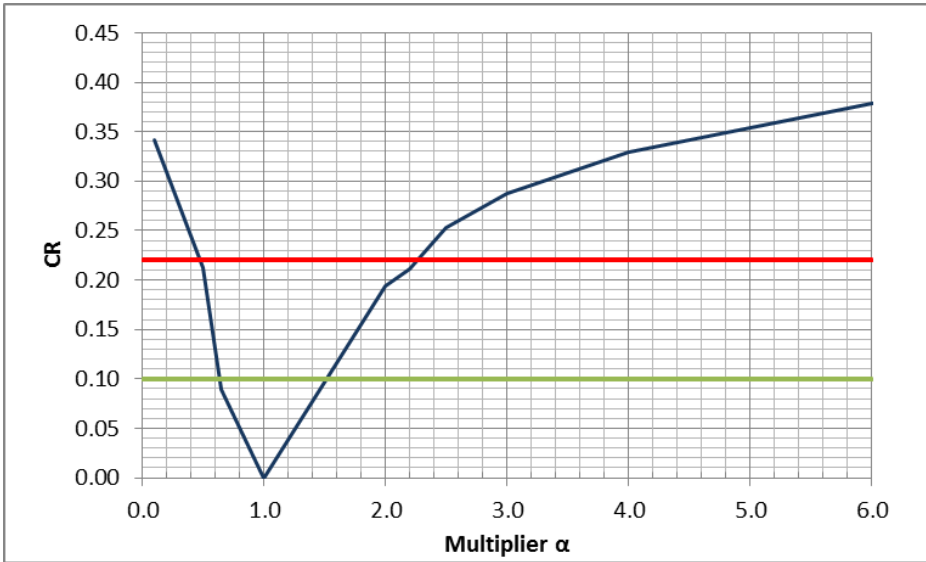


Figure 75 – FEBA 216: application of $\text{limit}=0.1 \text{ CR}(\alpha_{4j})$ for convection to vapor HTC.

Table 24 – FEBA 216: quantified variation ranges with $\text{limit}=0.1$.

α_i	Parameter	limit=0.22		limit=0.1	
		Min	Max	Min	Max
α_1	Interphase HTC multiplier	0.1	1.58	0.8	1.2
α_2	Interphase friction multiplier	0.86	1.62	0.96	1.08
α_3	Film boiling HTC multiplier	0.5	1.20	0.8	1.1
α_4	Convection to vapor HTC multiplier	0.35	2.3	0.63	1.53

It can be seen that the reduction by almost a factor of 2 in the value of a **limit** factor leads to significant change in ranges of some parameters such as interphase friction coefficient or convection to vapor HTC. The effect is especially noticeable in the part of the range (smaller or greater than reference value) that “leads” to improvement of code prediction with respect to experimental data.

The uncertainty analysis of thermal-hydraulic calculation has been repeated with ranges obtained with **limit** = 0.1 (Table 24) using the same setting of Table 23. The evaluated uncertainty bands of relevant responses are compared in the Figure 76, Figure 77 and Figure 78 with those obtained by ranges from Table 22.

It is evident that uncertainty bands obtained with ranges of input parameters, quantified with **limit** = 0.1, do not cover sufficiently the experimental data.

Therefore it is suggested not to modify the proposed value of **limit = 0.22** without further substantial justification.

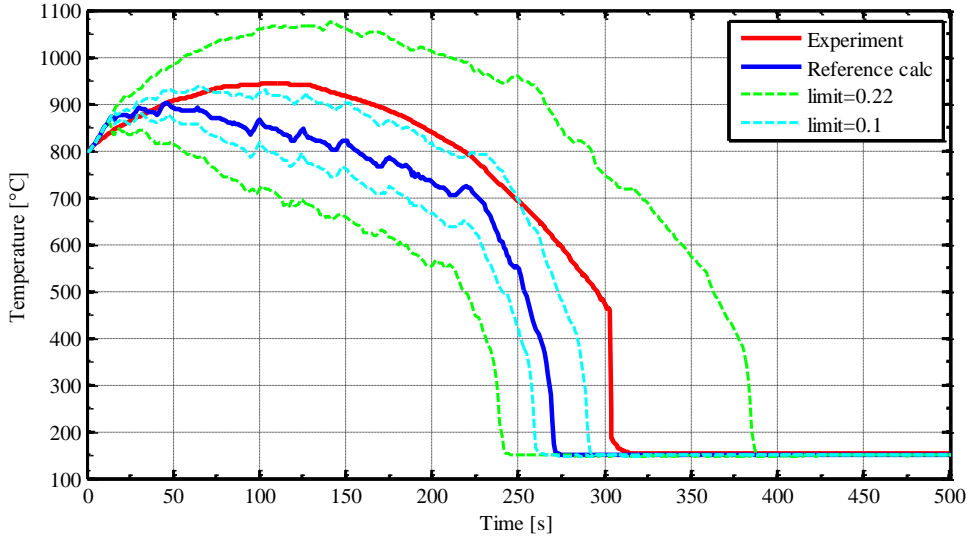


Figure 76 – FEBA 216: predicted uncertainty band with $limit=0.1$ for cladding temperature at 2/3 height.

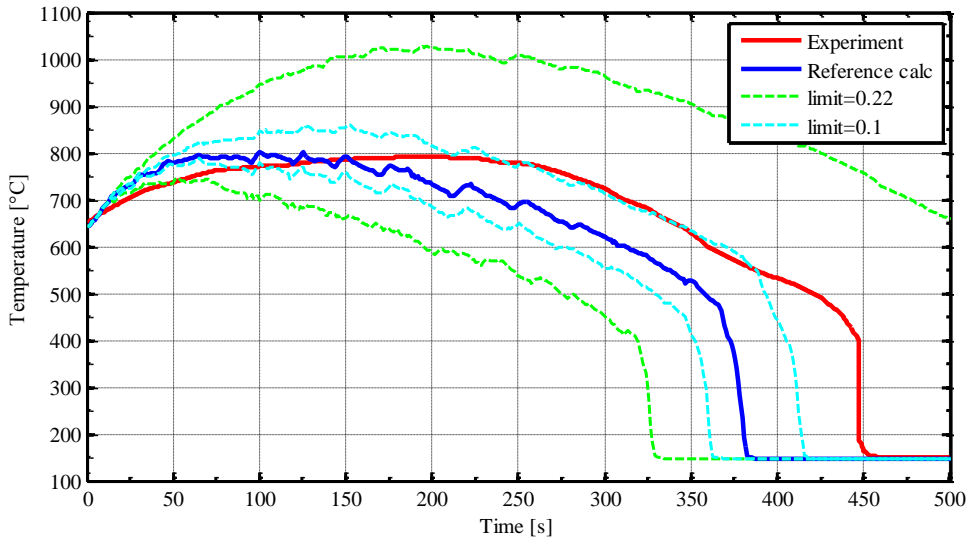


Figure 77 – FEBA 216: predicted uncertainty band with $limit=0.1$ for cladding temperature at top.

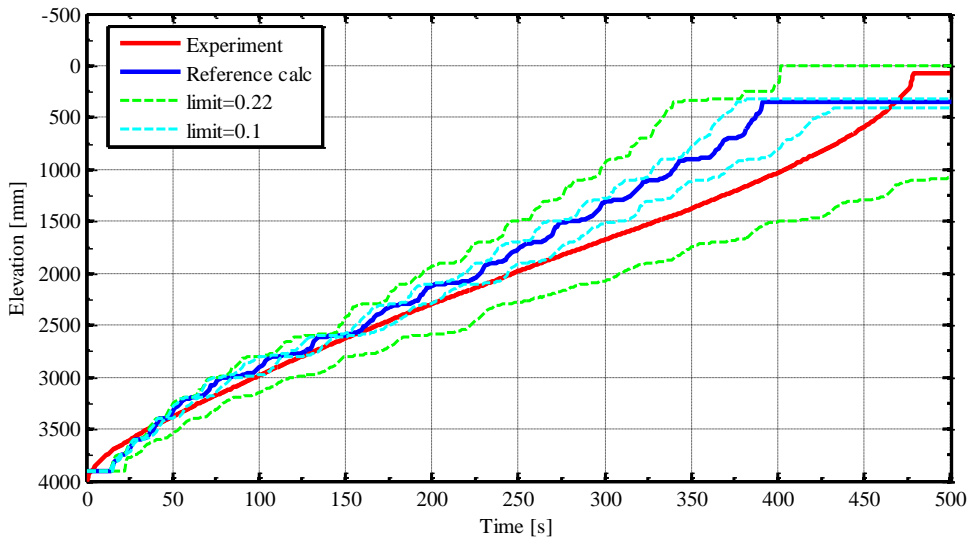


Figure 78 – FEBA 216: predicted uncertainty band with $limit=0.1$ for quench front elevation.

4.2.5.3. Sensitivity on type of Probability Density Function

The internal qualification for Edwards pipe problem and reflood test FEBA 216 has been performed so far through an uncertainty evaluation of thermal-hydraulic calculations of corresponding tests. The uncertainty evaluation has been performed with a statistically-based GRS method which requires to specify the type of Probability Density Function (PDF) for each considered input parameter. Being a non-statistical method, the IPREM allows to quantify the variation ranges of code input parameters of interest, but does not provide an information regarding the PDF of an analyzed parameter. However, three viable options are suggested to be used in the case of a limited knowledge on the statistical nature of a parameter:

- Uniform distribution
- Triangular distribution
- Histogram distribution

The uncertainty analyses (UA) performed in sections 3.4.3., 4.2.5.1 and 4.2.5.2 have been performed using the uniform PDF for each considered input parameter. Therefore, a sensitivity analysis has been performed on the type of the chosen PDF and presented in this subsection.

Additional two uncertainty analyses of calculation of FEBA test 216 have been carried out using triangular and histogram PDF. The settings for all compared analyses are presented in *Table 25*. For the histogram PDF the uncertainty analysis specifications with 50%/50% distribution to two bins (below and above reference value), proposed in PREMIUM benchmark have been used, ref. [51]. In all uncertainty analyses the same set of variation ranges of input parameters (*Table 22*) has been used. An example of calculated PDF of all three considered types is shown

in *Figure 79*. The evaluated uncertainty bands for three relevant responses are shown in *Figure 80*, *Figure 81* and *Figure 82*.

It may be noticed that the choice of PDF did not influence on uncertainty band of the quench front propagation (*Figure 82*). This can be explained by the fact that the weight of quench front response in calculation of AAG_{ij}^{S-R} and AAG_{ij}^{S-E} is smaller than those of two considered cladding temperature responses. Therefore, the determined input parameter variation ranges have greater influence on the predicted temperature than on the front propagation.

The choice of uniform PDF results in larger uncertainty bands of cladding temperature predictions, with PCT predicted almost by 100 °C higher (*Figure 80*). This could be expected since the uniform distribution represents the minimum state of knowledge about the parameter (only minimum and maximum value) and tend to enlarge the band of response when applied to uncertainty analysis. On the other hand, the use of triangular and histogram distribution show similar results in term of evaluated uncertainty bands. However, the uncertainty analysis performed with 50%/50% histogram distributions of input parameters has been carried out with 5th order statistics and the resulting bands provide larger tolerance internal - 95% (comparing to 90% interval in 1st order statistics applied for uniform and triangular distributions). Plus, there is no hard evidence that the actual probability to obtain a value of input parameter at the extrema of variation ranges in *Table 22* is zero.

Therefore, for all the subsequent uncertainty analysis carried out within the framework of the present research the 50%/50% histogram PDF has been applied to the quantified variation ranges of input parameters.

Table 25 – FEBA 216: settings for sensitivity analysis on type of PDF.

Parameter	PDF		
	uniform	triangular	histogram
Order statistics	1 st order	1 st order	5 th order
Tolerance limit	2-sided	2-sided	2-sided
Lower percentile	5%	5%	2.5%
Upper percentile	95%	95%	97.5%
Confidence level	95%	95%	95%
Number of code runs	93	93	200

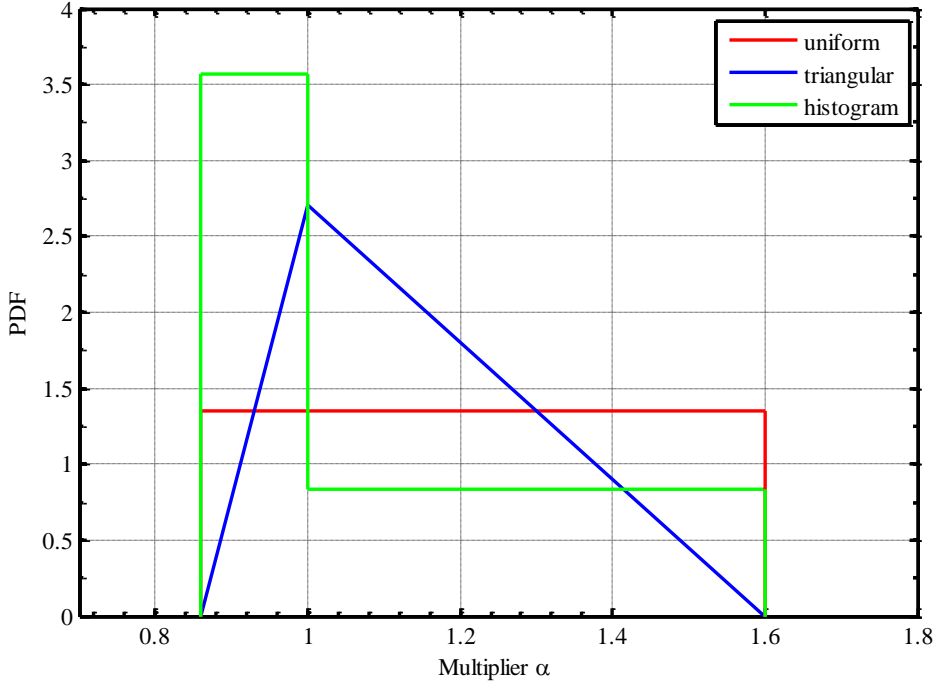


Figure 79 – FEBA 216: Probability Density Functions for interphase friction.

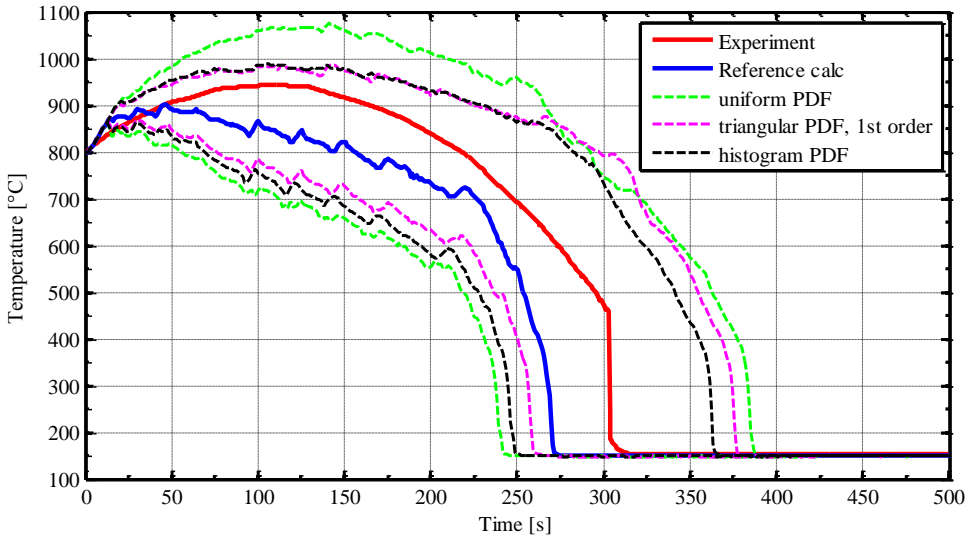


Figure 80 – FEBA 216: Results of PDF-sensitivity analysis for cladding temperature at 2/3 height.

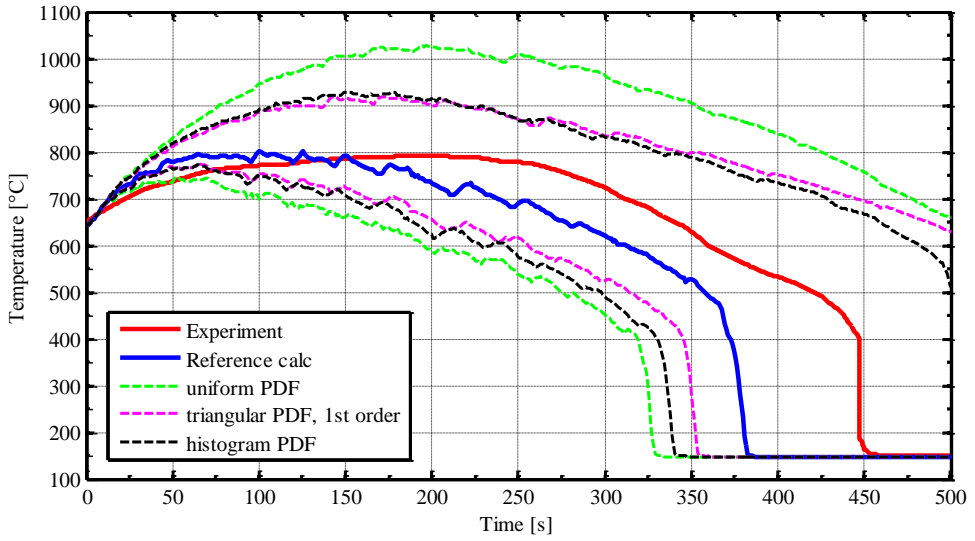


Figure 81 – FEBA 216: Results of PDF-sensitivity analysis for cladding temperature at top.

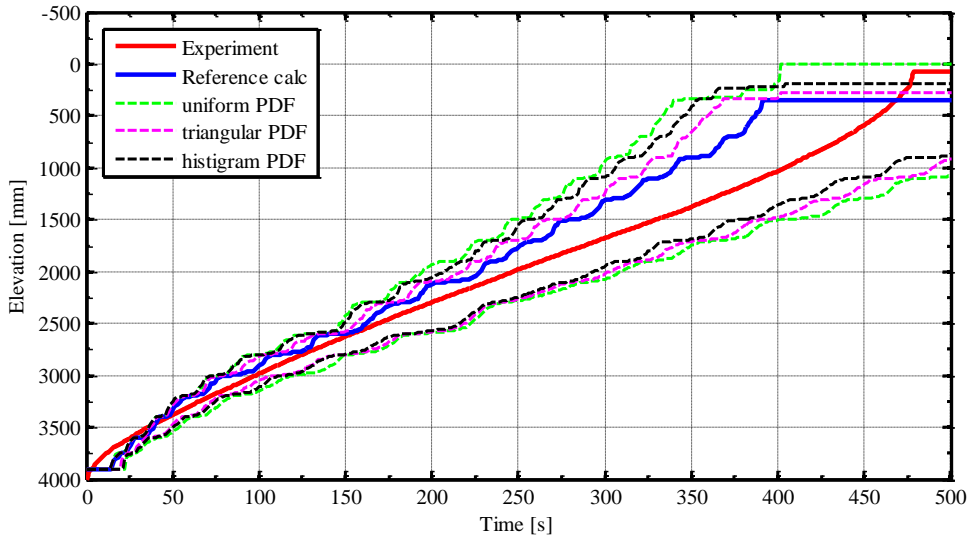


Figure 82 – FEBA 216: Results of PDF-sensitivity analysis for quench front elevation.

4.3. Validation of IPREM: uncertainty analysis of reflood simulation with thermal-hydraulic codes

The validation of the proposed methodology is a fundamental pre-requisite for the application of the method itself. Thus, the quantified variation ranges of reflood-related input parameters (*Table 22*) of RELAP5 Mod 3.3 code has been adopted to perform the uncertainty analysis of the thermal hydraulic calculations of various experimental reflood tests (*Table 8*, column “Validation”).

It shall be pointed out that the validation has been performed by simulating tests with identical geometry but different conditions (the FEBA tests) and tests with different geometry and conditions (the PERICLES and the ACHILLES tests) with respect to one used for the quantification of the ranges of input model parameters (i.e. FEBA test 216).

Considering the outcomes of the performed sensitivity analysis on the choice of PDF of input parameters, the 50%/50% histogram distribution has been assigned to all uncertain input parameters in the following uncertainty analysis. The settings for the uncertainty analysis of the performed thermal-hydraulic calculations in the framework of IPREM validation are shown in *Table 26*.

Table 26 – Validation: settings for uncertainty analysis.

Parameter	Value
Uncertainty analysis method	GRS
Order statistics	5 th order
Tolerance limit	2-sided
Lower percentile	2.5%
Upper percentile	97.5%
Confidence level	95%
Number of code runs	200
Input parameter PDF	histogram

4.3.1. Validation against FEBA facility

Thermal-hydraulic calculations with subsequent uncertainty analyses of five experimental tests in FEBA have been performed (see *Table 8*, *Table 9*). The calculation of the FEBA tests have been performed using the same RELAP5 model developed previously for test 216. No additional tuning has been applied to obtain better agreement of the reference calculations with the experimental data.

The resulting uncertainty bands for the relevant responses are shown in *Figure 82*, *Figure 83*, *Figure 84*, *Figure 85* and *Figure 86*. The uncertainty bands sufficiently encompass the experimental measurement data. The uncertainty in bundle quench time (qualitatively observed from Figures with quench front elevation vs time) cover the experimental data even in tests (223, 218 and 214) where the discrepancy between reference and experimental bundle quench time Δt_{rew} is more than 25%.

The evaluated upper uncertainty band of cladding temperature encompasses the experimentally observed PCT (in Figures with cladding temperature at 2/3 height, 12b4) in all five modelled tests. It shall be noted that the minimum margin between the predicted upper uncertainty band and experimental PCT is observed in tests performed at higher pressure (6.2 bar, tests 220 and 222).

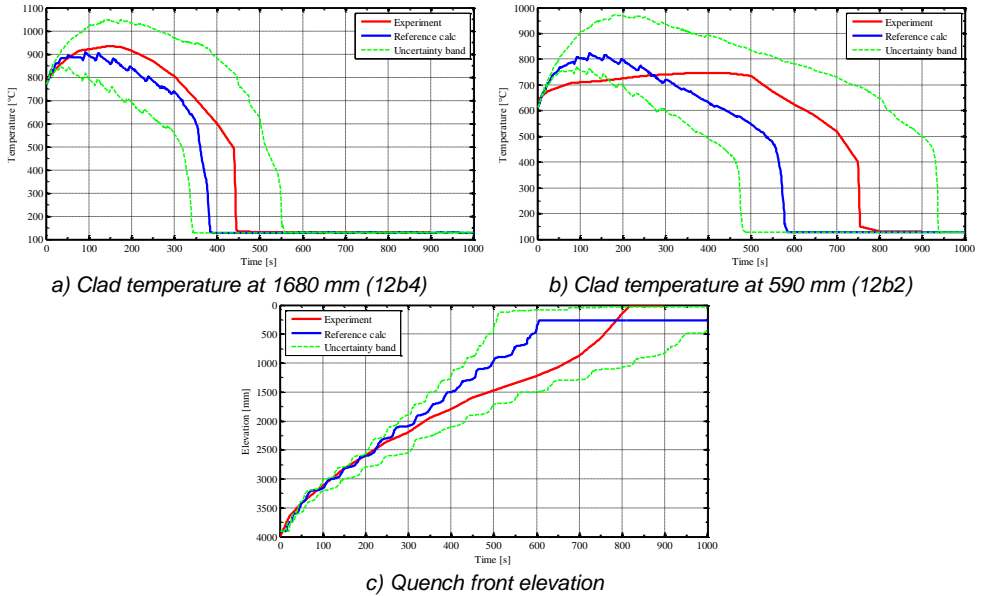


Figure 83 – Results of uncertainty analysis of RELAP5 calculation of FEBA 223.

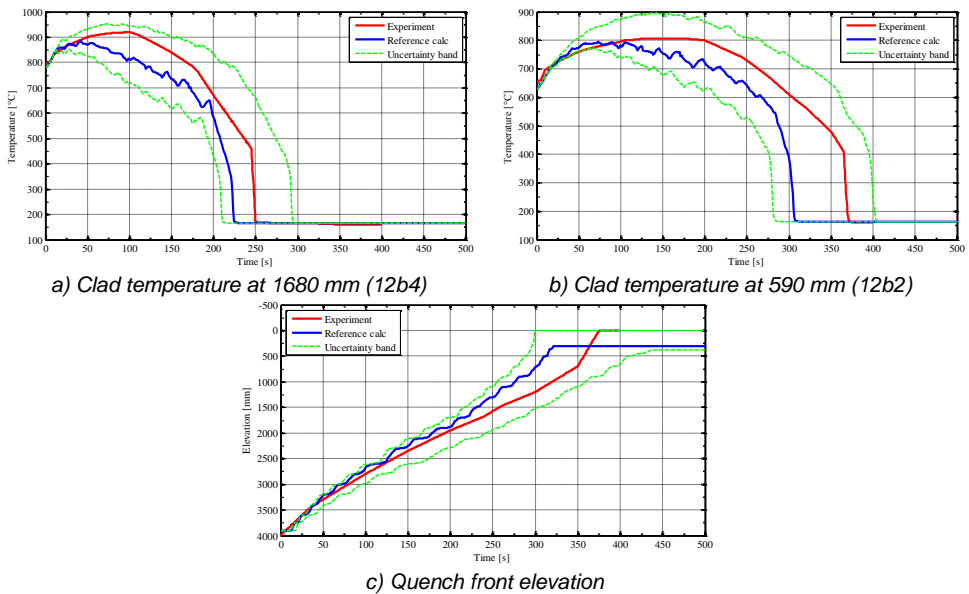
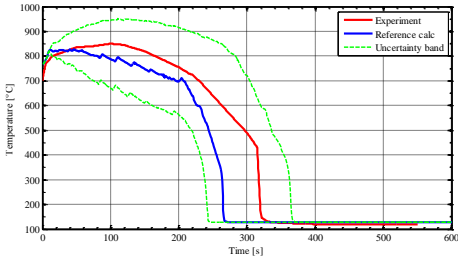
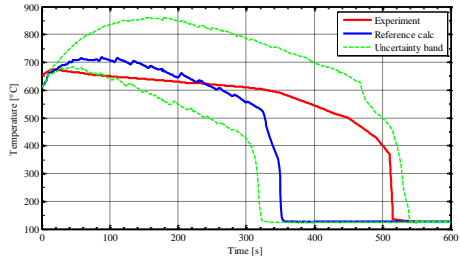


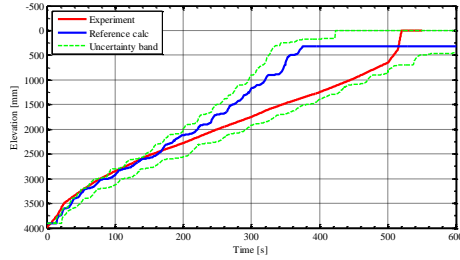
Figure 84 – Results of uncertainty analysis of RELAP5 calculation of FEBA 220.



a) Clad temperature at 1680 mm (12b4)

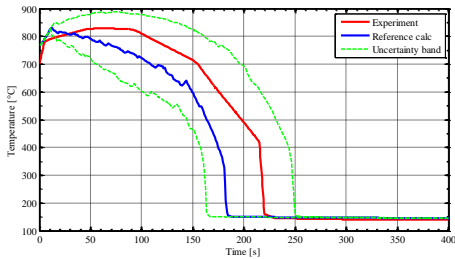


b) Clad temperature at 590 mm (12b2)

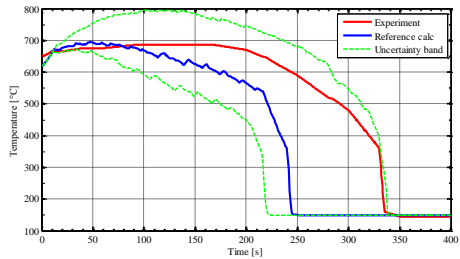


c) Quench front elevation

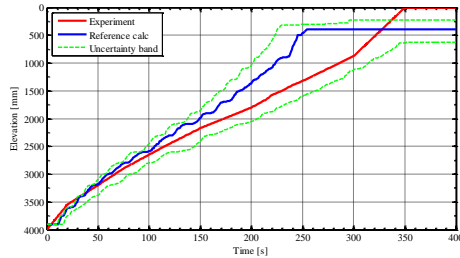
Figure 85 – Results of uncertainty analysis of RELAP5 calculation of FEBA 218.



a) Clad temperature at 1680 mm (12b4)



b) Clad temperature at 590 mm (12b2)



c) Quench front elevation

Figure 86 – Results of uncertainty analysis of RELAP5 calculation of FEBA 214.

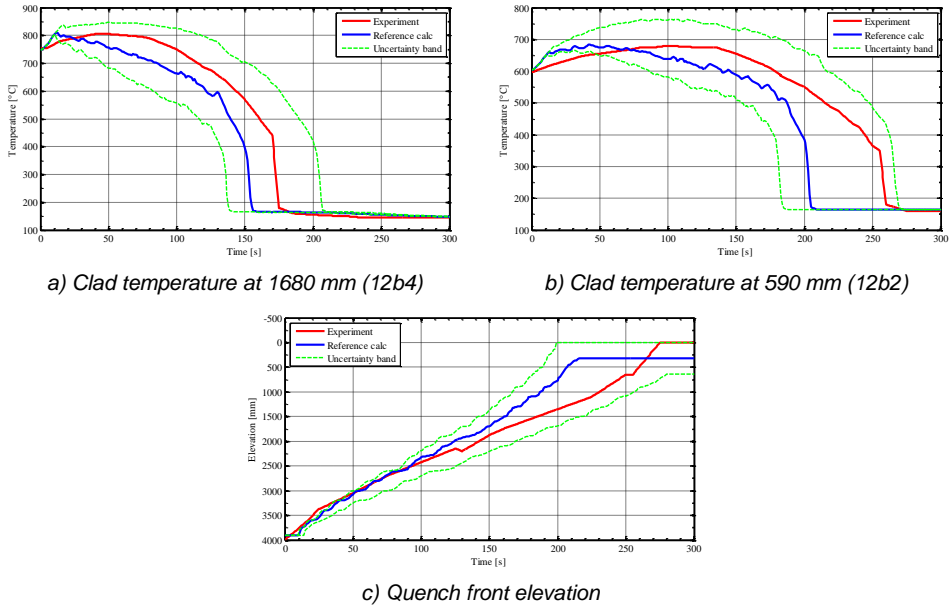


Figure 87 – Results of uncertainty analysis of RELAP5 calculation of FEBA 222.

4.3.2. Validation against PERICLES facility

As the next step, the variation ranges of reflow-related input parameters (*Table 22*) of RELAP5 Mod3.3 code have been validated against the experimental tests carried out at facility PERICLES that features different geometry with respect to FEBA facility.

4.3.2.1. Description of PERICLES facility

2D PERICLES, ref. [52], has been carried out to investigate 2-D effects (e.g. like cross flows) which can occur in a PWR core where the rod power is not identical from one assembly to the other ones. The experiment consists of three different assemblies, denoted here by A, B and C (*Figure 88*). These assemblies are contained in a vertical housing with a rectangular section, which is not heated unlike FEBA. Each assembly contains $7 \times 17 = 119$ full length heater rods. Thus, the total number of heater rods is 357. The dimensions of the assemblies are indicated on *Figure 88*.

The detailed section of one assembly is given on *Figure 89*. Each fuel rod simulator consists of 3 helical Nichrome wires embedded in boron nitride. The cladding is made of stainless steel. The rods are heated by two independent electrical power sources, giving the possibility to heat more the central assembly B (the ‘hot’ assembly) than the two lateral ones A and C (the ‘cold’ assemblies). The length of the rods is equal to the length of the channel (3656 mm) and their diameter is equal to 9.45 mm.

The axial power profile is not uniform, but depends on the elevation on the rod. The heating of the different rods in the three assemblies is shown on *Figure 90*. In this figure, ϕ designates the heat flux, ϕ_{nom} its nominal value and F_{xy} is the radial peaking factor (equal to 1 if the rod power lateral profile is flat). The values of ϕ/ϕ_{nom} are given in function of the axial location z by *Figure 90*.

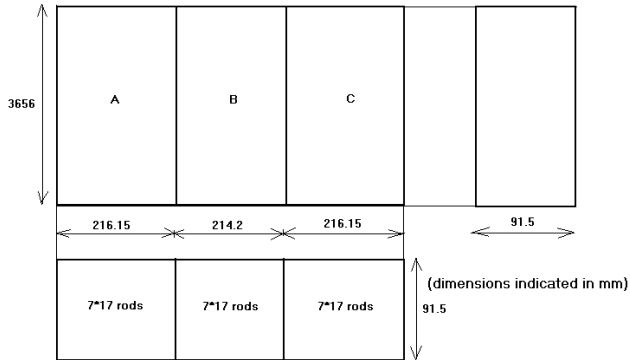


Figure 88 – Sketch of 2D PERICLES experimental test section.

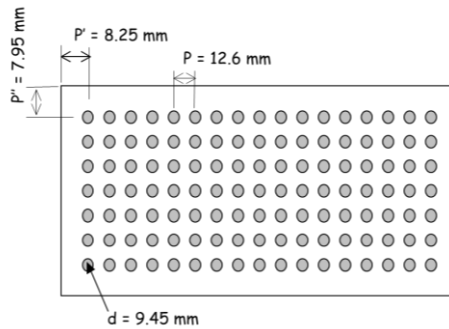


Figure 89 – Horizontal section of one assembly of 2D PERICLES.

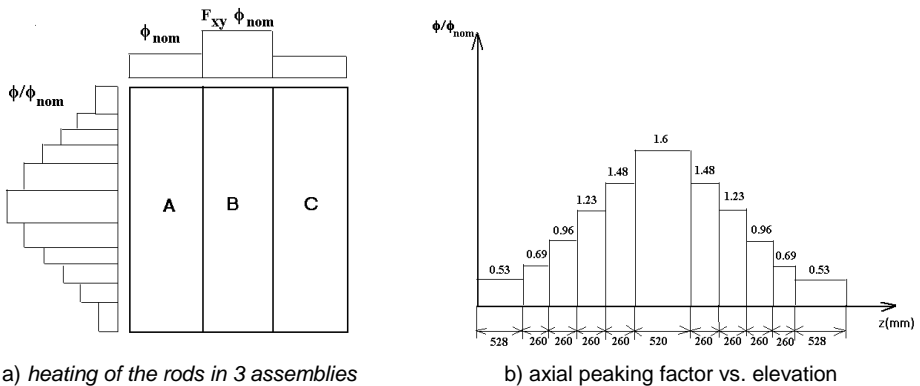


Figure 90 – Power profiles in 2D PERICLES.

The bottom plate, upper tie plate and upper core plate are installed at the bottom and top of the heated bundle respectively. The upper tie plate is 15 mm thick and perforated typically as in the reference reactor, corresponding to a flow area restriction of 30 % of that of the bundle. The upper core plate is 85 mm thick and perforated with 3 holes giving a flow area restriction of 21 %.

While carrying out experimental tests, the three assemblies are initially full of steam. At the time 0, the electrical power is put on. It is also kept constant during the whole transient. When a given value of the maximum clad temperature in the hot assembly is reached, the liquid enters each assembly, at a constant flow rate and with a constant sub-cooling. During the reflooding stage, a quench front goes up in each assembly. The reflooding stage is finished when the three quench fronts reach the top of the assemblies.

4.3.2.2. Modeling of PERICLES facility with RELAP5 code

The model of PERICLES test section for RELAP5 Mod3.3 code has been developed for “blind” calculations: only the geometrical specifications and the test conditions were available. Therefore, the same modelling, as the one adopted previously for the calculation of FEBA tests, has been used for the simulation of PERICLES facility: single 1-D hydraulic channel representing each assembly with 1 heat structure component representing each fuel bundle. The lengths of hydraulic nodes/meshes are similar to RELAP5 model of FEBA test section. The spacer grids have been taken into account by proper K_{loss} coefficients at corresponding locations, but the flow restriction due to grids has not been modeled (consistent with FEBA model) Resulting 3 parallel vertical channels has been connected by cross-flow junctions (Figure 91). The option 111 (vertical bundle with cross-flow) therefore has been activated in each heat structure representing rod bundles. The section housing has not been modeled according to the suggestions of the Specifications for Phase IV of PREMIUM benchmark, ref. [51]. The geometrical properties of the RELAP5 model of PERICLES are summarized in Table 27.

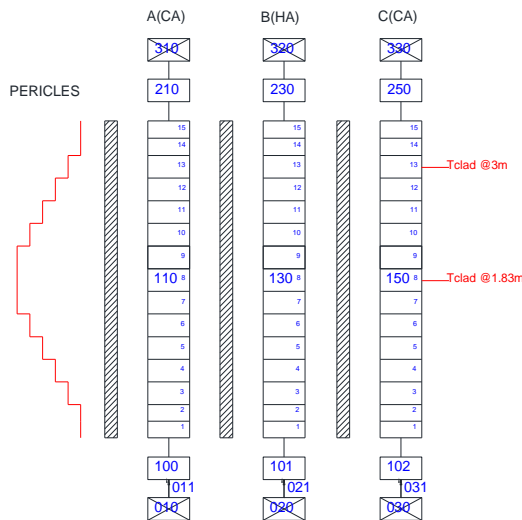


Figure 91 – Sketch of PERICLES nodalization for RELAP5 code.

Table 27 – Summary of RELAP5 model of PERICLES facility.

Parameter	Value
Total height/length	3656 mm
Nodes in heated length	15
Flow area, hot assembly (HA)	0.01143 m ²
Flow area, hot assembly (CA)	0.01125 m ²
Hydraulic diameter	1.127E-2 m ²
Wall roughness	2.E-5
Spacer grid K _{loss} , ref [51]	1.0
Cross flow K _{loss} , ref [51]	10.0
Maximum linear heat rate (HA)	2.00 kW/m
<i>Special options activated:</i>	
Rod bundle interphase friction (b=1 in hydraulic nodes)	
Vertical bundle with cross flow (111 in heat structures)	

It should be pointed out that a limited information regarding the geometry of 2D PERICLES facility has been available for model development. In particular this concerns the upper plenum above the heated part of the rod bundles, where steam-water separation devices are typically installed in such type of experimental facilities. Considering this issue and the fact that the calculations have been performed in 'blind' mode, it can be expected that reference calculation results do not provide the best prediction of experimental data.

4.3.2.3. Uncertainty analysis of PERICLES tests

Similar to activities performed with FEBA tests and presented in section 4.3.2.2., the uncertainty analysis of the thermal-hydraulic calculations of six PERICLES tests (*Table 8, Table 10*) has been performed. The same settings for the uncertainty analysis have been applied (*Table 26*). The obtained uncertainty bands are shown in *Figure 92, Figure 93, Figure 94, Figure 95, Figure 96* and *Figure 97* for the following three responses predicted for the "hot assembly": cladding temperature at 2/3 height (1828 mm), top (2998 mm) and quench front. However, only cladding temperature measurements data has been revealed to the analyst once the uncertainty analysis has been completed, therefore the predicted results for quench front elevation can only be judged qualitatively.

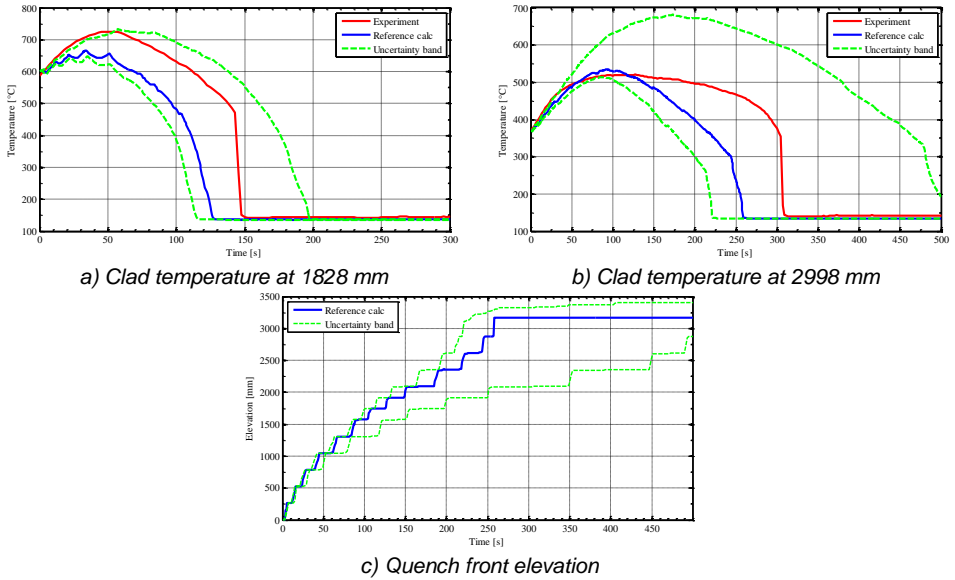


Figure 92 – Results of uncertainty analysis of RELAP5 calculation of PERICLES RE62.

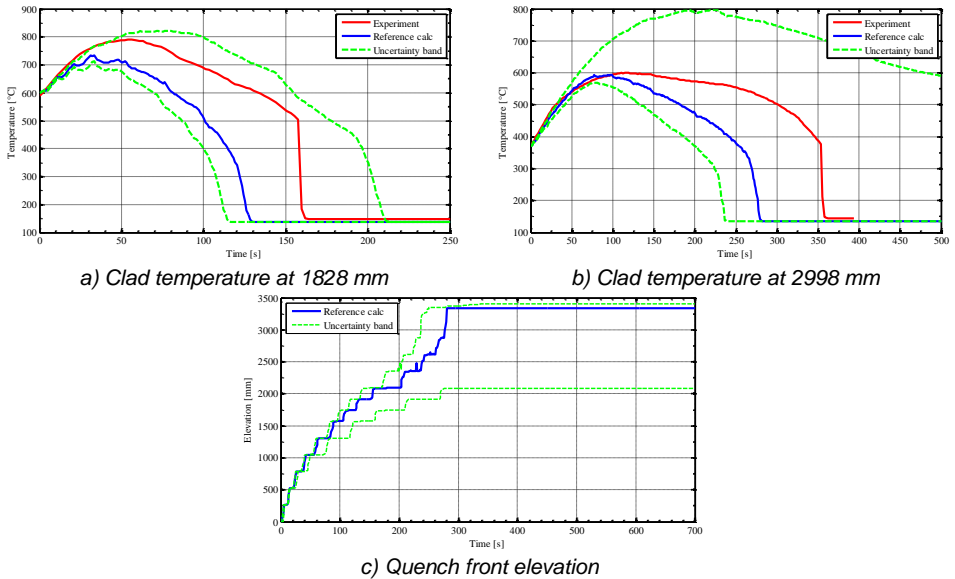
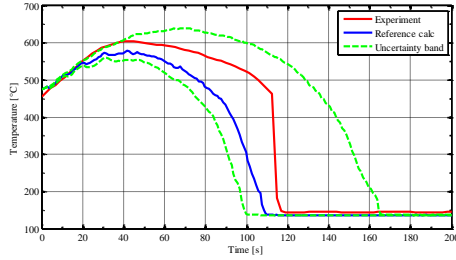
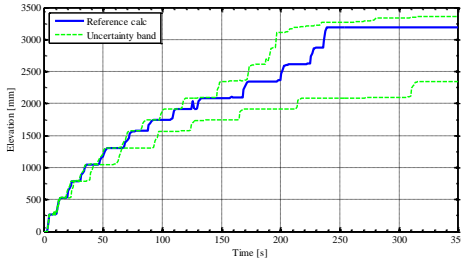


Figure 93 – Results of uncertainty analysis of RELAP5 calculation of PERICLES RE64.

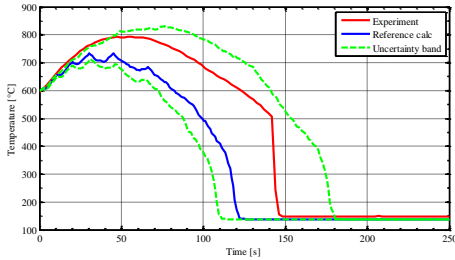


a) Clad temperature at 1828 mm

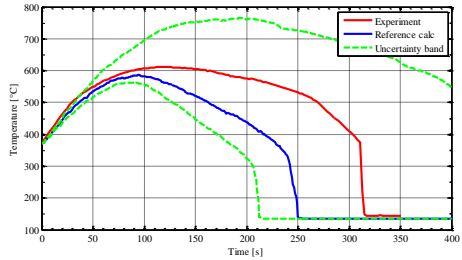


b) Quench front elevation

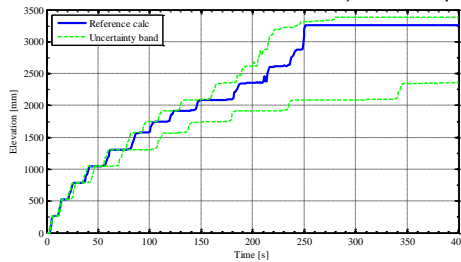
Figure 94 – Results of uncertainty analysis of RELAP5 calculation of PERICLES RE69.



a) Clad temperature at 1828 mm



b) Clad temperature at 2998 mm



c) Quench front elevation

Figure 95 – Results of uncertainty analysis of RELAP5 calculation of PERICLES RE79.

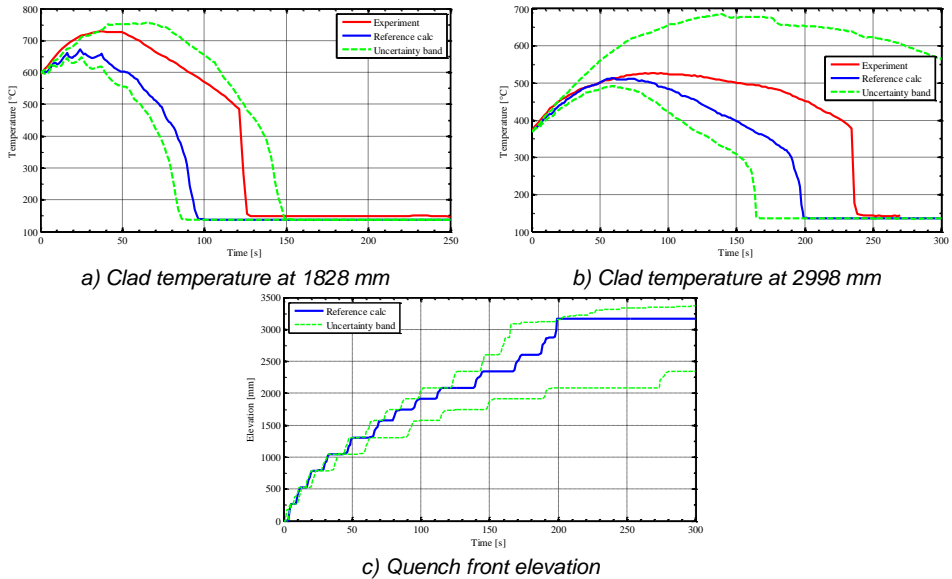


Figure 96 – Results of uncertainty analysis of RELAP5 calculation of PERICLES RE80.

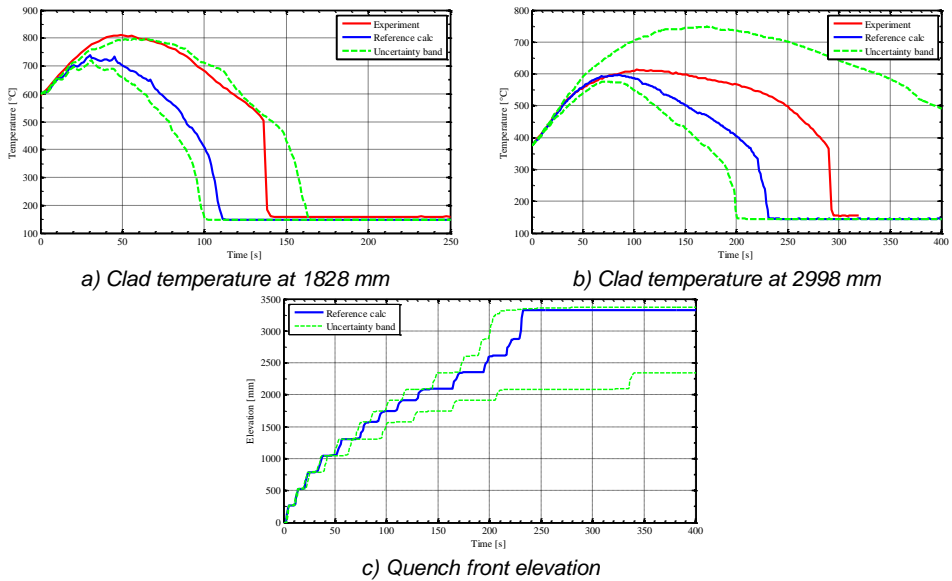


Figure 97 – Results of uncertainty analysis of RELAP5 calculation of PERICLES RE86.

It can be seen that for most of the simulated tests the evaluated uncertainty bands cover sufficiently the measurement data, although not encompass them completely. In a number of sampled calculations the bundles did not quench within the simulated timeframe. Therefore, there is no rewet observed in the upper uncertainty band of

the cladding temperature at the top. It can be pointed out that the initial cladding temperature increase (before PCT value is reached) at the 2/3 height is underpredicted by the code. However, the maximum value of upper uncertainty band does cover the correspondent experimental PCT in 5 tests out of 6 – except RE86 (*Figure 92*), where the PCT in test is underpredicted by 14 °C. However, it should be considered that the reference calculation of test RE86, which has been performed at higher pressure, showed the biggest underprediction of experimental data. This fact and the considerations mentioned above about the expected discrepancies due to the limited knowledge of hardware geometry, give the basis to judge in general as successful the validation against PERICLES tests.

4.3.3. Validation against ACHILLES facility

The variation ranges of reflood-related input parameters (*Table 22*) of RELAP5 Mod3.3 code have been validated against the experimental tests carried out at facility PERICLES that also features different geometry with respect to FEBA facility. However, ACHILLES facility consists of a single rod bundle, therefore bears more resemblance with FEBA facility comparing to PERICLES, where the non-uniform radial power distribution and 2-D geometry may affect the reflood phenomena.

4.3.3.1. Description of ACHILLES facility

The ACHILLES test facility, ref. [53] and [54], was designed to investigate the heat transfer in the core of a Pressurized Water Reactor (PWR) during the reflood phase of a postulated large break loss of coolant accident.

The ACHILLES test section consisted of 69 fuel rod simulators, assembled into a cluster using spacer grids, and mounted vertically within a cylindrical shroud vessel. A cross-sectional diagram of the cluster and shroud vessel is shown in *Figure 98*. The axial power distribution and the location of spacer grids and instrumentation positions are shown in *Figure 99*.

The cluster is surrounded by a circular shroud vessel which served both as a pressure vessel and as a duct to guide the flow of coolant up through the cluster. The shroud vessel was provided with 46 kW of electrical heating.

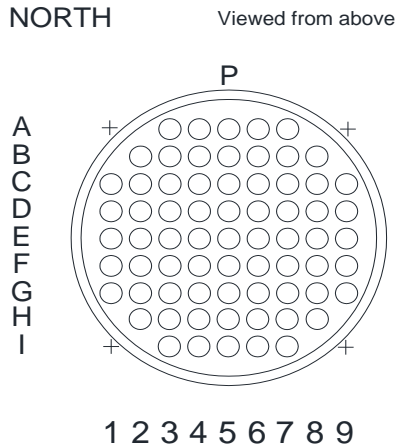


Figure 98 – Cross-section view of ACHILLES test section.

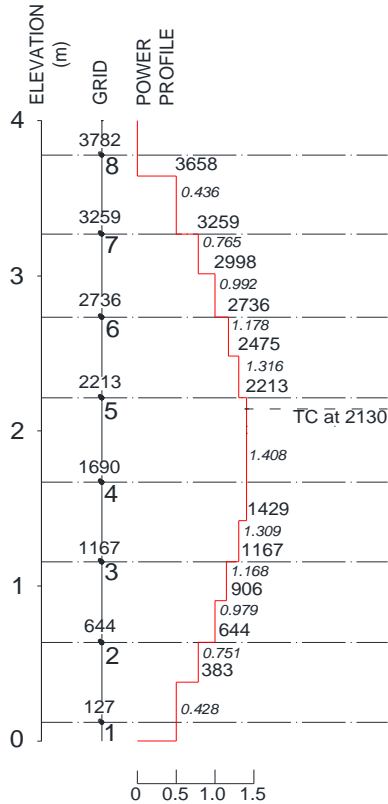


Figure 99 – Axial power profile and temperature measurement location in ACHILLES test section.

4.3.3.2. Modeling of ACHILLES facility with RELAP5 code

Similar to the validation against the PERICLES tests, the model of ACHILLES test section for RELAP5 Mod3.3 code have been developed for “blind” calculations: only the geometrical specifications and test conditions were available. The experimental measurements have been revealed to the analyst only after the uncertainty analysis results have been completed.

Therefore, the same modelling approach has been used for the simulation of the ACHILLES facility as adopted previously for the calculation of the FEBA test: single 1-D hydraulic channel representing the test section with 1 heat structure component representing the entire fuel bundle (*Figure 100*). The number of hydraulic nodes/meshes adopted is similar to the corresponding models of FEBA and PERICLES. The nodalization features are summarized in *Table 28*.

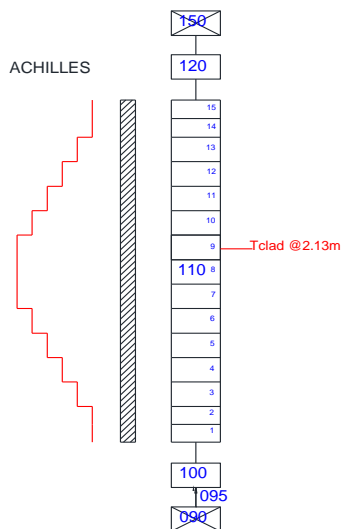


Figure 100 – Sketch of ACHILLES nodalization for RELAP5 code.

Table 28 – Summary of RELAP5 model of ACHILLES facility.

Parameter	Value
Total height/length	3.658 m
Node in heated length	15
Flow area	$7.977 \cdot 10^{-3} \text{ m}^2$
Hydraulic diameter	$1.296 \cdot 10^{-2} \text{ m}$
Wall roughness	$2.0 \cdot 10^{-5}$
Spacer grid K_{loss}	0.2
Maximum linear heat rate	1.2 kW/m
<i>Special options activated:</i>	
Rod bundle interphase friction (b=1 in hydraulic nodes)	
Vertical bundle without cross flow (110 in heat structures)	

4.3.3.3. Uncertainty analysis of ACHILLES tests

Once the RELAP5 model of ACHILLES facility has been set up, the uncertainty analysis of thermal-hydraulic calculation of two ACHILLES tests (*Table 8*, *Table 11*) has been carried out. The obtained uncertainty bands for two selected responses are shown in *Figure 101* and *Figure 102*: cladding temperature at 2.13 m (where the PCT has been observed in experiments) and quench front elevation.

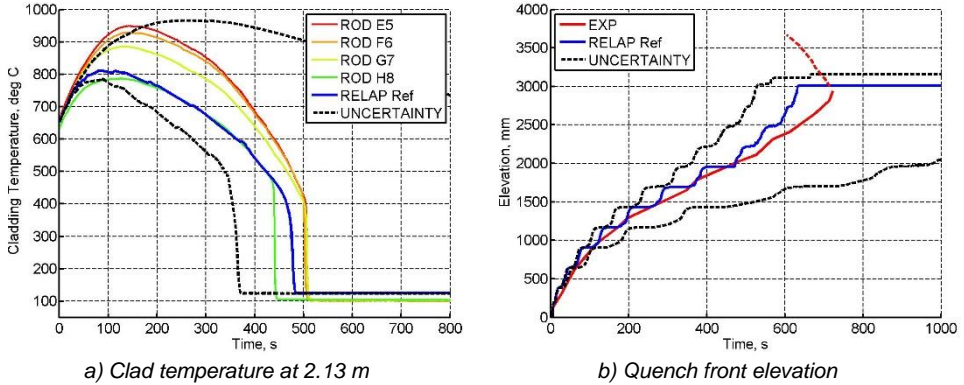


Figure 101 – Results of uncertainty analysis of RELAP5 calculation of ACHILLES A1R030.

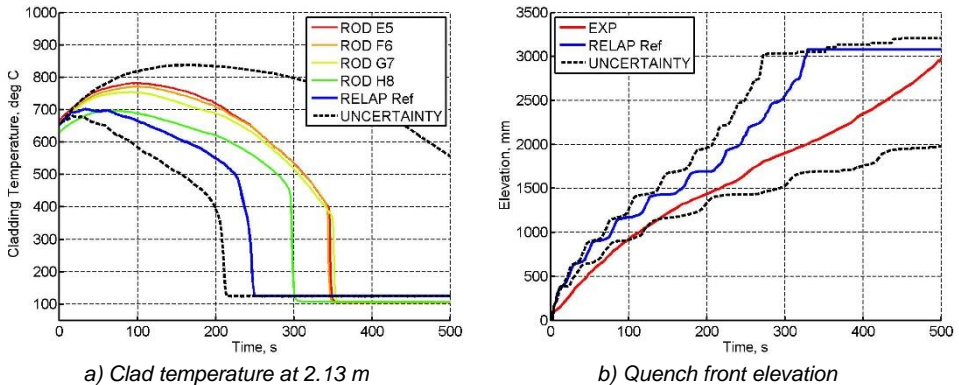


Figure 102 – Results of uncertainty analysis of RELAP5 calculation of ACHILLES A1R048.

In both tests, the predicted cladding temperature in the reference calculations corresponds rather to measurement at peripheral heater rods (H8) than to central one. Therefore the PCT is underestimated by the code, which is consistent with the code behavior at FEBA and PERICLES tests. The quench front propagation is predicted rather well by RELAP5 in the reference calculation of the test A1R030 with smaller reflood rate (Figure 101b). Instead, the model shows more consistent behavior (comparing to the simulations of FEBA and PERICLES) in the test A1R048 with higher reflood rate.

The evaluated uncertainty bands cover most of the experimental data, except the initial temperature increase in the test A1R030. However, the maximum value of the upper uncertainty band of cladding temperature is higher than experimentally measured PCT, which is relevant for nuclear safety. The effect of variation of input parameter on quenching time is rather large, and in some generated sample

calculations the bundle did not quench in the simulated timeframe (however there is clear indication of the cladding temperature decrease).

4.4. External qualification: test-independence and facility-independence checks

The IPREM has been applied to FEBA test 216 in order to quantify the variation ranges of reflood-related input parameters (*Table 22*). Further, these ranges have been subjected to “internal” qualification (via uncertainty analysis of FEBA test 216) and extensive validation through uncertainty analysis of RELAP5 calculations of various experimental reflood tests.

At this juncture, it is necessary to verify whether the validity of results (i.e. ranges of input parameters), obtained by the IPREM, are not strictly dependent on the chosen test (FEBA 216). For this purpose, two checks have been carried out, that constitute the “external” verification of the methodology:

- Test-independence check
- Facility-independence check

4.4.1. Quantification of input parameter uncertainties using FEBA test 222

The test-independence check consists in applying the IPREM to another test of the same facility in order to evaluate the uncertainty of input parameters. The resulting ranges are compared with those obtained from the test 216 and are further adopted to perform the uncertainty analysis of several thermal-hydraulic calculations of reflood tests. The evaluated uncertainty bands of the relevant responses are compared with the experimental data and the uncertainty bands obtained with the input parameter ranges quantified on the basis of FEBA test 216 (*Table 22*). Test FEBA 222 has been selected for this purpose, since it features different system pressure and reflood rate (*Table 9*).

The same steps, carried out previously in the framework of application of IPREM to FEBA 216, have been performed for FEBA 222:

- Calculation of reference case and computation of $\{AA^{R-E}\}$;
- Identification of influential input parameters (using procedure and criteria described in section 4.2.3.);
- Performing sensitivity calculations with variation of input parameters α_i ;
- Computation of values AAz_{ij}^{S-R} , AAz_{ij}^{S-E} , AAG_{ij}^{S-R} and AAG_{ij}^{S-E} ;
- Computation of $CR(\alpha_{ij})$ and application of **limit = 0.22**.

The Average Amplitude values for the reference calculation are presented in the *Table 29*. The same three responses have been selected: cladding temperature at 2/3 height and at the top, and the quench front elevation. The smaller value of $AA1^{R-E}$ for FEBA 222 indicates that in this test the reference calculation provides better agreement of predicted cladding temperature at 2/3 height (where PCT occurs) with experimental data comparing to FEBA 216. But the overall nodalization performance (indicated by AAG^{R-E}) is similar in both tests.

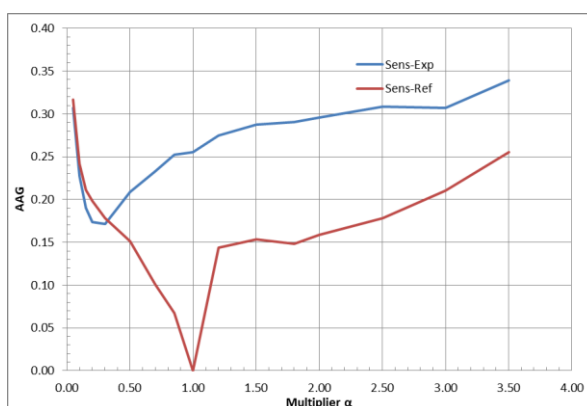
Table 29 – FEBA 222 reference calculation Average Amplitude values.

	Parameter	FEBA222	FEBA216
AAz ^{R-E}	AA1 ^{R-E} – 12b4	0.259	0.342
	AA2 ^{R-E} – 12b2	0.344	0.387
	AA3 ^{R-E} – quench front	0.154	0.135
AAG	AAG ^{R-E}	0.255	0.299

The preliminary sensitivity analysis results showed that 1 more parameter has been identified as an influential one: the transition boiling heat transfer coefficient. This parameter mainly influences the time of rewet. Therefore, the list of influential parameters for FEBA 222 is:

- α_1 – Multiplier to interphase heat transfer coefficient (HTC)
- α_2 – Multiplier to interphase friction
- α_3 – Multiplier to film boiling HTC
- α_4 – Multiplier to convection to vapor HTC
- α_5 – Multiplier to transition boiling HTC

As the next step, a series of *j* sensitivity calculations have been performed with various values for each of the five input parameters α_i and the values AAz_{ij}^{S-R} , AAz_{ij}^{S-E} , AAG_{ij}^{S-R} and AAG_{ij}^{S-E} have been computed. The trends of these values for the first four input parameters are quite similar to those obtained from test 216. Therefore, only the AAG_{5j}^{S-R} and AAG_{5j}^{S-E} for transition boiling HTC are presented below in Figure 103. The computed values of $CR(\alpha_{ij})$ are shown in Figure 104, Figure 105, Figure 106, Figure 107 and Figure 108. The resulting input parameter ranges are presented in Table 30.

Figure 103 – FEBA 222: AAG_{5j}^{S-R} and AAG_{5j}^{S-E} for transition boiling HTC.

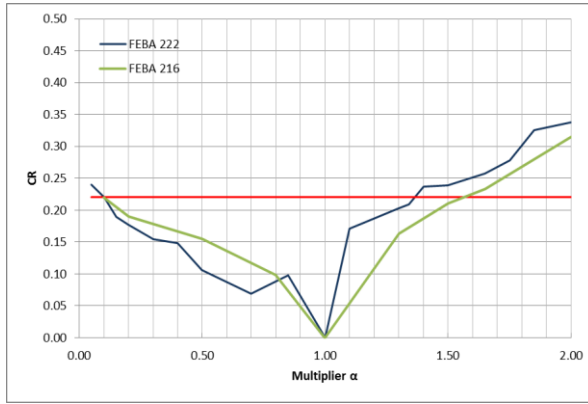


Figure 104 – FEBA 222: $CR(\alpha_{1j})$ for interphase HTC.

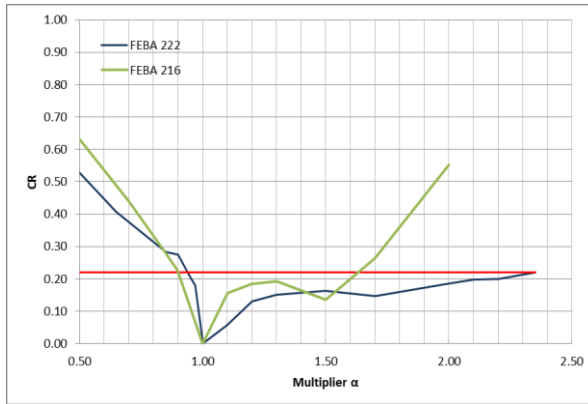


Figure 105 – FEBA 222: $CR(\alpha_{2j})$ for interphase friction coefficient.

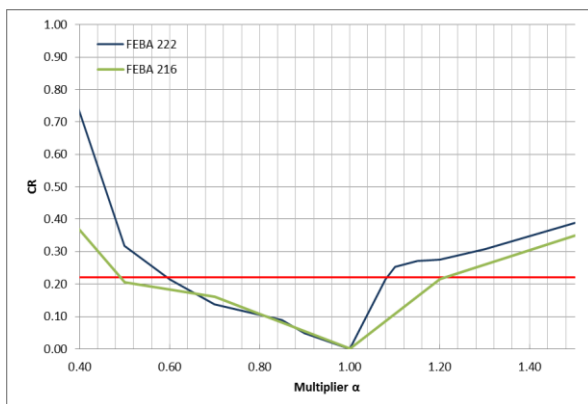


Figure 106 – FEBA 222: $CR(\alpha_{3j})$ for film boiling HTC.

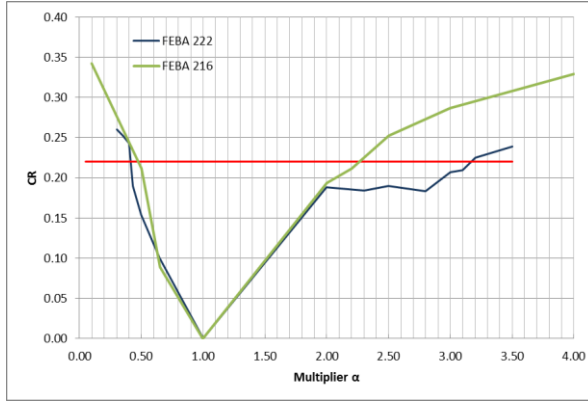


Figure 107 – FEBA 222: $CR(\alpha_{4j})$ for convection to vapor HTC.

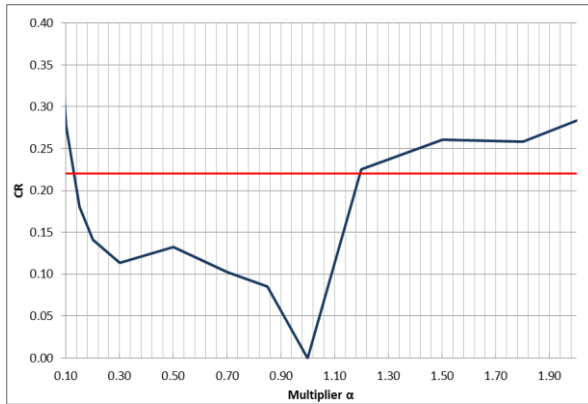


Figure 108 – FEBA 222: $CR(\alpha_{5j})$ for transition boiling HTC.

Table 30 – FEBA 222: quantified variation ranges.

α_i	Parameter	FEBA 222		FEBA 216	
		Min	Max	Min	Max
α_1	Interphase HTC multiplier	0.1	1.36	0.1	1.58
α_2	Interphase friction multiplier	0.96	2.35	0.86	1.62
α_3	Film boiling HTC multiplier	0.6	1.08	0.5	1.20
α_4	Convection to vapor HTC multiplier	0.41	3.2	0.35	2.3
α_5	Transition boiling HTC multiplier	0.12	1.2	-	-

The evaluated range of variation of the input parameters are consistent with those obtained from FEBA test 216 with 2 exceptions:

- the α^U of interphase friction coefficient is considerably larger when derived from test FEBA 222;
- the α^U of convection to vapor HTC is noticeably larger when derived from test FEBA 222.

An increase in interphase friction coefficient tends to postpone the progression of the quench front and, thus, to improve RELAP5 predictions (*Figure 66*). The reference calculation of FEBA test 222 results in worse agreement of the quench front elevation with the experimental data (*Figure 87*) if compared to that of FEBA 216 (*Figure 39*). This is also reflected in higher value of $AA3^{R-E}$ for FEBA 222 comparing to one of FEBA 216 (*Table 29*). Therefore, the higher value of the α^U of interphase friction coefficient is rather reasonable (in order to achieve better agreement with experimental results).

An increase in convection to vapor HTC tends to decrease cladding temperature values, i.e. to deteriorate RELAP5 predictions (*Figure 67*). Apparently, the change in multiplier to convection to vapor HTC in the range of 2.0 - 3.0 does not lead to significant changes in predicted responses. Only further increase of convection to vapor HTC causes the noticeable deviation of sensitivity calculation results with respect to the experimental data. Nevertheless, the upper range α^U of convection to vapor HTC is of lesser importance since it only reduces the predicted cladding temperature which RELAP5 typically underestimates.

The variation ranges of input parameters quantified on the basis of test FEBA 222 have been applied to evaluate uncertainty of thermal-hydraulic calculations of the following tests:

- Test FEBA 216
- Test PERICLES RE80

The obtained uncertainty bands for the relevant responses are shown on *Figure 109* and *Figure 110*.

The comparison of the uncertainty bands of cladding temperature and quench front elevation, evaluated with the input parameter uncertainty ranges derived from two tests with 2 different conditions, shows a difference, consistent with the difference found for the ranges of input parameters, and mainly for:

- the α^U of interphase friction coefficient;
- the α^U of convection to vapor HTC.

The evaluated maximum value of upper uncertainty band of cladding temperature at 2/3 height (where PCT is observed) is very similar for both sets of input parameter variation ranges in both calculated reflood tests. Instead, in both tests the shift of uncertainty bands of all responses in the “right” is noticed when using [α^L ; α^U] derived from FEBA 222. Taking into account the considerations mentioned above and the fact the prediction of the main figure-of-merit relevant for nuclear safety – PCT – is not affected, it can be concluded that the variation ranges of input parameters when obtained by IPREM from tests with different conditions are consistent. Therefore, it can be concluded that the methodology is test-independent.

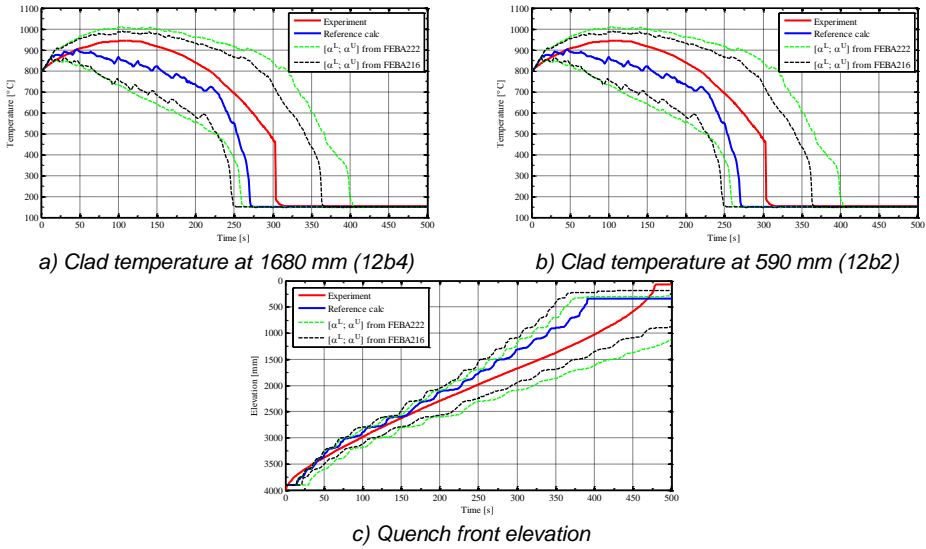


Figure 109 – Uncertainty analysis of RELAP5 calculation of FEBA 216 with $[\alpha^L ; \alpha^U]$ derived from FEBA 222

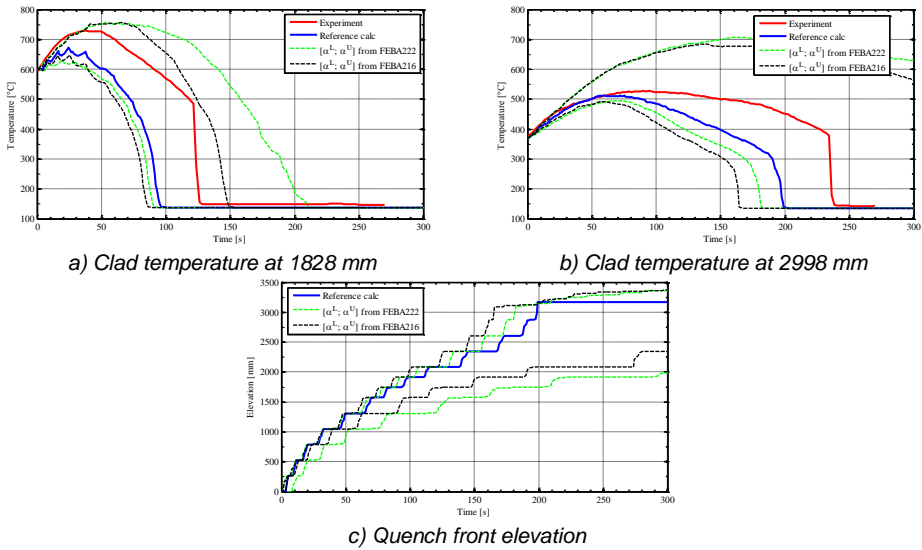


Figure 110 – Uncertainty analysis of RELAP5 calculation of PERICLES RE80 with $[\alpha^L ; \alpha^U]$ derived from FEBA 222.

4.4.2. Quantification of input parameter uncertainties using PERICLES facility

The facility-independence check consists in applying the IPREM to another experimental facility (but anyway to a test with similar conditions) in order to evaluate the uncertainty of input parameters. The resulting ranges are compared with those obtained from the FEBA tests 216 and 222 and are further applied to perform the uncertainty analysis of several thermal-hydraulic calculations of reflood tests. Within the framework of this task, the IPREM has been applied to PERICLES test RE79 which conditions (*Table 10*) are similar to those of the FEBA test 216.

4.4.2.1. Post-test calculation of PERICLES test RE79

In the framework of the validation of the IPREM for reflood-related parameters, the model of PERICLES test section for RELAP5 code has been developed and the calculations have been performed in “blind” mode: i.e. the measurement results have not been available until the uncertainty analyses have been completed.

Once the measurement data have been released, the post-test calculation of the PERICLES tests has been performed and the modifications have been introduced into the model in order to improve the agreement with the experimental data (*Table 31*). It should be pointed out the applied modification is consistent with the “best practice” approach in RELAP5 modeling: option 110 is better validated since most of code applications have been performed with 1-D geometry (either 1-D experimental facilities or simulation of 3-D nuclear reactor core with a single channel). The changes in model predictions of the test RE79 are shown in *Figure 111*, *Figure 112*, *Figure 113* and *Figure 114*.

Table 31 – Modification in post-test model of RELAP5 model of PERICLES facility.

Parameter	blind	post-test
Heat structure option	111 (vertical bundle with cross flow)	110 (vertical bundle without cross flow)

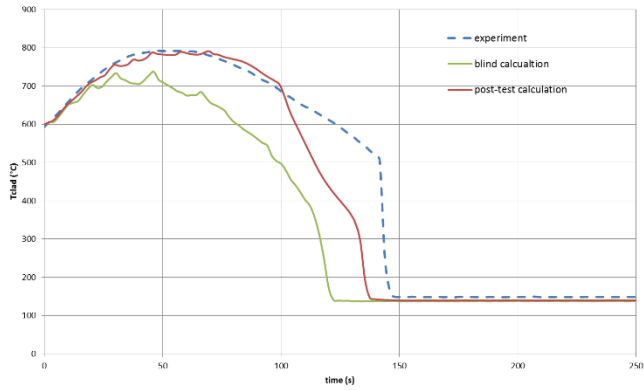


Figure 111 – Post-test calculation of PERICLES RE79: cladding temperature at 2/3 height of hot assembly.

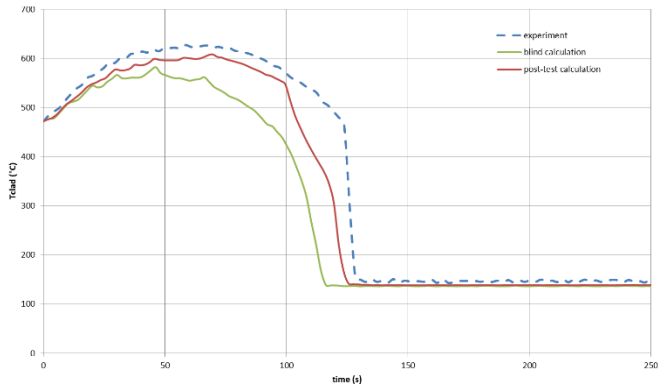


Figure 112 – Post-test calculation of PERICLES RE79: cladding temperature at 2/3 height of cold assembly.

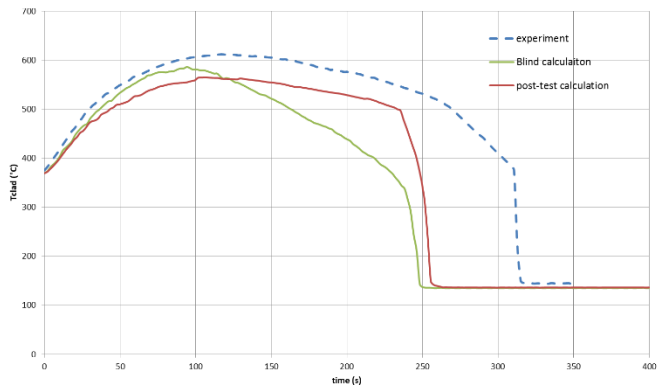


Figure 113 – Post-test calculation of PERICLES RE79: cladding temperature at top of hot assembly.

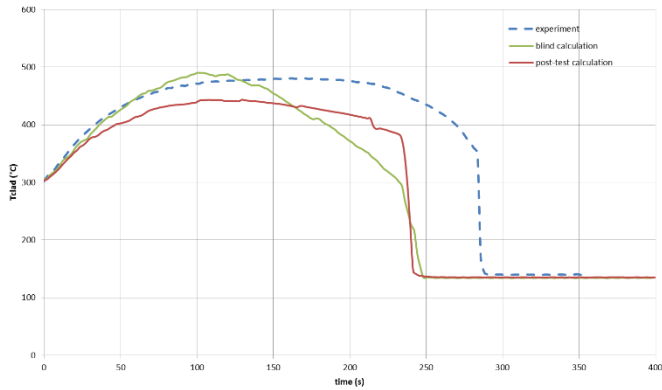


Figure 114 – Post-test calculation of PERICLES RE79: cladding temperature at top of cold assembly.

4.4.2.2. Quantification and input parameter uncertainties

The same steps, carried out previously in the framework of application of the IPREM to FEBA tests, have been performed for PERICLES test RE79:

- Calculation of reference case and computation of $\{AA^{R-E}\}$;
- Identification of influential input parameters (using procedure and criteria described in section 4.2.3.);
- Performing sensitivity calculations with variation of input parameters α_i ;
- Computation of values AAz_{ij}^{S-R} , AAz_{ij}^{S-E} , AAG_{ij}^{S-R} and AAG_{ij}^{S-E} ;
- Computation of $CR(\alpha_{ij})$ and application of **limit** = 0.22.

For the application of the IPREM to PERICLES test RE79 the following responses $\{R\}$ have been selected:

- 1) TC38A4 - cladding temperature at 2/3 height in cold assembly
- 2) TC38B4 - cladding temperature at 2/3 height in hot assembly
- 3) TC59A5 - cladding temperature at top of cold assembly
- 4) TC59B5 - cladding temperature at top of hot assembly

Unfortunately, quench front experimental measurement was not available, since many considered input parameters actually influence the quench front propagation and just few are important for PCT. At this juncture, an engineering judgment had to be introduced in order to separate the responses “responsible” for PCT from those “responsible” for quench front propagation:

- Cladding temperature at 2/3 height has been considered “responsible” for PCT: FFT analysis has been performed only for the first 135 s of the transient (to exclude the rewet from the consideration);
- Cladding temperature at top has been considered “responsible” for quench front propagation: FFT analysis has been performed for the entire transient timeframe, including the rewet.

The Average Amplitude values and applied weighting factors for the reference calculation are presented in the *Table 32*.

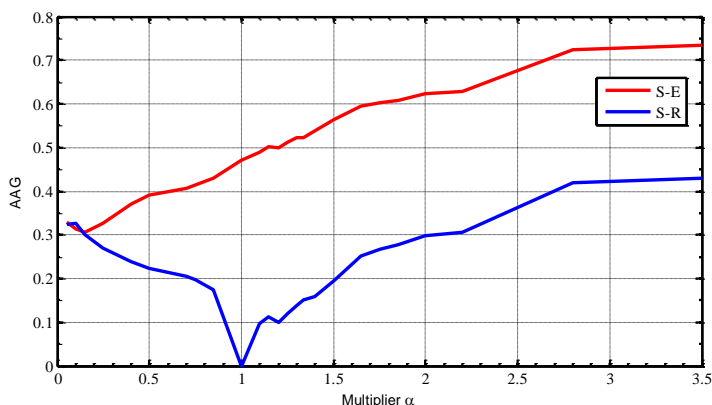
Table 32 – PERICLES RE79 IPREM settings for reference calculation.

	Parameter	Value
AAz ^{R-E}	AA1 ^{R-E} – TC38A4	0.285
	AA2 ^{R-E} – TC38B4	0.598
	AA3 ^{R-E} – TC59A5	0.531
	AA4 ^{R-E} – TC59B5	0.249
w _z	w _t – cladding temperature	0.25
AAG	AAG ^{R-E}	0.472

The preliminary sensitivity analysis results showed that transition boiling heat transfer coefficient is also influential (as for FEBA test 222). Therefore, the list of influential parameters for PERICLES RE79 is:

- α_1 – Multiplier to interphase heat transfer coefficient (HTC)
- α_2 – Multiplier to interphase friction
- α_3 – Multiplier to film boiling HTC
- α_4 – Multiplier to convection to vapor HTC
- α_5 – Multiplier to transition boiling HTC

As the next step, a series of *j* sensitivity calculations have been performed with various values for each of the five input parameters α_i and the values AAz_{ij}^{S-R} , AAz_{ij}^{S-E} , AAG_{ij}^{S-R} and AAG_{ij}^{S-E} have been computed. The Global AA values for all five input parameters are shown in *Figure 115*, *Figure 116*, *Figure 117*, *Figure 118* and *Figure 119*. The trends are consistent with those obtained for test FEBA 216 (*Figure 57*, *Figure 58*, *Figure 59* and *Figure 60*), which means the effect of variation of input parameters is similar in the simulations of both facilities.

Figure 115 – PERICLES RE79: AAG_{1j}^{S-R} and AAG_{1j}^{S-E} for interphase HTC.

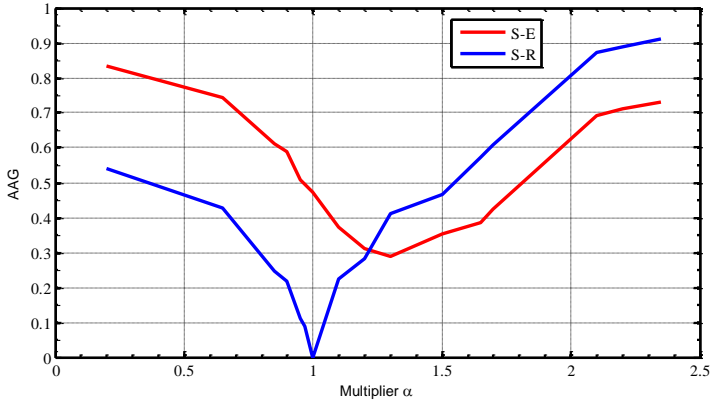


Figure 116 – PERICLES RE79: AAG_{2j}^{S-R} and AAG_{2j}^{S-E} for interphase friction coefficient.

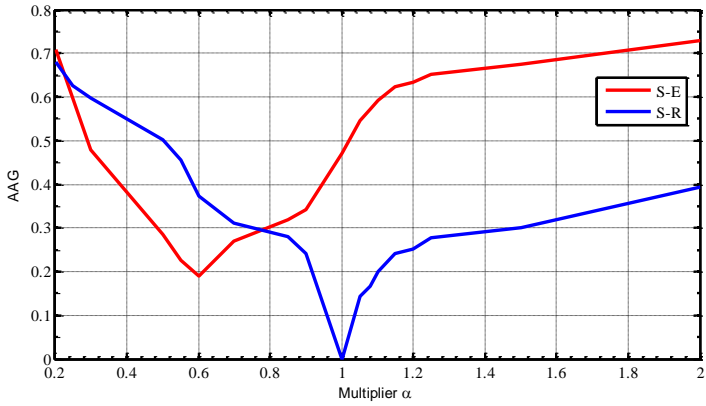


Figure 117 – PERICLES RE79: AAG_{3j}^{S-R} and AAG_{3j}^{S-E} for film boiling HTC.

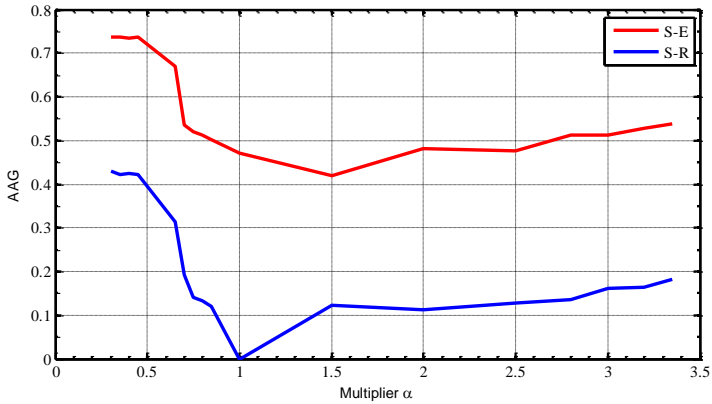


Figure 118 – PERICLES RE79: AAG_{4j}^{S-R} and AAG_{4j}^{S-E} for convection to vapor HTC.

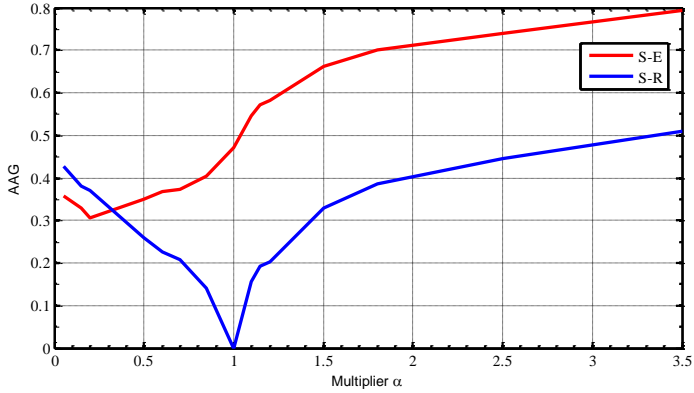


Figure 119 – PERICLES RE79: AAG_{4j}^{S-R} and AAG_{4j}^{S-E} for transition boiling HTC.

The computed values of $CR(\alpha_{ij})$ are shown in Figure 120, Figure 121, Figure 122, Figure 123 and Figure 124. The resulting input parameter ranges are presented in Table 33.

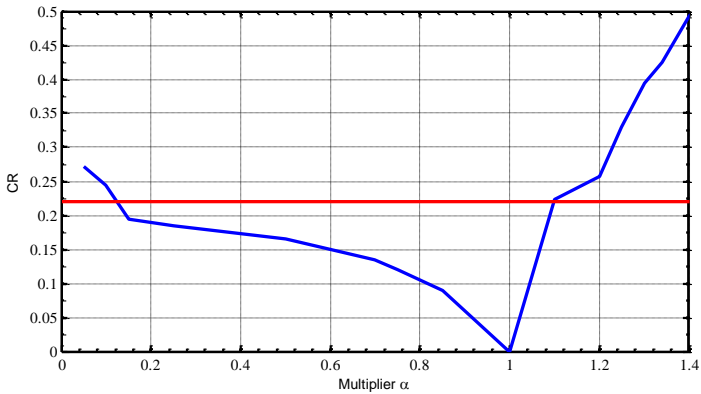


Figure 120 – PERICLES RE79: $CR(\alpha_{1j})$ for interphase HTC.

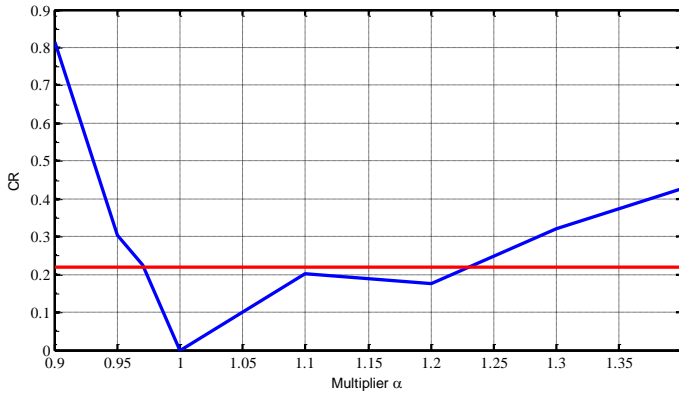


Figure 121 – PERICLES RE79: $CR(\alpha_{2j})$ for interphase friction coefficient.

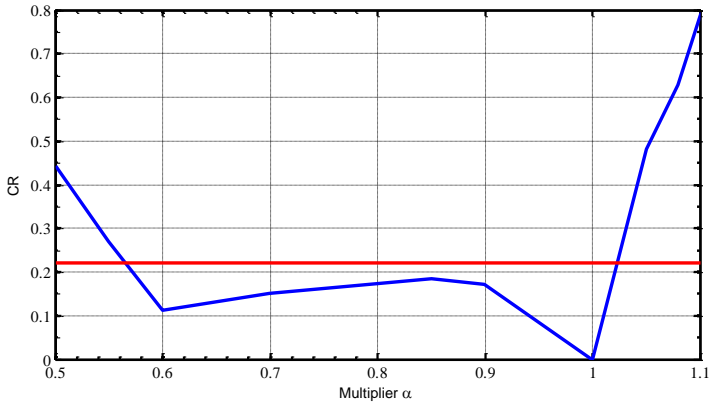


Figure 122 – PERICLES RE79: $CR(\alpha_{3j})$ for film boiling HTC.

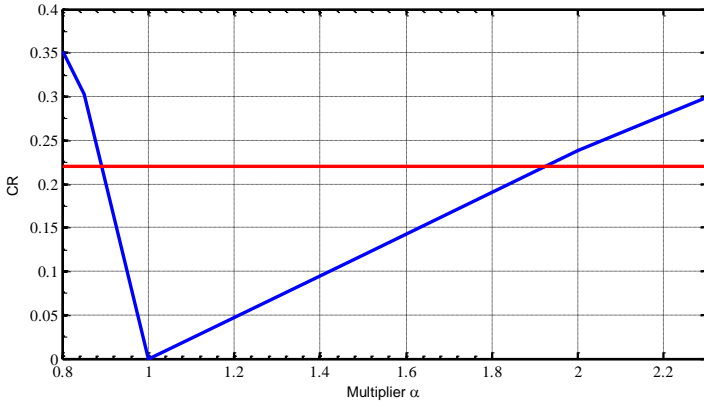


Figure 123 – PERICLES RE79: $CR(\alpha_{4j})$ for convection to vapor HTC.

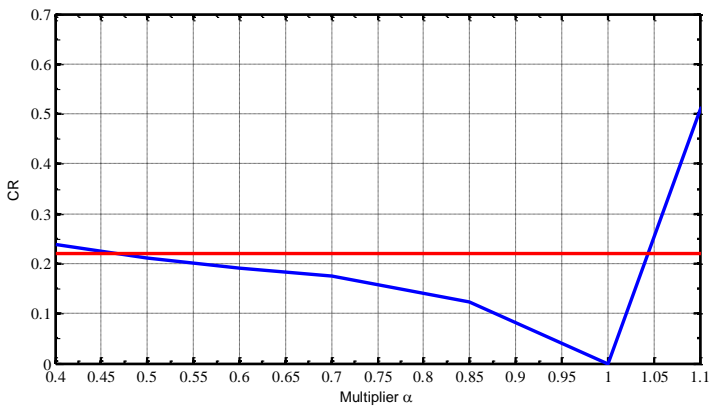


Figure 124 – PERICLES RE79: $CR(\alpha_{5j})$ for transition boiling HTC.

Table 33 – PERICLES RE79: quantified variation ranges.

α_i	Parameter	PERICLES RE79		FEBA 216		FEBA 222	
		Min	Max	Min	Max	Min	Max
α_1	Interphase HTC multiplier	0.12	1.14	0.1	1.58	0.1	1.36
α_2	Interphase friction multiplier	0.95	1.23	0.86	1.62	0.96	2.35
α_3	Film boiling HTC multiplier	0.56	1.03	0.5	1.2	0.6	1.08
α_4	Convection to vapor HTC multiplier	0.87	1.95	0.35	2.3	0.41	3.2
α_5	Transition boiling HTC multiplier	0.5	1.05	-	-	0.12	1.2

Since PERICLES and FEBA facilities are rather different in geometry and conditions, the direct comparison of quantified variation ranges of input parameter is not feasible. However, the ranges obtained on the basis of PERICLES test RE79 appear in general consistent with those obtained from FEBA tests. One may note that quantified value α^L of the convection to vapor HTC multiplier is rather high. This is due to the fact that the predicted cladding temperatures at 2/3 height in the reference calculation are in good agreement with experimental data. Thus, further decrease in convection to vapor HTC increases the maximum cladding temperature, anticipates the temperature peak and, therefore, deteriorates the prediction of the code with respect to experiment. The IPREM algorithm, thus, limits the α^L of the input parameter.

The variation ranges of input parameters quantified on the basis of test PERICLES RE79 have been applied to evaluate the uncertainty of the thermal-hydraulic calculations of the following tests:

- Test FEBA 216
- Test PERICLES RE80 (post-test model)

The obtained uncertainty bands for relevant responses are shown in *Figure 125* and *Figure 126*. The uncertainty bands encompass the experimental measurements (*Figure 126*) of test RE80 when the variation ranges [α^L ; α^U] are derived from the different test (RE79) but performed at the same facility (PERICLES). On the other hand, the input parameter variation ranges [α^L ; α^U] derived from PERICLES test RE79 result in “narrower” uncertainty bands of responses (comparing to those derived from FEBA tests (*Table 33*)) predicted for test at different facility (FEBA 216). The experimental quench front and cladding temperature at the top (*Figure 125 b,c*) are encompassed by the evaluated uncertainty band. Instead, the part of cladding temperature trend at 2/3 height, where the temperature starts to decrease after reaching its PCT, is not covered by the uncertainty band (*Figure 125 a*). However, the maximum value of upper uncertainty band, even if postponed in time, is marginally greater than the experimentally observed PCT, which is important from the nuclear safety point of view. Therefore, it may be concluded that the IPREM methodology is facility-independent. Nevertheless, in the possible industrial application of IPREM for evaluation of uncertainties of input parameters, it is suggested to use the data from experimental facilities that would be coherent with the adopted nodalization approach for modeling of the actual nuclear power plant.

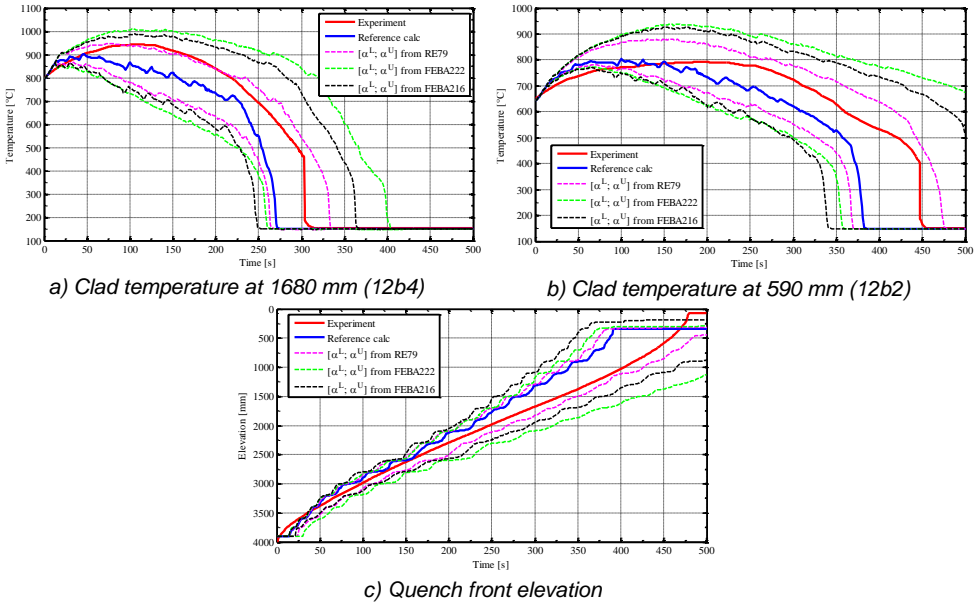


Figure 125 – Uncertainty analysis of RELAP5 calculation of FEBA 216 with $[\alpha^L; \alpha^U]$ derived from PERICLES RE79.

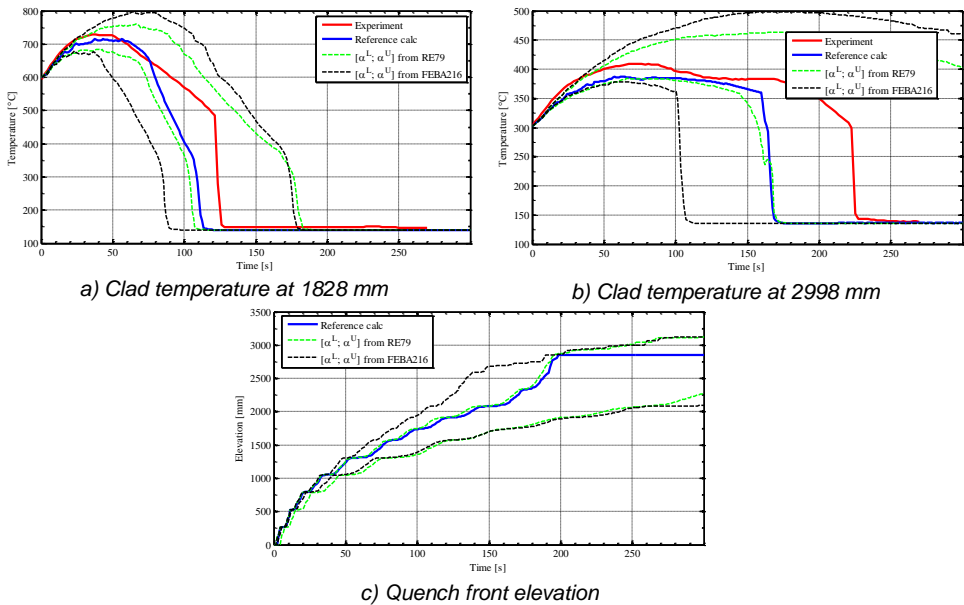


Figure 126 – Uncertainty analysis of RELAP5 calculation of PERICLES RE80 with $[\alpha^L; \alpha^U]$ derived from PERICLES RE79.

4.5. External qualification: application of IPREM to CATHARE2 code

The IPREM methodology has been applied to evaluate the uncertainty of reflood-related input parameters of thermal-hydraulic code RELAP5 Mod3.3. Obtained results have been subjected to various “internal”, “external” qualifications and extensive validation through uncertainty analysis of RELAP5 calculations of various experimental reflood tests.

As a final step of the validation of the IPREM methodology, it is necessary to verify whether the IPREM is not strictly dependent on the type of thermal-hydraulic code. For this purpose, a final code-independence check has been carried out, that contributes to the “external” verification of the methodology. The CATHARE2 thermal-hydraulic code has been selected. At this step, the following activity has been performed:

- To apply IPREM to FEBA test 216 and evaluate uncertainties of reflood-related input parameters [α^L ; α^U];
- To validate quantified variation ranges of input parameters through uncertainty analysis of thermal-hydraulic calculations of several reflood-tests performed at different experimental facilities.

4.5.1. Modeling of FEBA facility with CATHARE2 code

The CATHARE 2 (Code for Analysis of Thermal-Hydraulics during an Accident of Reactor and safety Evaluation) is a best estimate system code, ref. [56], originally devoted to calculations of thermal-hydraulic transients in Light Water Reactors such as PWR, VVER or BWR. All CATHARE modules are based on a six-equation two-fluid model (mass, energy and momentum equations for each phase), with additional optional equations for non-condensable gases and radio-chemical components. It has been developed in Grenoble by the Commissariat à l’Energie Atomique (CEA), Electricité de France (EDF), AREVA and Institut de Radioprotection et de Sûreté Nucléaire (IRSN). More detailed description of CATHARE2 are provided in Appendix A.

The FEBA test assembly has been modeled by CATHARE2 V2.5 Mod 7.1 code by one single 1-D component representing the core bundle (heated part, 3900 mm), inlet and outlet boundary conditions and connected with junctions. The nodalization is built-up based upon the drawings shown in *Figure 32*, *Figure 33* and *Figure 34*, and also on the code user-guide recommendations, ref. [57]. However, no special tuning and adjustments have been applied to achieve the best possible agreement with experimental data. The general modeling scheme is illustrated in the *Figure 127*.

The 1D component is composed of 39 vertical meshes in the core (length of 1 mesh is 100 mm). No cross-flow inside the bundle is modeled. In order to simulate the pressure loss due to flow restriction, the 7 grid spacers are modeled according to the specifications. The form loss coefficient (K_{loss}) is set to 1.68 for each spacer grid. However, no change in hydraulic diameter or flow area reduction is modeled at the spacer grids elevations. Locations of the implemented thermocouples 12b1, 12b2, 12b3, 18a1, 18a2, 18a3 and 18a4 correspond exactly to scalar nodes of the meshing.

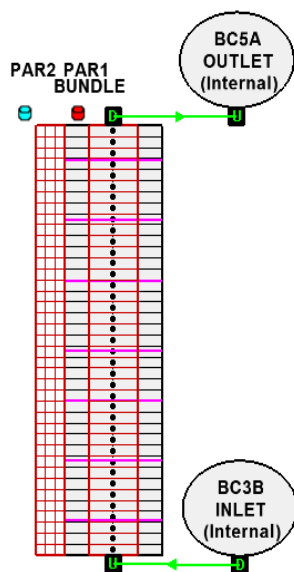


Figure 127 – CATHARE model of the FEBA rod bundle.

The heater rods are represented with a single heat structure component with axial power profile imposed as in the experiment specifications. In radial direction the fuel rod is divided into 3 parts: heater, insulator and cladding (*Figure 33*). The thick-wall housing is modelled (thickness is 6.5 mm), whereas unheated part of rods, lower and upper plenum are not modelled. The test section is assumed to be a well insulated, hence no heat losses are simulated.

Thermal properties of the materials (Nichrome Ni Cr 80 20 for cladding and heating elements, Magnesium oxide as a filler and insulator material in the fuel rod simulator and the V2A Chrome Nickel Steel for the test section housing) are obtained by a polynomial interpolation from FEBA data given by GRS, ref. [57]. The CATHARE reflood correlations (REFLCHAR option) are used, ref. [58] and [59], for both the heater rods to fluid and housing to fluid heat transfers.

The following boundary conditions are modelled:

- Inlet boundary conditions:
 - BC3B (for steady-state critical power calculations: HL, HG, ALFA, VL and VG). Here: HL, HG - liquid and gas enthalpies (J/kg), ALFA - void fraction, VL and VG - liquid and gas velocities (m/s);
- Outlet boundary conditions:
 - BC5A (outlet pressure, Pa);
- Power vs. time law:
 - Is imposed to the bundle heat structure by means of general table with specified power curve.

Table 34 – Summary of CATHARE2 model of FEBA facility.

Parameter	Value
Total height/length	3.90 m
Node in heated length	39
Flow area	$3.893 \cdot 10^{-3} \text{ m}^2$
Hydraulic diameter	$1.347 \cdot 10^{-2} \text{ m}$
Spacer grid K_{loss}	1.68
Total heat transfer area of the heated part of heater rods	3.2928 m^2
Maximum linear heat rate	2.441 kW/m

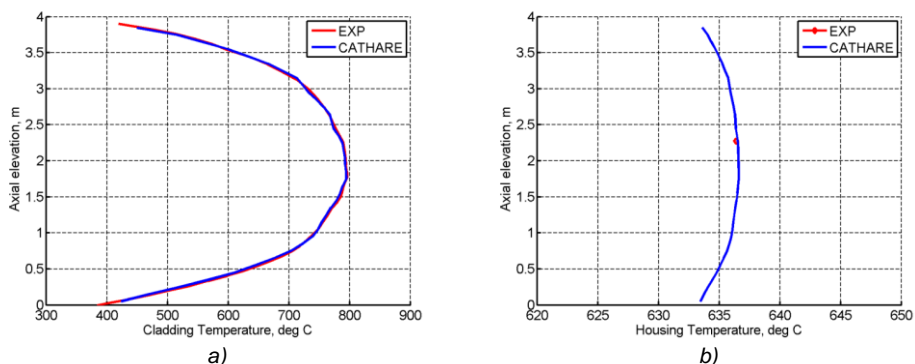


Figure 128 – FEBA test 216: predicted by CATHARE2 steady-state clad (a) and housing (b) temperature distributions.

The main model properties are summarized in *Table 34*. In order to reach the Start of Transient (SoT) conditions, no steady state calculation was performed but a set-up of the clad and shroud vessel temperatures. As to the initial conditions, all junction flow was set to stagnation (0.0 m/s), while the steam temperature was set to the value slightly above the saturation all along the volumes (200°C). Comparison of the cladding and housing axial temperature distributions to the experimental one is shown in *Figure 128*.

The transient begins when the experimental initial clad temperature at 1.625 m is reached. By starting of the test run the bundle power is increased to the required level simulating decay heat according to 120% ANS-standard about 40 s after reactor shut down. Simultaneously the water supply was activated.

The results of reference calculation of test 216 are shown in *Figure 129* and *Figure 130*. CATHARE2 calculation underestimates the peak cladding temperature (PCT) and predicts faster quench front propagation comparing to experimental data. The quench at the very top of the bundle is simulate by the code as top-down reflow, on the contrary to the shown bottom-up reflow in *Figure 131*, and is not considered in the framework of evaluation of uncertainty of input parameters. It should be noted

that calculations have been performed as “post-test”, i.e. experimental results were available to the analyst. However, no special tuning has been applied to the model in order to achieve best agreement possible with experimental data. Instead, the observed discrepancies of calculation results using the standard nodalization practices with respect to the experimental data were deemed as acceptable.

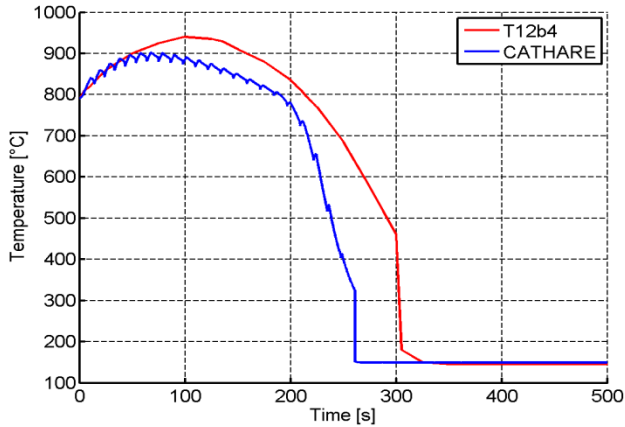


Figure 129 – FEBA test 216: predicted by CATHARE2 cladding temperature at 2/3 height.

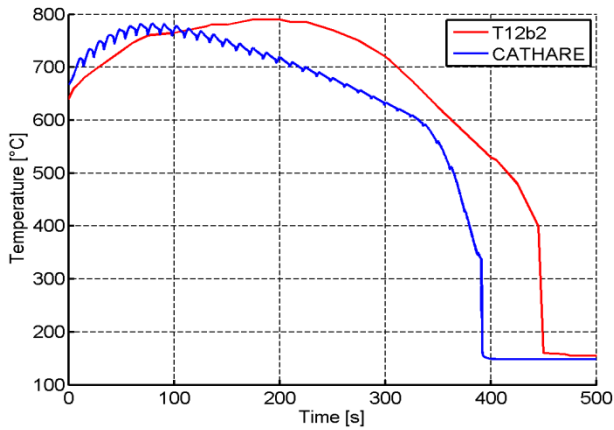


Figure 130 – FEBA test 216: predicted by CATHARE2 cladding temperature at TAF.

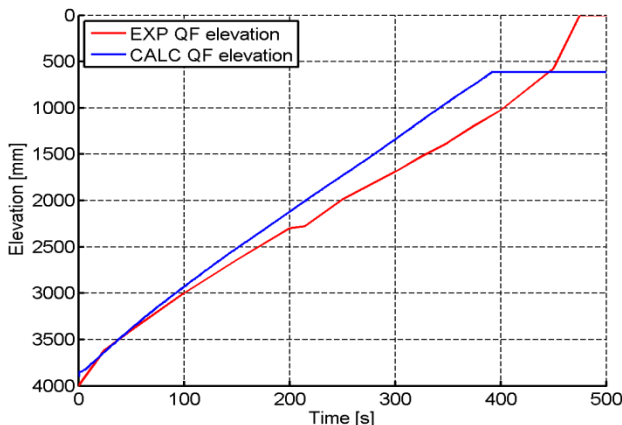


Figure 131 – FEBA test 216: predicted by CATHARE2 quench front propagation.

4.5.2. Quantification of input parameter uncertainties

The IPREM has been applied to FEBA test 216 simulated with CATHARE code in order to evaluate the uncertainties of input parameters:

- Calculation of reference case and computation of $\{AA^{R-E}\}$;
- Identification of influential input parameters;
- Performing sensitivity calculations with variation of input parameters α_i ;
- Computation of values AAz_{ij}^{S-R} , AAz_{ij}^{S-E} , AAG_{ij}^{S-R} and AAG_{ij}^{S-E} ;
- Computation of $CR(\alpha_{ij})$ and application of **limit** = 0.22.

The same 3 responses $\{R\}$ have been used in CATHARE calculations as in RELAP5 applications:

- 1) Cladding temperature at location 12b4 (where PCT is observed)
- 2) Cladding temperature at location 12b2 (top of heated part)
- 3) Quench front elevation (QF)

The Average Amplitude values and applied weighting factor for the reference calculation are presented in the *Table 35*. The obtained values of calculate $\{AA^{R-E}\}$ are consistent with the time trends presented in *Figure 129*, *Figure 130* and *Figure 131*: the code underprediction of the cladding temperature at 2/3 height results in relatively high $AA1^{R-E}$.

The preliminary sensitivity analysis has been applied to identify the influential input parameters of CATHARE2 code. The procedure and criteria described in section 4.2.3 have been applied for this purpose. Finally, three code input parameters (corresponding to physical models of CATHARE2 code) have been identified as influential (*Table 36*), ref. [17]:

- α_1 – Multiplier to wall-fluid global heat transfer;
- α_2 – Multiplier to conduction near quench front;
- α_3 – Multiplier to interfacial friction.

The identified influential parameters are coherent with the findings of participants of PREMIUM benchmark who use CATHARE2 code, ref. [49]. It should be noticed that CATHARE2 code allows user to use multipliers to many correlations directly in the input data deck and thus no re-compilation is needed, ref. [59]. The variations of the selected responses due to variation in influential input parameters are presented in Figure 132, Figure 133 and Figure 134, ref. [60].

Table 35 – FEBA 216 IPREM settings for reference calculation with CATHARE2.

	Parameter	CATHARE2	RELAP5
AAz ^{R-E}	AA1 ^{R-E} – 12b4	0.576	0.342
	AA2 ^{R-E} – 12b2	0.328	0.387
	AA3 ^{R-E} – quench front	0.126	0.135
Wz	w _l – cladding temperature	0.357	0.357
	w _{qf} – quench front	0.286	0.286
AAG	AAG ^{R-E}	0.359	0.299

Table 36 – Identified influential reflood-related input parameters for CATHARE2.

α	Parameter	Keyword	Affected response
α_1	wall-fluid global heat transfer	PQFDT	$\Delta T_{clad}, t_{rew}$
α_2	conduction near quench front	P1K2FDT	t_{rew}
α_3	interfacial friction	TOIFDT	$\Delta T_{clad}, t_{rew}$

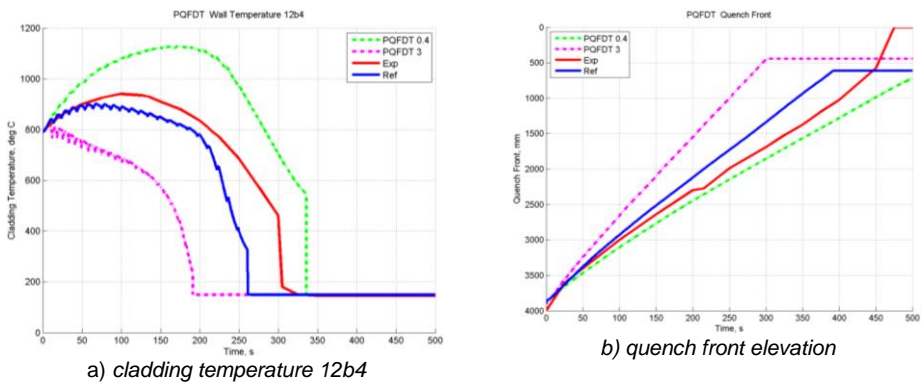


Figure 132 – CATHARE2 sensitivity to variations in wall-fluid global heat transfer.

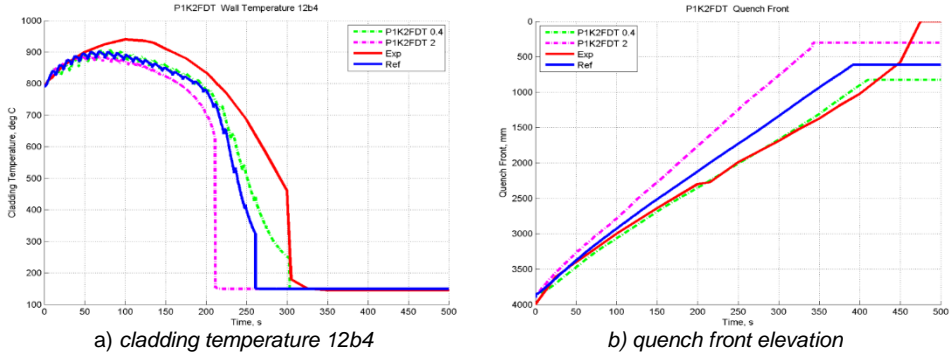


Figure 133 – CATHARE2 sensitivity to variations in conduction near quench front.

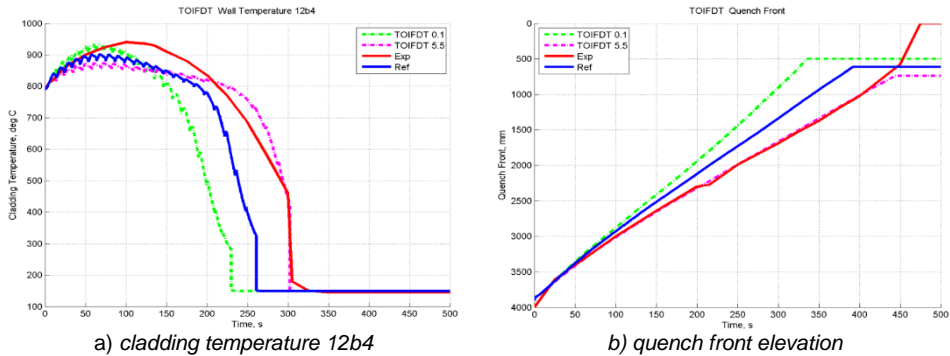


Figure 134 – CATHARE2 sensitivity to variations in interfacial friction.

As the next step, a series of j sensitivity calculations have been performed with various values for each of three input parameters α_i and the values AAZ_{ij}^{S-R} , AAZ_{ij}^{S-E} , AAG_{ij}^{S-R} and AAG_{ij}^{S-E} have been computed. The trends of AAG_{ij}^{S-R} and AAG_{ij}^{S-E} are presented in Figure 135, Figure 136 and Figure 137. The improvement of code prediction is noticeable from values AAG_{ij}^{S-E} have while decreasing the global heat transfer and conduction near quench front (Figure 135 and Figure 136), which can also be visually confirmed by Figure 132 and Figure 133. The AAG_{ij}^{S-E} indicates that the best agreement of calculation results with experimental data occurs when $\alpha_1 \sim 1$. Increasing the multiplier for interfacial friction leads to constant improvement (Figure 137) and the predicted quench front almost matches the experimental data at $\alpha_3 \sim 5.5$.

Next, the $CR(\alpha_{ij})$ is computed for each of 3 input parameters according to equation (27). The results are shown in Figure 138, Figure 139 and Figure 140. The **limit** = 0.22 (red line in Figures) has been applied to each $CR(\alpha_{ij})$ in order to quantify the variation ranges of input parameters (Table 37). It should be pointed out, that there was no significant changes in CATHARE2 prediction of the cladding temperature while decreasing the parameter “conduction near quench front” (Figure 133 a), because this input parameter almost exclusively affects the quench front propagation. Since the quench front response has lower weight in calculation of AAG, there is no significant change in $CR(\alpha_{2j})$ at $\alpha_2 < 0.8$ (Figure 139). Therefore,

an engineering judgment had to intervene and a lower limit of 0.5 has been assumed for this input parameter.

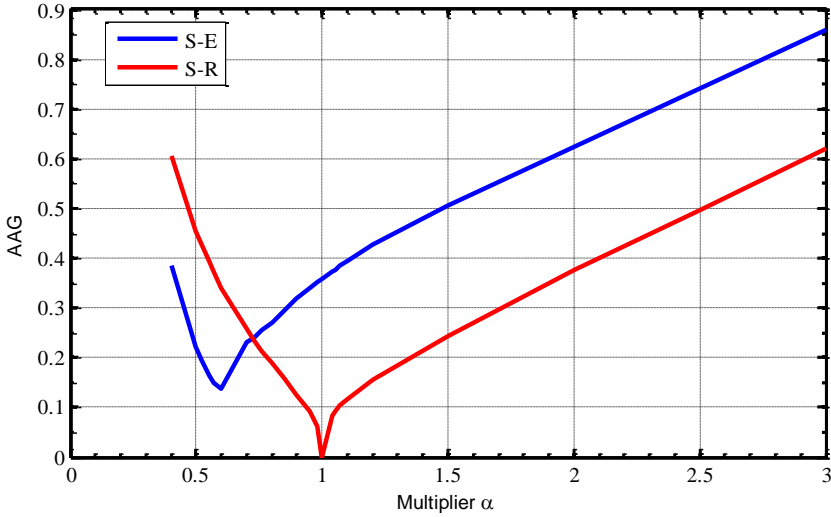


Figure 135 – CATHARE2: AAG_{1j}^{S-R} and AAG_{1j}^{S-E} for wall-fluid global heat transfer.

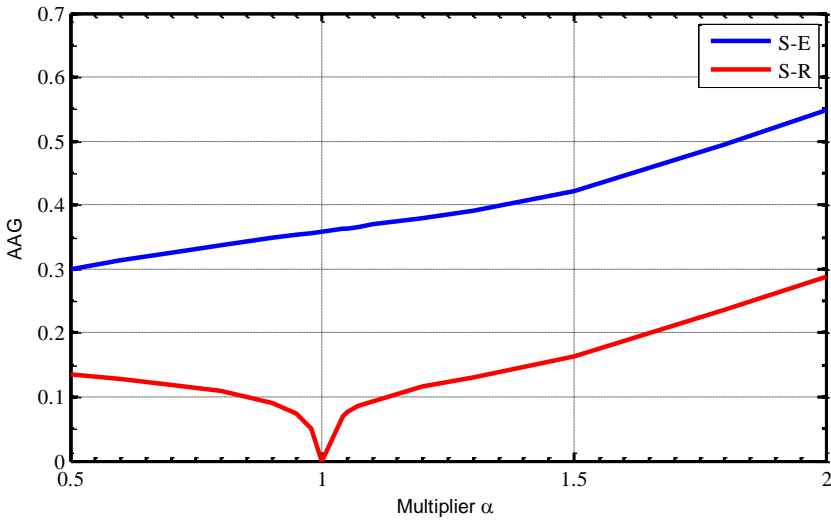


Figure 136 – CATHARE2: AAG_{2j}^{S-R} and AAG_{2j}^{S-E} for conduction near quench front.

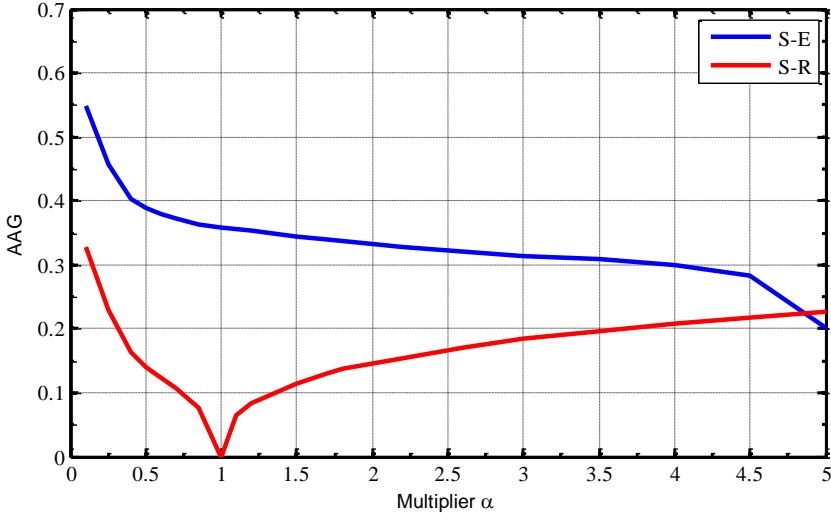


Figure 137 – CATHARE2: AAG_{3j}^{S-R} and AAG_{3j}^{S-E} for interfacial friction.

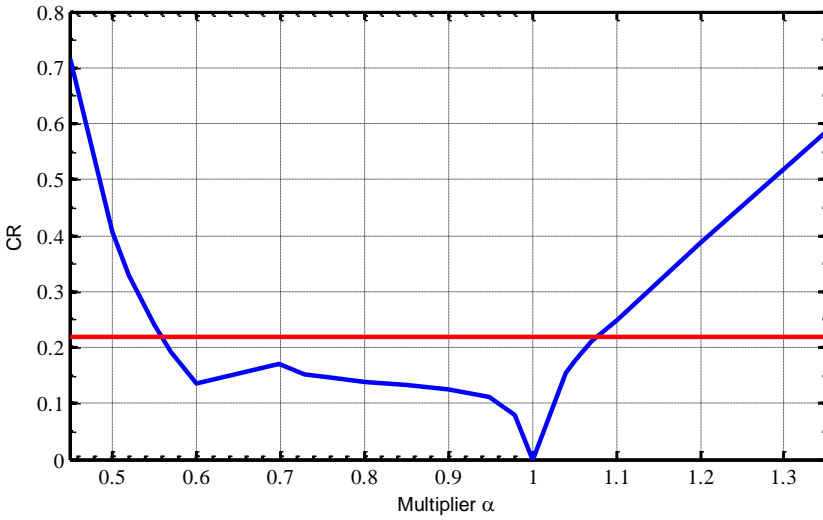


Figure 138 – CATHARE2: $CR(\alpha_{1j})$ for wall-fluid global heat transfer.

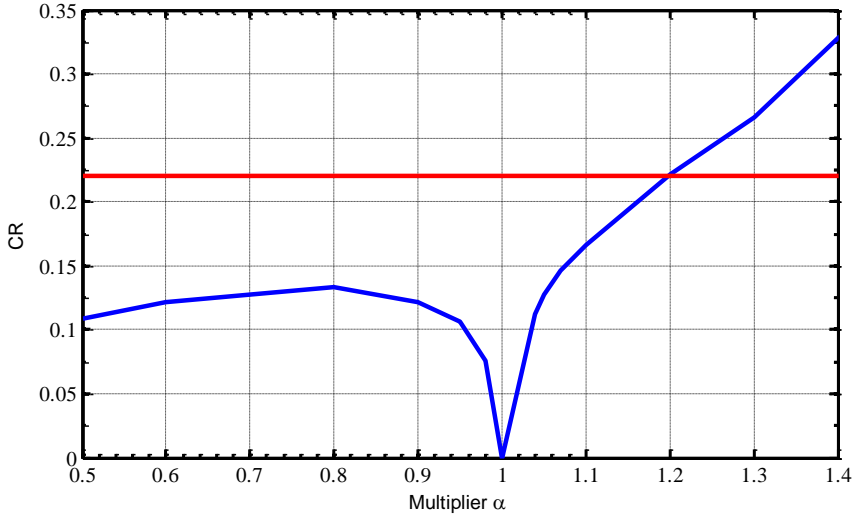


Figure 139 – CATHARE2: $CR(\alpha_{2j})$ for conduction near quench front.

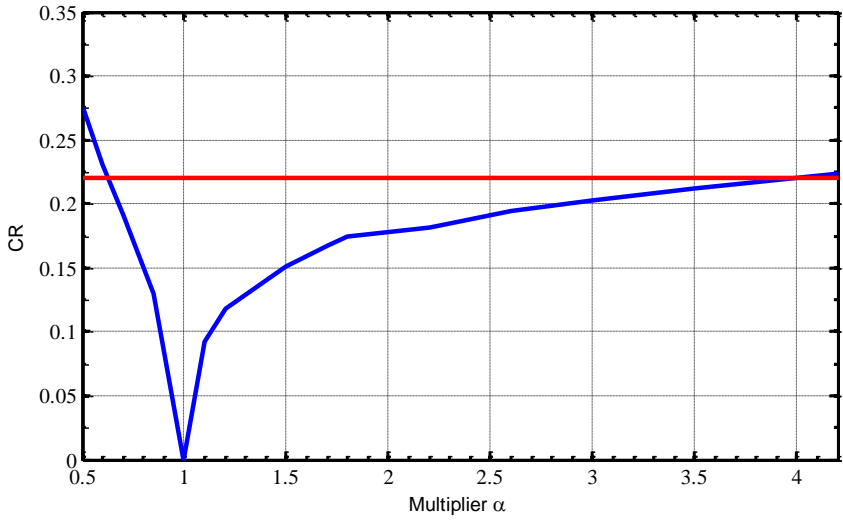


Figure 140 – CATHARE2: $CR(\alpha_{3j})$ for interfacial friction.

Table 37 – FEBA 216: quantified variation ranges of input parameters for CATHARE2.

α_i	Parameter	Ref	Min	Max
α_1	wall-fluid global heat transfer	1.0	0.56	1.08
α_2	conduction near quench front	1.0	0.5	1.2
α_3	interfacial friction	1.0	0.77	4.0

4.5.3. Validation of input parameter uncertainties

As part of the validation process, the variation ranges of input parameters quantified for CATHARE2 code on the basis of test FEBA 216 have been applied to evaluate uncertainty of thermal-hydraulic calculations of the following tests (*Table 8*):

- Test FEBA 214 (*Table 9*)
- Test ACHILLES A1R030 (*Table 11*)
- Test ACHILLES A1R048

4.5.3.1. Modeling of ACHILLES facility with CATHARE2 code

The calculations of ACHILLES tests with CATHARE2 code have been performed in “blind” mode: only the geometrical features of the experimental facility and test initial and boundary (BIC) conditions were available. The experimental data has been revealed only after the uncertainty analysis results have been completed.

The ACHILLES test assembly is modeled by CATHARE2 V2.5 Mod 7.1 by one single 1D component representing the core bundle (heated part, 3658 mm), inlet and outlet boundary conditions and connected with junctions. The same modeling approach has been adopted as for the FEBA facility. The nodalization is built-up based upon the drawing shown in *Figure 98* and *Figure 99*, and also on the code user-guide recommendations, ref. [56]. The general nodalization scheme is illustrated in the *Figure 141*.

The axial element is of the type “rod bundle” with 28 axial segments. No cross-flow inside the bundle is modeled. In order to simulate the pressure loss due to flow restriction, the 7 grid spacers are modeled according to the specifications. The form loss coefficient (K_{loss}) is set to 1.2 for each spacer grid. However, no change in hydraulic diameter or flow area reduction is modeled at the spacer grids elevations.

The heater rods are represented with a single heat structure component with axial power profile imposed as in the experiment specifications. In the radial direction the fuel rod was divided into 3 parts: insulator, heater, and sheath. The thick-wall housing is modelled (thickness is 6.5 mm), whereas unheated part of rods, lower and upper plenum are not modeled. The test section is assumed to be well insulated, hence no heat losses are simulated.

Thermal properties of the materials (filler for the heating elements and insulator material in the fuel rod simulator; sheath for the cladding and shroud for the external vessel) are obtained by a linear or a polynomial regression from ACHILLES data, ref. [53].

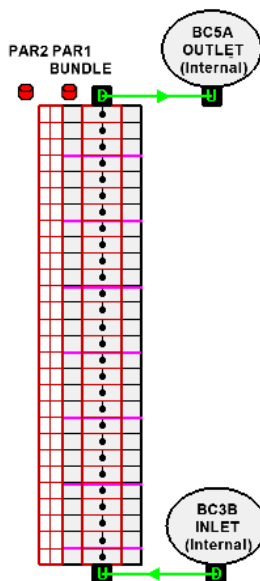


Figure 141 – CATHARE model of the ACHILLES rod bundle.

Table 38 – Summary of CATHARE2 model of ACHILLES facility.

Parameter	Value
Total height/length	3.658 m
Node in heated length	28
Flow area	$7,977 \cdot 10^{-3} \text{ m}^2$
Hydraulic diameter	$1,296 \cdot 10^{-2} \text{ m}$
Spacer grid K_{loss}	1.2
Total heat transfer area of the heated part of heater rods	7.53 m^2
Maximum linear heat rate	1.15 kW/m

The following boundary conditions are modelled:

- Inlet boundary conditions:
 - BC3B (for steady-state critical power calculations: HL, HG, ALFA, VL and VG). Here: HL, HG - liquid and gas enthalpies (J/kg), ALFA – void fraction, VL and VG - liquid and gas velocities (m/s);
- Outlet boundary conditions:
 - BC5A (outlet pressure, Pa);
- Power vs. time law:
 - Is imposed to the bundle heat structure by means of general table with specified power curve.

The main model properties are summarized in Table 38.

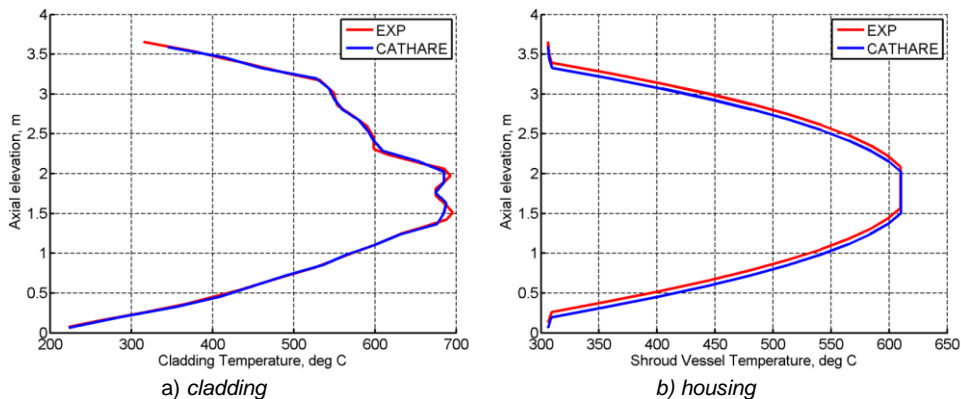


Figure 142 – ACHILLES A1R030: predicted by CATHARE2 steady-state temperature distributions.

In order to reach the Start of Transient (SoT) conditions, no steady state calculation was performed but a set-up of the clad and shroud vessel temperatures. As to the initial conditions, all junction flow was set to stagnation (0.0 m/s), while the steam temperature was set to the value slightly above the saturation all along the volumes (200°C). Comparison of the cladding and housing axial temperature distributions to the experimental once of the test A1R030 is shown in *Figure 142 (a, b)*.

4.5.3.2. Uncertainty analysis of reflood tests simulations

The uncertainty analysis of thermal-hydraulic calculations of selected FEBA and ACHILLES reflood test with CATHARE2 code have been performed with GRS method according to the settings indicated in *Table 26* (applied previously to validation of uncertainty of reflood-related input parameters for RELAP5 code). The obtained uncertainty bands for two responses are shown in *Figure 143*, *Figure 144* and *Figure 145*: cladding temperature at elevation where PCT has been observed and quench front elevation.

It should be pointed out, that CATHARE2 reference calculations underestimate the cladding temperature (to bigger extent comparing to FEBA tests) and predict slightly faster quench front propagation comparing to experimental data. It should be also noted that in the experiments the quench front propagation at the top of fuel assembly (dashed red line in *Figure 144* and *Figure 145*) is affected by a top-down reflood caused by liquid fall-back from the separation devices installed above test section. These components were not modeled and, therefore, the top-down reflood phenomenon was not modeled to full extent and, hence, should not be taken into consideration.

The evaluated uncertainty bands cover sufficiently the experimental data, except the initial cladding temperature rise in ACHILLES test A1R030. However the maximum value of upper uncertainty band encompass the experimentally observed PCT, which is the important issue for nuclear safety. The uncertainty bands of quench front elevation encompasses the considered part of the experimental trend in all simulated tests.

Therefore, it shall be concluded that application of the IPREM for evaluating the uncertainty of reflood-related input parameters of CATHARE2 code has been successful. Hence, it can be confirmed that the IPREM methodology is code-independent.

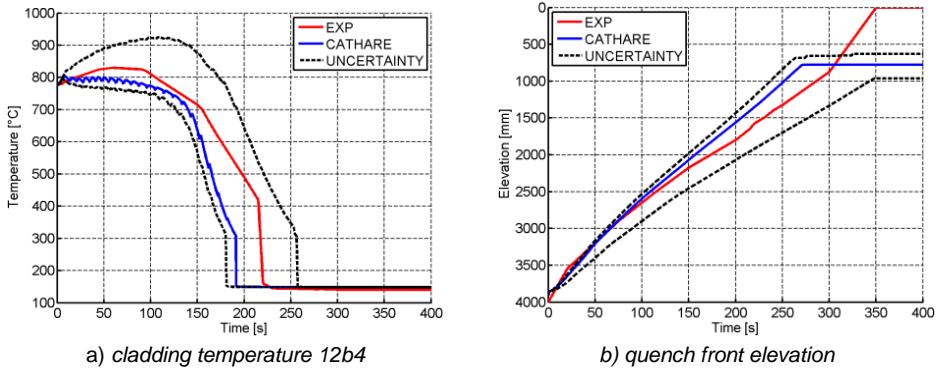


Figure 143 – Uncertainty analysis of CATHARE2 calculation of FEBA test 214 with $[\alpha^L ; \alpha^U]$ derived from FEBA 216.

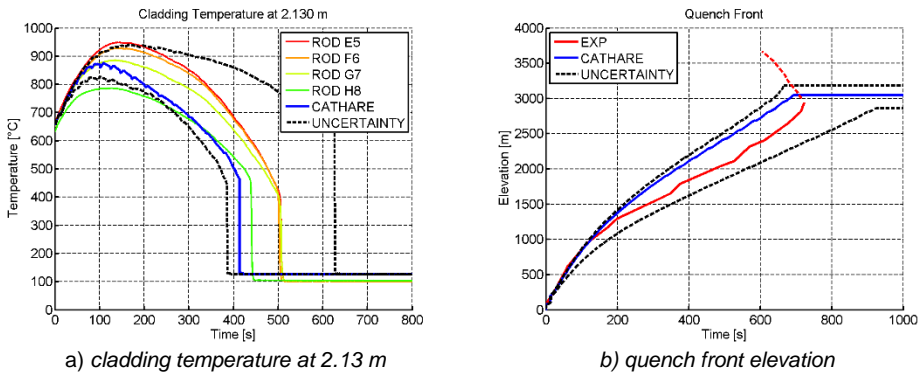


Figure 144 – Uncertainty analysis of CATHARE2 calculation of ACHILLES test A1R030 with $[\alpha^L ; \alpha^U]$ derived from FEBA 216.

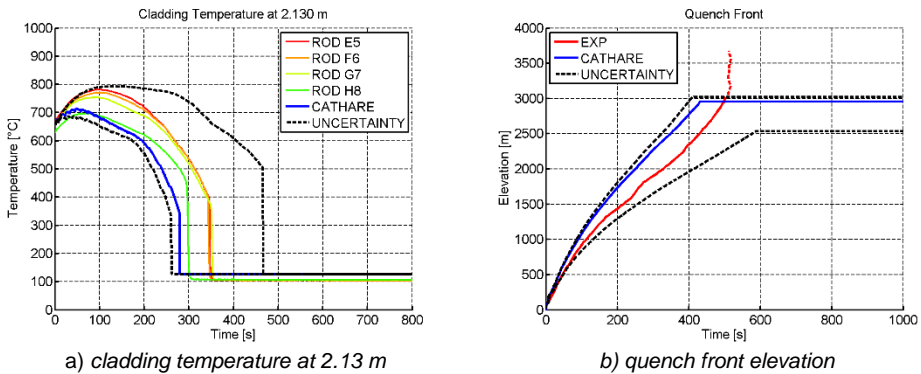


Figure 145 – Uncertainty analysis of CATHARE2 calculation of ACHILLES test A1R048 with $[\alpha^L ; \alpha^U]$ derived from FEBA 216.

4.6. Summary of performed analysis

As the milestone of the present research activity, the IPREM methodology has been applied for evaluating the uncertainty of reflood-related input parameters and models of RELAP5 Mod3.3 code. The obtained results in the form of variation ranges of input parameters have been subjected to various “internal” qualifications (sensitivities on criteria and choice of PDF) and extensive validation. The validation has been carried out through uncertainty analysis of thermal-hydraulic calculations of numerous reflood tests performed at different experimental facilities and at different conditions. The sufficient coverage of experimental data by resulting uncertainty bands is the success criteria for the validation.

Additional analyses have been performed to verify that the IPREM methodology does not depend on particular test, facility or thermal-hydraulic code applied.

As the main nuclear safety issue related to reflood phenomena is the peak cladding temperature, the corresponding values of PCT from the results of the validation activity are summarized in *Table 39* (uncertainty analyses with $[\alpha^- ; \alpha^+]$ derived from FEBA 216).

Table 39 – Summary of reflood calculations for validation of IPREM.

Code	Facility	Test	Exp PCT, °C	Ref PCT, °C	Max Upper Band, °C
RELAP5	FEBA	223	935	905	1050
		220	920	883	948
		218	850	828	956
		214	830	833	892
		222	805	803	847
	PERICLES	RE0062	725	665	733
		RE0064	789	735	821
		RE0069	605	578	640
		RE0079	792	734	830
		RE0080	729	671	755
		RE0086	810	739	796
	ACHILLES	A1R030	946	817	972
A1R048		778	705	842	
CATHARE2	FEBA	214	830	802	938
	ACHILLES	A1R030	946	875	945
		A1R048	778	712	796

The uncertainty analysis has been performed according to GRS method using the histogram distribution of input parameters (50% in each bin below and above

reference value of input parameter) and quantifying the 2.5% and 97.5% percentiles, representative of uncertainty band, with a 5th order statistics.

The majority of evaluated uncertainty bands encompass the measured values of PCT. The considerations regarding blind model of RELAP5 for simulation of PERICLES facility, provided in section 4.3.2.3., allow to confirm the validity of application of the IPREM methodology for evaluating the uncertainty of code input parameters.

The IPREM methodology proved:

- To allow evaluation of input parameter uncertainty from a single 'intermediate' experimental test. However, the use of a number of other experimental test is required to validate the obtained ranges [α^L ; α^U];
- To be test, facility, and code independent;
- That any code input parameter and any code output parameter can be used in the process of quantification of input parameter ranges;
- That methodology does not require modifications of source of thermal-hydraulic code – only the post-processing of calculation results is required;
- That resulting evaluated uncertainty of code input parameters is applied with reference/default values of these parameters (no calibration);
- That no significant resources are needed to implement and apply the methodology. The process of running sensitivity calculations with a code, post-processing the results and performing FFT analysis can be easily automated by use of various scripts (bash, C-shell, perl) and/or mathematical software (e.g. MATLAB, ref. [61]);
- That the IPREM methodology reduces the use of engineering judgment thanks to a proper procedure, mathematical apparatus and corresponding criteria. Engineering judgment is still present and connected with the selection of the input parameters and responses of interest, the characterization of the criteria and of its threshold, but in all these situations, the engineering judgment is embedded into the method itself and is not changed from one application to the other. In addition it shall be noted that in some particular cases the **CR(α)** does not reach the **limit** value: in this case, therefore the engineering judgment is still unavoidable, even though it is reduced.

5 CONSIDERATIONS ON BEST-ESTIMATE MODEL QUALIFICATION

The Best Estimate Plus Uncertainty (BEPU) approach in safety analysis implies the availability of two key assets:

- Best-Estimate (BE) model
- Uncertainty Analysis method

The uncertainty analysis provides the evaluation of likely variation in code predictions due to imperfect knowledge and approximations in models, correlations, boundary and initial conditions etc. However, the currently applied uncertainty analysis methods are not able to take into account other sources of uncertainty such as uncertainty due to nodalization choices, code user effect etc., i.e. the effects which are hardly quantifiable. Therefore, the validity of the uncertainty analysis results is ensured by the use of the Best-Estimate model, i.e. the non-quantifiable effects are considered either overcome or negligible when a so called “best modeling practice” is used.

A “best modeling practice” is established through the consistent code assessment programme and corresponding procedures for quality assurance. Thus, the independent code assessment constitutes an important part in the qualification of an analytical tool for performing licensing or NPP support activities. The consistent application of adopted modeling procedures together with qualified experimental database plays a key role in the code assessment process. It should be pointed out that a consistent code assessment supported by a qualified experimental database is an important step for developing a solid ground for the uncertainty evaluation in the frame of BEPU approach.

Therefore, the availability of an experimental qualified database is of outmost importance for the validation and qualification of code calculation. Such database can be used to demonstrate that the code results are reliable [9], it can constitute the basis for an independent code assessment [11] and finally the basis for an uncertainty evaluation methodology [33, 64]. As discussed in several papers and guidelines, an uncertainty methodology must rely on the availability of a qualified code and qualified procedures. The development of a Standard Consolidated Reference Experimental Database (SCRED) including the Reference Data Set (RDS) of the facility and of the tests, the Qualification Report (QR) of the code calculations and the Engineering Handbook (EH) constitutes an approach, envisaged by IAEA [1, 64].

In the present research, the proposed requirements, forms and procedures for development of SCRED are outlined. The SCRED development and application is illustrated by demonstrating the assessment of thermal-hydraulic code RELAP5-3D© against large and small break loss-of-coolant scenarios performed at LOBI Integral Test Facility.

5.1. Use of qualified experimental database for a system code assessment

The experimental database for the nuclear technology is mainly constituted by the experiments available through the OECD/CSNI Integral Test Facility (ITF), ref. [46], and Separate Effect Test Facility (SETF), ref. [45] matrix. These databases collect over thirty years of experiments: separate effects tests for individual phenomena, integral tests for large break LOCA, small break LOCA, transients, beyond design basis accidents and accident management in PWRs, BWRs and WWERs type of reactor. The enormous amount of information has been used for the code assessment in the framework of V&V activities. The availability of the experimental database constitutes also the pre-requisite for the development of a qualified 'error' database of system thermal-hydraulic responses to be used for the uncertainty evaluation in the method based on "extrapolation of output errors".

The information contained in the experimental reports together with the code input nodalization are the sources to be elaborated in a systematic way by a qualified database made up of the following documents, ref. [65]:

- The Reference Data Set for the selected facility, RDS-facility;
- The Reference Data Set for the selected experimental test, RDS-test;
- The Qualification Report, QR;
- The Engineering Handbook, EH.

Figure 146 shows the link between the RDS, the Input deck, the QR and the EH. The black lines indicate the activities carried out in sequence, the blue lines constitute the feedback for review and the red lines are the required input to development of the input deck and the EH. The whole process is based on continuous review and exchange of information between the analysts involved in these activities. An independent review of each report is achieved through an approach when the input deck and EH are developed by different analysts. Similarly, the code input deck developer shall be not extensively involved in RDS development.

Block A in *Figure 146* is related to the collection of relevant drawings and reports of the selected facility. This documentation constitutes the basis for writing down the RDS (block B). The writing of the RDS is also the first step of the review process, when each document is checked against its consistency with other sources of information, which result in establishment of a final documentation set for the particular facility.

The subsequent block of the chart (block C) is related to the creation of a RDS for the selected experimental test that has to be analyzed. The RDS of the test contains the definition of test conditions, the set points and the boundary conditions. The RDS of the facility and of the test constitute the basis for the code input deck development.

The development of an input deck (block D) must follow a preconfigured set of nodalization strategies described in a dedicated document (description of which is outside of the present paper's scope) which goal is to collect the nodalization approaches, user choices and model selections to be used for the development of any other input deck.

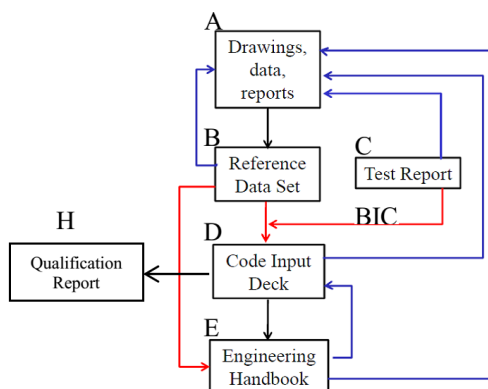


Figure 146 – Flow chart of the RDS, Input Deck, QR and EH interconnections.

A review process of the RDS takes place at this phase: the input developer uses the RDS to extract the necessary information for the input preparation together with the availability of the original documentation already collected. Potential errors and misinterpretations maybe identified and further corrected in the RDS. The writing down of the RDS-test also constitutes a review process of the RDS-facility.

One of the reasons for the need of an RDS is connected with the duration of an experimental campaign performed at each facility (typically from five to ten years). During those years, different modifications can be made to the facility configuration in order to improve the fidelity of the facility with respect to the reference plant, to reduce the heat losses, to install a more sophisticated instrumentation apparatus, etc. Such information and modifications are obviously not part of the original documentation and, in general, could be only partially reflected in separated reports and documents. Thus, the goal of an RDS is to analyze the amount of available documentation and to solve possible contradictions coming out from different reports in order to produce a consistent and homogenous set of data of the facility.

Once the code input file has been produced and the calculations performed, there is a need to qualify the achieved code results following appropriate procedures as discussed in the UMAE methodology. The Qualification Report (QR) (block H) collects the results of the application of qualification procedures to the code input.

The engineering handbook (block E) constitutes the final step for the set-up of a qualified database useful for the uncertainty methodology. The IAEA report, ref. [1], states that a “document contains a full description of how the database has been converted into an input data deck for a specific computer code” should be available. This is the goal of the EH: it does not only describe the nodalization of the facility based on the input file and the calculation notes made available by the input developer, but it also provides the engineering justifications of the user choices and the explanation of possible discrepancies with the general nodalization strategies.

At this step, a final review process of the entire set of documents is also performed: any entry in the input deck is checked against the calculation notes and the RDS of the facility. Any errors or inconsistencies found in the input are tracked and reported and appropriate countermeasures are taken. For the criterion of the independence of the review process, it is of utmost importance that the engineer in charge of the

EH is different from the input deck developer (the latter one is involved in the preparation of the EH only for the description of the “nodalization rationale” and for the “user choices”).

5.1.1. Setting up RDS facility and RDS test

The first step for the database creation is constituted by the collection of the relevant experimental information in a document called Reference Data Set handbook. The relevant design data of the facility and of the test are organized in order to be ready to be used for the development of the code input data file. The data and the organization of the data are not dependent on the code selected for the analysis.

To perform a proper data collection, the IAEA suggest to:

- Check the quality of input data,
- Resolve the contradiction coming out from the data,
- Explain information on geometry, thermal and hydraulic properties,
- Perform an independent review,
- Carry-out a quality control of the database by means of relevant quality assurance procedures,
- Develop a database in a code independent form.

Two kinds of RDS are necessary to the creation of an input deck: the RDS of the facility (RDS-facility) and the RDS of each test (RDS-test) that has to be included in the database. *Figure 147* shows the relationship between those documents.

The RDS related with the design of a facility may consist of the following sections, ref. [66]:

- Layout of the facility,
- Collection of geometrical data (length, volumes, areas, elevations) for each subsystem and component of the facility,
- Collection of specific data for complex component (pumps, valves, heaters, etc...),
- Identification of geometrical discontinuities and evaluation of pressure loss coefficients (normal operation),
- Material properties,
- Measurement system,
- Nominal heat losses.

The RDS of a particular test in a facility may consists of the following sections, ref. [67]:

- Description of the test and phenomena occurring in the experiment,
- Characterization of the Boundary and Initial Conditions (BIC),
- Characterization of trips and logic signals occurring during the transient,
- Measurement data,
- Specific heat losses,
- Evaluation of possible additional pressure loss coefficients,
- Thermal hydraulic system behavior description.

Examples of an RDS-facility and RDS-test (selected parts) are provided in Appendix D.

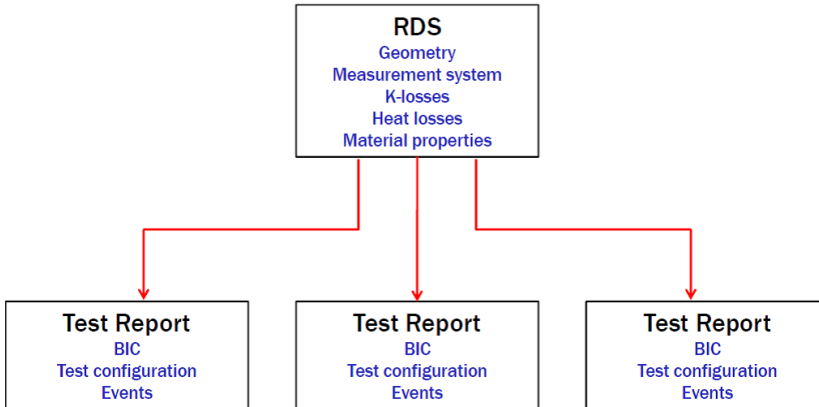


Figure 147 – The RDS-facility and the RDS-Tests.

5.1.2. Writing an input deck

A preliminary consideration to set up a nodalization should first address the kind of facility and the related type of problem to be investigated. It should be noted that in the present context the word “facility” is intended here both as a power plant and a test rig as well. The level of details of either full or reduced scale facilities should be comparable even though, in case of an experimental rig, some auxiliary systems are simplified or even not reproduced, while in case of a power plant the simulation of some of auxiliary systems must be considered though it consumes code resources.

The set-up of a nodalization passes through different steps:

- Nodalization preparation: main choices of the model characteristics and preliminary code resources distribution;
- Nodalization schematization: buildup of the discretization of the various parts of the considered facility;
- Input writing: translation of the schematization into the code language/syntax.

The input data file is developed starting from the RDS-facility and RDS-test. Together with the data file, calculation notes have to be elaborated to document modelling decisions made by the code input developer. Input data file and calculation notes pass through a peer review process (see *Figure 146* and *Figure 149*) before the final version of the input is issued.

The process of nodalization preparation includes the analysis of the facility lay-out, its main geometrical characteristics and its working modalities. In addition the analyst shall have in mind which phenomena are expected to occur in the considered facility (due to geometrical specificities and/or constraints) and in the specific (or set of) transient. At this regard, the OECD code validation matrices, ref. [45] and [46], constitute an irreplaceable tool in which most of the ITF and SETF operated in the world are considered.

An assessment on code resources distribution shall be made by the analyst prior to set up of the related model, to ensure that sufficient level of details (e.g. number of active channels, number of equivalent U-tubes, etc.) is put in relevant part of the plant without neglecting or oversimplifying the rest of the model of a plant. Assessment of sufficient level of detail shall take into account the objectives of the analysis. As an example, an ultra-detailed simulation of a RPV could be viable in case of very short term core analysis, but it becomes penalizing in case of long-term global plant simulations.

Outcome of this initial stage of the code input development is a draft of the nodalization sketch with the indication of the main features of the nodalization (e.g. number of active channels, number of equivalent U-tubes, etc.).

The nodalization development is the logical subsequent step of the nodalization preparation, during which the basic idea of the model is fully developed up to design a complete nodalization. Feedbacks on the previous stage could come out during the development of the nodalization, especially when the code user starts to have a more complete picture of the model. The availability of the report containing the guidelines for the development of the nodalization and the main strategies to be adopted (block F in *Figure 149*) is a fundamental supporting tool for the code input developers.

The writing/implementation of the input deck consists in the translation of the developed nodalization into the code language. In principle, it needs 'just' the knowledge of the code's syntax and the use of the related manual. Attention shall be put in order to avoid typing errors (very difficult to be detected in case of plausible value from the code internal check point of view). In addition, a rational in the deck structure shall be followed: readability of the input deck may suggest to clearly identifying the main sections which include trips, hydrodynamic data, heat structures data, neutron kinetic data, control variables, additional requested variable (if any).

The "spot info" comments should be added at various input cards and words providing an explanation and facilitating the understanding of an input deck. The comments may be such as

- description of what a logic trip is further used for (signal)
- the total elevation change of a pipe component with ascending and descending parts
- description of junctions in the branch components (connection to which parts of hardware)
- description of the origin of K_{loss} (due to pipe bend, orifice etc.)
- etc.

It is recommended to assign meaningful names to the components of the code input deck, which would facilitate the further use of the deck e.g. component searching, input verification etc. and therefore add to the overall quality of the product. The names of control variable components should bear a certain meaning also. It is recommended to include the name of the related system zone and to specify a parameter which is the outcome of this control variable.

Example 1: hot leg piping may be modeled with 2 components. A component modeling a first piece of loop 1 hot leg piping at the outlet from the reactor vessel may be named as HL1-a, second piece as HL1-b.

Example 2: A control variable component that calculates collapsed level in pressurizer may be named as PRZ-L.

The numbering of the hydraulic components is a matter of a free choice and convenience for user. It is recommended though to dedicate an easily remembered and understandable range of numbers for each system zone. For example in 2-loop reactor model the 100 series (all numbers from 100 to 199) can be dedicated to components representing the loop 1, 200 series for loop 2, 300 series for reactor, 400 series for pressurizer, 900 series for safety systems etc.

It is also suggested to adopt a meaningful scheme for numbering of control logic components. The numbers should be assigned in such way that the input deck user shall easily remember the numbers of the most important control components (power, levels in SG and PRZ, scram signal, MCP motor signal etc.).

5.1.3. Qualification Report

The Qualification Report (QR) is necessary to demonstrate that the code results are qualitatively and quantitatively acceptable with respect to fixed acceptance criteria, ref. [33]. In particular, for the uncertainty method based on extrapolation of output error, the availability of QR is a pre-requisite to demonstrate the qualification level of the 'error' database.

Without going into the details of the qualification procedure, ref. [33] (illustrated in *Figure 148*), it is however important to outline the minimum amount of information that shall be contained in a qualification report:

- The demonstration of the geometrical fidelity (block **e** in *Figure 148*) of the model with respect to the facility;
- The qualification at steady-state level (block **d** in *Figure 148*), i.e. the demonstration of the capability of the model to reproduce the steady-state qualified condition of the test;
- The qualification at transient level (block **h** in *Figure 148*). *This activity is necessary to demonstrate the capability of the code nodalization to reproduce the relevant thermal-hydraulic phenomena expected during the transient. This step also permits to verify the correctness of modeling of the systems that are in operation only during transient events (e.g. accumulators). Criteria, both qualitative and quantitative, are established to define the acceptability of the transient calculation.*

When the acceptability criteria at blocks **f** and **j** are met the input deck is considered qualified.

5.1.4. Engineering Handbook

The engineering handbook constitutes the technical rationale for the input model. It summarizes for each component of the model's input file the documentation used and provides engineering justification of the adopted assumptions. Each input's entry is fully described and documented and the calculation notes of the input developer are included in the EH allowing an easier understanding of the input values.

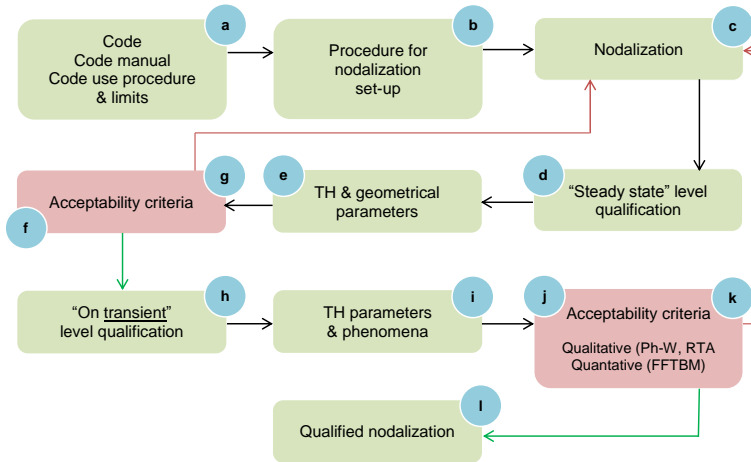


Figure 148 – Flow chart of the nodalization qualification procedure.

The Engineering Handbook finally makes a cross-link between the RDS (both for the facility and for the test), the code and the input data files.

Since the EH documents in detail how the RDS have been converted into an input deck for the particular computer code, one can say that the final goal of the EH is to preserve and to make easier the transfer of knowledge about the input (i.e. the user choices and the technical rationale behind the development of the input) from one group to another one.

A typical Engineering Handbook shall contain:

- The methods and the assumptions used to convert the RDS information into the code input data;
- All calculations made to convert the technical plant data to the necessary format for the input deck (i.e. the traceability of the information);
- The nodalization schemes of the components as well as for the complete system being modeled;
- The adequate description and explanation of all adopted modeling assumptions.

The EH is set up once the input deck has been qualified and frozen. Any changes to the input deck, prior peer review approval, must be documented in the EH.

In the process described in the present paper, the writing down of the EH constitutes the final step of the review activities for the whole process (from the blue prints to the input deck and the EH). The availability of the calculation notes (block G in Figure 149), prepared by the input developer, allows to check possible inconsistencies in the input deck respect to the RDS data and any revealed discrepancy is carefully reviewed and solved through the proper corrective action that also has to be documented.

5.2. Application of SCRED for assessment of RELAP5 code against LOCA scenarios in LOBI facility

5.2.1. Description of LOBI facility

The LOBI-MOD2 test facility, ref. [68], is a high pressure integral system test facility and represents an approximately 1:712 scale model of a four-loop, 1300 MWe PWR of KWU design. It has two primary loops, the Intact Loop (IL) representing three loops and the Broken Loop (BL) representing one loop of the reference PWR. Each primary loop contains a main circulation pump (MCP) and a steam generator (SG). The simulated core consists of a directly electrically heated 64 rod bundle arranged in a 8 x 8 square matrix inside the pressure vessel model; nominal heating power is 5.3 MW. Lower plenum, upper plenum, an annular downcomer and an externally mounted upper head simulator are additional major components of the reactor model assembly. The system pressurizer is normally connected to the Intact Loop hot leg. The primary cooling system, which is shown schematically in *Figure 150*, operated at normal PWR conditions: approximately 158 bar and 294 – 326 °C pressure and temperature respectively. Main design and operation parameters of the experimental facility are reports in *Table 40*.

The emergency-core-cooling (ECC) water can be supplied by the high pressure injection system (HPIS) and by the accumulator injection system (AIS); there are also provisions for the simulation of the low pressure injection system (LPIS). Provisions are made for cold leg, hot leg or combined cold and hot leg ECC injection into both primary loops.

Heat is removed from the primary loops by the secondary cooling circuit containing a condenser and a cooler, the main feedwater pump, and the auxiliary feedwater system. The normal operating conditions of the secondary cooling circuit are approximately 210 °C feedwater temperature and 64.5 bar pressure.

The whole LOBI-MOD2 test facility and individual components are scaled to preserve, insofar as possible or practical, similarity of thermal hydraulic behavior with respect to the reference plant during normal and off-normal conditions. The particular objectives of the LOBI-MOD2 experimental program required rigorously scaled and heavily instrumented shell and inverted U-tube type steam generators having geometrical configuration similar to that in the reference plant. The scaling rationales which required a capacity ration between the IL and the BL steam generator 3:1 with respect to major thermal and hydraulic parameters, led to a heat transfer exchange power of 1.32 MW, and 8 U-tubes (+ 1 installed spare) for the BL-SG and to a heat exchange of 3.96 MW and 24 U-tubes (+ 1 installed spare) for the IL-SG.

Each steam generator consists of a single cylindrical pressure vessel with an annular downcomer separated from the riser region by a skirt tube. This tube is supported above the tube plate, and carries the coarse separator. A fine separator is arranged in the uppermost part of the steam dome. The U-tubes are arranged in a circle within the riser region, around an axially mounted filler tube, with the U-bend crossing over one another above it. An adjustable throttle device is installed at the lower end of the downcomer to allow the recirculation rates in the two SGs to be set up. A proper connection between the secondary side at the tube-plate elevation and the inlet or

outlet plenum on the primary side can be established for the simulation of Steam Generator Tube Rupture (SGTR) accident conditions.

Each heated rod of the simulated reactor core consist of an hollow tube with an active heated length of 3.9 m, outer diameter of 10.75 mm and a pitch of 14.3 mm. The wall thickness is varied in 5 steps to provide a cosine-shaped axial heat flux distribution. The upper unheated part of the heater rod bundle extends entirely in the upper plenum to the upper power connecting plate.

The LOBI-MOD1 facility, ref. [69], features essentially the same geometrical features in the primary side as LOBI-MOD2 facility. The main differences with the LOBI-MOD2 facility are the different type of SGs, secondary side system more suitable for LBLOCA experiments and a less detailed measurement system (since it is an earlier version of LOBI facility configuration).

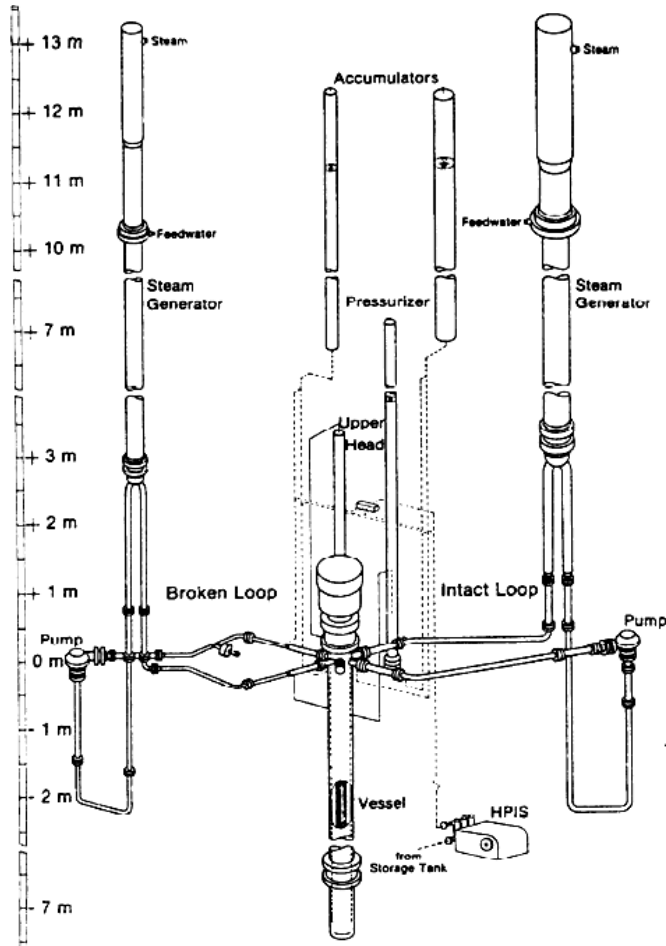


Figure 150 – LOBI MOD2 Primary Cooling System Configuration.

Table 40 – Summary of reflood calculations for validation of IPREM.

Object	Parameter	Value or Explanation
Reference Plant	Siemens-KWU Loops Power	Biblis B 4 1300 MW
LOBI-MOD2	Volume scaling factor Height scaling factor Number of loops Scaling factor of loops BL (IL) Number of accumulators Operating organization	1:712 1:1 2 1:1 (1:3) 2 JRC, Ispra, Italy
Primary System	Nominal pressure Nominal temperature (cold leg/hot leg) Total volume Nominal mass flow (IL/BL)	15.8 MPa 294/326 °C 0.6 m ³ 21/7 kg/s
Secondary System	Nominal pressure Nominal temperature (inlet/outlet)	6.4 MPa 210/326 °C
Core	Power Length Numbers of heated rods Matrix Heated rod outer diameter Pitch Electrical heating	5.28 MW 3.9 m 64 8x8 10.75 mm 14.3 mm Direct
Vessel Downcomer	Type Gap	Annular 12 mm
Main Coolant Pumps	Type Specific speed (DIN) Velocity range	Centrifugal 29.2 ±8500 rpm
Steam Generators	Type Number of tubes in use (available)	Vertical U-tubes BL/IL: 8/24 (9/25)
Accumulators	Maximum pressure Maximum temperature Nominal temperature Pressure of intervention	6.0 MPa 50 °C 30 °C 2.7 MPa
LPIS	Available	
HPIS	Nominal temperature Pressure of intervention Maximum mass flow Total head	30 °C 11.7 MPa 0.39 kg/s 200 bar
Pressurizer	Power of heaters Number of heater rods Number of cooling coils Water level	20 kW 8 5 4.8 m

5.2.2. Reference Data Set of LOBI facility

The two documents, RDS-facility and RDS-test, are the starting point for the thermal-hydraulic model development. The LOBI-MOD1 and LOBI-MOD2 facilities have been analyzed and subsequently subdivided in code-independent modules according to the geometrical and functional characteristics (*Figure 151*). An example of module description for Upper Plenum is shown on *Figure 152*. For each module an engineering analysis has been performed and the main quantities necessary to describe the specific part of the facility are calculated (e.g. flow area, length, heat transfer area etc.), with the formula used shown, and for traceability reasons the reference to the original document is given. The description of the facility is not limited to the geometry - the measuring system, the material properties, and the data for special components such as valves and pumps has been provided, the pressure loss coefficients at the geometry discontinuity locations have been evaluated, ref. [70], and the complete evaluation process is reported. Therefore, the RDS of LOBI-MOD2 facility constitute a comprehensive document that summarizes in a systematic way all the characteristics of the facility, taking track also of the modifications made during the experimental campaign, to be used as a reference to set up the model for the thermal-hydraulic analysis. More examples of RDS for LOBI-MOD2 facility are provided in Appendix D.

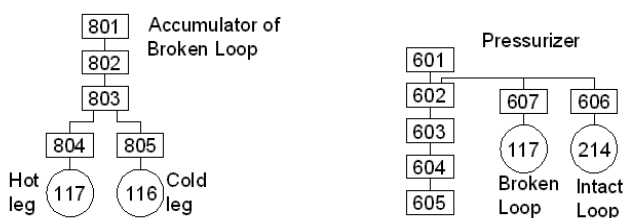


Figure 151 – Example of modules of RDS for LOBI-MOD2 facility.

The RDS of the test is issued for 2 analyzed experimental tests: A1-06 (Large Break LOCA) and A1-83 (Small Break LOCA). Each RDS-test summarizes the facility configuration, the test procedures, the initial conditions and boundary conditions. It also provides an engineering explanation of the test behavior together with the time trend of the most important parameters characterizing the test (around 40-50 time trends). The examples from RDS-test for test LOBI A1-83 are provided in Appendix D.

5.2.3. Modeling of LOBI facility with RELAP5-3D© code

A qualified experimental database to be used for safety analysis and assessment or uncertainty analysis must be consistent. The meaning of “consistent” in this context can be considered as follows: “the results of different transient performed on different facility should be obtained with models that follow the same rationale and user choices; for different experiments performed on the same facility the model should not be changed for the different transient; the process thus allows only modification of the initial and boundary conditions, set points of the different systems and K-losses adjustment only for the part of the facility with a different geometry (i.e. different break area)”.

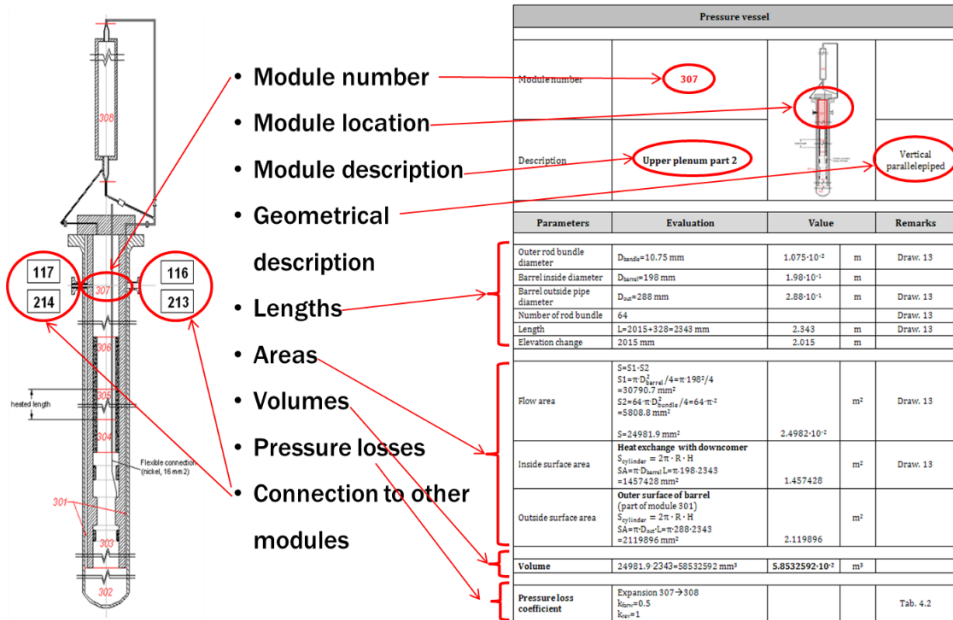


Figure 152 – Example of Upper Plenum module of RDS for LOBI-MOD2 facility.

Therefore, 2 nodalizations for RELAP5-3D© thermal-hydraulic code has been developed, ref. [67] and [71], and applied for simulation of 2 experimental tests: LOBI MOD1 A1-06 (ref. [72]) and LOBI-MOD2 A1-83 (ref. [73]). However, it should be pointed out that only the nodalization of the steam generators is different, while the nodalization of the primary side remains essentially the same.

The database developed at the University of Pisa follows codified nodalization strategy that comes from the vast experience, best practice and code guidelines. These strategies cover a wide spectrum of aspects, from the more general numerical solver to be used to the detailed suggestion on how to model the connection between the PRZ and the surge line. The few examples of choices used for the RELAP5 input deck development are as follow:

- Use of EPRI correlation for bundle interphase friction,
- Use of the original RELAP5 break flow model,
- Sliced nodalization with mandatory planes (i.e. BAF, TAF, HL/CL centerline etc.,
- Volumes adopted for primary side schematization should have a node length in the range 0.2 – 0.8 m.,
- The ratio of lengths of adjacent nodes may not be greater than 2.

Geometrical fidelity has been checked of the developed models and the steady-state of the calculation has been achieved and qualified against available experimental data. More details on model description and steady-state qualification of RELAP5-3D© model of LOBI-MOD2 test A1-83 is provided in Appendix C.

The RELAP5-3D[®] code, ref. [74], is an outgrowth of the one-dimensional RELAP5/MOD3 code developed at the Idaho National Laboratory. More detailed description is provided in Appendix A.

While writing the ASCII file of the input deck for of RELAP5-3D[®] model of LOBI facility, an extensive deck commenting has been applied, rendering traceable every created RELAP component and introduced geometrical parameters and coefficients. The smart system of numbering of RELAP5 hydraulic components, heat structures and control logic components has been introduced, making intuitive deck understanding and providing aid for the further knowledge transfer. An example of input deck comments is provided on *Figure 153* and *Figure 154*.

```

*
* IL SG OUTLET PLENUM
*
* (MODULES 204, 205)
1250000 ILSG-OUT  branch      * from 2.900m (U-TUBES OUTLET) TO 2.588m (LOOP SEAL INLET)
1250001 2
1250101 0. 0.336 1.074e-02 0. -90. 2.312 4.e+5 0.0 0000000
1250200 100 15.70e+06 1.283e+06 2.439e+06 0. *
1251101 120260002 125010001 0.000 0.64 0.223 00000000 * outlet from U-tubes bundle
1252101 125010002 130010001 0.000 0.5 1.0 00000000 * outlet to LS
1251201 21.3 0.0 0.0 0.0
1252201 21.3 0.0 0.0 0.0
* IL LOOP SEAL
*
* SG OUTLET PLENUM - PUMP INLET (MODULES 209, 210, 211, 212)
1300000 ILLS-1 pipe * from 2.588m (SG OUTLET PLENUM) to -0.200m (PUMP INLET) with bottommost @ -2.515m
1300001 23
1300101 1.088e-02 5
1300102 4.266e-03 23
1300301 0.215 1
1300302 0.300 2
1300303 0.400 3
1300304 0.400 4
1300305 0.458 5
    
```

Figure 153 – Example of RELAP5 ASCII input deck commenting: hydraulic components.

```

*
* PRESSURE DROPS
*
* all CV are numbered CCC3
* RPV RISER PRESSURE DROP 3453 (PDR3YA), MPa
20534530 PVRSR-PD sum 1.e-6 0.0 1
20534531 0.0 1.0 p 310010000
20534532 -1.0 p 345010000
*
* RPV DOWNCOMER PRESSURE DROP 3003 (PDR3DB), MPa
20530030 PVDC-PD sum 1.e-6 0.0 1
20530031 0.0 1.0 p 300100000
20530032 -1.0 p 300100000
*
* RPV CORE PRESSURE DROP 3303 (PDR3UG), MPa
20533030 FVCCR-PD sum 1.e-6 0.0 1
20533031 0.0 1.0 p 315030000
20533032 -1.0 p 340010000
    
```

Figure 154 – Example of RELAP5 ASCII input deck commenting: control logic components.

Once the input deck has been developed, the Engineering Handbooks have been produced, ref. [75], which document for each component of the RELAP5-3D[®] model the input entries providing engineering justification of the adopted assumptions (rationale and user choice). The visual aids in form of figures and tables have been

utilized to describe the cross-link between the Reference Data Set and the code model. An example of use of colors to facilitate the explanation of correspondence between RDS and RELAP5 nodalization of LOBI-MOD2 pressure vessel is shown on *Figure 155*.

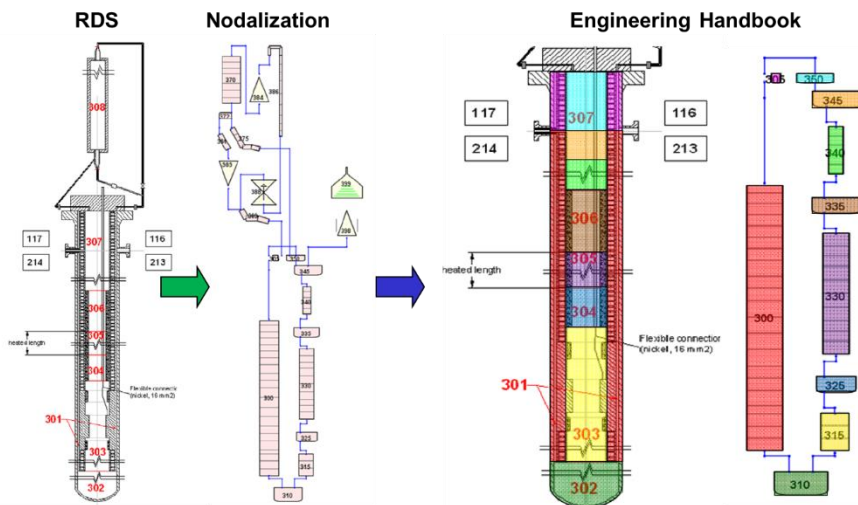


Figure 155 – Engineering Handbook: example of description of LOBI-MOD2 RPV nodalization for RELAP5 code.

5.2.4. Code validation for LBLOCA scenario

Analyzed experimental test A1-06 is a 2A cold leg break with combined HL/CL injection in the intact loop and HL injection the broken loop.

After initiation of blowdown, the saturation pressure in the hot legs is reached after about 100 ms. Flashing in the hot legs starts and the depressurization rate decreases. After 18s, the accumulator actuation pressure is reached and the accumulator injection starts. Further, the pressure in the system is mainly governed by the break flow. During this test DNB occurred over the whole bundle at 0.8 s to 1.3 s into the transient and caused the temperature to increase sharply. The cladding temperature excursion is further terminated by the ACC injection.

The calculation results, ref. [65], summarized in *Figure 156*, *Figure 157*, *Figure 158*, *Figure 159* and *Figure 160*, show an excellent agreement with the experimental data from a qualitatively point of view. Additionally, the analysis of the Relevant Thermal-hydraulic Aspects (RTA), ref. [76], has been performed in order to provide a qualitative judgment (marked as “Excellent”, “Reasonable”, “Minimum” and “Unqualified”) to model performance in terms of phenomena prediction. The results of calculation of test A1-06 has been judged as “E” and “R”, which provide a good qualification basis for code assessment.

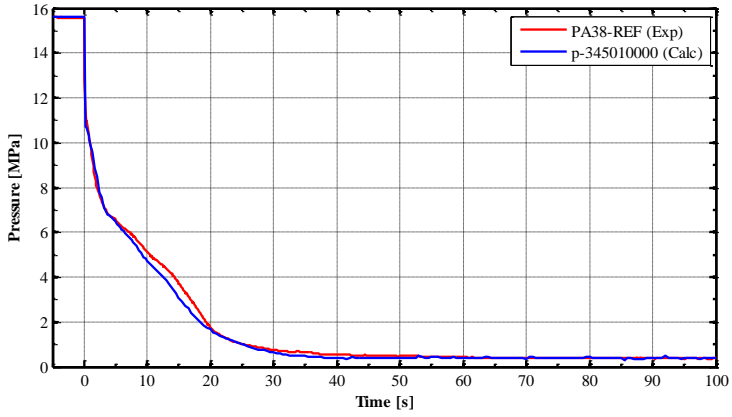


Figure 156 – LOBI A1-06 RELAP5 calculation: primary side pressure.

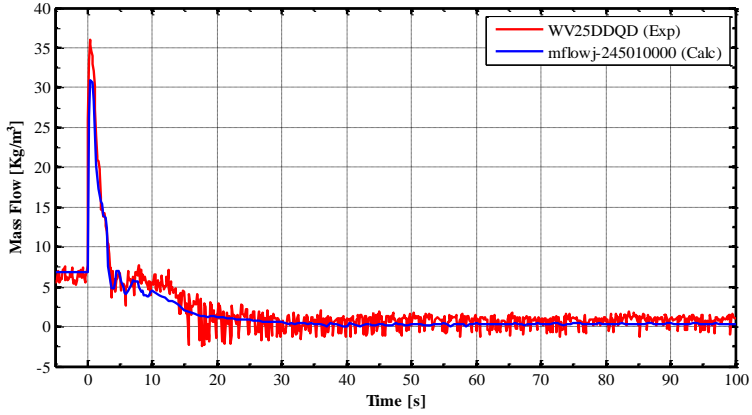


Figure 157 – LOBI A1-06 RELAP5 calculation: Break mass flow rate (pump side).

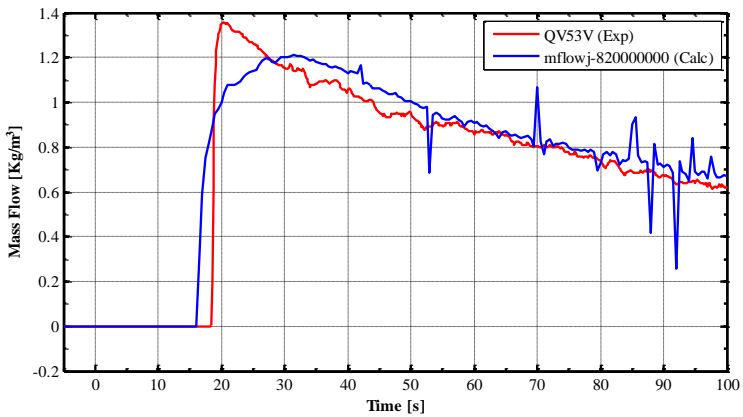


Figure 158 – LOBI A1-06 RELAP5 calculation: Mass flow rate ACC HL IL.

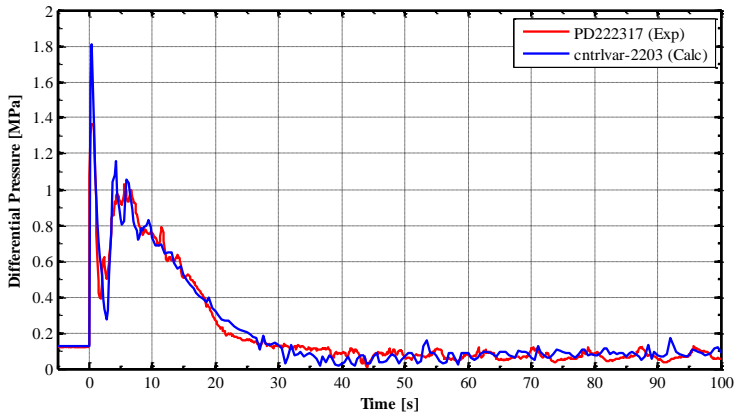


Figure 159 – LOBI A1-06 RELAP5 calculation: Differential pressure across BL SG U-tubes.

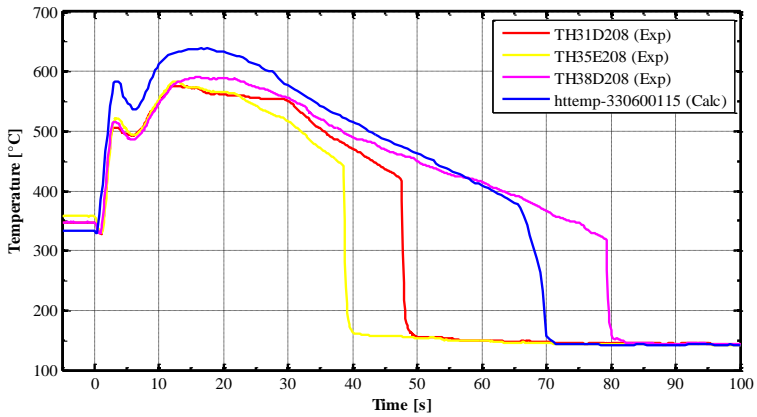


Figure 160 – LOBI A1-06 RELAP5 calculation: Heater rod temperature 2/3 of the core height.

Table 41 – Example of Analysis of Relevant Thermal-hydraulic Aspects.

		LOBI A1-06			
		UNIT	EXP	R5	Judg.
RTA: break mass flow behavior					
TSE	Upper plenum in saturation conditions	s	0.4	0.45	E
IPA	Integral break flow rate at dryout time	kg	82.0	70	R
	Integral break flow rate at ACC injection time	kg	350.0	364.0	E
	Integral break flow rate at core quenching time	kg	450.0	474.0	E
	Integral break flow rate at 100 s	kg	482.0	524.0	E
TSE	Time of emptying	s	-	14.12	-
RTA: Pressurizer behavior					
NDP	PRZ pressure/primary pressure at 5 s	-	2.06	2.08	E
	PRZ pressure/primary pressure at 10 s	-	2.19	2.37	R
	PRZ pressure / primary pressure at emptying time	-	-	2.52	-
TSE	Time of PRZ – primary pressure equalization	s	65.0	60	R

Note: TSE – time sequence of event; IPA – Integral Parameter; NDP – Non Dimensional Parameter; E – excellent agreement; R – reasonable agreement.

5.2.5. Code validation for SBLOCA scenario

For test A1-83 the LOBI/MOD2 test facility was predisposed in the basic configuration for cold leg break LOCA experiments. It simulates a 0.1A cold leg break loss-of-coolant experiment with HPIS injection in the HL of the intact loop and ACC injection in HL/CL of the intact loop and HL of the broken loop.

After initiation of blowdown the primary system depressurized rather quickly. At 1.8s into the transient, the 132 bar low primary system set point pressure enabled the core heating power and the secondary system cooldown trip signals. The isolation and the automatic cooldown at a rate of 100 K/h of the secondary system was effectively started at 2s which overlays the initial responses of the primary and secondary system pressures. Within 2.5s the primary system pressure had fallen to saturation pressure of fluid in the hot legs. This caused a moderate change in system depressurization which continued at reduced rate as the fluid in the upper vessel internals started to flash.

At 5.4s into the transient, the 117 bar low primary system pressure set point tripped the HPIS-ECC water injection which was sequenced to initiate with a delay of about 3s. The 110 bar low primary system set point which tripped the main coolant pumps coastdown was reached at 6.7s after the blowdown.

Transition from subcooled to saturated critical flow at the break orifice occurred at about 15.8s into the transient; at this time the fluid in the primary system cold legs saturated. The primary system depressurization rate diminished as the outflow from the break orifice decrease. Following the actuation at 316s of ECC water injection from the accumulator injection system which was tripped by a primary system pressure of 26 bar, the depressurization rate decreased as the outflow from the break was offset by the inflow from the accumulators.

The code predicted very well the overall thermal-hydraulic response of the system and showed the acceptable results in core phenomena simulation, ref. [77]. The list of resulting events is shown in *Table 42* and a set of selected time trends is shown from *Figure 161*, *Figure 162*, *Figure 163* and *Figure 164*.

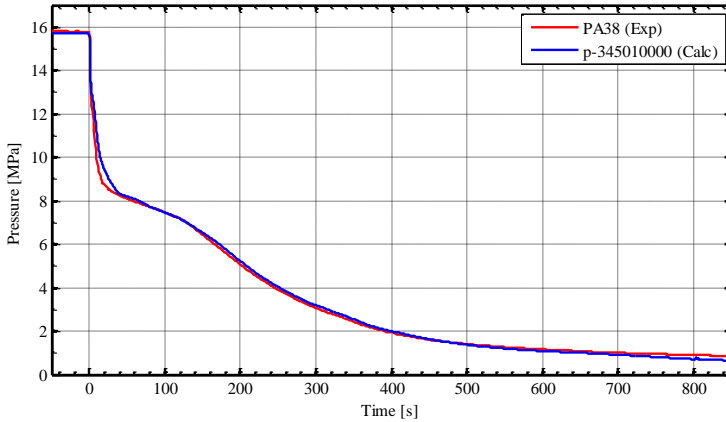


Figure 161 – LOBI A1-83 RELAP5 calculation: primary side pressure.

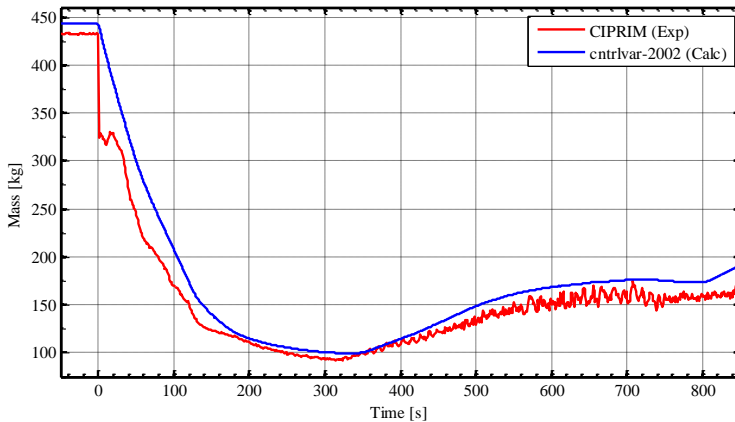


Figure 162 – LOBI A1-83 RELAP5 calculation: primary side residual mass.

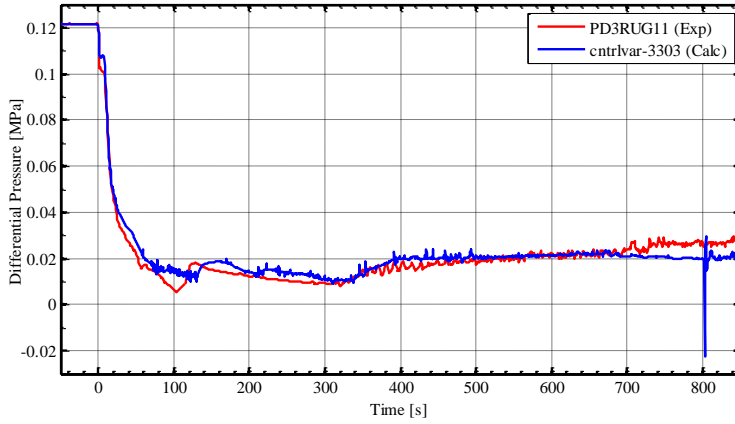


Figure 163 – LOBI A1-83 RELAP5 calculation: core differential pressure.

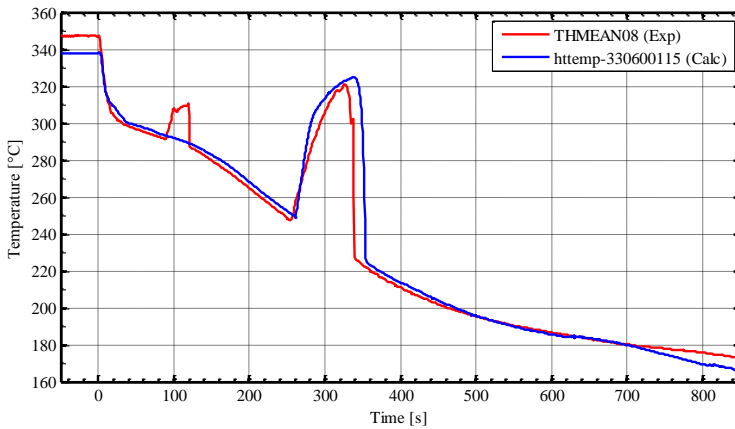


Figure 164 – LOBI A1-83 RELAP5 calculation: Heater rod temperature 2/3 of the core height.

Table 42 – List of predicted events in LOBI A1-83.

EVENTS	EXP [s]	CALC [s]
Break valve starts to open	0	0
Primary system pressure equal 132 bar	1.8	2.9
Primary system pressure equal 110 bar	6.7	10.1
Saturation in CL	15.8	41
PRZ surge line uncovers	21.0	29.0
Saturation in lower plenum	31.0	37.2
HPIS water injection initiated	41.0	43.0
First core dry out detected at level 8 (2.7 m)	88.0	-
Broken loop seal clears out	89.0	71.0
PCT during first dry out	98.6	-
Primary system pressure below secondary system pressure	105	105
Intact loop, loop seal clears out	111	96
Break uncovers	120	113
Second core dry out detected at level 12 (3.86 m elevation)	210	261
Second core dry out reaches level 7 (2.2 m elevation)	255	274
Accumulator water injection initiates	316	243
PCT during second dry out	326	341
Second core rewet attained	349	351

5.3. Summary considerations

In this part of the research activity, the features and structure of the Standard Consolidated Reference Experimental Database (SCRED), that includes a series of documents which goal is to demonstrate the qualification level of the achieved code results, has been presented. The quality level of the “RDS-facility”, the “RDS-test”, the “Qualification Report” and the “Engineering Handbook” is achieved through a structured approach focused on multiple and independent review process.

By-product of this activity is the clear possibility to make traceable any input’s value and any user choice respectively derived and taken from the blue prints to the final achieved code results.

In the framework of application of the SCRED to validation of thermal-hydraulic code RELAP5-3D©, the RDS, model for LOBI-MOD1 and LOBI-MOD2 facilities and Engineering Handbook have been developed. The calculation of test A1-06 (LBLOCA) and A1-83 (SBLOCA) has been performed and calculation results have been subjected to qualification process. An extract of the RELAP5-3D code calculation results of 2 selected transients performed following the presented procedures is shown to demonstrate the maturity level and the effectiveness of the procedures itself, which is reflected in the excellent results of the presented simulations.

This confirms that the use of qualified experimental databases has the key role in providing the Quality Assurance to the “best nodalization practices”, which is currently the only viable approach in consideration of the nodalization-related uncertainties.

6 CONCLUSIONS

This doctoral thesis is a result of research activity carried out at San Piero a Grado Nuclear Research Group of University of Pisa. During the designated period, the Author took part in many activities related to application and validation of thermal-hydraulic codes, safety studies of nuclear reactors of PWR, BWR, WWER and CANDU types, participated in various international benchmarks, meetings, workshops and projects related to use of system thermal-hydraulic codes and application of uncertainty methodologies. The expertise, acquired from this work and from collaboration with many experts from foreign institutions (both research and industry), provided an invaluable basis for conducting a solid and coherent research.

In this context, the emphasis can be given to two international projects which provided the possibilities and means to profit from state-of-the-art methodologies in evaluating the uncertainties of code input parameters and the access to required experimental databases:

- OECD/NEA PREMIUM (Post-BEMUSE REFlood Models Input Uncertainty Methods) benchmark which was launched with the aim to progress on the issue of uncertainty of the physical models involved in the prediction of core reflooding;
- NURESAFE European collaborative project which aims at developing advanced tools and methods for a multi-scale and multi-physics analysis and new methods for evaluation of accuracy, sensitivity and uncertainty of coupled simulation tools.

A part of the present research activity constituted the synthesis of the work performed by all PREMIUM benchmark participants in the frame of Phase II and largely contributed to the writing of the corresponding OECD/NEA report.

The present research activity has been aimed to progress on the two issues identified in the framework of use of BEPU approach in nuclear safety studies:

- Estimation of code input parameter uncertainties, and
- Quality assurance in qualification of best-estimate models.

The review of the currently available methodologies for model calibration and evaluation (e.g. CIRCE, DAA) of uncertainty of code input parameter revealed a series of frailties and disadvantages inherent to the adopted approaches. Therefore, a new Input Parameter Range Evaluation Methodology (IPREM) have been developed in order to overcome the aforementioned issues and to reduce the uncertainty method user effect.

The mathematical apparatus and figures-of-merit of the Fast Fourier Transform Based Method (FFTBM), that allow a quantifiable comparison of time trends resulting from thermal-hydraulic calculations, has been adopted. The procedure, factors and criteria have been developed and set up in order to quantify the variation ranges of considered code input parameters.

The developed IPREM is based rather on engineering considerations than on statistical treatment. Therefore, it does not take account or provides as a result the

Probability Density Function for each input parameter. However, for practical thermal-hydraulic applications, the use of uniform or histogram distribution (which correspond to a minimum knowledge on the statistical nature of a parameter) proved to provide the valid uncertainty analysis results for relevant thermal-hydraulic responses.

As milestone of the present research activity, the IPREM has been applied to the evaluation of uncertainty of the reflood-related input parameters and models of RELAP5 Mod3.3 and CATHARE2 codes. The obtained results in the form of variation ranges of input parameters have been subjected to various “internal” qualifications (sensitivities on criteria and choice of PDF) and extensive validation. The validation has been carried out through uncertainty analysis of “blind” thermal-hydraulic calculations of numerous reflood tests performed at different experimental facilities and at different conditions. As the main nuclear safety issue related to reflood phenomena is the peak cladding temperature, the corresponding values of measured PCT have been compared against the maximum of evaluated upper uncertainty ranges of predicted temperature trends. The majority of evaluated uncertainty bands encompasses the measured values of PCT and allows to confirm the validity of the application of the IPREM methodology for the evaluation of uncertainty of code input parameters.

The IPREM proved:

- To allow the evaluation of input parameter uncertainty from a single ‘intermediate’ experimental test. However, the use of a number of other experimental test is required to validate the obtained ranges [α^L ; α^U];
- To be test, facility, and code independent;
- That any code input parameter and any code output parameter can be used in the process of quantification of input parameter ranges;
- That the methodology does not require modifications of the source of thermal-hydraulic code – only the post-processing of the calculation results is required;
- That resulting evaluated uncertainty of code input parameters is applied with reference/default values of these parameters (no calibration), which is relevant for industrial applications and acceptance by regulatory bodies;
- That no significant resources are needed to implement and apply the methodology.

The developed IPREM methodology reduces the use of engineering judgment (and thus the uncertainty method user effect) thanks to a proper procedure, mathematical apparatus and corresponding criteria. Engineering judgment is still present and connected with the selection of the input parameters and responses of interest, the characterization of the criteria and of its threshold, but in all these situations, the engineering judgment is embedded into the method itself and is not changed from one application to the other. In addition it shall be noted that in some particular cases the proposed figures-of-merit did not allow to quantify the one side of the range of variation of an input parameter. In this case, therefore the engineering judgment is still unavoidable, even though it is reduced.

Finally, the issue of quality assurance in qualification of best-estimate codes, models and “best modeling practices” has been analyzed. It has been pointed out that a consistent code assessment supported by a qualified experimental database is an important step for developing a solid ground for the uncertainty evaluation in the frame of BEPU approach.

The solution to quality assurance problem has been proposed in a form of a Standard Consolidated Reference Experimental Database (SCRED), which includes a series of documents which goal is to demonstrate the qualification level of the achieved code results. The quality level of the “RDS-facility”, the “RDS-test”, the “Qualification Report” and the “Engineering Handbook” is achieved through a structured approach focused on multiple and independent review process which is part of SCRED.

In the framework of application of the SCRED to the validation of thermal-hydraulic code RELAP5-3D©, the RDS, the model for LOBI-MOD1 and LOBI-MOD2 facilities and the Engineering Handbook have been developed. The calculations of test A1-06 (LBLOCA) and A1-83 (SBLOCA) have been performed and calculation results have been subjected to qualification process. An extract of the RELAP5-3D© code calculation results of two selected transients performed following the presented procedures is shown to demonstrate the maturity level and the effectiveness of the procedures itself, which is reflected in the excellent results of the presented simulations.

This confirms that the use of qualified experimental databases has the key role in providing the Quality Assurance to the “best nodalization practices”, which is currently the only viable approach in consideration of the nodalization-related uncertainties.

REFERENCES

- [1] IAEA, "Accident Analysis for Nuclear Power Plants", Safety Reports Series No. 23, Vienna, A, 2002.
- [2] A. Kovtonyuk, A. Petruzzi and F. D'Auria, *Error sources considered in the "UMAE driven" CIAU methodology*, The 14th International Topical Meeting on Nuclear Reactor Thermalhydraulics, NURETH-14, Toronto, Ontario, Canada, September 25-30, 2011
- [3] A. Petruzzi and F. D'Auria, *Approach and method to evaluate the uncertainty in system thermal-hydraulics calculations. Key applications by CIAU method*, The 12th International Topical Meeting on Nuclear Reactor Thermal Hydraulics (NURETH-12), Pittsburgh, Pennsylvania, U.S.A. September 30-October 4, 2007.
- [4] US NRC, 10 CFR 50 <Acceptance Criteria for Emergency Core Cooling Systems for Light Water Nuclear Power Reactors> and Appendix K, <ECCS Evaluation Models> to 10 CFR Part 50, Code of Federal Regulations, 1996.
- [5] Boyack B.E., Catton I., Duffey R.B., Griffith P., Katsma K.R., Lellouche G.S., Levy S., Rohatgi U.S., Wilson G.E., Wulff W. and Zuber N., *An Overview of the Code Scaling, Applicability and Uncertainty Evaluation Methodology*, J. Nucl. Eng. and Des. 119, pp 1-16, 1990.
- [6] Glaeser H., Hofer E., Kloos M., Skorek T., 1994. *Uncertainty and sensitivity analysis of a post-experiment calculation in thermal hydraulics*. Reliability Engineering & System Safety Vol. 45 (1-2), 19-33.
- [7] Hofer E. Probabilistische Unsicherheitsanalyse von Ergebnissen umfangreicher Rechenmodelle, GRS-A-2002, 1993.
- [8] Wilks S.S., 1941. *Determination of sample sizes for setting tolerance limits*. *Annals of Mathematical Statistics* 12, 91-96.
- [9] F. D'Auria, N. Debrecin, G.M. Galassi, "Outline of the Uncertainty Methodology based on Accuracy Extrapolation", J. Nuclear Technology, 109 No. 1, 1995, pp. 21-38
- [10] Ambrosini W., Bovalini R., D'Auria F., 1990. *Evaluation of Accuracy of Thermal-hydraulic Codes Calculations*. Energia Nucleare 7.
- [11] D'Auria F. and Giannotti W., *Development of Code with capability of Internal Assessment of Uncertainty*, J. Nuclear Technology 131, pp 159-196, 2000.
- [12] Petruzzi, A., D'Auria, F., Giannotti, W. and Ivanov K., *Methodology of Internal Assessment of Uncertainty and Extension to Neutron-Kinetics / Thermal-Hydraulics Coupled Codes*, J. Nucl. Scie. and Eng. 149, pp 1-26, 2005.
- [13] A. Petruzzi, F. D'Auria, *Uncertainties in predictions by thermal-hydraulic codes: approaches and results*, *Proceedings of the 3rd Joint US-European Fluids Engineering Summer Meeting and 8th International Conference on Nanochannels, Microchannels and Minichannels*, ASME 2010, August 1-5, Montreal, Canada, 2010.
- [14] Cacuci D.G., *Sensitivity and Uncertainty Analysis, Theory*, Vol. I, Chapman & Hall/CRC, Boca Raton (FL, US), ISBN 1-58488-115-1, 2003.
- [15] Cacuci D.G., Ionescu-Bujor M. and Navon I.M., *Sensitivity and Uncertainty Analysis, Application to Large Scale Systems*, Vol. II, Chapman & Hall/CRC, Boca Raton (FL, US), ISBN-10 1-58488-116-X, 2005.
- [16] M. Perez, F. Reventos et al., *Uncertainty and sensitivity analysis of a LBLOCA in a PWR Nuclear Power Plant: Results of the Phase V of the BEMUSE*

- programme*, Nuclear Engineering and Design, Volume 241, Issue 10, October 2011, pp. 4206–4222.
- [17] A. Kovtonyuk, S. Lutsanych, A. Petruzzi, F. Moretti and F. D'Auria, *Validation of the IPREM methodology for evaluation of uncertainty of system code input parameters*, Proceedings of the 22th International Conference on Nuclear Engineering, ICONE22, July 7-11, Prague, Czech Republic, 2014
- [18] NEA-CSNI, 2012. *OECD/NEA PREMIUM benchmark: Phase I: Methodology and data review, Appendix B: CIRCÉ description*. Tech. Rep., Committee on the Safety of Nuclear Installations, OECD, Nuclear Energy Agency.
- [19] A. de Crécy: “*Determination of the uncertainties of the constitutive relationships of the CATHARE 2 code*”, M&C 2001, Salt Lake City, Utah, USA, September 2001
- [20] Dempster, A.P., Rubin, D. B., Tsutakawa, R.K.: “*Estimation in Covariance Components Models*”, Journal of the American Statistical Association, Vol. 76, Number 374, (1981)
- [21] Cacuci D.G., *On the Use of Adjoint Operators for Global Optimization and Data Assimilation*, Lectures Notes, Workshop on Predictability, Observations, and Uncertainties in Geosciences, Tallahassee (FL, US), March 13-15, 2006.
- [22] A.F. Badea, D.G. Cacuci, “*Uncertainty reduction in coupled neutron-kinetics /thermalhydraulics computational predictions following assimilation of BWR-TT benchmark experimental data*”, The 15th International Topical Meeting on Nuclear Reactor Thermal - Hydraulics, NURETH-15, Pisa, Italy, May 12-17, 2013
- [23] A. Petruzzi, D.G. Cacuci, “*Best-Estimate Model Calibration and Prediction Through Experimental Data Assimilation—II: Application to a Blowdown Benchmark Experiment*”, Nuclear Science and Engineering Volume 165, pp. 1–52 (2010).
- [24] M. C. Badea, D. G. Cacuci, A. F. Badea, “*Best-Estimate Predictions and Model Calibration for Reactor Thermal Hydraulics*”, Nuclear Science and Engineering Volume 172, Number 1, pp. 1-19 (2012).
- [25] A. F. Badea, D. G. Cacuci, M. C. Badea, *Uncertainty reduction in calibrated FLICA4 thermal-hydraulics computational predictions following assimilation of multiple BFBT benchmark experimental data*, The 15th International Topical Meeting on Nuclear Reactor Thermal - Hydraulics, NURETH-15, Pisa, Italy, May 12-17, 2013.
- [26] OECD/NEA, “*Best-Estimate Methods (Including Uncertainty Methods and Evaluation) Qualification and Application. First Meeting of the Programme Committee*”, NEA/SEN/SIN/AMA(2003)8, Issy-les-Moulineaux, France, February 12-13, 2003.
- [27] OECD/NEA, “*First Meeting of the BEMUSE Programme (Best-Estimate Methods – Uncertainty and Sensitivity Evaluation) –BEMUSE Phases 1 and 2*”, NEA/SEN/SIN/AMA(2003)27, Cadarache, France, September 4-5, 2003.
- [28] NEA-CSNI, 2012. *OECD/NEA PREMIUM benchmark: General requirements and description specification of methodologies and experimental data to be used in PREMIUM benchmark*. Tech. Rep., Committee on the Safety of Nuclear Installations, OECD, Nuclear Energy Agency.
- [29] C. Chauliac, J.M. Aragonés, D. Bestion, D. G. Cacuci et al., *NURESIM – A European simulation platform for nuclear reactor safety: Multi-scale and multi-*

- physics calculations, sensitivity and uncertainty analysis*, Nuclear Engineering and Design 241(9), pp. 3416-3426, 2011.
- [30] NURESAFE, 2013. *Detailed Program of Work of the Work Package 3.1: Multiscale and Multiphysics Simulation of LOCA. NUclearREactorSAFEty simulation platform*, Collaborative Project - Seventh Framework Programme EURATOM, European Commission, NURESAFE – D3.1.0.1.
- [31] Leonardi M., D'Auria F., Pochard R., *The FFT based method in the frame of the UMAE*, Spec. Workshop on Uncertainty Analysis Methods, London, March 1994.
- [32] Wickett T., D'Auria F., Glaeser H. et al, "*Report of the Uncertainty Method Study for Advanced Best Estimate Thermalhydraulic Code Applications*" OECD/NEA/CSNI R (97) 35, I and II, June 1998.
- [33] Petruzzi A., D'Auria F., *Thermal-Hydraulic System Codes in Nuclear Reactor safety and Qualification procedures*, Science and Technology of Nuclear Installations, ID 460795, 2008.
- [34] OECD/NEA/CSNI, BEMUSE Programme. Phase 3 report "*Uncertainty and Sensitivity Analysis of the LOFT L2-5 experiment*", OECD/CSNI Report NEA/CSNI/R(2007)4.
- [35] A. Del Nevo, E. Coscarelli, A. Kovtonyuk, F. D'Auria, *Analytical Exercise On OECD/NEA/CSNI PKL-2 Project Test G3.1: Main Steam Line Break Transient In PKL-III Facility Phase 2: Post-Test Calculations*, TH/PKL-2/02(10) Rev. 1, Universita di Pisa, Pisa, March 2011.
- [36] Coscarelli E., 2013. *An Integrated Approach to Accident Analysis in PWR. Tesi di Dottorato di Ricerca*, Scuola di Dottorato in Ingegneria "Leonardo da Vinci", Università di Pisa.
- [37] Nyquist H., "*Certain topics in telegraph transmission theory*". Transactions AIEE, vol. 47, 1928, pp. 617–644.
- [38] Shannon C. E., "*Communication in the presence of noise*". Proceedings Institute of Radio Engineers, vol. 37(1), 1949, pp. 10–21.
- [39] Bovalini R., D'Auria F., Leonardi M., "*Qualification of the Fast Fourier Transform based methodology for the quantification of thermal-hydraulic system code accuracy*", DCMN NT 194(92), Pisa, 1992.
- [40] A. Kovtonyuk, A. Petruzzi, F. D'Auria. "*Proposal of Methodology for Assessment of Uncertainty of System Codes' Input Parameters*". 7th Workshop on OECD/NEA Uncertainty Analysis Methodology program, OECD/NEA Headquarters, Issy-les-Moulineaux, France, 2013.
- [41] A. R. Edwards and F. P. O'Brien, "*Studies of Phenomena Connected with the Depressurization of Water Reactors*," Journal of the British Nuclear Energy Society, 9, 1970, pp. 125-135.
- [42] US NRC, 2003. RELAP5/MOD3.3 *Code Manual Volume I: Code Structure, System Models, and Solution Methods*. NUREG/CR-5535/Rev P3.
- [43] R. E. Henry and H. K. Fauske. "*The Two-Phase Critical Flow of One-Component Mixtures in Nozzles, Orifices, and Short Tubes*." Transactions of ASME, Journal of Heat Transfer. 93.1971. pp. 179-187.
- [44] US NRC, 2003. RELAP5/MOD3.3 *Code Manual Volume 3: Developmental Assessment Problems*. NUREG/CR-5535/Rev P3.
- [45] CSNI/NEA. *CSNI Separate Effects Test Matrix for Thermal-Hydraulic Code Validation*, NEA/CSNI/R(93)14, September 1993.

- [46] CSNI/NEA. *CSNI Integral Test Facility Validation Matrix for the Assessment of Thermal-Hydraulic Codes for LWR LOCA and Transients*, NEA/CSNI/R(96)17, July 1996.
- [47] Kfk Karlsruhe, 1984. *FEBA – Flooding Experiments with Blocked Arrays, Evaluation Report*. Tech. Rep. KfK 3657.
- [48] Kfk Karlsruhe, 1984. *FEBA – Flooding Experiments with Blocked Arrays, Data Report 1*, Test Series I through IV. Tech. Rep. KfK 3658.
- [49] NEA-CSNI, 2012. *OECD/NEA PREMIUM benchmark: Phase II: Identification of influential input parameters*. Tech. Rep., Committee on the Safety of Nuclear Installations, OECD, Nuclear Energy Agency.
- [50] NEA-CSNI, 2011. *OECD/NEA PREMIUM benchmark: Specifications for phase II*. Tech. Rep., Committee on the Safety of Nuclear Installations, OECD, Nuclear Energy Agency.
- [51] NEA-CSNI, 2013. *OECD/NEA PREMIUM benchmark: Specifications for the phase IV using the 2-D reflooding PERICLES tests*. Tech. Rep., Committee on the Safety of Nuclear Installations, OECD, Nuclear Energy Agency.
- [52] CEA, 1985. *Study of Two-Dimensional Effects in the Core of a Light Water Reactor during the Reflooding Phase of LOCA*. Commissariat à l'énergie atomique. Note TT/SETRE/146.
- [53] ACHILLES, 1989. *Achilles Unballooned Cluster Experiments - Part 1: Description of the Achilles Rig, Test Section and Experimental Procedures*. Tech. Rep. AEEW-R 2336. United Kingdom Atomic Energy Authority, Winfrith Technology Centre.
- [54] ACHILLES, 1989. *Achilles Unballooned Cluster Experiments - Part 3: Low Flooding Rate Reflood Experiments*. Tech. Rep. AEEW 2338. United Kingdom Atomic Energy Authority, Winfrith Technology Centre.
- [55] CATHARE 2 V2.5_1: *General Description of the CATHARE 2 V25_2mod8.1 System Code*. DEN/DANS/DM2S/STMF/LMES/RT/12-008/A, Laviaille G. et al., 2012.
- [56] CATHARE 2 V2.5_1: *User Guidelines*, DER/SSTH/LDAS/EM/2005-034, G. Laviaille, 2005.
- [57] NEA-CSNI, 2011. *OECD/NEA PREMIUM benchmark: Specifications for phase II. Appendix B: Thermal properties of FEBA test facility*. Tech. Rep., Committee on the Safety of Nuclear Installations, OECD, Nuclear Energy Agency.
- [58] CATHARE 2 V2.5_2mod8.1: *Dictionary of Directives and Operators*, DEN/DANS/DM2S/STMF/LMES/RT/11-004/A, J. Darona, 2011.
- [59] CATHARE2 V2.5_1: *User's Manual*, SSTH/LDAS/EM/2005-035, G. Laviaille, 2006.
- [60] A. Kovtonyuk, S. Lutsanych, F. Moretti. "Validation and improvement of the uncertainty quantification method based on FFTBM", NURESAFE-SP3 3rd Meeting, Rez, Czech Republic, 2013.
- [61] <http://www.mathworks.nl/products/matlab/>
- [62] A. Kovtonyuk, A. Petruzzi, F. Fiori, M. Kovtonyuk and F. D'Auria. "Development of Qualified Experimental Database for Code/Nodalization Assessment". Technical Meeting on BEPU in Safety Analyses, IAEA J4-TM-44906, Pisa, Italy, 10 -14 June, 2013.
- [63] Petruzzi A., Giannotti W., D'Auria F., "Development, Qualification and Use of a Code with the Capability of Internal Assessment of Uncertainty", CNS, Sixth

- International Conference on Simulation Methods in Nuclear Engineering, Montreal, Canada 2004.
- [64] IAEA. “*Best Estimate Safety Analysis for Nuclear Power Plants: Uncertainty Evaluation*”, Safety Report Series N° 52, Vienna, 2008.
- [65] A. Kovtonyuk, F. Fiori, A. Petruzzi, M. Kovtonyuk and F. D’Auria, “*Use of qualified experimental database for a system code assessment*”. The 15th International Topical Meeting on Nuclear Reactor Thermal - Hydraulics, NURETH-15, Pisa, Italy, May 12-17, 2013.
- [66] Agreement Atucha-II - UNIPI N°3. “*RELAP5-3D© Post-test analysis and accuracy quantification of LOFT L2-5 LBLOCA test*”, REP-210_U-NII_DIT_217_E1.3.7e_ChFin_FR_rev0. Fiori F., 2013.
- [67] Agreement Atucha-II - UNIPI N°3. “*RELAP5-3D© post-test analysis and accuracy quantification of LOBI test A1-06*”, REP-132_U-NII_DIT_237_E1.3.7a_ChFin_FR_rev0. Fiori F. and Veronese F., 2013.
- [68] NEA-CSNI. “*LOBI-MOD2: Facility Description and Specifications for OECD-CSNI International Standard Problem N° 18 (ISP 18)*”, Reactor Safety Program N° 4010, July 1983.
- [69] C. Addabbo, L. Piplies, “*Difference between the MOD1 and MOD2 configuration of the LOBI test facility*”, Technical Note N° I.06.C1.85.41, Ispra Italy, April 1985.
- [70] И. Е. Идельчик, “Справочник по гидравлическим сопротивлениям”, 3-е издание Москва, Машиностроение 1992 г. (rus. for I.E. Idel’chik, Handbook of Hydraulic Resistance).
- [71] Agreement Atucha-II - UNIPI N°3. “*RELAP5-3D© post-test analysis and accuracy quantification of LOBI test A1-83*”, REP133_U-NIII_DIT219_E1.3.7b_Ch15Fin_FR_rev0. Kovtonyuk A. and Fiori F., 2012.
- [72] L. Piplies, N. Granner, “*Quick Look Report on LOBI Test A1-06*”, N° 3955, September 1982, Ispra Research Center, Italy.
- [73] C. Addabbo, G. Gressani, “*Quick Look Report on LOBI-MOD2 Test A1-83*”, N° 4028, May 1985, Ispra Research Center, Italy.
- [74] The RELAP5-3D© Code Development Team, “*RELAP5-3D© Code Manual Volume I: Code Structure, System Models, And Solution Methods*”, INEEL-EXT-98-00834, Revision 2.4, Idaho National Laboratory, June 2005
- [75] Agreement Atucha-II - UNIPI N°3. “*Engineering Handbook of RELAP5-3D© LOBI/MOD2 facility nodalization*”, REP138_U-NIII_DIT140_E1.3.8b_FR_Ch15Fin_Rev1. Fiori F., O. Lysovii and Kovtonyuk A., 2012.
- [76] Bonuccelli M., D’Auria F., Debrechin N., Galassi G. M., “*A Methodology for the Qualification of Thermalhydraulic Code Nodalizations*”, Proceedings of NURETH-6 Conference, Grenoble, France, October 5-8, 1993.
- [77] F. Fiori, A. Kovtonyuk, et al. “*RELAP5-3D assessment using a qualified experimental database*”. Proceedings of the 21th International Conference on Nuclear Engineering ICONE21, China, 2012.

APPENDIX A. CODES APPLIED IN THE FRAMEWORK OF RESEARCH

A.1. RELAP5 Mod3.3 code

A.1.1. Code overview

The light water reactor transient analysis code, RELAP5, was developed at Idaho National Engineering Laboratory (INEL) for the U.S. Nuclear Regulatory Commission (NRC), ref. [A-1]. Code uses include analyses required to support rulemaking, licensing audit calculations, evaluation of accident mitigation strategies, evaluation of operator guidelines, and experiment planning analysis. Specific applications have included simulations of transients in LWR systems such as loss of coolant, anticipated transients without scram (ATWS), and operational transients such as loss of feedwater, loss of offsite power, station blackout, and turbine trip. RELAP5 is a highly generic code that, in addition to calculating the behavior of a reactor coolant system during a transient, can be used for simulation of a wide variety of hydraulic and thermal transients in both nuclear and nonnuclear systems involving mixtures of steam, water, non-condensable, and solute.

RELAP5/MOD3.3 has been developed jointly by the NRC and a consortium consisting of several countries and domestic organizations that were members of the International Code Assessment and Applications Program (ICAP) and its successor organization, Code Applications and Maintenance Program (CAMP). Credit also needs to be given to various Department of Energy sponsors, including the INEL laboratory-directed discretionary funding program.

The RELAP5/MOD3.3 code is based on a nonhomogeneous and non-equilibrium model for the two phase system that is solved by a fast, partially implicit numerical scheme to permit economical calculation of system transients. The objective of the RELAP5 development effort from the outset was to produce a code that included important first-order effects necessary for accurate prediction of system transients but that was sufficiently simple and cost effective so that parametric or sensitivity studies were possible.

The code includes many generic component models from which general systems can be simulated. The component models include pumps, valves, pipes, heat releasing or absorbing structures, reactor point kinetics, electric heaters, jet pumps, turbines, separators, accumulators, and control system components. In addition, special process models are included for effects such as form loss, flow at an abrupt area change, branching, choked flow, boron tracking, and non-condensable gas transport.

A.1.2. Reflood-related correlations

A reflood heat transfer model has been designed specifically for the reflood process which normally occurs at low flow and low pressure, ref. [A-2]. The fine mesh rezoning scheme is applied at the quench front elevation. Changes were made to default code models of interfacial heat transfer, interfacial drag, and wall heat transfer. Whenever a code user activates "reflood," the code uses these models.

A.1.2.1. Interphase friction

The modified Bestion correlation is used for interfacial drag in vertical bubbly-slug flow at pressures below 10 bars in place of the EPRI correlation. Above 20 bars the EPRI correlation is used. Between 10 and 20 bars the interfacial drag is interpolated. The modified Bestion correlation for the code interfacial drag coefficient, C_i , is coded in subroutine FIDISJ as:

$$C_i = \frac{65\alpha_g\rho_g(1-\alpha_g)^3}{D} \quad (\text{A-1})$$

where

C_i = interfacial drag coefficient (the variable name is *fic* in subroutine FIDISJ)

α_g = donored junction vapor void fraction

ρ_g = donored junction vapor density

D = junction hydraulic diameter

The void distribution parameter C_0 is set to 1.2.

A.1.2.2. Dispersed flow interphase heat transfer

In RELAP5/MOD3.3, the interfacial heat transfer between the gas and liquid phases in the bulk actually involves both heat and mass transfer. Temperature-gradient-driven bulk interfacial heat transfer is computed between each phase and the interface. The temperature of the interface is assigned the saturation value for the local pressure. Heat transfer correlations for each side of the interface are provided in the code. Since both superheated and subcooled temperatures for each phase are allowed, the heat transfer may be either into or away from the interface for each phase. All of the thermal energy transferred to the interface from either side contributes to vaporization as it is used to compute the mass transfer Γ_{ig} to the gas phase. Conversely, all of the heat transfer away from the interface contributes to condensation, since it is used to compute the mass transferred to the liquid phase ($-\Gamma_{ig}$). In other words, the cases of superheated liquid and superheated gas contribute to vaporization, while both subcooled liquid and subcooled gas contribute to condensation. The net rate of mass transfer is determined by summing the contributions, positive and negative, from each side of the interface.

The form used in defining the heat transfer correlations for superheated liquid (SHL), subcooled liquid (SCL), superheated gas (SHG), and subcooled gas (SCG) is that for a volumetric heat transfer coefficient (W/m^3K). Since heat transfer coefficients are often given in the form of a dimensionless parameter (usually Nusselt number, Nu), the volumetric heat transfer coefficients are coded as follows:

$$H_{ip} = \frac{k_p}{L} Nu a_{gf} = h_{ip} a_{gf} \quad (\text{A-2})$$

where

H_{ip} = volumetric interfacial heat transfer coefficient for phase p ($\text{W}/\text{m}^3 \cdot \text{K}$)

k_p = thermal conductivity for phase p ($\text{W}/\text{m} \cdot \text{K}$)

L = characteristic length (m)

a_{gf} = interfacial area per unit volume (m^2/m^3)

h_{ip} = interfacial heat transfer coefficient for phase p ($\text{W}/\text{m}^2 \cdot \text{K}$)

p = phase p (either f for liquid for g for gas)

and where Nu takes different form for different phases

- Subcooled liquid
- Superheated liquid
- Subcooled gas
- Superheated gas

In the reflood mode the interfacial area is changed in a control volume next to a heat structure with "reflood" activated.

Both the wet and dry wall interfacial areas are changed in subroutine FIDISV for reflood simulation. The wet wall droplet size maximum was reduced from 2.5 mm to 1.5 mm. The dry wall Weber number was reduced from 12 to 3.

A.1.2.3. Wall to fluid Heat Transfer (film boiling and transition boiling)

Changes occur in transition and film boiling heat transfer coefficients, both with and without the hydraulic bundle flag activated, when reflood is active.

Quenching can occur at both ends of rod bundles. Quench front advancement is determined in subroutine QFHTRC and keys off the mode number. The current fine mesh is considered to be wetted when the mode number is less than 5. Quench fronts can also recede if dryout reoccurs. *Figure 165* illustrates a bottom and top wetted regime along with distance variables used by the code and variables used in this section of the manual.

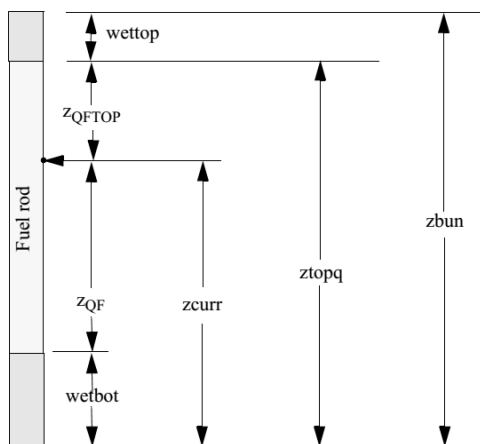


Figure 165 – Fuel Rod Showing Variables used by the Reflood Model.

A modified Weismann correlation replaces the Chen transition boiling correlation. The correlation is:

$$h_w = h_{max} (e^{-0.02\Delta T_{wchf}}) + 4500 \left(\frac{G}{G_R}\right)^{0.2} (e^{-0.012\Delta T_{wchf}}) \quad (\text{A-3})$$

Where

$$h_{max} = \frac{0.5 CHF}{\Delta T_{chf}}$$

CHF = critical heat flux

$$\Delta T_{wchf} = \max[3, \min(40, T_w - T_{spt})]$$

$$\Delta T_{chf} = \max(0, T_w - T_{spt})$$

G = total mass flux

$$G_R = 67.8 \text{ kg/m}^2\text{s}$$

The original Weismann correlation used 0.04 in place of 0.02. The 0.5 multiplier in h_{max} was not in the PSI updates as received but was added to reduce the magnitude of the spike in heat flux to the fluid which occurs near the critical heat flux temperature. Reducing this spike is the whole motivation behind the reflood model. The reduction is physically justified because of the hysteresis in going from nucleate boiling to transition boiling and back.

Code use of the Weismann correlation depends on the distance from the point in question to the quench front position. The transition boiling heat transfer coefficient to liquid h_{TB} , is given by:

$$h_{fTB} = \begin{cases} \max(h_{max}, h_w) & z_{QF} \leq 0.1 \text{ m} \\ h_{low} & z_{QF} \geq 0.2 \text{ m} \\ \text{Interpolate } 0.1 \text{ m} < z_{QF} < 0.2 \text{ m} & \end{cases} \quad (\text{A-4})$$

where

h_{fTB} = transition boiling heat transfer coefficient to liquid

z_{QF} = distance from the point in question to the bottom quench front

$h_{low} = 0.0001 \text{ W/m}^2\text{K}$

The heat flux to liquid, q_{fTB} , is $h_{fTB}(T_w - T_{spt})$.

The transition boiling heat transfer coefficient to vapor, h_{gTB} , comes from a call to the DITTUS subroutine. This coefficient, h_{Ditt} , is then void fraction ramped so that it goes to zero as the void fraction goes to zero and is given by:

$$h_{gTB} = h_{Ditt} \alpha_g \quad (\text{A-5})$$

The heat flux to vapor, q_{gTB} , is $h_{gTB}(T_w - T_g)$.

The film boiling heat transfer coefficient to liquid h_{fFB} , uses the maximum of a film coefficient, h_{fBB} , and a Forslund-Rohsenow coefficient, h_{FR} . The film coefficient, h_{fFB} , is given by:

$$h_{fBB} = [1400 - 1880 \min(0.05, z_{QF})] \min(0.999 - \alpha_g, 0.5) + h_{FBGR} (1 - \alpha_g)^{0.5} \quad (\text{A-6})$$

The first part of h_{fBB} is an empirical length dependent expression and the second part includes a modified Bromley correlation coefficient, h_{FBGR} , which uses z_{QF} for the length in the denominator instead of the wave length as does the normal RELAP5 Bromley correlation. The modified Bromley correlation coefficient used here is given by:

$$h_{FBGR} = 0.62 \left\{ \frac{g k_g^3 \rho_g (\rho_f - \rho_g) [h_{fg} + 0.5(T_w - T_{spt}) c_{pf}]}{\max(0.005, z_{QF}) \mu_g (T_w - T_{spt})} \right\}^{0.25} \quad (\text{A-7})$$

The Forslund-Rohsenow correlation coefficient is given by:

$$h_{FR} = h1 \left\{ \frac{g \rho_g \rho_f h_{fg} k^3}{[(T_w - T_{spt}) \mu_g d (\frac{\pi}{6})^{\frac{1}{3}}]} \right\}^{0.25} \quad (\text{A-8})$$

Where

$$h1 = 0.4 \left(\frac{\pi}{4} \right) \left[\frac{6(0.999 - \alpha_g)}{\pi} \right]^{\frac{2}{3}}$$

$$d = \min \left(0.003, \max \left\{ 0.0004, 3 \frac{\sigma}{\rho_g} \max MEMP \left[0.01, (v_g - MEMP v_f)^2 \right] \right\} \right) \quad (\text{A-9})$$

where

v_g = vapor velocity

v_f = liquid velocity

Radiation to droplets is added to the final film boiling coefficient to liquid, h_{IFB} , which is the maximum of Equation (A-6) and (A-8). The final value is multiplied times $T_w - T_{spt}$ to get the heat flux to liquid.

The heat flux to vapor is the same as the transition boiling value.

A.1.2.4. Weber number

The We number is used to compute the interfacial transfer area per unit volume:

$$a_{gf} = \frac{3.6\bar{\alpha}}{d_o} \quad (A-10)$$

where the average diameter d_o is obtained by assuming that $d_o = (1/2) d_{max}$. The maximum diameter, d_{max} is related to the critical Weber number, We_c , by:

$$We_c = \frac{d_{max}\rho_c(v_g - v_f)^2}{\sigma} \quad (A-11)$$

A.1.2.5. Minimum droplet diameter

The minimum droplet diameter is a preset constant in RELAP5 subroutines that is used for calculation of interphase friction and interphase heat transfer. The droplet diameter is computed for each volume and junction by:

$$D_{min} = MAX \left[\frac{We_c \cdot \sigma}{\rho_g \cdot (v_g - v_f)^2}, present_D' \right] \quad (A-12)$$

This value is further used to compute other parameter, e.g. Re number:

$$Re_p = \frac{|v_g - v_f| d_o \rho_c}{\mu_m} \quad (A-13)$$

where $d_o = MIN[D_{min}; preset_D]$

A.2. CATHARE2 code

The CATHARE2 (Code for Analysis of Thermal-Hydraulics during an Accident of Reactor and safety Evaluation) is a best estimate system code originally devoted to calculations of thermalhydraulic transients in Light Water Reactors such as PWR, VVER or BWR. It has been developed in Grenoble by the Commissariat à l'Energie Atomique (CEA), Electricité de France (EDF), AREVA and Institut de Radioprotection et de Sûreté Nucléaire (IRSN).

All CATHARE modules, ref. [A-3], are based on a six – equation two - fluid model (mass, energy and momentum equations for each phase), with additional optional equations for non-condensable gases and radio-chemical components.

CATHARE has a flexible modular structure for the thermal hydraulic modeling in applications ranging from simple experimental test facilities to large and complex installations like Nuclear Power Plants. Several modules can be assembled to represent the primary and secondary circuits of any Reactor and of any separate-effect test or integral effect test facility.

The modules are:

- The 1-D (or axial) module to describe pipe flow. A TEE sub-module used to represent a main pipe (1-D module) with a lateral branch can be added to the 1-D module;
- The 0-D (or volume) module, a two-node module used to describe large size plena with several connections, such as the pressurizer, the accumulator, the steam generator dome or the lower plenum of a PWR. The volume predicts swell level, total or partial fluid stratification and phase separation phenomena at the junctions;
- The 3-D module to describe multidimensional effects in the vessel;
- The boundary conditions (BC) module.

To complete the modeling of the circuits, sub-modules can be connected to the main modules:

- The multi-layer wall module in which radial conduction is calculated;
- The reflooding model with 2-D heat conduction in the wall or fuel rod for predicting quench front progression;
- The fuel pin thermo-mechanics sub-module which can predict fuel cladding deformation, creep, rupture, clad oxidation and thermal exchanges;
- Heat exchangers between two circuits or between two elements of a circuit;
- The point neutronics module (a 3-D neutronics code can also be coupled to CATHARE);
- Various reactor components (accumulator, pressurizer, 1-node pump, valves, safety valves, check valves, flow limiters);
- Sources and sinks, breaks, steam generator tube rupture;
- The counter-current flow limitation (CCFL) sub-module to be used in complex geometries such as the upper core plate and the steam generator tubes.

The discretization of all terms of the equations is fully implicit in 1-D and 0-D modules and semi implicit in 3-D elements including inter-phase exchange, pressure and convection terms, and the resulting non-linear equations are solved using an iterative Newton solver. The code allows efficient use of several processors in parallel. The space discretization uses the staggered mesh and the donor cell principle. A specific treatment of the residual phases exists in order to manage their appearance and disappearance while minimizing convergence problems and with a quasi-perfect mass and energy conservation.

A.3. RELAP5-3D© code

The RELAP5-3D© code, ref. [A-4] is an outgrowth of the one-dimensional RELAP5/Mod3 code developed at the INL. The most prominent attribute that distinguishes RELAP5-3D© from its predecessors is the fully integrated, multi-dimensional thermal-hydraulic and neutron kinetic modeling capability.

The code models the coupled behavior of the reactor coolant system and the core (3-D neutron kinetic model) for simulating accidents in LWR: such as loss of coolant, Anticipated Transients Without Scram (ATWS) and operational transients. A generic modeling approach is used that permits simulating a variety of thermal hydraulic systems such as turbines, condensers and secondary feed-water systems.

Based on one-dimensional, transient, and non-homogeneous and non-equilibrium hydrodynamic model for the steam and liquid phases, RELAP5 code uses a set of six partial derivative balance equations and can treat a non-condensable component in the steam phase and a non-volatile component (boron) in the liquid phase. A choked-flow model developed by Ransom and Trapp is included primarily in RELAP5-3D© as the standard choked flow model for calculation of the mass discharge from the system at a pipe break or a nozzle. An optional choked flow model (modified Henry-Fauske) is also available.

A semi-implicit numeric scheme is used to solve the equations inside control volumes connected by junctions. The fluid scalar properties (pressure, energy, density and void fraction) are the average fluid condition in the volume and are viewed located at the control volume center. The fluid vector properties, i.e. velocities, are located at the junctions and are associated with mass and energy flows between control volumes that are connected in series, using junctions to represents flow paths. The direction associated to the control volume is positive from the inlet to the outlet.

Heat flow paths are also modeled in a one-dimensional sense, using a staggered mesh to calculate temperatures and heat flux vectors. Heat structures and hydrodynamic control volumes are connected through heat flux, calculated using a boiling heat transfer formulation. These structures are used to simulate pipe walls, heater elements, nuclear fuel pins and heat exchanger surfaces.

A.3. References to APPENDIX A

- [A-1] United States Nuclear Regulatory Commission, 2003. *RELAP5/MOD3.3 Code Manual Volume I: Code Structure, System Models, and Solution Methods*. NUREG/CR-5535/Rev P3.
- [A-2] United States Nuclear Regulatory Commission, 2003. *RELAP5/MOD3.3 Code Manual Volume IV: Models and Correlations*. NUREG/CR-5535/Rev P3.
- [A-3] *General Description of the CATHARE 2 V25_2mod8.1 System Code*, DEN/DANS/DM2S/STMF/LMES/RT/12-008/A, G. Laviaille, 2012.
- [A-4] The RELAP5-3D© Code Development Team, "*RELAP5-3D© Code Manual Volume I: Code Structure, System Models, and Solution Methods*", INEEL-EXT-98-00834, Revision 2.4, Idaho National Laboratory, June 2005

APPENDIX B. MODIFICATIONS OF RELAP5 SOURCE CODE

B.1. RELAP5 Mod3.3 source package

The RELAP5 Mod3.3 distribution package contains different folders and files. The focus is given to the folder “Source”, which actually contains the package with the source files for RELAP5 compilation.

Before proceeding further, one must read carefully the files *ReadmeFirst*, *Pre_install* and *ReadmeInstall* which are available in the root of the distribution package.

In the preset research, the successful compilation of RELAP5 Mod3.3 patch 03 has been performed with Intel Fortran Compiler under Linux Ubuntu 32-bit operating system.

In order to compile, the *make* command is used. In case the compilation succeeds, an executable *relap.x* (equivalent to *relap.exe*) is created in the “run” folder, otherwise, the error log *.errors* located in “relap” folder should be consulted to find out the compilation errors.

B.2. Modifications of main subroutine

It is possible to introduce the modification to RELAP5 source in the dedicated subroutines which are created after running the configuration scripts (*.ff files in a subfolder called “relap”).

There are 2 options available for introducing the modifications into the RELAP5 source:

- 1) Introduce the necessary modification (add a new line or multiplier, change a coefficient etc.) in the selected subroutine, compile the code and run the executable. This approach is relatively straightforward, easy and does not require any additional modification to the RELAP5 source except the introduced change to the model. But in this for every new sensitivity run (e.g. new value of introduced multiplier) the source must be modified, the code must be re-compiled and the model must be calculated with the “new” executable.
- 2) Incorporate into RELAP5 main program source (relap5.ff) some code lines in order to read a text file with values of the multipliers and store them in new FORTRAN variables of a common block. Perform an overview of all the stipulated subroutines/models to be modified and introduce into them the multipliers for the FORTRAN variables of interest in the form of the new FORTRAN variables of the common block. Compile once RELAP5 and obtain an executable which reads the values for the multipliers in the text file, allowing running all the necessary sensitivities without needing to perform additional compilations (i.e. if a value of a multiplier needs to be changed, only the text file has to be edited before running RELAP5). This solution is more elegant, in a long term time-saving and reduces the risk of

user errors, but requires an additional knowledge in FORTRAN programming in order to develop such an additional subroutine.

The second option has been used in the present research activities. The source code of the main routine *relap5.ff*, located in the “relap” folder, has been edited adding these two blocks of lines:

```
(...)  
c ----- PREMIUM ----- (1/2)  
common /premium/ mulval, multxt  
real mulval(14)  
character multxt(14)*30  
integer g  
c ----- PREMIUM -----  
  
(...)  
c ----- PREMIUM ----- (2/2)  
c Assign values to multipliers  
c  
    open(90,status='old',file='data.txt')  
    write(*,*) 'Uncertainty multipliers >>>>'  
    do 10 g=1,14  
        read(90,*) multxt(g)  
        read(90,*) mulval(g)  
        write(*,*) multxt(g),' multiplier set to: ', mulval(g)  
10  continue  
    read(*,*)  
    close(90)  
c ----- PREMIUM -----  
  
(...)
```

Line number 200,
where variables are
defined

Line number 237, just
after the input file
processing subroutines
are called

Figure 166 – Modification to *relap5.ff*.

The main objective of writing these lines is reading the file *data.txt* and storing its information in the variables “*mulval*” (vector of real numbers that correspond to the value of multipliers) and “*multxt*” (vector of character strings that correspond to the name of the multipliers).

Additionally, the information written in the output window while it is read in order to allow the analyst to check that everything is OK before beginning of the calculation.

As it can be observed, the maximum number of multipliers (e.g. dimension of vectors “*mulval*” and “*multxt*”) has been set to 14 in the example. This number could be changed as long as it remains greater or equal to the number of multipliers that the analyst intends to vary.

After this *relap5.ff* modification, the values and names of the multipliers are stored in the variables “*mulval*” and “*multxt*”, which belong to the block “*premium*”. A block is a set of variables that can be used in all the subroutines. Therefore, the stored values of “*mulval*” and “*multxt*” can be accessed from any subroutine, as long as we make reference to the block in the variable declaration.

In order to introduce the multipliers the variables of the common block have to be declared by inserting the following lines in their source code (at the beginning of the

file, after the long list of “*call” and just before local variables are supposed to be declared):

```
(...)
c
c ----- PREMIUM ----- (1/2)
common /premium/ mulval, multxt
real mulval(14)
character multxt(14)*30
c ----- PREMIUM -----
(...)
```

Figure 167 – Modification at the beginning of all affected *.ff.

The structure of adopted *data.txt* file is shown on Figure 168 (in reference calculations all the multipliers set to unity).

```
=1=Interphase-fr-bundle-fic
1.
=2=Interphase-drg-fic
1.
=3=Droplet-min-D-dcon(2)
1.
=4=Interphase-drg-final-fij
1.
=5=Interphase-HT-wet-hif,hig
1.
=6=Interphase-HT-dry-hif,hig
1.
=7=Interphase-HT-tot-hif,hig
1.
=8=FilmB-HTC-2fluid-hfb
1.
=9=FilmB-HTC-2gas-hv
1.
=10=TrB-HTC-2fluid-qtb
1.
=11=TrB-HTC-2gas-htbg
1.
=12=QF-threshold-0.1-(dis1)
1.
=13=QF-threshold-0.2-(dis2)
1.
=14=QF-threshold-(zqfmin)
1.
=15=N/A
1.
```

Figure 168 – Structure of externally read *data.txt*.

B.3. Reflood-relevant subroutines and parameters

B.3.1. Interphase friction

There are 2 main models adopted in RELAP5 for calculation of interphase friction: drag coefficient and drift-flux. In its turn, the drag coefficient model takes different forms depending on the flow regime. Nevertheless, 3 subroutines may be identified:

- **FIDISJ**: calculates the effective interphase drag coefficient for dispersed vapor flows. In the framework of RELAP5 calculations of FEBA facility, this subroutine calculates the bundle interface friction (if the corresponding flag is activated in hydraulic volumes of the model) based on EPRI drift-flux correlation. This subroutine is called by numerous subroutines which calculate interphase friction in different flow regimes.
- **FIDIS2**: computes the junction interphase drag term for bubbles and droplets. This subroutine is called by numerous subroutines which calculate interphase drag in different flow regimes.
- **PHANTJ**: computes the resulting interphase drag.

The following table contains the information on the FORTRAN variables in mentioned above subroutines to be modified in order to assess the sensitivity and/or uncertainty of physical models.

Table 43 – RELAP5 subroutine modifications for interphase friction.

Subroutine	Variable	Line number	Added/modified line
FIDISJ	fic	517	Added line: "fic = fic*mulval(1)"
FIDIS2	fic	123	Modified: "fic = mulval(2)*rhogj(i)*surfa*cd"
PHANTJ	fij	511	Modified: "fij(jj) = mulval(4)*fij(jj)*vlgfj".

B.3.2. Interphase heat transfer

3 subroutines were identified as those of interest for reflood:

- **DISPWETHIF**: computes wetted wall interphase heat transfer.
- **DISPDRYHIF**: computes interphase heat transfer for dry walls.
- **PHANTV**: computes resulting interphase heat transfer

All 3 subroutine have been modified in order to provide a possibility to perform sensitivities on separate models.

Table 44 – RELAP5 subroutine modifications for interphase heat transfer.

Subroutine	Variable	Line number	Added/modified line
DISPWETHIF	- hifc	- 132	- "hifc(ivx) = mulval(5)*hifc1(ivx)"
	- higc	- 133	- "higc(ivx) = mulval(5)*higc1(ivx)"
	- hgfc	- 134	- "hgfc(ivx) = mulval(5)*hgfc1(ivx)"
DISPDRYHIF	- hifc	- 107	- "hifc(ivx) = mulval(6)*hifsb1**xintrp*hifsp1**(1.0 - xintrp)"
	- higc	- 115	- "higc(ivx) = (((2.0 + ...)*mulval(6))
	- hgfc1	- 120	- "hgfc1(ivx) = (((2.0+ ...)*mulval(6))
PHANTV	- hif	655	Added:
	- hig		- "hif(iv) = mulval(7)*hif(iv)"
	- hgf		- "hig(iv) = mulval(7)*hig(iv)" - "hgf(iv) = mulval(7)*hgf(iv)"

B.3.3. Film/Transition boiling heat transfer

The subroutine which is in charge of calculating the heat transfer coefficient in post-DNB forced convection conditions is *PSTDNB*. Both Transition Boiling heat transfer and Film Boiling heat transfer are calculated by this subroutine. For either heat transfer mode 2 heat transfer coefficients are computed: wall-to-liquid and wall-to-gas.

Table 45 – RELAP5 subroutine modifications for film boiling heat transfer.

Subroutine	Variable	Line number	Added/modified line
PSTDNB	hfb (wall-to-liquid)	393	Added line: "hfb = mulval(8) * hfb" ¹
PSTDNB	hv (wall-to-gas)	393	Added line: "hv = mulval(9) * hv"

Table 46 – RELAP5 subroutine modifications for transition boiling heat transfer.

Subroutine	Variable	Line number	Added/modified line
PSTDNB	qtb	381	Added line: "qtb = mulval(10)* qtb" ¹
PSTDNB	htbg	381	Added line: "htbg = mulval(11)* htbg"

B.3.4. Minimum droplet diameter

There were 2 subroutines identified where the minimum droplet diameter is specified as a constant which is further used to calculate interphase area, which in its turn affects the calculation of both interphase friction and interphase heat transfer:

- **FIDISV**: computes interphase drag term for bubbles and droplets in volumes.
- **FIDIS2**: computes the junction interphase drag term for bubbles and droplets. This subroutine is called by numerous subroutines which calculate interphase drag in different flow regimes.

The same multiplier to minimum droplet diameter has been introduced to both subroutines, since it has been considered as a single uncertain parameter that can affect different correlations.

Table 47 – RELAP5 subroutine modifications for minimum droplet diameter.

Subroutine	Variable	Line number	Modified line
FIDISV	dcon(2)	68	"dcon(2) = 1.5e-03*mulval(3)"
FIDIS2	dcon(2)	56	"dcon(2) = 1.5e-03*mulval(3)"

B.5. References to APPENDIX B

- [B-1] United States Nuclear Regulatory Commission, 2003. *RELAP5/MOD3.3 Code Manual Volume IV: Models and Correlations*. NUREG/CR-5535/Rev P3.
- [B-2] United States Nuclear Regulatory Commission, 2003. *RELAP5/MOD3.3 Code Manual Volume VIII: Programmers Manual*. NUREG/CR-5535/Rev P3.

APPENDIX C. DESCRIPTION OF THE LOBI-MOD2 NODALIZATION FOR RELAP5-3D© CODE

C.1. Description of the nodalization

The Relap5-3D© input deck developed for simulating the LOBI/MOD2 test A1-83 behavior is a detailed nodalization carried out with a “sliced” approach⁵ based on the module subdivision reported in the LOBI Reference Data Set (RDS) [C-1]. The data used in order to build the nodalization are reported also in references [C-2], [C-3].

The nodalization has been developed following the nodalization techniques developed and adopted at GRNSPG [C-4]. Detailed description of the developed nodalization together with the rationale and the user choices are provided in the LOBI Engineering Handbook [C-5].

The RELAP-3D© nodalization sketch of the LOBI facility is shown in *Figure 169*. The correspondence between the zones of the facility and the nodes of the code model is presented in Table 48. In this table the facility is divided in zones, composed by various hydraulic elements. These components are reported in the table according to flow paths in nominal conditions. Number and type of the hydraulic nodes are indicated in the table itself.

The utilized code resources for the LOBI nodalization are summarized in [C-5]. In particular, the numbers of hydraulic components and of heat structure are reported.

Hereafter some significant aspects of the developed nodalization are summarized.

The RPV is modeled with 12 1-D components (*Figure 170*). The downcomer is modeled with two pipes 300 and 302 as parallel channels interconnected by a multiple cross-flow junctions in order to allow simulation of the mixing phenomena. The active part of the core is represented by a pipe component 330 consisting of 10 nodes. The length of the nodes is determined by a discrete power profile provided in specifications. The Upper Head is modeled as a pipe component 370 and its connection piping is represented by a series of pipe and valve components. All the bypass connections are present in the model:

- from DC top (component 305) to UP (component 345) representing 2 holes in the barrel;
- from DC top to IL hot leg (component 100) representing a gap in the sealing flange;
- from DC top to BL hot leg (component 200) representing a gap in the sealing flange;
- From DC top to UH representing the corresponding piping;
- From UH to UP top (component 350) representing the corresponding piping.

⁵ The slice approach scheme is suitable for a better code response, especially during natural circulation and/or during low flow rate regimes.

The Intact Loop is modeled using 10 hydraulic components of the 1XX series and the Broken Loop is modeled using the 14 hydraulic components of the 2XX series. The flow restrictions due to instrumental insertions are not modeled as a change in flow area but rather taken into account by appropriate form loss coefficients. The SG U-tubes bundles are modeled by a single pipe components each 120 (IL) and 220 (BL) with total flow area and average length, thus preserving the heat exchange surface area. The main coolant pumps of LOBI are modeled with a special RELAP5 pump components. The head and torque homologous curves as well as two-phase multipliers are specified in the component's corresponding cards. After the pump trip the pumps' velocity is provided by a time-velocity tables which are supplied from available experimental data. The Broken Loop locked rotor resistance simulator in LOBI MOD2 facility, which is representing via orifices in a two-way valve, is simulated in RELAP5-3D© model it by use of the motor valve 251 which is initially open and partially closes, leaving the flow area as provided in specifications, when the corresponding signal is generated. Full abrupt area change is set in order to take into account the additional pressure losses due to geometrical discontinuity.

Both PRZ surgeline configurations are present in the input deck: connection to IL and connection to BL. For the test A2-81 the connection to BL is disabled. The pressurizer vessel bottom part up to the outlet from the surge line is modeled with 2 branch components of equal length. The top part of the PRZ is modeled as a branch component. The rest of the PRZ is modeled with a pipe component.

The HPIS is simulated as time-dependent imposed mass flow rate by means of time-dependent junction component 855 with fluid properties specified by corresponding time-dependent volume component 850.

The pump seal water, injected into the IL and BL are modeled as a boundary condition by mean of time-dependent junction and time-dependent volume (components 180 and 181 for IL and components 280 and 281 for BL). The pump seal water drain is simulated as time-dependent imposed mass flow rate extracted from the primary side by means of time-dependent junction component 398 connected to the UP branch 345.

The break spool is modeled with motor valve 090 simulating the break and time-dependent volume 092 simulating the discharge line and containment back-pressure. The motor valve is connected to the outlet face of component 260 representing the location of the break spool in the broken loop cold leg.

During the first 50 s of the steady-state calculation the PRZ pressure and level are regulated by artificial controllers represented by time-dependent volume 491 (for pressure regulation) and time-dependent junction 495 (for PRZ level regulation). After the 50s of the steady-state these components are isolated/deactivated.

All the passive heat structures of the primary side are modeled by cylindrical and rectangular heat structure components according to the hardware geometry. The geometrical properties of the heat structure were set to preserve the heat transfer area and metal volume. The active part of the core heater rods is modeled by 10 separate heat structures each connected to the corresponding node of the pipe 330. The corresponding power fraction is assigned to each active heat structure in order

to reproduce the specified cosine power shape. The “unheated” part of the heater rods are modeled as well with the specified stray power input. The heat losses from the primary side are simulated by specifying a heat transfer coefficient at the right boundary of the heat structures representing the pressure boundary of the primary side.

The secondary side of the IL and BL steam generators is modeled by 7 hydraulic components each: components series 6XX for the IL SG and components series 7XX for the BL SG. Both annular and cylindrical parts of the riser participating in heat exchange with the primary side as well as the cylindrical and conical parts above the tube bundle are modeled as a single vertical channel (pipes 605/705). The lengths of the nodes of these pipes are chosen in order to comply with “sliced” nodalization of the SG U-tubes. The coarse separator of the SG is modeled by a special RELAP5-3D© separator component (separator 610/710). While the steam dome is considered as a free volume (branch 620/720) available for the steam and the presence of a fine separator is taken into account by subtracting a volume occupied by it.

The steam pressure is imposed in the SG during the steady-state and in the first part of the transient by connecting the steam dome to the time-dependent volume component via a motor valve: components 660 and 661 for the IL SG and components 760 and 761 for the BL SG. The steam pressure in IL SG during the Cooldown procedure is imposed by connecting the SG steam dome with time-dependent volume component where the time-dependent pressure curve is specified (components 680/780 and 681/781).

The main feedwater system is represented by an artificial controller modeled with time-dependent junction (686/786) and time-dependent volume (685/785) components. This model supplies the necessary mass flow rate to the SG downcomer in order to maintain the SG downcomer level during the steady-state and the initial part of the transient.

All the passive heat structures of the secondary side are modeled by cylindrical and rectangular heat structure components according to the hardware geometry. The geometrical properties of the heat structure were set to preserve the heat transfer area and metal volume. The heat losses from the secondary side are simulated by specifying a heat transfer coefficient at the right boundary of the heat structures representing the SG vessel.

The nodalization contains various control variables to calculate levels, masses, power and pressure drops in the different zone of the facility model.

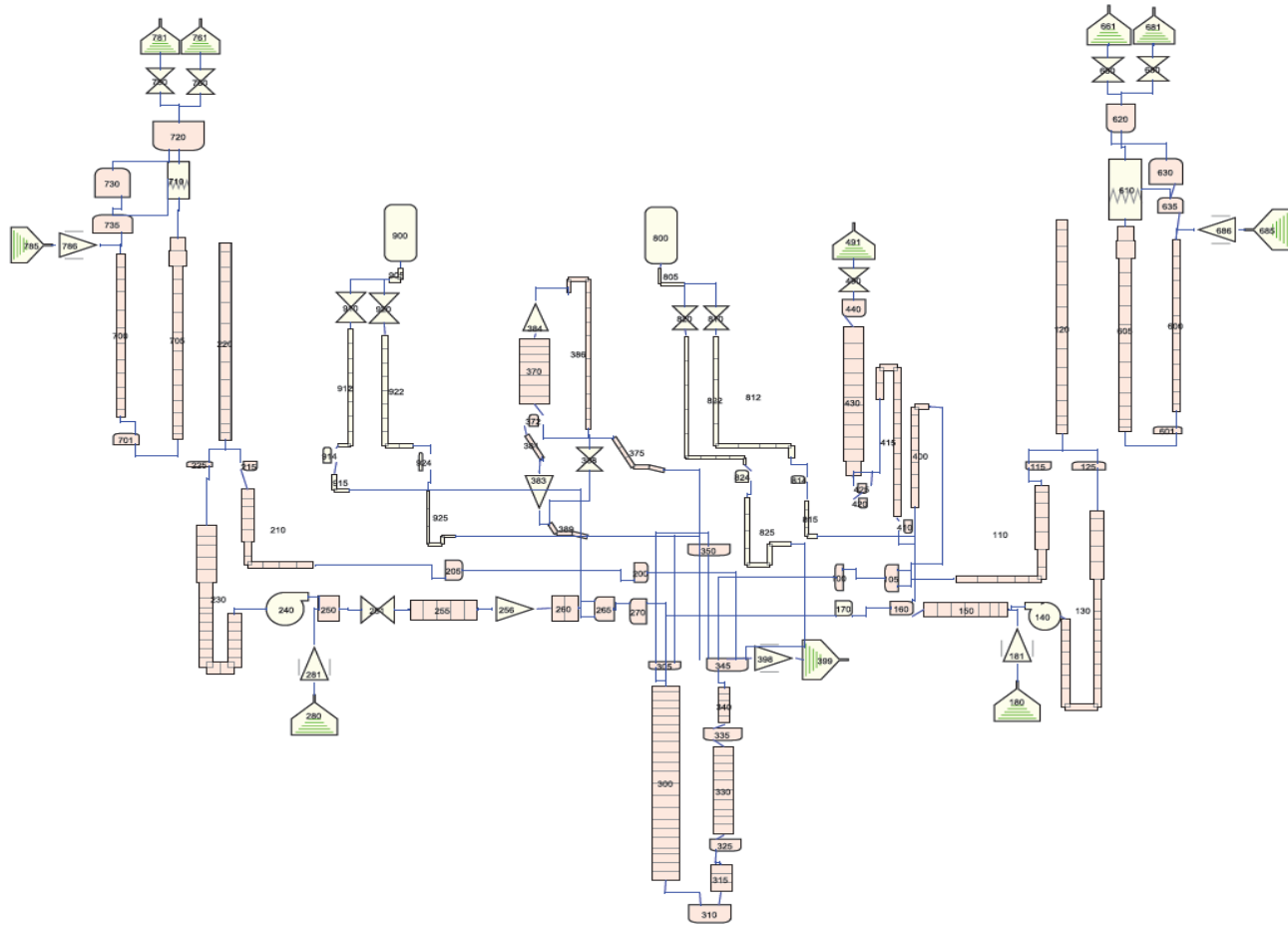


Figure 169 – RELAP5-3D© - LOBI/MOD2 nodalization, general scheme.

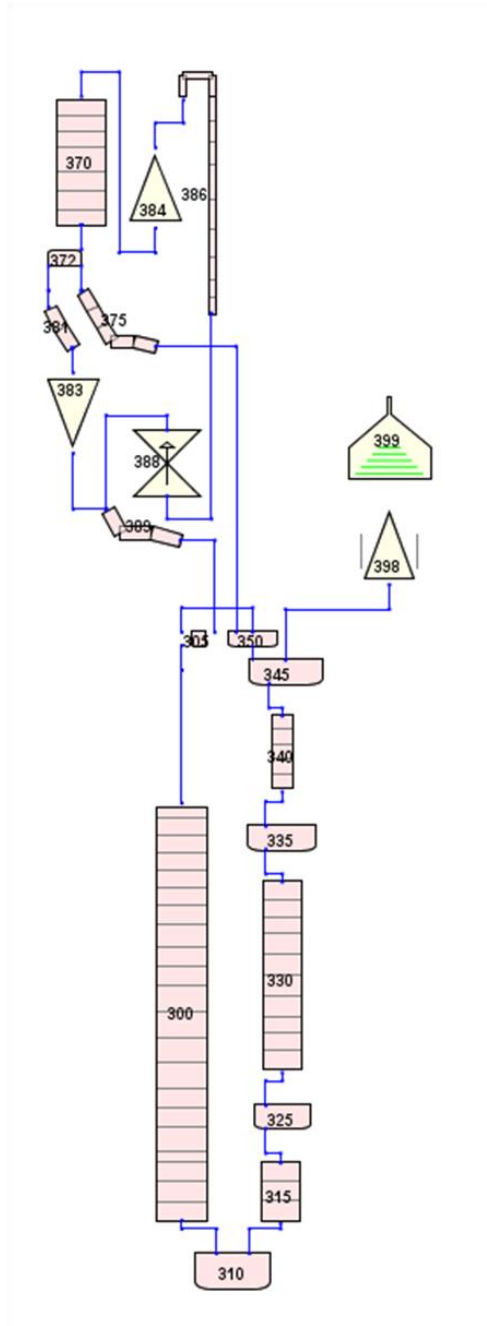


Figure 170 – RELAP5-3D© of LOBI/MOD2 reactor pressure vessel and upper head simulator.

Table 48 – Code nodes and hydraulic zones correspondence, RELAP5-3D®.

GENERAL ZONE	ZONE	NUMBER	TYPE
PRIMARY SIDE			
Intact Loop	IL HL	100	BRANCH
		105	BRANCH
		110	PIPE
	IL SG	115	BRANCH
		120	PIPE
		125	BRANCH
	IL LOOP SEAL	130	PIPE
	IL PUMP	140	PUMP
	IL CL	150	PIPE
		160	BRANCH
170		BRANCH	
Broken Loop	BL HL	200	BRANCH
		205	BRANCH
		210	PIPE
	BL SG	215	BRANCH
		220	PIPE
		225	BRANCH
	BL LOOP SEAL	230	PIPE
	BL PUMP	240	PUMP
	BL CL	250	SINGLVOL
		251	VALVE
		255	PIPE
		256	SINGLJUN
		260	PIPE
		265	BRANCH
270	BRANCH		
Vessel	DOWNCOMER	300	PIPE
		305	BRANCH
	LOWER PLENUM	310	BRANCH
		315	PIPE
	CORE	325	BRANCH
		330	PIPE
		335	BRANCH
	UP	340	PIPE
		345	BRANCH
		350	BRANCH
370		PIPE	
Upper Head	UH	372	BRANCH
		375	PIPE
		381	PIPE
		383	SINGLJUN
		384	SINGLJUN
		386	PIPE
		388	VALVE
		389	PIPE

(to be continued)

Table 48 – Code nodes and hydraulic zones correspondence, RELAP5-3D©.
(Continued).

GENERAL ZONE	ZONE	NUMBER	TYPE
PRZ	IL SURGE LINE	400	PIPE
	BL SURGE LINE	405	PIPE
	SURGE LINE	410	BRANCH
		415	PIPE
	PRZ VESSEL	420	BRANCH
		425	BRANCH
		430	PIPE
		440	BRANCH
SECONDARY SIDE			
IL SG	DOWNCOMER	600	PIPE
		601	BRANCH
	RISER	605	PIPE
	SEPARATOR and STEAM DOME	610	SEPARATR
		620	BRANCH
	IL SG ANNULUS	630	BRANCH
		635	BRANCH
BL SG	DOWNCOMER	700	PIPE
		701	BRANCH
	RISER	705	PIPE
	SEPARATOR and STEAM DOME	710	SEPARATR
		720	BRANCH
	BL SG ANNULUS	730	BRANCH
		735	BRANCH
IL Pump	Seal Water	180	TMDPVOL
		181	TMDPJUN
BL Pump	Seal Water	280	TMDPVOL
		281	TMDPJUN
Pump	Seal Water drainage	398	TMDPJUN
		399	TMDPVOL
Break Spool	Break	090	VALVE
	Tank	092	TMDPVOL
IL SG P Control	-	660	VALVE
	-	661	TMDPVOL
BL SG P Control	-	760	VALVE
	-	761	TMDPVOL
IL SG Cooldown	-	680	VALVE
		681	TMDPVOL
BL SG Cooldown	-	780	VALVE
	-	781	TMDPVOL
IL SG Main Feedwater	Feedwater tank	685	TMDPVOL
	Feedwater Main	686	TMDPJUN
BL SG Main Feedwater	Feedwater tank	785	TMDPVOL
	Feedwater Main	786	TMDPJUN

(to be continued)

Table 48 – Code nodes and hydraulic zones correspondence, RELAP5-3D©.
(Continued).

GENERAL ZONE	ZONE	NUMBER	TYPE
ECCS			
IL ACCUM	IL ACC TANK	800	ACCUM
	ACC LINE	805	PIPE
		810	VALVE
		812	PIPE
		814	BRANCH
		815	PIPE
		820	VALVE
		822	PIPE
		824	BRANCH
825	PIPE		
BL ACCUM	BL ACC TANK	900	ACCUM
	ACC LINE	905	PIPE
		910	VALVE
		912	PIPE
		914	BRANCH
		915	PIPE
		920	VALVE
		922	PIPE
		924	BRANCH
925	PIPE		

Table 49 – Adopted code resources for RELAP5-3D© LOBI/MOD2 nodalization.

Number of nodes	439
Number of junctions	465
Number of heat structures	421
Number of mesh points	5460
Number of core active structures	10*

* + 10 more active HS for heater rods below and above the core

C.2. Model qualification

A nodalization representing an actual system (ITF or plant) can be considered qualified when:

- it has a geometrical fidelity with the involved system;
- it reproduces the measured nominal steady state condition of the system;
- it shows a satisfactory behavior in time dependent conditions.

Taking into account these statements, a standard procedure to obtain a “qualified nodalization” has been defined (see [C-3], [C-6] and [C-7]). The qualification process consists of two main phases:

1) Steady state level: the nodalization is qualified against data available from nominal stationary conditions measured in the simulated system. To this aim:

a) Relevant geometrical parameters of the facility (e.g. volume, heat transfer area, elevations, pressure drops distribution etc.) are compared with the input data and the differences among them must be acceptably small. The adopted acceptability criteria are reported in the first part of Table 50.

b) The nominal steady state conditions are simulated with a code running (a hundred seconds time interval is considered acceptable to reach correct steady state values); ‘significant’ parameters are selected and compared with the measured results. A parameter is considered ‘significant’ when it is of major relevance in determining the plant behavior and can be reliably measured. The adopted acceptability criteria for this step are reported in the second part of Table 50.

2) Transient level: the nodalization is tested in time-dependent conditions reproducing the available experimental transients.

Three main calculation types can be distinguished in a meaningful code assessment process:

- a) at least 100s steady state;
- b) reference calculation results;
- c) results from sensitivities studies.

It may be noted that item a) may constitute a part of the nodalization qualification process, described in the previous chapter; however, the fulfillment of criteria reported in Table 50 is necessary each time a new experiment is considered an before starting transient calculations by using the previous qualified nodalization.

The reference calculation results, item b), must outcome from the qualified nodalization and satisfy qualitative and quantitative accuracy related criteria. The reference calculation is not the “best” calculation achievable by the code. In order to get the reference calculation, boundary and initial conditions of the considered experiment may be changed within their uncertainty ranges; if a user choice is introduced, its validity and acceptability must be checked by repeating the nodalization qualification process.

Sensitivities analyses, item c), must be carried out to demonstrate the robustness of the calculation, to characterize the reasons for possible discrepancies between measured and calculated trends that appear in the reference calculation, to optimize code results and user option choices, to improve knowledge of the code by the user.

The attention is focused hereafter towards the analysis of the reference calculation results, item b), considering that steady state calculation, item a), is part of the nodalization qualification process and sensitivities analysis, item c), can be designed following the analyses at the previous step. Typical results are provided in relation to the three steps.

The geometrical fidelity of the nodalization representing an actual system (ITF or plant) is demonstrated by providing the Volume vs. Elevation curve and comparing the pressure drops distribution with the model input data and results.

Figure 171 shows the comparison between the facility and the RELAP5-3D© model of the primary system volume against the elevation. All discrepancies are within the acceptance criteria #1 and #7 in Table 50.

The comparison of the relevant geometrical parameters of the part 1 of Table 50 is performed systematically in the Engineering Handbook [C-5]. All discrepancies are within the corresponding acceptance criteria.

A steady state calculation has been performed by running a 'null transient' case of 300 s, the last 250s of the null transient have been performed without the artificial control of the PRZ level and PRZ pressure, only the PRZ heater were used to control the primary side pressure. The following results have been achieved.

- 1) All time trends show a stable behavior, i.e. an inherent drift less than 1%/100 sec in the last 100 seconds of null transient;
- 2) The comparison between calculated and experimental pressure drop curves (*Figure 172* and *Figure 173*) fulfills the acceptance criteria #19 in Table 50;
- 3) The capability of the developed model to reproduce the measured nominal steady state conditions of the facility is verified through the comparison in Table 51.

As summary, the developed model is qualified at steady state level as it satisfies the geometrical fidelity with the involved system and reproduces the measured nominal steady state.

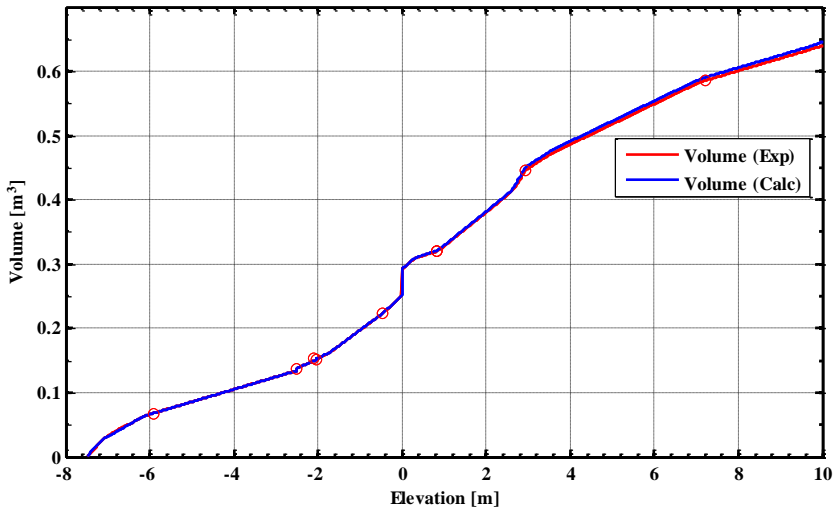


Figure 171 – PS volume vs. elevation.

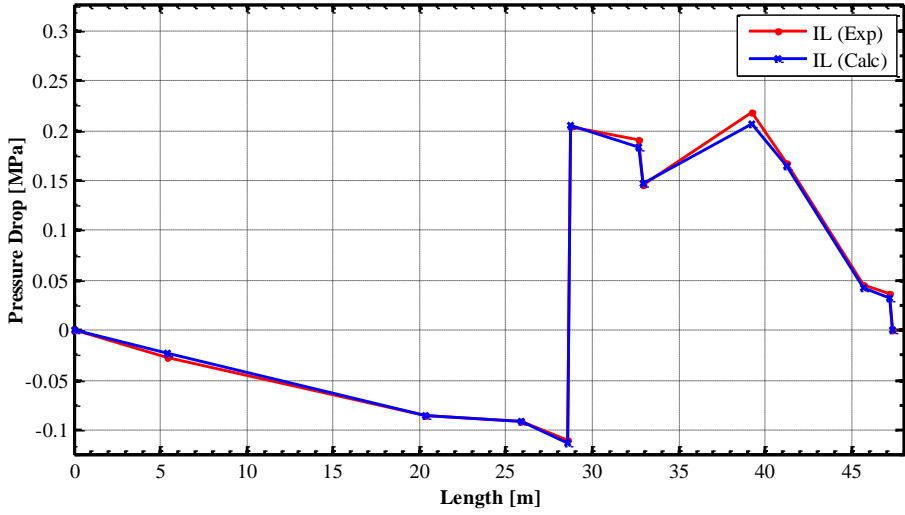


Figure 172 – Pressure drop Vs. length in IL.

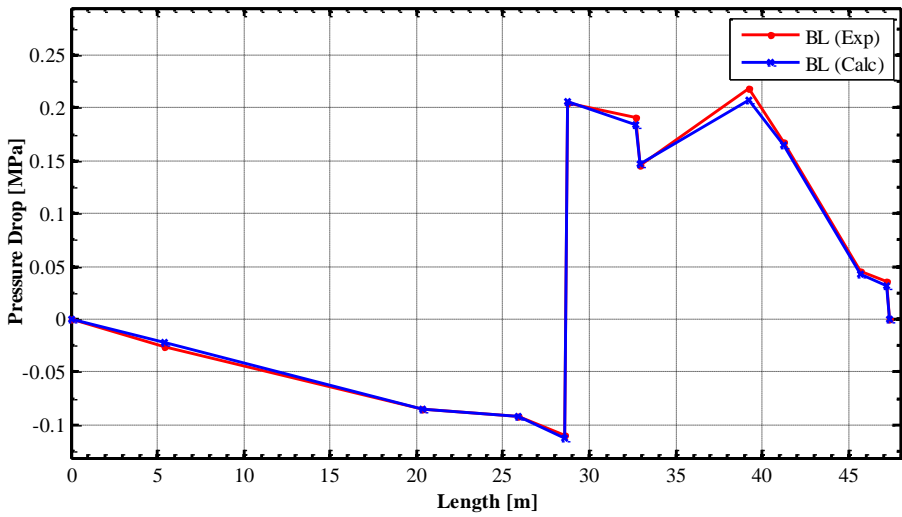


Figure 173 – Pressure drop Vs. length in BL.

Table 51 – Comparison between measured and calculated relevant initial and boundary conditions.

QUANTITY	UNIT	EXP	CALC R5	ERROR [%]	ACCEPTED ERROR
Core power	MW	5.20	5.20	0.0 %	2 %
Upper Plenum pressure	MPa	15.8	15.8	0.0 %	0.1 %
Pressurizer level	m	c. 5.2 ^{/1/}	5.4	-	0.05 m
IL mass flow rate	kg/s	20.8	20.75	0.0%	2 %
BL mass flow rate	kg/s	6.7	6.74	0.0%	2 %
IL MCP speed	rad/s	510.1	510.0	0.0%	1 %
BL MCP speed	rad/s	391.1	403.3	1.0% ^{/2/}	1 %
IL cold leg temperature	°C	295.4	296.2	0.0%	0.5 %
BL cold leg temperature	°C	296.2	295.5	0.0%	0.5 %
IL hot leg temperature	°C	327.9	328.0	0.0%	0.5 %
BL hot leg temperature	°C	327.8	327.6	0.0%	0.5 %
Accumulators temperature	°C	30.0	30.0	0.0%	0.5%
IL SG pressure	MPa	6.62	6.62	0.0%	0.1 %
BL SG pressure	MPa	6.62	6.62	0.0%	0.1 %
IL SG downcomer level	m	c. 8.29 ^{/1/}	8.31	0.0%	0.10 m
BL SG downcomer level	m	c. 8.11 ^{/1/}	8.03	0.0%	0.10 m
IL SG feedwater temperature	°C	210.3	210.3	0.0%	0.5 %
BL SG feedwater temperature	°C	207.4	207.4		0.5%
IL SG feedwater flow rate	kg/s	2.0	2.04	2% ^{/2/}	2 %
BL SG feedwater flow rate	kg/s	0.66	0.66	0.0%	2 %

/1/ The error band on the measured level is large but unknown, the value should be taken only as indicative.

/2/ Considering the experimental measurement error

C.3 References to APPENDIX C

- [C-1] Agreement Atucha-II - UNIPI N°3. "*Reference Data Set for LOBI-MOD2 facility*", REP124_U-NIII_DIT130_E1.3.6a_FR_Ch15Fin_Rev1, S. Giovannetti, O. Lisovyy, Pisa, May 2011.
- [C-2] Agreement Atucha-II - UNIPI N°3. "*Reference Data Set of LOBI/MOD2 test 10% Cold Leg LOCA*", REP129_U-NIII_DIT135_E.1.3.6h_FR_Ch15Fin_Rev2", S. Giovannetti, F. Fiori, Pisa, 2011.
- [C-3] Bonucelli M., D'Auria F., Debrecin N., Galassi G. M., "*A methodology for the Qualification of Thermalhydraulic Code Nodalization*", Proceedings to NURETH-6 Conference, Grenoble, France, 1993.
- [C-4] Agreement Atucha-II - UNIPI N°3. "*Qualification of the Nodalization Strategies*", A. Kovtonyuk, M. Cherubini, W. Giannotti, A. Petruzzi, Pisa, 2013.
- [C-5] Agreement Atucha-II - UNIPI N°3. "*Engineering Handbook of RELAP5-3D© LOBI/MOD2 Test Facility Nodalization*", REP138_U-NIII_DIT140_E1.3.8b_FR_Ch15Fin_Rev1, Fiori F., Lisovyy O., Kovtonyuk A., Pisa, July 2011.
- [C-6]. Petruzzi A., D'Auria F., Giannotti W., "*Description of The Procedure to Qualify the Nodalization and To analyze the Code Results*" DIMNP NT 557 (05) Rev.0, Pisa, 2005.
- [C-7]. Petruzzi, A., D'Auria, F., "*Accuracy Quantification: Description of the Fast Fourier Transform Based Method (FFTBM)*", DIMNP NT 556(05) Rev. 0, Pisa, 2005.

APPENDIX D. EXAMPLE OF REFERENCE DATA SET FOR LOBI FACILITY

In this Appendix a few examples from Reference Data Set for LOBI-MOD2 facility and Reference Data Set for test A1-83 are provided. To provide the idea of the typical scope of RDS it may be noted that the original RDS for LOBI-MOD2 facility is a 280 pages document, while RDS for A1-83 test is a 52 pages document.

D.1. Reference Data Set for Facility

As a first step, the geometrical layout of the facility has been analyzed and subdivided into modules, *Figure 174*. These module are based on common geometrical properties and hardware which they represent. It should be pointed out that the RDS modules are independent of the code nodalization that may be further set up for simulation.

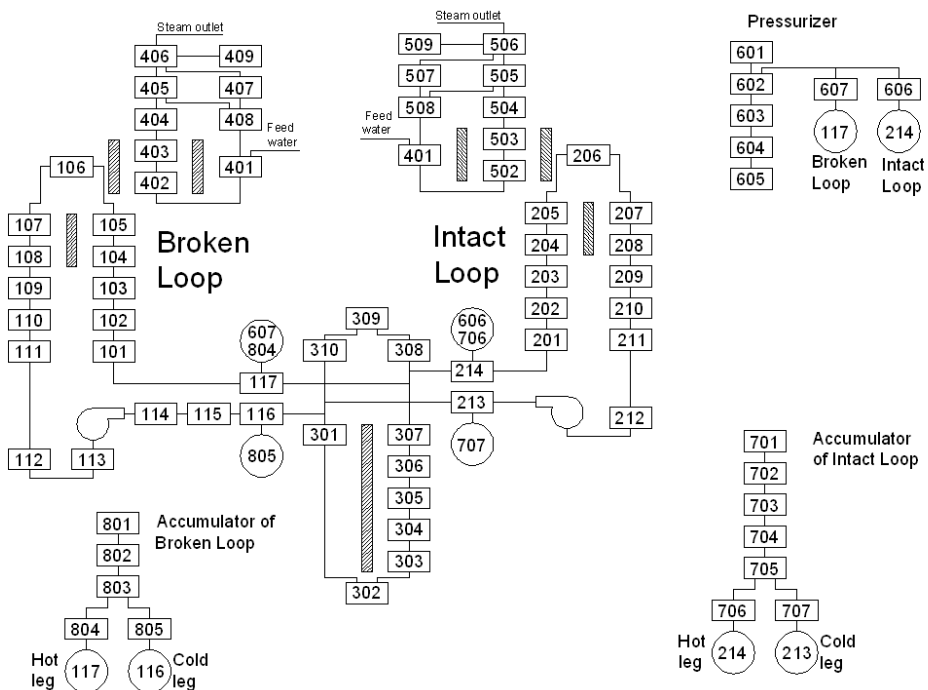


Figure 174– Subdivision of LOBI facility into modules.

The volume versus elevation curve of the primary side of LOBI-MOD2 facility is shown in *Figure 175*.

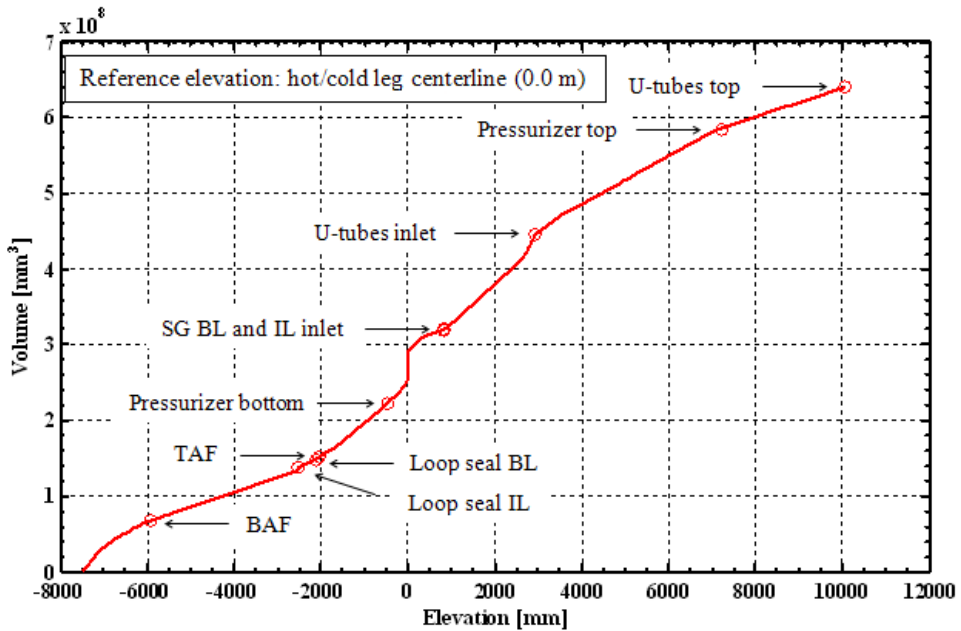


Figure 175 – Primary Side Volume versus Height Curve.

Below, the examples of several **modules** (primary side of a steam generator and pressurizer surge line) are provided.

The steam generator is subdivided into modules from n° 101 to n° 111, as shown in *Figure 176*, whereas all the geometrical information of the modules is available in *Table 52*.

Geometrical data of the pressurizer surge line piping are shown in *Figure 177*. The piping is divided into modules 606 and 607, for the intact and broken loop, respectively. Geometry summary information is available in *Table 53*.

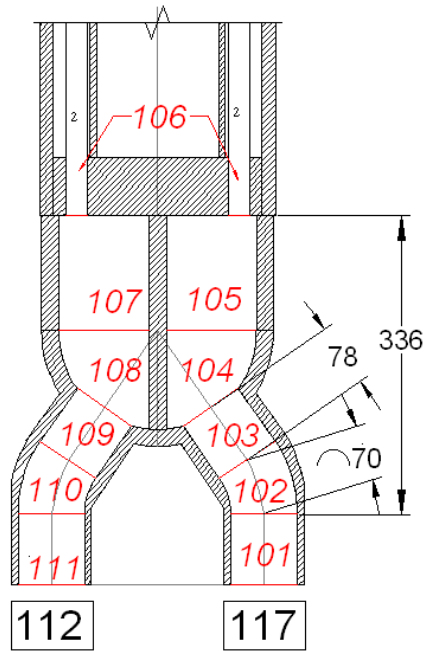


Figure 176 – Modules of Steam Generator of Primary Side Broken Loop.

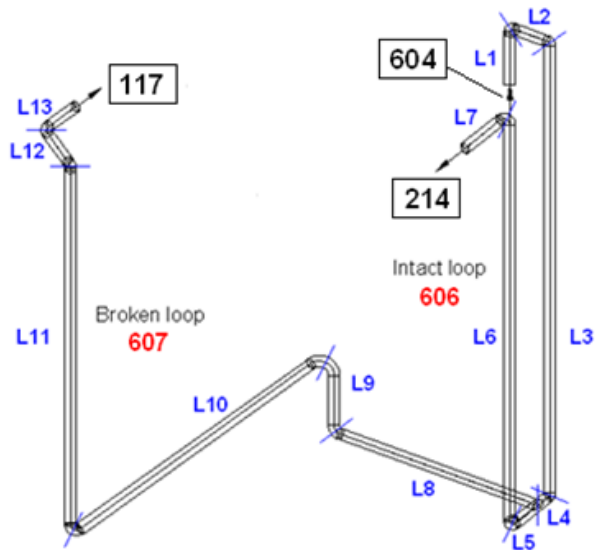


Figure 177 – Modules of Surge Line Piping.

Table 52 – Steam Generator Geometrical Data:
Primary Side Broken Loop. Module 101.

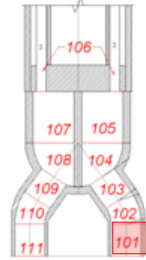
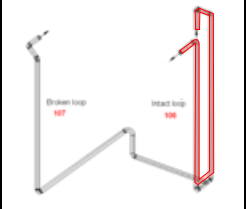
Primary Side Broken Loop Steam Generator				
Module number	101			Vertical cylinder
Description	Inlet pipe of SG BL			
Parameters	Evaluation	Value		Remarks
Outside diameter	$D_o = 82.5 \text{ mm}$	$8.25 \cdot 10^{-2}$	m	
Wall thickness	$t = 7.1 \text{ mm}$	$7.1 \cdot 10^{-3}$	m	
Inside diameter	$D_i = 82.5 - 2 \cdot (7.1) = 68.3 \text{ mm}$	$6.83 \cdot 10^{-2}$	m	
Length of piping	$L = 2081 - 303 = 1752 \text{ mm}$	1.752	m	
Outside radius	$R_o = 82.5/2 = 41.25$	$4.12 \cdot 10^{-2}$	m	
Inside radius	$R_i = 68.3/2 = 34.15 \text{ mm}$	$3.415 \cdot 10^{-2}$	m	
Elevation change	$\Delta H = 1752 \text{ mm}$	1.752	m	
Flow area	$A_f = \pi \cdot R_i^2 = \pi \cdot 34.15^2 = 3664 \text{ mm}^2$	$3.664 \cdot 10^{-3}$	m^2	
Inside surface area	$S_i = 2\pi \cdot R_i \cdot L$ $= 2\pi \cdot 34.15 \cdot 1752 = 375928 \text{ mm}^2$	$3.75928 \cdot 10^{-1}$	m^2	
Outside surface area	$S_o = 2\pi \cdot R_o \cdot L$ $= 2\pi \cdot 41.25 \cdot 1752 = 454086 \text{ mm}^2$	$4.54086 \cdot 10^{-1}$	m^2	
Metal volume	$V_m = \pi \cdot L \cdot (R_o^2 - R_i^2)$ $= \pi \cdot 1752 \cdot (41.25^2 - 34.15^2)$ $= 2946549 \text{ mm}^3$	$2.946549 \cdot 10^{-3}$	m^3	
Hydraulic volume	$V_h = \pi \cdot R_i^2 \cdot L = \pi \cdot 34.15^2 \cdot 1752$ $= 6418971 \text{ mm}^3$	$6.418971 \cdot 10^{-3}$	m^3	
Pressure coefficient loss	Expansion $k_{\text{forw}} = 0.183$ $k_{\text{rev}} = 0.03$			

Table 53 – Pressurizer Surge Line Geometrical Data. Module 606.

Pressurizer Surge Line Piping				
Module number	606			
Description	Intact Loop Piping			
Parameters	Evaluation	Value		Remarks
Inside diameter	$D_i = 13.2 \text{ mm}$	$1.32 \cdot 10^{-2}$	m	
Wall thickness	$t = 2 \text{ mm}$	$2 \cdot 10^{-3}$	m	
Outside diameter	$D_o = D_i + 2 \cdot t = 17.2 \text{ mm}$	$1.72 \cdot 10^{-2}$	m	
Inside radius	$R_i = 13.2/2 = 6.6 \text{ mm}$	$6.6 \cdot 10^{-3}$	m	
Outside radius	$R_o = 17.2/2 = 8.6 \text{ mm}$	$8.6 \cdot 10^{-3}$	m	
Length	$L_1 = 630 \text{ mm}$ $L_2 = 200 \text{ mm}$ $L_3 = 3400 \text{ mm}$ $L_4 = 105 \text{ mm}$ $L_5 = 105 \text{ mm}$ $L_6 = 2500 \text{ mm}$ $L_7 = 200 \text{ mm}$ $L = \sum_i L_i = 7140 \text{ mm}$	7.14	m	
Elevation change	$\Delta H = 270 \text{ mm}$	$2.7 \cdot 10^{-1}$	m	
Flow area	$A_f = \pi \cdot R_i^2 = \pi \cdot 6.6^2 = 137 \text{ mm}^2$	$1.37 \cdot 10^{-4}$	m^2	
Inside surface area	$S_i = 2\pi \cdot R_i \cdot L = 2\pi \cdot 6.6 \cdot 7140 \text{ mm}^2 = 296089 \text{ mm}^2$	$2.96089 \cdot 10^{-1}$	m^2	
Outside surface area	$S_o = 2\pi \cdot R_o \cdot L = 2\pi \cdot 8.6 \cdot 7140 \text{ mm}^2 = 385813 \text{ mm}^2$	$3.85813 \cdot 10^{-1}$	m^2	
Metal volume	$V_m = \pi \cdot (R_o^2 - R_i^2) \cdot L = \pi \cdot (8.6^2 - 6.6^2) \cdot 7140 = 681901 \text{ mm}^3$	$6.81901 \cdot 10^{-4}$	m^3	
Hydraulic volume	$V_h = \pi \cdot R_i^2 \cdot L = \pi \cdot 6.6^2 \cdot 7140 = 977093 \text{ mm}^3$	$9.77093 \cdot 10^{-4}$	m^3	
Pressure loss coefficient	Bend $k_{forw} = k_{rev} = 0.098$ T-junction 606 $k_{forw} = k_{rev} = 0.1$ Outlet 606 → 214 $k_{forw} = 1.27 (0.24, 5.93, 11.44)$ $k_{rev} = 1.14 (0.74, 7.04)$			

Below the examples of documentation of **facility instrumentation system** is provided (for the reactor pressure vessel).

Each experimental measurement in the LOBI-system is identified by a code formed by eight alphanumerical symbols. The code describes the type of measurement and the measurement point location in the system. It has the following scopes:

- Identification of measurement in the system
- Data identifier for data storage and processing
- Identifier in plots or graphical presentation of experimental data and results.

Measurement location in reactor pressure vessel model

The absolute pressure is taken in the upper plenum. Differential pressure measurements can be provided over all the main sections and subsections along the complete flow path of the pressure vessel, *Figure 178*. A second density measurement indicates void measurement of the lower plenum. Fluid temperatures are measured at all representative locations and wall temperatures in the downcomer region. The downcomer fluid temperature measurements are provided at different circumferential locations for each level, to detect possible local temperature differences. Mass flow information is provided by flow and density measurements in the core inlet box.

Liquid inventories can be obtained from the differential pressure measurements when flow velocities are small.

Measurement location in heater rod bundle

Each heater rod in the bundle is supplied with three thermocouples in the tube wall (except two rods, on which the heater voltage drop is measured). The location of this instrumentation within the bundle is shown in *Figure 179*.

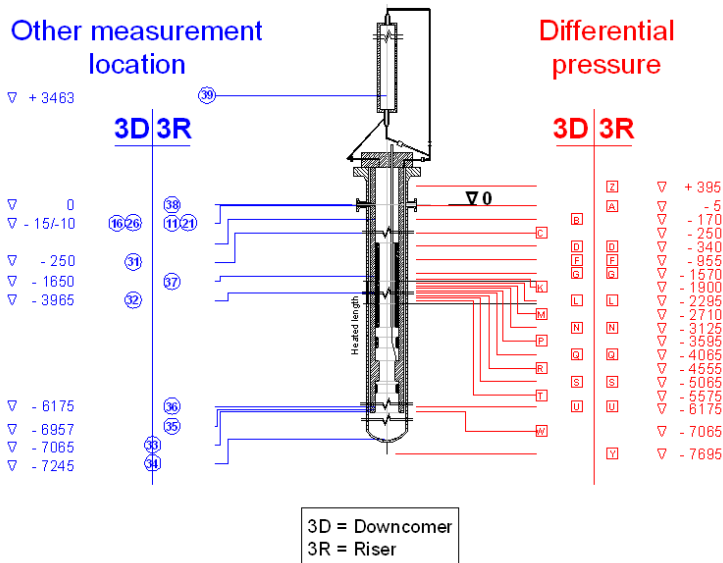


Figure 178 – Measurement Insert Location in Reactor Pressure Vessel.

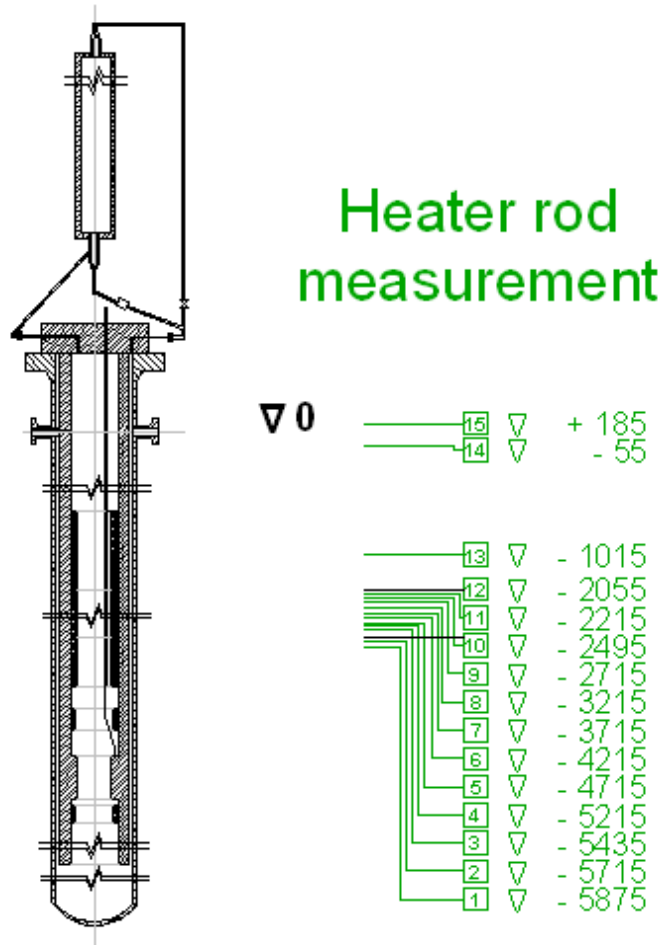


Figure 179 – Heater Rod Measurement Insert Location in Reactor Pressure Vessel.

Pressure Losses Evaluation

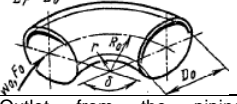
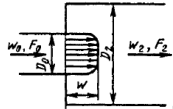
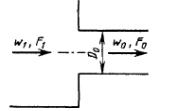
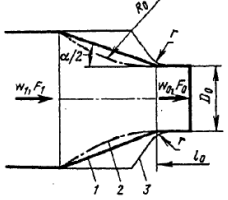
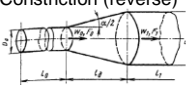
The losses due to entries and exits, fittings and valves, induced by curvature or recirculation are traditionally referred to as “minor losses” and they represent an additional energy dissipation in the flow.

Flow resistance coefficient, k_{loc} , is expressed in terms of the upstream or downstream velocity of the component. Loss term can be added to upstream or downstream velocity with the same net effect. “Base area”, F_0 , for all flow resistances shown in this section is given based on the smallest cross sectional area of the component hence the largest velocity.

For the evaluation of the k-loss coefficient due to the local pressure losses, the following parameters and formulas were used:

- G – Mass flow (kg/s);
- T – Temperature ($^{\circ}\text{C}$);
- ν – Cinematic viscosity (m^2/s);
- ρ – Density (kg/m^3);
- w_i – Flow velocity (m/s);
- Re – Reynolds number;
- A_i – Cross sectional area (mm^2);
- P_i – Perimeter of cross sectional area;
- D_i – Hydraulic diameter (mm).

Table 54 – Example of pressure losses evaluation.

N°	Element of system	Parameters	G _i kg/s	T °C	v _i ·10 ⁻⁷ m ² /s	ρ kg/m ³	w _i m/s	Re·10 ⁶	Evaluation	k _{loc}	Remarks
102	Bend 	$\frac{R_0}{D_0} = \frac{242}{68.4} = 3.538$ $\delta=35^\circ$	7	326	1.26	654	2.9	1.58	$k_{loc} = A_1 \cdot B_1 \cdot C_1$ $= 0.5162 \cdot 0.1116 \cdot 1$	0.058	Ref. D3 Sec. 6-1 (p. 260, 277)
103- 104	Outlet from the piping (forward) 	F ₂ considered as an infinite plane	7	326	1.26	654	6.41	2.34	$k_{loc} = \left(1 - \frac{F_0}{F_2}\right)^2$	1	Ref. D3 Sec. 4-1 (p. 158), Sec. 4-9 (p. 165)
	Outlet from the piping (reverse): 	F ₁ considered as an infinite plane	7	326	1.26	654	6.41	2.34	$k_{loc} = 0.5 \cdot \left(1 - \frac{F_0}{F_1}\right)^{\frac{3}{4}}$	0.5	Ref. D3 Sec. 4-9 (p. 151, 165)
111- 112	Constriction (forward) 	$\frac{F_0}{F_1} = \frac{1669}{3664} = 0.456$ $\alpha=30^\circ$	7	294	1.26	740	3.48	1.60	$k_{loc} = (-0.0125 \cdot n_0^4 + 0.0224 \cdot n_0^3 - 0.00723 \cdot n_0^2 + 0.00444 \cdot n_0 - 0.00745) \cdot (\alpha_T^3 - 2 \cdot \pi \cdot \alpha_T^2 - 10 \cdot \alpha_T)$ $\alpha_T = 0.01745\alpha$ $n_0 = \frac{F_0}{F_1}$	0.030	Ref. D3 Sec. 5-23 (p. 249)
	Constriction (reverse) 	$\frac{F_0}{F_2} = \frac{1669}{3664} = 0.456$ $\alpha=30^\circ$	7	294	1.26	740	3.48	1.60	$k_{loc} = 3.2 \cdot k_d \cdot \text{tg}^{1.25}\left(\frac{\alpha}{2}\right) \cdot \left(1 - \frac{F_0}{F_1}\right)^2$ $k_d=3.2$	0.183	Ref. D3 Sec. 5-1 (p. 192) Sec. 5-2 (p. 213)

Physical properties of materials

As an example the summary table on the materials of passive (non-heated) structures is provided below.

Table 55 – Material Properties of Passive Structures.

Heat Structure	Material	Table N°	Ref.
Reactor Pressure Vessel			
Pressure vessel	INCONEL 625	Tab. 5.2	Ref.[D4], p.18
All flanges	INCONEL 718	Tab. 5.3	Ref.[D4], p.18
Ceramic fillers	Al2O3 (99.5%)	Tab. 5.7	Ref.[D4], p.18
Heater rods	1.4948, Ni 201	Tab. 5.4	Ref.[D4], p.19
Core support barrel	1.4571	Tab. 5.6	Ref.[D4] p.19
“Upper head” tank	1.4571	Tab. 5.6	Ref.[D4], p.19
Primary Circuit			
Pipes of intact and broken loops	1.4571	Tab. 5.6	Ref.[D4], p.19
Pressurizer	1.4571	Tab. 5.6	Ref.[D4], p.19
ECC accumulators	1.4571	Tab. 5.6	Ref.[D4], p.19
Steam Generator			
SG vessel, bottom, flanges	1.4571	Tab. 5.6	Ref.[D4], p.19
Shroud, central tube	1.4571	Tab. 5.6	Ref.[D4], p.19
U-tubes	INCOLOY 800	Tab. 5.8	Ref. [D4]

Heat losses

The results of the two heat losses tests are shown in *Figure 180*. Data are valid for stationary operation: heat losses during transient may differ. Moreover uncertainties could be caused by changes in the reference temperatures, pump seal flow or fluid condition in the loop.

The losses of the individual loop components, determined as a combination of measurements and model calculation, are listed in *Table 56*. Measurements are made for heat losses caused by pump seal water and by instrument cooling water. Calculations are made for heat losses caused by heat conduction through the loop insulation, uninsulated components and metal fins.

The distribution of the local heat losses for the HL1 is:

- 60% pump seal water
- 20% instrument cooling water
- 13% uninsulated components and fins

- 7% loop insulation

This distribution shows that, for example, during a 100 k/h cooldown, the stored heat in the metal pipe walls is not removed by conduction via the loop insulation but it heats the liquid and is removed mainly by other heat sinks.

The sum of the total heat losses is 84.06 kW for test HL1 and 46.67 for test HL2, respectively.

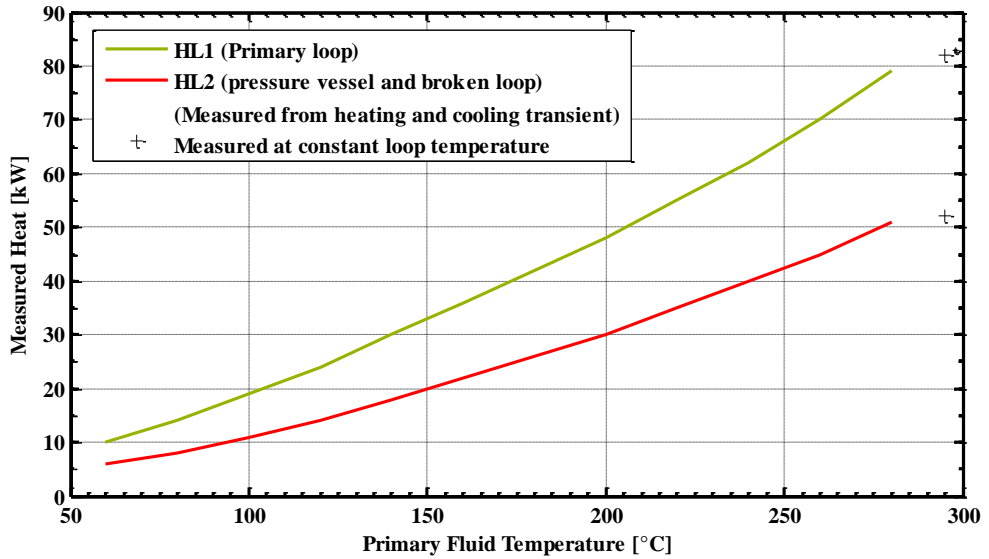


Figure 180 – Heat Losses of LOBI-MOD2 primary Loop at Steady State.

Table 56 – Example of data of facility individual heat losses.

Component	Heat losses, kW			
	Intact loop	Broken loop		Pressure vessel
Pump seal water	28.2	16.5 (HL1)	18.1 (HL2)	-
Seal water return	2.5	2.5		-
Cooling water				
Upper power connection plate	-	-	-	4.54
Pump cooling water	0.91	0.78	-	-
Pressure cooling adapters	2.8	1.4	-	3.76
Densitometer cooling water + conduction loss ¹⁾	1.0	2.0	-	-
Conduction				
Loop insulation	1.78	1.20	-	2.78
Upper flange	-	-	-	0.88
Lower flange	-	-	-	1.76
Lower power connector incl. uninsulated parts	-	-	-	2.85
Vessel support	-	-	-	0.96
Lower vessel support	-	-	-	0.63
Pump bowl (not insulated)	1.07	1.00	-	-
Bunker entrance/exit (6)	-	1.08	-	-
Support in lower bunker	-	0.19	-	-
Pipe support below entrance of steam generator	0.13	0.13	-	-
Break insert	-	0.13	-	-
TOTAL, kW	38.99	26.91 (HL1)	28.51 (HL2)	18.16

1) should be adjusted to conditions of test facility for each test

D.2. Reference Data Set for Experimental Test

The selected examples from RDS for test A1-83 are provided.

Facility configuration

The facility configuration for the execution of this test is summarized in *Table 57*. Certain components and controls outlined in the table, although not reactor typical, were nevertheless required for either operational reasons or simulation requirements.

Table 57 – Configuration of the Facility in test A1-83.

Parameters	Description
Break	Position: CL break between MCP and vessel inlet Size: 0.1A (break orifice 9.5 mm \varnothing), <i>Figure 181</i> and <i>Figure 182</i> . Type: communicative, side oriented
Upper Head	Connected to upper plenum and upper downcomer
Pressurizer	Connected to IL HL
SCRAM	132 bar + delay 0.5 s The primary system low pressure trip signals refers to the upper plenum pressure
High Pressure Injection System	Injection position: intact loop hot leg Injection rate: 2 of 4 pumps Actuation: 117 bar + delay 35 s
Accumulator Injection System:	Injection position: <ul style="list-style-type: none"> • intact loop: hot and cold leg • broken loop: hot leg Injection rate: normal Actuation: 26 bar (gas pressure)
Main Coolant Pump	Start of coastdown: 110 bar Seal water drainage: continuous draining from upper plenum up to initiation of rupture; thereafter the draining system is isolated Locked rotor resistance simulator: <ul style="list-style-type: none"> • intact loop: not used • broken loop: inserted 4 s after pump coastdown to zero speed
Auxiliary feedwater	Not used
Secondary Side	Feedwater and main steam line isolation: 132 bar Cooldown actuation: 132 bar Cooldown rate: 100 K/h
Containment	Connected to the atmosphere

Break Assembly

The break assembly, *Figure 181* and *Figure 182*, consisted of a T-shaped spool piece inserted within the cold leg pipework that provide a communicative break configuration. It included a side oriented break orifice, a quick opening on/off valve for initiation of the rupture and a measurement insert for density, velocity, pressure and temperature of the outflow.

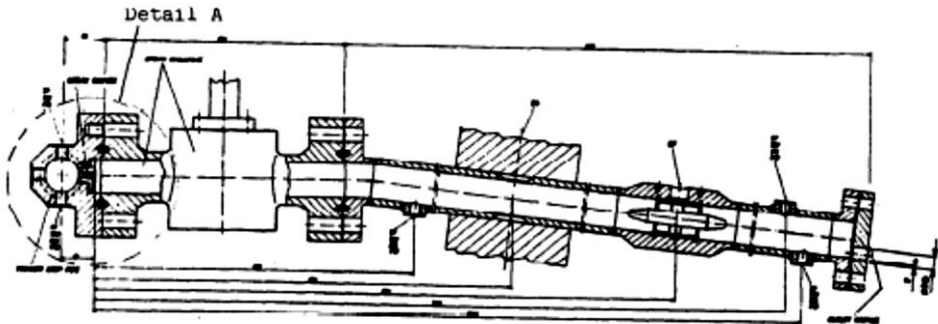


Figure 181 – Break Insert with Discharge Line, [D-2].

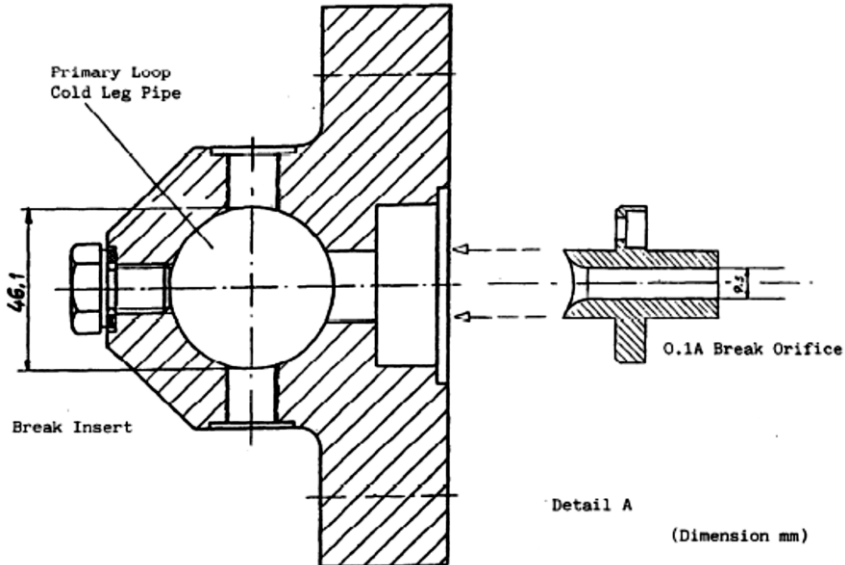


Figure 182 – Break Assembly: Configuration for Small Break, [D-2].

Simulation of the Pump Locked Rotor Resistance

The locked-rotor hydraulic resistance of the LOBI main coolant pumps is too low compared to the ideal scaled reference reactor resistance; also, since the two pumps are identical there exists the potential for asymmetry of flow distribution in the two loops during the period of natural circulation following pump coast-down. To ensure a more symmetrical mass flow behaviour in the two loops in such conditions, pump locked-rotor resistance simulators can be installed at the pump discharge, each consisting of a valve which can be properly orificed to provide the required additional resistance. In the BL the perforated plate type orifices provide a flow area reduction up to 18% of the normal full flow area. This orifice is normally inserted 4 s after pump coastdown to zero speed. For pump operational reasons, full flow area must exist in the BL pipe-work during steady-state phase of the experiment.

Test description

Initial Conditions

The system was brought with the normal run up procedure to the stable stationary operation conditions, the loop control and monitoring system was enabled at -300 s before initiation of rupture. At -240 s the shut-off valve in the pipework connecting the top of the upper head was signalled to close (closure time 8 s). At -3 s the pump seal water drain valve in the upper plenum was sequenced to close (closure time 3 s). Thereafter the sequence of controlled events was dictated by ensuing primary system depressurization.

The stationary operation conditions prior the beginning of the transient are given in *Table 58*. *Figure 183* shows the pressure drop curve against the circuit length in the intact loop.

Boundary Conditions

An appropriate power-time curve was applied to the electrically heated rod bundle to simulate the heat release from nuclear fuel rods during a similar transient, *Figure 184*. The heating power remained constant at the initial value (100 %) until trip at 3s on low primary system pressure; thereafter, the power was controlled to simulate decay power and release of stored energy.

The speed of both main coolant pumps remained constant at the initial value (100%) until trip at 8 s on low primary system pressure; thereafter the pumps coasted down reaching zero speed within 102 s after blowdown initiation. The rotors of the pumps were then locked at zero speed (mechanical brakes on) and at 107 s the locked rotor resistance simulator was inserted in the broken loop.

The normal feedwater flow to both SGs remained at the initial value until 4 s when low primary system pressure (132 bar in the UP) tripped the closure of the shut-off valves in the feedwater lines and in the main steam line at the inlet of the condenser. The secondary sides of the intact and broken loop SGs remained however connected during the whole test. According to the reference plant mitigation procedures, the secondary side cooldown at a rate of 100 K/h was initiated at 2 s upon reception of the low primary system pressure trip signal. Cooldown was

automatically controlled and was achieved via steam venting from the SG relief valves.

ECC water, from the high pressure injection system, was directed into the intact loop hot leg only. The mass flow was programmed to match the expected capacity of 2 out of 4 HPIS trains. Injection started at 41 s into transient, at this time the primary cooling system pressure was about 83 bar. The actual HPIS flow is shown in *Figure 185* as function of time.

Accumulator injection became active at 316 s into transient. Injection from the intact loop accumulator was directed into both cold leg and hot leg; whereas, injection from the broken loop accumulator was directed into hot leg only.

Thermal Hydraulic System Behavior

This section presents an analysis of the system thermal hydraulic behaviour. In particular, major phenomena affecting the response of each system component are analysed by means of relevant thermal hydraulic quantities.

Transition from subcooled to saturated critical flow at the break orifice occurred at about 15.8 s into the transient; at this time the fluid in the primary system cold legs saturated. The primary system depressurization rate diminished as the outflow from the break orifice decrease. At 21 s the pressurizer surge line uncovered and by 31 s the lower plenum and hence the entire primary system saturated. Injection of ECC water from the HPIS at 41 s had no discernible influence on primary system pressure response which continued to depressurize at a fairly constant rate up to the uncover of the break orifice which occurred at about 120 s. Following the actuation at 316 s of ECC water injection from the accumulator injection system which was tripped by a primary system pressure of 26 bar, the depressurization rate decreased as the outflow from the break was offset by the inflow from the accumulators.

The primary and secondary system pressure responses are given in *Figure 186*. At 105 s the primary system pressure fell below the secondary system pressure, *Figure 186*; however inverse heat transfer was negligible as the primary side of the U-tube voided rather earlier into the transient.

After initiation of blowdown, the primary cooling system fluid inventory rapidly depleted due to the initial subcooled outflow from the break. Following the establishment of saturated critical flow at the break orifice (at 15.8 s), the outflow from the primary system was considerably reduced. Initiation of HPIS-ECC water injection had no relevant influence on primary system mass content which continued to decrease throughout the initial transient. Mass depletion for the primary system was however arrested by initiation at 316 s of ECC water injection from the accumulator injection system. Thereafter, the primary system fluid inventory recovered as the inflow from the accumulator offset the outflow from the break. The transient behaviour of the primary inventory is depicted in *Figure 187*. It is worth noting that collapsed liquid level is indicative only for the gravity dominated period of the transient. The formation of a liquid seal in both the IL and the BL pump suction U-tubes caused an initial depression of water level in the vessel, *Figure 188*.

The initial depression of water level in the vessel caused by loop seal formation in both primary loops was sufficient to uncover the upper elevation of the rod bundle "heated length". Dry out was first detected in the uppermost instrumented level of the middle high powered section of the rod bundle, (*Figure 189*). Within 125 s into the transient nucleate boiling conditions were re-established over the entire heated length of the core. The initial rewet was clearly coupled to an insurge into the core due to loop seal clear-out. By 304 s, however, dry out conditions were reinstated in the uppermost elevations of the core as boiloff increased the local void content. Nucleate boiling conditions were quickly re-attained following actuation of ECC water injection from the accumulator injection system, which was configured in the combined injection mode.

The core thermal response within the vessel is depicted in *Figure 189*, which shows the mean temperature of the heater rod at different axial elevation.

Table 58 – Test Relevant Initial Conditions.

Parameters	Location	Value
Primary System:		
Mass Flow	Intact loop Broken loop	20.8 kg/s 6.7 kg/s
Pressure	Upper plenum	15.8 MPa
Fluid Temperature	Vessel outlet • Intact loop • Broken loop Vessel inlet • Intact loop • Broken loop	327.9 °C 327.8 °C 296.2 °C 295.4 °C
Water Level	Pressurizer	c. 5.2 m
Temperature	Pressurizer	346 °C
Power	Core	5.20 MW
Water Volume	Accumulator • Intact loop • Broken loop	246 l 76 l
Gas Volume	Accumulator • Intact loop • Broken loop	34 l 18 l
Temperature	Accumulator • Intact loop • Broken loop	c. 30 °C c. 30 °C
Mass Flow	MCP seal water injection Intact loop Broken loop	0.01 kg/s 0.0087 kg/s
Temperature	MCP seal water injection	c. 30 °C
Water Temperature	HPIS	28 °C
Secondary System:		
Mass Flow	Steam generator Intact loop Broken loop	2.0 kg/s 0.66 kg/s
Pressure	Steam dome Intact Loop Broken Loop	6.62 MPa 6.62 MPa
Temperature	Steam Generator inlet • Intact Loop • Broken Loop Steam Generator outlet • Intact Loop • Broken Loop	210.3 °C 207.4 °C 282.4 °C 281.9 °C
Recirculation Ratio	Steam generator Intact loop Broken loop	c. 5.8 c. 4.0
Water Level	Downcomer Intact loop Broken loop	c. 8.29 m c. 8.11 m

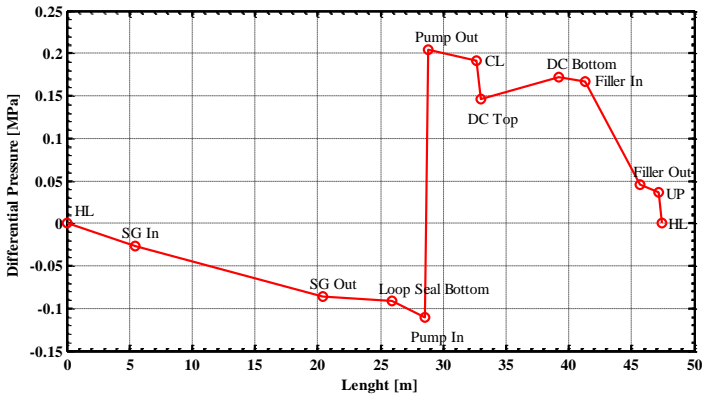


Figure 183 – Pressure Drop versus Length in the Intact Loop.

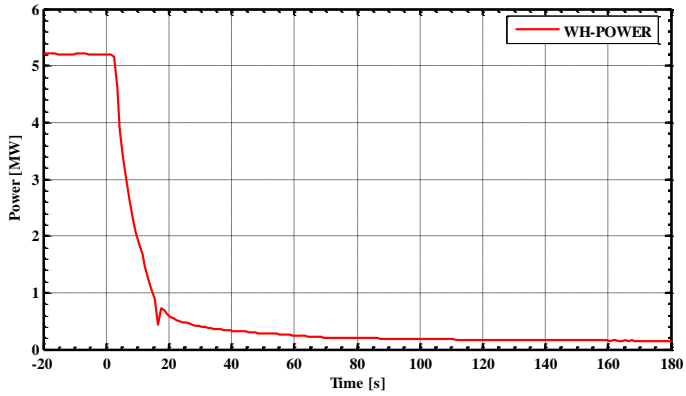


Figure 184 – Core Power, Short Time.

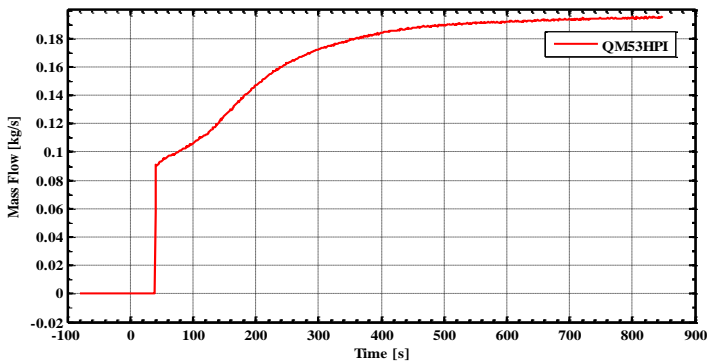


Figure 185 – HPIS Mass Flow as Function of Time.

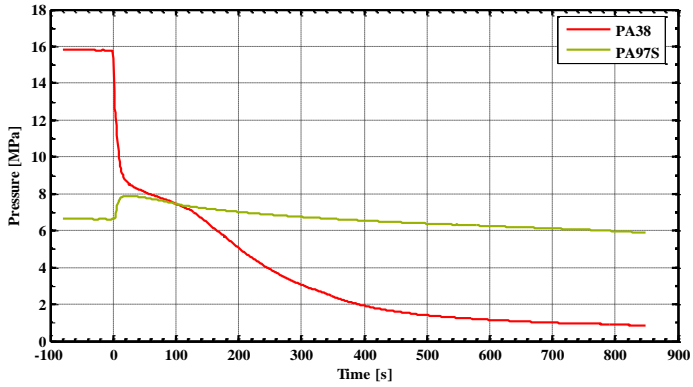


Figure 186 – Primary and Secondary System Pressure.

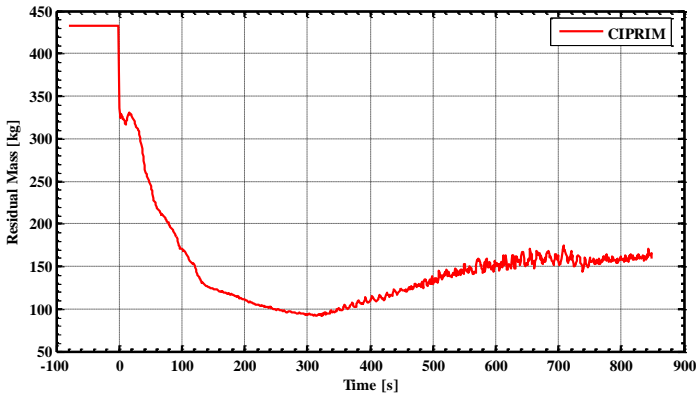


Figure 187 – Primary System Fluid Inventory.

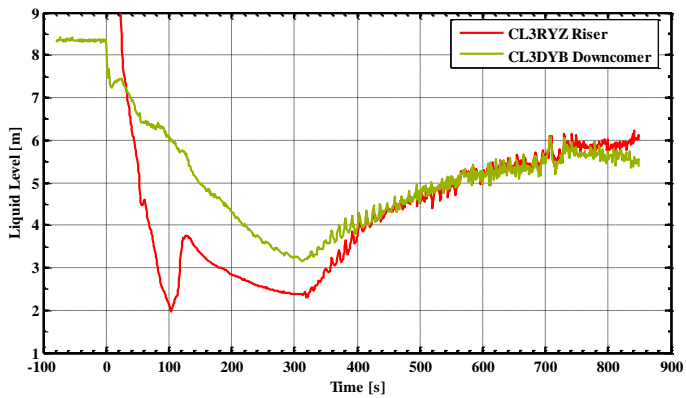


Figure 188 – Collapsed Liquid Level in the Vessel.

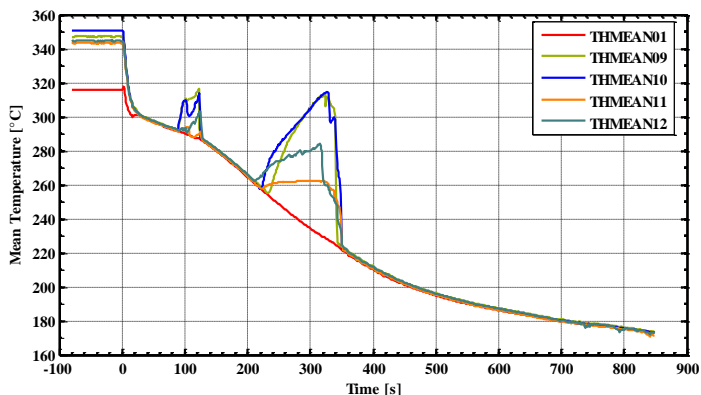


Figure 189 – Mean Temperature in Heater Rods.

D.3. References to APPENDIX D

- [D-1] F. D'Auria, M. Frogheri, W. Gianotti, "RELAP5/MOD3.2 post test analysis and accuracy quantification of LOBI Test BL-34(44)", NUREG/IA-0152(53), February 1999
- [D-2] C. Addabbo, G. Gressani, "Quick Look Report on LOBI-MOD2 Test A1-83", N° 4028, May 1985, Ispra Research Center, Italy
- [D-3] И. Е. Идельчик, "Справочник по гидравлическим сопротивлениям", 3-е издание Москва, Машиностроение 1992 г.
- [D-4] OECD-CSNI. "LOBI-MOD2: Facility Description and Specifications for OECD-CSNI International Standard Problem N° 18 (ISP 18)", Reactor Safety Program N° 4010, July 1983.

APPENDIX E. EXAMPLE OF ENGINEERING HANDBOOK OF RELAP5 MODEL OF LOBI FACILITY

In this Appendix a few examples from Engineering Handbook of RELAP5-3D© model of LOBI-MOD2 facility are provided. To provide the idea of the typical scope of Engineering Handbook it may be noted that the original EH of RELAP5-3D© model of LOBI-MOD2 facility is a 270 pages document.

The Engineering Handbook (EH) constitutes the technical rationale and description of the input model. It documents for each component of the RELAP5-3D© model the input entries providing engineering justification of the adopted assumptions (rationale and user choice). It finally makes a cross link between the Reference Data Set (RDS) of the ITF, the code and the input deck.

The EH describes the RELAP5-3D© input model. It documents for each component of the RELAP5-3D© model the input entries providing engineering justification of the adopted assumptions (rationale and user choice). It finally makes a cross link between the Reference Data Set (RDS) of the ITF, the code and the input deck. The approach used to developed the EH content and to write the document also help to find errors in the input and discrepancies between the RDS and the R5 input deck. The independent review of the input is assured by the fact that the input developer has only to write the “rationale” and the “user choice” sections of the present document, all the other part of the EH have been elaborated and written by RDS developers whom continuously checked the consistency of the input development calculation notes and the RDS data.

The approach used for the development of the present document intrinsically constitute a review of the three documents increase the overall quality of the RDS, Input file and EH, ensuring high quality of the products.

E.1. Pressure Vessel hydraulic model

Subdivision of the Reactor Pressure Vessel (RPV) and Upper Head (UH) in modules is shown in *Figure 190*, the corresponding R5 nodalization is shown in *Figure 191*. *Figure 192 and Figure 193* showed in the following represent the detailed subdivision in module of the RPV with the correspondence, highlighted with the use of different colors, to the R5 nodalization scheme. To facilitate the use of the present document the RPV has been divided in six parts: downcomer, Lower Plenum (LP), core, Upper Plenum (UP), upper head simulator and the seal water drainage.

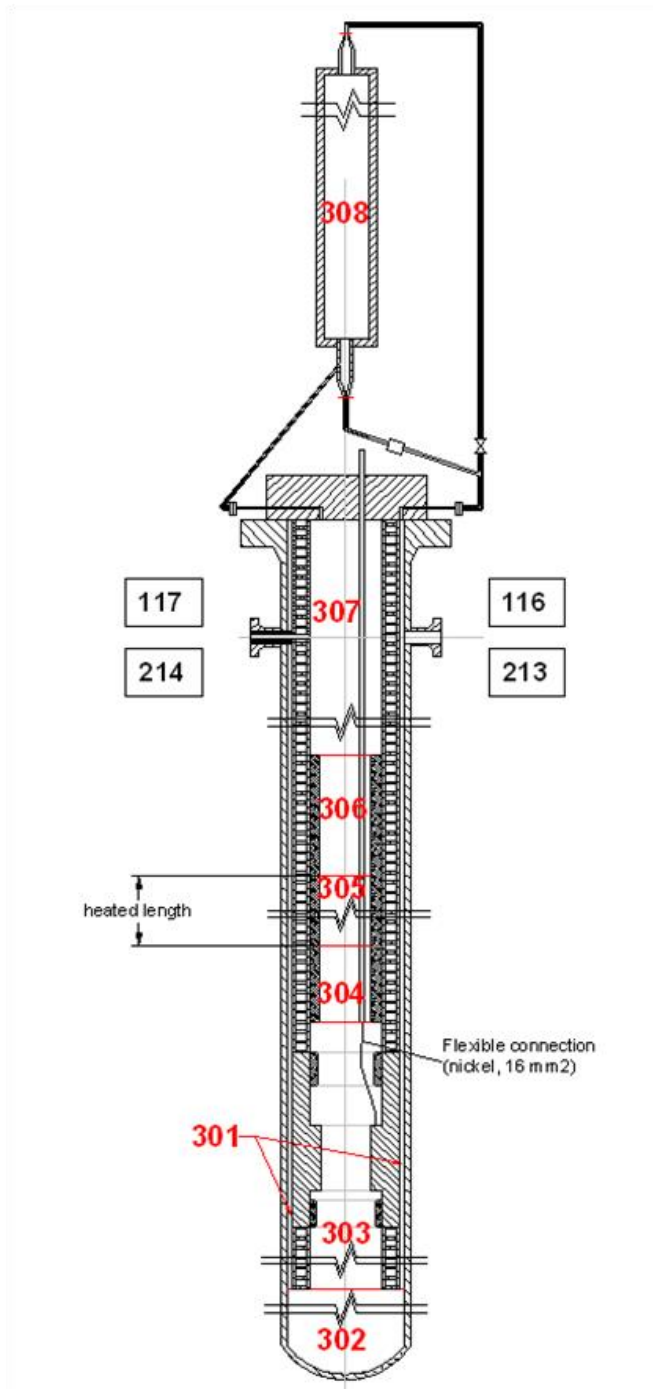


Figure 190 – LOBI/MOD2 RPV and UH simulator with subdivision in modules [E1].

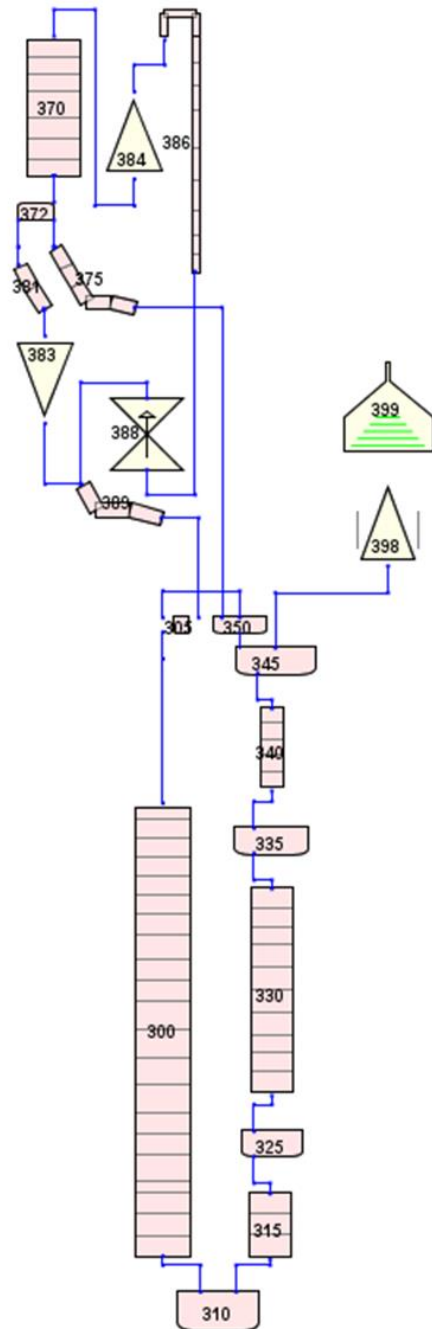


Figure 191 – RELAP5-3D[®] nodalization of LOBI/MOD2 RPV and UH simulator.

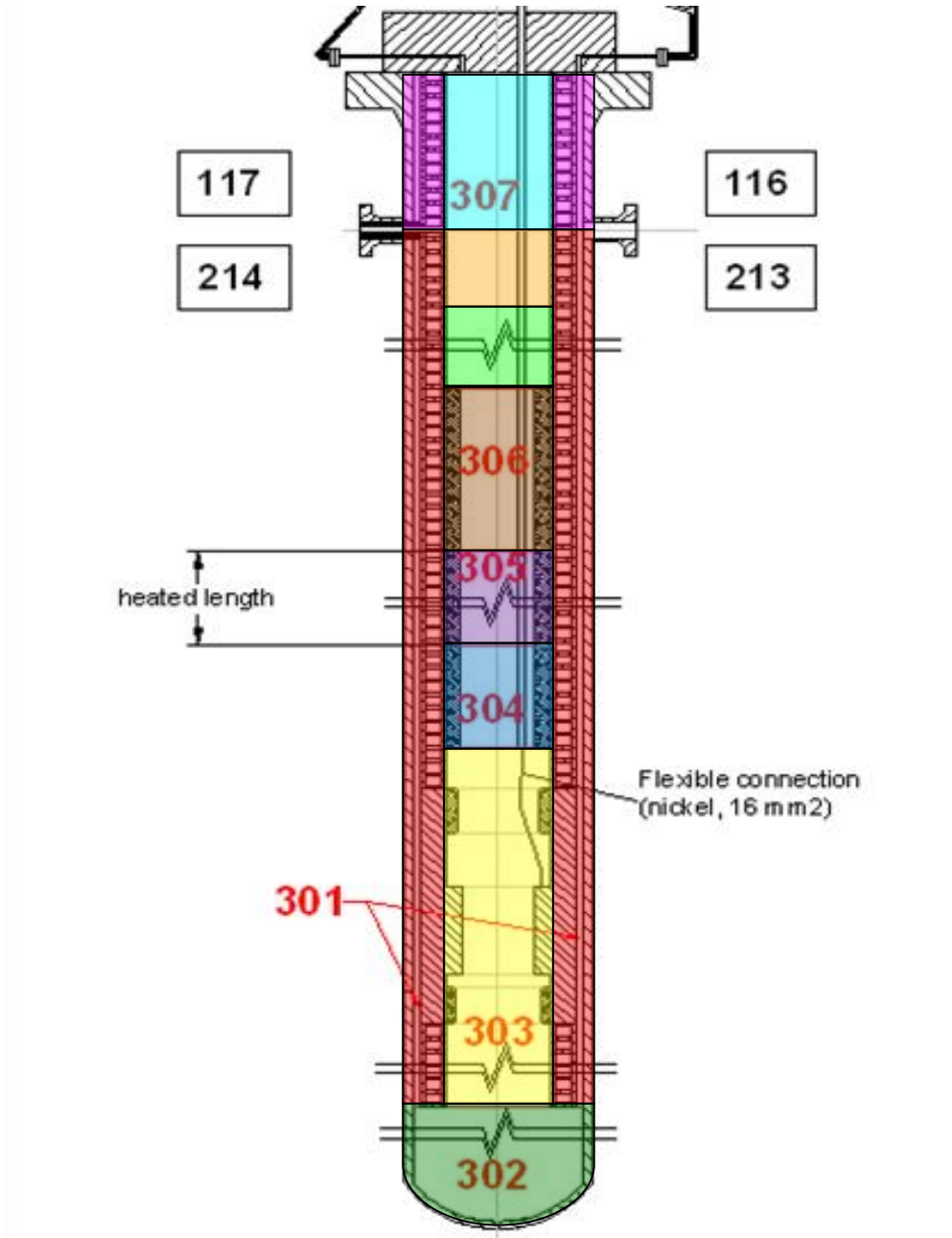


Figure 192 – LOBI/MOD2 Reactor Pressure Vessel.

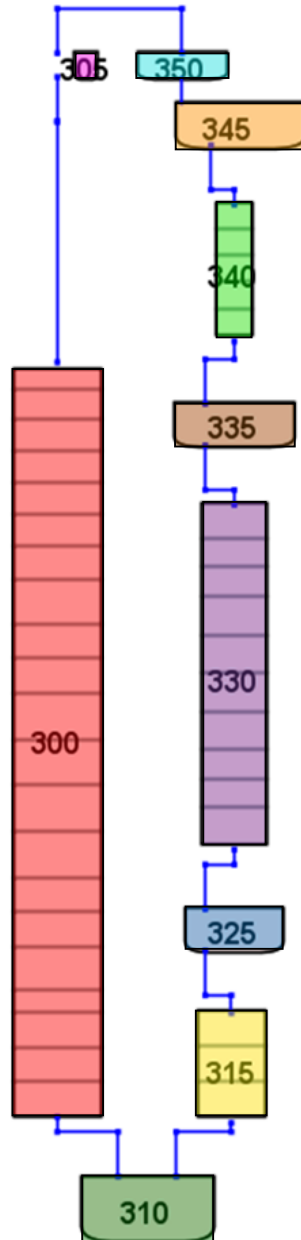


Figure 193 – RELAP5-3D[®] nodalization of LOBI/MOD2 Reactor Pressure Vessel.

E.1.1. Downcomer hydraulic model

○ Rationale

The downcomer is modeled as a single vertical stack of volumes, implying a total mixing in azimuthal direction.

○ User choices

The part of downcomer above the centerline of cold legs is modeled by a single branch. The part of downcomer below the centerline of cold legs until the hemispherical bottom is modeled as a pipe component. The lengths of the nodes of this pipe are chosen to comply with the “sliced” nodalization approach (core and loop seal).

○ Models (flag)

- PIPE 300 (FROM COLD LEG DOWNCOMER TO LP)

Volume: default;

Junctions: default.

- BRANCH 305 (FROM COLD LEG UP TO VESSEL COVER)

Volume: default;

Junctions 1, 6: default;

Junctions 2, 3, 4 and 5: flag v=2.

○ Geometry Data

- PIPE 300 (FROM COLD LEG DOWNCOMER TO LP)

Component 300 models the annular space between the reactor vessel and the core barrel vessel from the central level of the legs to the lower plenum. It is vertically oriented with downward direction and it is subdivided into 21 cells. The length of each cell varies according to the cutting plane used for the slice nodalization approach. The internal diameter is 0.288 m, the external diameter is 0.312 m and the flow area is $1.131 \cdot 10^{-2} \text{ m}^2$. The total length of the component is 7.121 m (E-1)

$$L_{300} = L_{M300} - L_{305} = 7.436 - 0.315 = 7.121 \text{ m} \quad (\text{E-1})$$

See *Table 59* for detailed geometry summary.

- BRANCH 305 (FROM COLD LEG UP TO VESSEL COVER)

Component 305 models the upper part of the downcomer (from the level of the Cold Leg to the top of the core barrel). The component is upward directed. The hydraulic diameter of the component is 0.024 m (see E-2) and the flow area is $1.131 \cdot 10^{-2} \text{ m}^2$. The length of the branch is 0.315 m (E-3).

$$D_{hd305} = D_{M305,ext} - D_{M305,int} = 0.312 - 0.288 = 0.024 \text{ m} \quad (\text{E-2})$$

$$L_{305} = L_{M300} - L_{300} = 7.436 - 7.121 = 0.315 \text{ m} \quad (\text{E-3})$$

See *Table 59* for detailed geometry summary.

- **Junction Data**

- PIPE 300 (FROM COLD LEG DOWNCOMER TO LP)

The junction flow area is not specified. See *Table 60* for detailed junction summary.

- BRANCH 305 (FROM COLD LEG UP TO VESSEL COVER)

Component 305 (upper part of the downcomer) has three junctions. The first one connects its “inlet face” to the first cell “inlet face” of component 300 (downcomer). The second junction connects the “outlet face” of component 305 to the first cell “outlet face” of component 350 (top of the upper plenum) simulating the by-pass between the top of the downcomer and the UP, and third one connects its “outlet face” to the third cell “outlet face” of the component 389 (pipeline of the upper head), that simulates the by-pass to the UH. The specified area is $3.927 \cdot 10^{-5} \text{ m}^2$ for the junction number two and $3.14 \cdot 10^{-4} \text{ m}^2$ for the junction number three. K-loss coefficient is applied in the second junction with value 8.5 and in the third junction with value 100. See *Table 60* for detailed junction summary.

E.2. Pressure Vessel heat structure data

Figure 194 shows the nodalization of the RPV and the upper head simulator with the corresponding heat structure that are detailed in the following of this section.

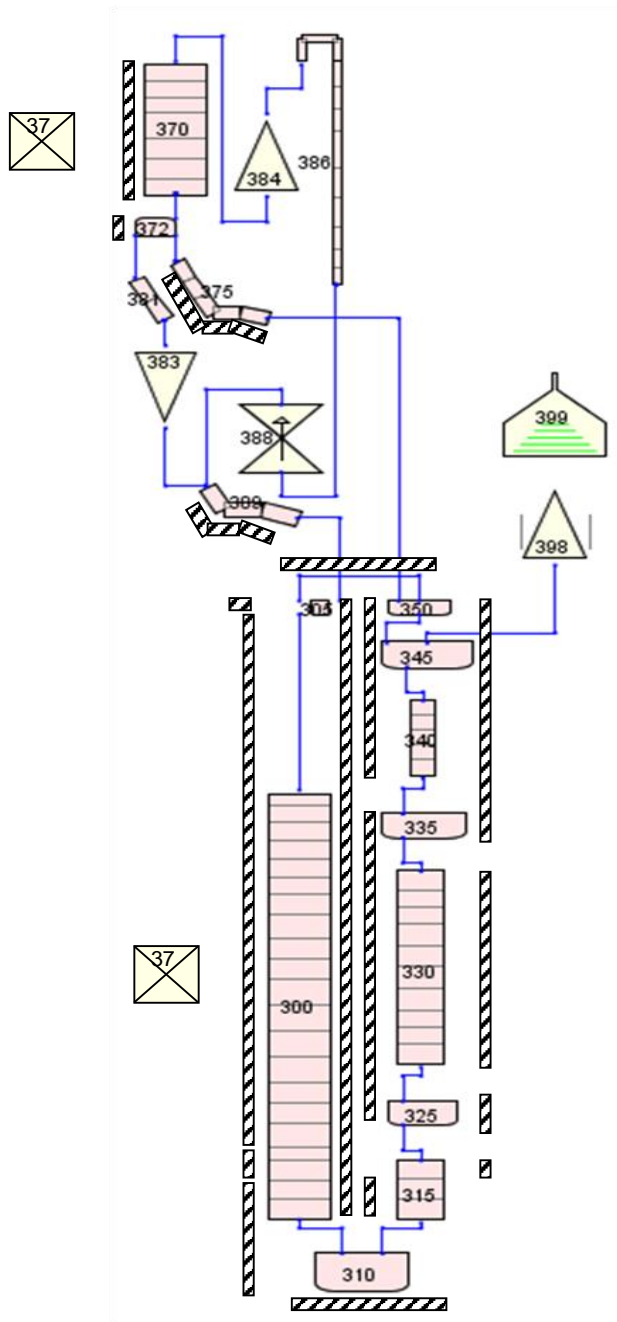


Figure 194 – LOBI/MOD2 Pressure Vessel, Heat Structures.

Table 59 – Summary Table: Geometry Data of Pressure Vessel and Upper Head.

Comp. Name	Comp. N°	Volume N°	Comp. Type	Length	Area	Volume	D _{hd}	Elevation change	Angle	Outlet Elevation	Wall Roughness	Volume Control Flag tlpvbf	Comment
DC-1	300	1	PIPE	0.200	$1.131 \cdot 10^{-2}$	-	0.024	-0.200	-90°		$4.5 \cdot 10^{-5}$	0000000	
		2		0.287				-0.287					
		3		0.300				-0.300					
		4		0.300				-0.300					
		5		0.300				-0.300					
		6		0.300				-0.300					
		7		0.328				-0.328					
		8		0.412				-0.412					
		9		0.331				-0.331					
		10		0.332				-0.332					
		11		0.437				-0.437					
		12		0.438				-0.438					
		13		0.438				-0.438					
		14		0.437				-0.437					
		15		0.332				-0.332					
		16		0.331				-0.331					
		17		0.412				-0.412					
		18		0.200				-0.200					
		19		0.335				-0.335					
		20		0.335				-0.335					
		21		0.336				-0.336					
DC-2	305	1	BRANCH	0.315	$1.131 \cdot 10^{-2}$	-	0.024	0.315	90°		$4.0 \cdot 10^{-5}$	0000000	
LP-1	310	1	BRANCH	0.373	-	$2.647 \cdot 10^{-2}$	0.024	0.315	90°		$4.0 \cdot 10^{-5}$	0000000	
LP-2	315	1	PIPE	0.336	$2.565 \cdot 10^{-2}$	-		0.336	90°		$4.0 \cdot 10^{-5}$	0000000	
		2		0.335				0.335					
		3		0.335				0.335					
CORE-B	325	1	BRANCH	0.200	$8.126 \cdot 10^{-3}$			0.200	90°		$4.0 \cdot 10^{-5}$	0000000	
CORE-A	330	1	PIPE	0.412	$8.1152 \cdot 10^{-3}$	-	-	0.412	90°		$4.0 \cdot 10^{-5}$	0000100	Squared cross-section
		2		0.331				0.331					
		3		0.332				0.332					
		4		0.437				0.437					
		5		0.438				0.438					
		6		0.438				0.438					
		7		0.437				0.437					
		8		0.332				0.332					
		9		0.331				0.331					
		10		0.412				0.412					

Table 60 – Summary Table: Junction Data of Pressure Vessel and Upper Head.

Component Name	Comp. N°	Component Type	Junction Number	From Component	To Component	Junction Area	Junction Flag jefvcahs	Loss Coefficient		Description
								K _t	K _r	
DC-1	300	PIPE	1	30001	30002	-	00000000	0	0	
			2	30002	30003					
			3	30003	30004					
			4	30004	30005					
			5	30005	30006					
			6	30006	30007					
			7	30007	30008					
			8	30008	30009					
			9	30009	30010					
			10	30010	30011					
			11	30011	30012					
			12	30012	30013					
			13	30013	30014					
			14	30014	30015					
			15	30015	30016					
			16	30016	30017					
			17	30017	30018					
			18	30018	30019					
			19	30019	30020					
			20	30020	30021					
DC-2	305	BRANCH	1	300010001	305010001	-	00000000	0.000	0.000	
			2	305010002	350010002	$3.927 \cdot 10^{-4}$		4.500	4.500	
			3	305010002	389030002	$3.142 \cdot 10^{-4}$		1.669	1.669	
LP-1	310	BRANCH	1	300210002	310010002	-	00000000	0.723	0.443	
			2	310010002	315010001			0.341	0.360	
LP-2	315	PIPE	1	31501	31502	-	00000000	0.000	0.000	
			2	31502	31503			2.200	2.200	
CORE-B	325	BRANCH	1	315030002	325010001	-	00000000	0.393	0.526	
			2	325010002	330010001	-		0.220	0.220	

E.2.1. Downcomer heat structure data

The downcomer structure is simulated by heat structures 3000, 3001, 3002, 3003 and 3004.

- **Rationale**

The cylindrical heat structures of the RPV and barrel are modeled according to the general nodalization techniques.

- **User choices**

The lengths (surface factor) of the cylindrical axial heat structures are set equal to the length of the corresponding hydraulic nodes.

- **Models (flag)**

- Downcomer Barrel (3000)

The left boundary condition type is 0.

The right boundary condition type is 101.

- Pressure Vessel, Lower Cylindrical part (3001)

The left boundary condition type is 101.

The right boundary condition type is 3300.

- Pressure Vessel, Lower Flange (3002)

The left boundary condition type is 101.

The right boundary condition type is 3300.

- Pressure Vessel, Upper Cylindrical part (3003)

The left boundary condition type is 101.

The right boundary condition type is 3300.

- Pressure Vessel, Upper Flange (3004)

The left boundary condition type is 101.

The right boundary condition type is 3300.

- **Calculation notes: Geometry Data**

- Downcomer Barrel (3000)

The heat structure 3000 represents the outer half of the core barrel, that has an honeycomb structure, which is in contact with the downcomer. It is composed of twenty two axial heat structures of the same geometry. The component is of cylindrical geometry type. Its right surface is connected with hydrodynamic components 300 and 305. The inner and outer diameters of the HS are taken from RDS module 301: $D_{in} = 0.274$ m and $D_{out} = 0.288$ m. The HS has a total length of 7.436 m. For more detailed HS information see *Table 61*.

- Pressure Vessel, Lower Cylindrical part (3001)

The heat structure 3001 models the lower cylindrical part of the pressure vessel, from the downcomer region to the lower plenum. The HS is of cylindrical geometry type. It is composed of two axial heat structures of the same geometry. The left side of the heat structure is connected with the last cell of hydrodynamic component 300 (30021) and with component 310. The right surface of the heat structure is connected to the environment, simulated with the component 030. The inner and outer diameters of the HS are taken from RDS module 301: $D_{in} = 0.312$ m and $D_{out} = 0.3436$ m. HS has a total length of 0.623 m (E-4). For more detailed HS information see *Table 61*.

$$L_{3001} = L_{310(1)} + L_{300(21)} = 0.287 + 0.336 = 0.623 \text{ m} \quad (\text{E-4})$$

- Pressure Vessel, Lower Flange (3002)

The heat structure 3002 represents the region of the lower flange. The geometry of the heat structure is cylindrical type. The structure is composed of two equal axial HS. The left side of the heat structure is connected with cells 19 and 20 of component 300. The right surface of the heat structure is connected to the environment, simulated with the component 030. The inner diameter of the HS is taken from RDS module 301 and the outer diameter is calculated as an average diameter of the flange, preserving the facility metal's volume and so the stored energy. In the following the calculation notes for this process are explained: $D_{in} = 0.312$ m and $D_{out} = 0.4177$ m. (E-10). HS has a total length of 0.415 m (E-11). For more detailed HS information see *Table 61*.

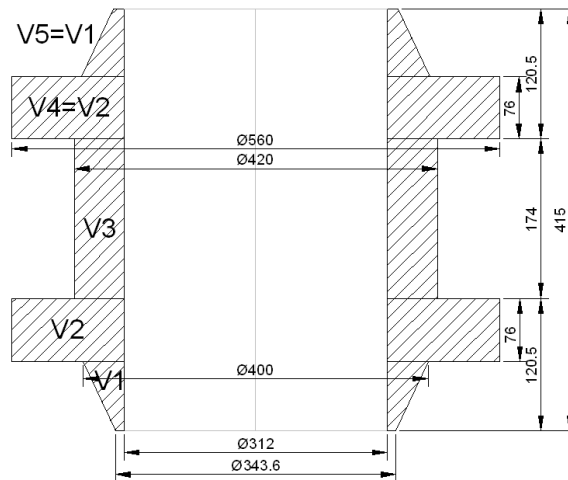


Figure 195 – LOBI/MOD2 Lower Flange of the Pressure Vessel.

$$V_1 = \frac{\pi}{12} \cdot (0.1205 - 0.076) \cdot (0.4^2 + 0.4 \cdot 0.3436 + 0.3436^2) - \frac{\pi}{4} \cdot 0.312 \cdot (0.1205 - 0.076) \quad (\text{E-5})$$

$$V_2 = \frac{\pi}{4} \cdot (0.56^2 - 0.312^2) \cdot 0.076, \quad V_3 = \frac{\pi}{4} \cdot (0.42^2 - 0.312^2) \cdot 0.174 \quad (\text{E-6})$$

$$V_3 = \frac{\pi}{4} \cdot (0.42^2 - 0.312^2) \cdot 0.174 \quad (\text{E-7})$$

$$V_{tot} = 2 \cdot V_1 + 2 \cdot V_2 + V_3 = 0.0252 \text{ m}^3 \quad (\text{E-8})$$

$$A_{eq} = \frac{V_{tot}}{L} = 0.0606 \text{ m}^2 \quad \text{and} \quad A_{eq} = \frac{\pi}{4} \cdot \left((D_{out}^{eq})^2 - D_{in}^2 \right) \quad (\text{E-9})$$

from these two equations the equivalent diameter is evaluated:

$$D_{out}^{eq} = \sqrt{4 \cdot \frac{A_{eq}}{\pi} + D_{in}^2} = 0.4177 \text{ m} \quad (\text{E-10})$$

$$L_{3002} = L_{300(19.2)} + L_{300(20)} = 0.080 + 0.335 = 0.415 \text{ m} \quad (\text{E-11})$$

- Pressure Vessel, Upper Cylindrical part (3003)

The heat structure 3003 represents the upper cylindrical part of the pressure vessel. The HS is of cylindrical geometry type. It is composed of twenty axial heat structures of the same geometry. The left side of the heat structure is connected with the hydrodynamic component 305 and with component 300 from the first cell to the nineteenth cell (30001-30019). The right surface of the heat structure is connected to the environment, simulated with the component 030. The inner and outer diameters of the HS are taken from RDS module 301: $D_{in} = 0.312 \text{ m}$ and $D_{out} = 0.3436 \text{ m}$. HS has a total length of 6.569 m (E-12). For more detailed HS information see *Table 61*.

$$L_{3003} = L_{305(01)} + L_{300(01-18)} + L_{300(19.1)} = 0.199 + 6.115 + 0.255 = 6.569 \text{ m} \quad (\text{E-12})$$

- Pressure Vessel, Upper Flange (3004)

The heat structure 3004 models the upper flange. The HS has cylindrical geometry and it is composed of one structure. The left side of the heat structure is connected with the hydrodynamic component 305. The right surface of the heat structure is connected to the environment, simulated with the component 030. The inner diameter of the HS is taken from RDS module 301 and the outer diameter is calculated as an average diameter of the flange preserving the actual metal's volume: $D_{in} = 0.312 \text{ m}$ and $D_{out} = 0.5032 \text{ m}$. (E-17). HS has a total length of 0.080 m (E-18). For more detailed HS information see *Table 61*.

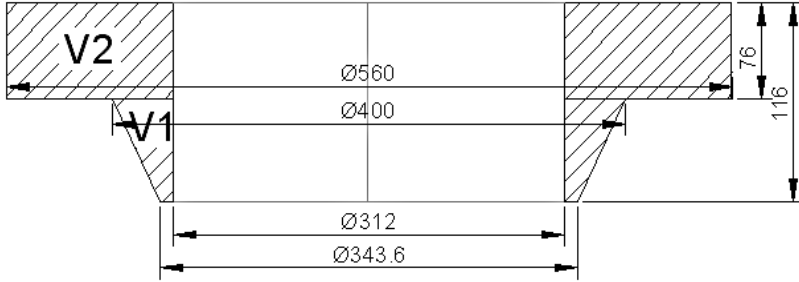


Figure 196 – LOBI/MOD2 Upper Flange of the Pressure Vessel.

$$V_1 = \frac{\pi}{12} \cdot (0.116 - 0.076) \cdot (0.4^2 + 0.4 \cdot 0.3436 + 0.3436^2) - \frac{\pi}{4} \cdot 0.312^2 \cdot (0.116 - 0.076) \quad (\text{E-13})$$

$$V_2 = \frac{\pi}{4} \cdot (0.56^2 - 0.312^2) \cdot 0.076 \quad (\text{E-14})$$

$$V_{tot} = V_1 + V_2 = 0.0192 \text{ m}^3 \quad (\text{E-15})$$

$$A_{eq} = \frac{V_{tot}}{L} = 0.1224 \text{ m}^2 \quad \text{and} \quad A_{eq} = \frac{\pi}{4} \cdot \left((D_{out}^{eq})^2 - D_{in}^2 \right) \quad (\text{E-16})$$

from these 2 equations the equivalent diameter is evaluated:

$$D_{out}^{eq} = \sqrt{4 \cdot \frac{A_{eq}}{\pi} + D_{in}^2} = 0.5032 \text{ m} \quad (\text{E-17})$$

$$L_{3004} = L_{305(1.2)} = 0.080 \text{ m} \quad (\text{E-18})$$

Table 61 – Summary Table: Heat Structure Data of RPV.

Heat Structure N°	N° of Axial Heat Structure	N° mesh point	Geometry Type	N° of mesh intervals	Materials	Mesh Size	Left Coordinate	Right Coordinate	Source Type	Source multiplier	Description
3000	22	15	2	14	3	-	0.137	0.144	-	-	
3001	2	20	2	19	1	-	0.156	0.1718	-	-	
3002	2	20	2	19	7	-	0.156	0.20885	-	-	
3003	20	20	2	19	1	-	0.156	0.1718	-	-	
3004	1	20	2	19	7	-	0.156	0.266	-	-	
3101	1	20	2	19	1	-	0.0	0.0158	-	-	
3150	1	15	2	14	4	-	0.0	0.00225	900	0.047	
3151	3	15	2	14	3	-	0.0909	0.106	0	0.0	
3250	1	20	2	19	4	-	0.0	0.005375	900	0.005	
3300	1	15	2	14	5	-	0.003225	0.005375	900	0.065	
3301	1	15	2	14	5	-	0.003875	0.005375	900	0.07	
3302	1	15	2	14	5	-	0.003875	0.005375	900	0.07	
3303	1	15	2	14	5	-	0.004175	0.005375	900	0.11275	
3304	1	15	2	14	5	-	0.004175	0.005375	900	0.11275	
3305	1	15	2	14	5	-	0.004175	0.005375	900	0.11275	
3306	1	15	2	14	5	-	0.004175	0.005375	900	0.11275	
3307	1	15	2	14	5	-	0.003875	0.005375	900	0.071	
3308	1	15	2	14	5	-	0.003875	0.005375	900	0.071	
3309	1	15	2	14	5	-	0.003225	0.005375	900	0.066	
3310	12	10	2	9	2	-	0.075	0.105	-	-	
3350	1	15	2	14	4	-	0.0025	0.005375	900	0.0112	
	2									0.0102	
	3									0.0102	
	4									0.0102	
	5									0.0102	
	6									0.0098	
	7									0.068	
	8									0.0152	
3400	7	15	2	14	3	-	0.099	0.106	-	-	
3500	1	20	1	19	1	-	0.0	0.13	-	-	
3700	7	20	2	19	1	-	0.06	0.08	-	-	
3720	1	15	2	14	1	-	0.01725	0.02225	-	-	
3750	5	10	2	9	1	-	0.01	0.012	-	-	
3890	17	10	2	9	1	-	0.01	0.012	-	-	

E.3. General tables

The steady state power for each test is imposed on card 20290000 (see *Table 62*). General table 900 is used to impose the decay power as specified for each experiment. The table is activated with the trip 1900 (see corresponding section). The entries of *Table 62* may change with the test condition.

Table 62 – Core Power Table.

Table number	Time [s]	Fraction of Test Nominal Power
20290001	0.	1.0
20290002	5.25	0.7561302
20290003	10.4	0.3840996
20290004	15.6	0.2160919
20290005	26.04	0.1088122
20290006	31.26	0.0881226
20290007	72.8	0.0459770
20290008	166.5	0.0354406
20290009	331.5	0.0266283
20290010	762.5	0.0208620
20290011	1459.5	0.0178160
20290012	4907.5	0.0122605

E.4. Material properties

This section of the engineering handbook documents the material properties of materials used in the input deck. The stored material properties in the RELAP5 codes have not been used. The option TBL/FCTN in card 201MMM00 has been used for the different materials: the thermal conductivity and the heat capacity are input as a function of temperature. *Table 63* lists the input entries for the Inconel 625 thermal conductivity.

Table 63 – Inconel 625 Thermal Conductivity.

Table number	Temperature [K]	Heat conductivity [W/(m K)]
20100101	93.	12.
20100102	473.	12.5
20100103	573.	13.9
20100104	673.	15.3
20100105	2073.	16.3

E.5. Control logic

E.5.1. Control variables

Level

Table 64 summarizes the level control variables that are present in the RELAP5 input. In the present *Table 64*, the control variables, related to a particular part of the ITF, are grouped together (the same approach has been used in the input file). For each control variable the location of the level measurement is identified (second column), the correspondence with the ITF measurement channel is given in the fifth column. For each control variable the last column of *Table 64* provides the reference to the section that the described the specific control variable.

Pressurizer level

The pressurizer level is calculated summing the liquid void fraction in each cells multiplied by the elevation change of each cell for which the variable “voidf” is calculated (E–19 and E–20). Two control variables are used to calculate the actual collapsed level of the pressurizer: 4209 and 4309.

Control variable 4209:

$$\begin{aligned}
 &PRZ_L1 \\
 &= 0.395 \cdot voidf\ 420_01 + 0.395 \cdot voidf\ 425_01 + 0.585 \\
 &\cdot voidf\ 430_01 + \\
 &\quad + 0.5 \cdot voidf\ 430_02 + 0.5 \cdot voidf\ 430_03 + 0.5 \\
 &\quad \cdot voidf\ 430_04 + \\
 &\quad + 0.5 \cdot voidf\ 430_05 + 0.345 \cdot voidf\ 430_06
 \end{aligned}
 \tag{E-19}$$

Control variable 4309:

$$\begin{aligned}
 PRZ_L &= 0.336 \cdot voidf\ 430_07 + 0.5 \cdot voidf\ 430_08 + 0.5 \\
 &\cdot voidf\ 430_09 + \\
 &\quad + 0.6 \cdot voidf\ 430_10 + 0.6 \cdot voidf\ 430_11 + 0.705 \\
 &\quad \cdot voidf\ 430_12 + \\
 &\quad + 0.705\ voidf\ 440_01 + 1.0 \cdot cntrlvar\ 4209
 \end{aligned}
 \tag{E-20}$$

E.5.2. Trips

Upper plenum pressure signal

Trip 345

Trip 345 is widely used in the control system of the present input deck. The trip is a low pressure signal in the upper plenum of the RPV (E-21).

$$p\ 345_01\ lt\ null\ 0\ 13.2e + 6\ l$$

E.6 References to APPENDIX E

[E-1] Agreement Atucha-II - UNIP I N°3. "Reference Data Set for LOBI-MOD2 facility", REP124_U-NIII_DIT130_E1.3.6a_FR_Ch15Fin_Rev1, S. Giovannetti, O. Lisovsky, Pisa, May 2011.

Table 64 – Summary Table for Level control variables.

General Location	Location	Control Variable Number	Control variable Name	Experimental Channel Measurement Correspondence	Description	Reference	
IL LEVEL	Pressurizer	4209	PRZ_L1	-			
		4309	PRZ_L	-			
	IL SG inlet global	1159	ILSGIN-L	CL90AB+1.19m-0.055m			
	IL U-tubes ascending side	1189	ILUTAS-L	CL90BP+2.995m			
		1199	ILUTAS-L				
	IL U-tubes descending side	1219	ILUTDS-L	-			
		1229	ILUTDS-L	CL92BP+2.955m			
	IL SG outlet Global level	1259	ILSGOT-L	-			
				CL93AB+1.19m-0.055m			
	IL Loop Seal		1299	ILLS-1	-		
1309			ILLS-2	-			
1319			ILLS-L	CL1792X3			
RPV LEVEL	RPV Core Level	3295	RPVCOR-1	-			
		3309	RPVCOR-L	-			
	RPV Riser Level	3159	RPVRSR-1	-			
		3409	RPVRSR-3	-			
		3459	RPVRSR-L	CL3RYA	Approximately		
	RPV Downcomer Level		3009	RPVDC-1	-		
			3019	RPVDC-2	-		
			3029	RPVDC-3	-		
3059			RPVDC-L	CL3DYB+0.17m			
BL SG	BL SG Downcomer level	7009	BLSGDC-1	-			
		7359	BLSGDC-L	-			
BLSG	BL SG Riser level	7049	BLSGRS-1	-			
		7059	BLSGRS-L	-			